

MIRT

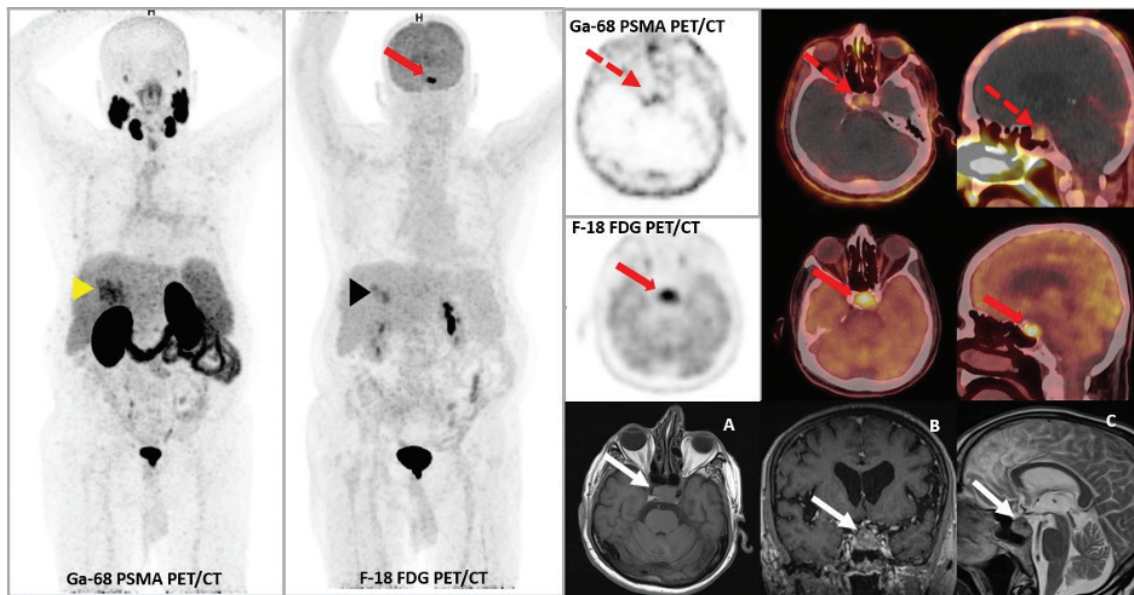
Molecular Imaging and Radionuclide Therapy

October 2022

Volume 31

Issue 3

www.tsnm.org



"Official Journal of the Turkish Society of Nuclear Medicine"

Scientific Advisory Board

Ayşegül Akgün

Ege University, Medical School, Department of Nuclear Medicine, İzmir, Turkey

Esma Akin

The George Washington University, Medical School, Department of Diagnostic Radiology, Washington DC, USA

Claudine Als

Hopitaux Robert Schuman Zitha Klinik, Médecine Nucléaire, Luxembourg

Vera Artiko

Clinical Center of Serbia, Center for Nuclear Medicine, Belgrade, Serbia

Nuri Arslan

University of Health Sciences Turkey, Gülhane Medical School, Gülhane Training and Research Hospital, Clinic of Nuclear Medicine, Ankara, Turkey

Lütfiye Özlem Atay

Gazi University Faculty of Medicine, Department of Nuclear Medicine, Ankara, Turkey

Marika Bajc

Lund University Hospital, Clinic of Clinical Physiology, Lund, Sweden

Lorenzo Biassoni

Great Ormond Street Hospital for Children NHS Foundation Trust, Department of Radiology, London, United Kingdom

Hans Jürgen Biersack

University of Bonn, Department of Nuclear Medicine, Clinic of Radiology, Bonn, Germany

M. Donald Blafox

Albert Einstein College of Medicine, Department of Radiology, Division of Nuclear Medicine, New York, USA

Patrick Bourguet

Centre Eugène Marquis Department of Nuclear Medicine, Clinic of Radiology, Rennes, France

Murat Fani Bozkurt

FEBNM Hacettepe University, Medical School, Department of Nuclear Medicine, Ankara, Turkey

A. Cahid Civelek

NIH Clinical Center, Division of Nuclear Medicine, Bethesda, USA

Arturo Chiti

Humanitas University, Department of Biomedical Sciences; Humanitas Clinical and Research Center, Clinic of Nuclear Medicine, Milan, Italy

Josep Martin Comin

Hospital Universitari de Bellvitge, Department of Nuclear Medicine, Barcelona, Spain

Alberto Cuocolo

University of Naples Federico II, Department of Advanced Biomedical Sciences, Napoli, Italy

Tevfik Fikret Çermik

University of Health Sciences Turkey, İstanbul Training and Research Hospital, Clinic of Nuclear Medicine, İstanbul, Turkey

Angelika Bischof Delaloye

University Hospital of Lausanne, Department of Radiology, Lausanne, Switzerland

Mustafa Demir

İstanbul University, Cerrahpaşa Medical School, Department of Nuclear Medicine, İstanbul, Turkey

Hakan Demir

Kocaeli University Medical School, Department of Nuclear Medicine, Kocaeli, Turkey

Peter Josef Ell

University College Hospital, Institute of Nuclear Medicine, London, United Kingdom

Tanju Yusuf Erdil

Marmara University, Pendik Training and Research Hospital, Clinic of Nuclear Medicine, İstanbul, Turkey

Türkan Ertay

Dokuz Eylül University, Medical School, Department of Nuclear Medicine, İzmir, Turkey

Jure Fettich

University Medical Centre Ljubljana, Department for Nuclear Medicine, Ljubljana, Slovenia

Christiane Franzius

Klinikum Bremen Mitte Center, Center for Modern Diagnostics, Bremen, Germany

Lars Friberg

University of Copenhagen Bispebjerg Hospital, Department of Nuclear Medicine, Copenhagen, Denmark

Jørgen Frøkiær

Aarhus University Hospital, Clinic of Nuclear Medicine and PET, Aarhus, Denmark

■ **The Owner on Behalf of Turkish Society of Nuclear Medicine**

Prof. Dr. Tevfik Fikret Çermik

University of Health Sciences Turkey, İstanbul Training and Research Hospital, Clinic of Nuclear Medicine, İstanbul, Turkey

E-mail: tevfik.cermik@sbu.edu.tr

ORCID ID: 0000-0001-7622-7277

■ **Publishing Manager**

Prof. Murat Fani Bozkurt, MD.

FEBNM Hacettepe University, Medical School, Department of Nuclear Medicine, Ankara, Turkey

E-mail: fanibozkurt@gmail.com

ORCID ID: 0000-0003-2016-2624

■ **Editor in Chief**

Prof. Murat Fani Bozkurt, MD.

FEBNM Hacettepe University, Medical School, Department of Nuclear Medicine, Ankara, Turkey

E-mail: fanibozkurt@gmail.com

ORCID ID: 0000-0003-2016-2624

■ **Associate Editors**

Prof. Tanju Yusuf Erdil, MD.

Marmara University Medical School, Department of Nuclear Medicine, İstanbul, Turkey

E-mail: yerdil@marmara.edu.tr

ORCID ID: 0000-0002-5811-4321

Prof. Nalan Selçuk, MD.

Yeditepe University, Medical School, Department of Nuclear Medicine, İstanbul, Turkey

E-mail: nalanselcuk@yeditepe.edu.tr

ORCID ID: 0000-0002-3738-6491

■ **Statistics Editors**

Prof. Gül Ergör, MD.

Dokuz Eylül University, Medical School, Department of Public Health, İzmir, Turkey

E-mail: gulergor@deu.edu.tr

Prof. Sadettin Kılıçkap, MD.

Hacettepe University, Medical School, Department of Preventive Oncology, Ankara, Turkey

E-mail: skilickap@yahoo.com

■ **English Language Editor**

Dr. Didem Öncel Yakar

İstanbul, Turkey

Maria Lyra Georgosopoulou

University of Athens, 1st Department of Radiology, Aretaieion Hospital, Radiation Physics Unit, Athens, Greece

Gevorg Gevorgyan

The National Academy of Sciences of Armenia, H. Buniatian Institute of Biochemistry, Yerevan, Armenia

Seza Güleç

Florida International University Herbert Wertheim College of Medicine, Departments of Surgery and Nuclear Medicine, Miami, USA

Liselotte Højgaard

University of Copenhagen, Department of Clinical Physiology, Nuclear Medicine and PET, Rigshospitalet, Copenhagen, Denmark

Ora Israel

Tel Aviv University Sackler Medical School, Assaf Harofeh Medical Center, Clinic of Otolaryngology-Head and Neck Surgery, Haifa, Israel

Csaba Juhász

Wayne State University Medical School, Children's Hospital of Michigan, PET Center and Translational Imaging Laboratory, Detroit, USA

Gamze Çapa Kaya

Dokuz Eylül University, Medical School, Department of Nuclear Medicine, İzmir, Turkey

Metin Kır

Ankara University, Medical School, Department of Nuclear Medicine, Ankara, Turkey

Irena Dimitrova Kostadinova

Alexandrovska University Hospital, Clinic of Nuclear Medicine, Sofia, Bulgaria

Lale Kostakoğlu

The Mount Sinai Hospital, Clinic of Nuclear Medicine, New York, USA

Rakesh Kumar

All India Institute of Medical Sciences, Department of Nuclear Medicine, New Delhi, India

Georgios S. Limouris

Athens University, Medical School, Department of Nuclear Medicine, Athens, Greece

Luigi Mansi

Second University of Naples, Medical School, Department of Nuclear Medicine, Naples, Italy

Yusuf Menda

University of Iowa Health Care, Carver College of Medicine, Department of Radiology, Iowa City, USA

Vladimir Obradović

University of Belgrade, Faculty of Organizational Sciences, Department of Human Development Theory, Business Administration, Organizational Studies, Belgrade, Serbia

Zehra Özcan

Ege University Faculty of Medicine, Department of Nuclear Medicine, İzmir, Turkey

Yekta Özer

Hacettepe University, Faculty of Pharmacy, Department of Radiopharmaceutical, Ankara, Turkey

Francesca Pons

Hospital Clinic, Clinic of Nuclear Medicine, Barcelona, Spain

Monica Rossleigh

Sydney Children's Hospital, Clinic of Nuclear Medicine, Sydney, Australia

Dragana Sobic Saranovic

University of Belgrade, Medical School, Departments of Radiology, Oncology and Cardiology, Belgrade, Serbia

Mike Sathekge

University of Pretoria, Steve Biko Academic Hospital, Department of Nuclear Medicine, Pretoria, South Africa

Kerim Sönmezöğlü

İstanbul University, Cerrahpaşa Medical School, Department of Nuclear Medicine, İstanbul, Turkey

Zsolt Szabo

The Johns Hopkins Hospital, Divisions of Radiology and Radiological Science, Baltimore, USA

Istvan Szilvasi

Semmelweis University, Medical School, Department of Nuclear Medicine, Budapest, Hungary

Berna Okudan Tekin

Ankara Numune Training and Research Hospital, Clinic of Nuclear Medicine, Ankara, Turkey

Mathew L. Thakur

Thomas Jefferson University, Department of Radiology, Pennsylvania, USA

Bülent Turgut

Cumhuriyet University, Medical School, Department of Nuclear Medicine, Sivas, Turkey

Turgut Turoğlu

Marmara University, Medical School, Department of Nuclear Medicine, İstanbul, Turkey

Gülin Uçmak

University of Health Sciences Turkey, Ankara Oncology Training and Research Hospital, Clinic of Nuclear Medicine, Ankara, Turkey

Doğangün Yüksel

Pamukkale University, Medical School, Department of Nuclear Medicine, Denizli, Turkey

Turkish Society of Nuclear Medicine

Cinnah Caddesi Pilot Sokak No: 10/12 Çankaya 06650 Ankara, Turkey Phone: +90 312 441 00 45 Fax: +90 312 441 12 95 Web: www.tsnm.org E-mail: dernekmerkezi@tsnm.org
"Formerly Turkish Journal of Nuclear Medicine"

Reviewing the articles' conformity to the publishing standards of the Journal, typesetting, reviewing and editing the manuscripts and abstracts in English, creating links to source data, and publishing process are realized by Galenos.

**Galenos Publishing House****Owner and Publisher**

Derya Mor
Erkan Mor

Publication Coordinator

Burak Sever

Web Coordinators

Fuat Hocalar
Turgay Akpınar

Graphics Department

Ayda Alaca
Çiğdem Birinci
Gülşah Özgül
Gülay Saday

Finance Coordinator

Sevinç Çakmak
Emre Kurtulmuş

Project Coordinators

Aybuke Ayvaz
Aysel Balta
Gamze Aksoy
Gülay Akın
Hatice Sever
Melike Eren
Nuran Akti
Özlem Çelik Çekil
Pınar Akpınar
Rabia Palazoğlu
Sümeyye Karadağ

Research&Development

Nihan Karamanlı

Digital Marketing Specialist

Ümit Topluoğlu

Publisher Contact

Address: Molla Gürani Mah. Kaçamak Sk. No: 21/1
34093 İstanbul, Turkey

Phone: +90 (212) 621 99 25 Fax: +90 (212) 621 99 27

E-mail: info@galenos.com.tr/yayin@galenos.com.tr

Web: www.galenos.com.tr

Publisher Certificate Number: 14521

Online Publication Date: October 2022

ISSN: 2146-1414 E-ISSN: 2147-1959

International scientific journal published quarterly.



Molecular Imaging and Radionuclide Therapy (formerly Turkish Journal of Nuclear Medicine) is the official publication of Turkish Society of Nuclear Medicine.

Focus and Scope

Molecular Imaging and Radionuclide Therapy (Mol Imaging Radionucl Ther, MIRT) is a double-blind peer-review journal published in English language. It publishes original research articles, invited reviews, editorials, short communications, letters, consensus statements, guidelines and case reports with a literature review on the topic, in the field of molecular imaging, multimodality imaging, nuclear medicine, radionuclide therapy, radiopharmacy, medical physics, dosimetry and radiobiology. MIRT is published three times a year (February, June, October). Audience: Nuclear medicine physicians, medical physicists, radiopharmaceutical scientists, radiobiologists.

The editorial policies are based on the "Recommendations for the Conduct, Reporting, Editing, and Publication of Scholarly Work in Medical Journals (ICMJE Recommendations)" by the International Committee of Medical Journal Editors (2016, archived at <http://www.icmje.org/>) rules.

Molecular Imaging and Radionuclide Therapy is indexed in Pubmed, Pubmed Central (PMC), Emerging Sources Citation Index (ESCI), TUBITAK-ULAKBIM, DOAJ, Scopus, Gale/Cengage Learning, EBSCO databases, Embase, ProQuest Health & Medical Complete, CINAHL, Index Copernicus, J-Gate, IdealOnline, ROOT INDEXING, Türkiye Atif Dizini-Turkiye Citation Index, Turk Medline, EuroPub, Hinari, GOALI, ARDI, OARE and AGORA.

Open Access Policy

This journal provides immediate open access to its content on the principle that making research freely available to the public supports a greater global exchange of knowledge.

Open Access Policy is based on rules of Budapest Open Access Initiative (BOAI) (<http://www.budapestopenaccessinitiative.org/>). By "open access" to [peer-reviewed research literature], we mean its free availability on the public internet, permitting any users to read, download, copy, distribute, print, search, or link to the full texts of these articles, crawl them for indexing, pass them as data to software, or use them for any other lawful purpose, without financial, legal, or technical barriers other than those inseparable from gaining access to the internet itself. The only constraint on reproduction and distribution, and the only role for copyright in this domain, should be to give authors control over the integrity of their work and the right to be properly acknowledged and cited.

Subscription Information

Manuscripts can only be submitted electronically through the Journal Agent website (<http://www.journalagent.com/mirt/?plng=eng>) after creating an account. This system allows online submission and review.

All published volumes in full text can be reached free of charge through the website <http://mirt.tsnmjournals.org>

Copyright Statement

Turkish Society of Nuclear Medicine holds the international copyright of all the content published in the journal.

Republication and reproduction of images or tables in any published material should be done with proper citation of source providing authors names; article title; journal title; year (volume) and page of publication; copyright year of the article.

The author(s) hereby affirms that the manuscript submitted is original, that all statement asserted as facts are based on author(s) careful investigation and research for accuracy, that the manuscript does not, in whole or part, infringe any copyright, that it has not been published in total or in part and is not being submitted or considered for publication in total or in part elsewhere.

Completed Copyright Statement form should be submitted to the online article system.

By signing this form,

1. Each author acknowledge that he/she participated in the work in a substantive way and is prepared to take public responsibility for the work.
2. Each author further affirms that he or she has read and understands the "Ethical Guidelines for Publication of Research".
3. The author(s), in consideration of the acceptance of the manuscript for publication, does hereby assign and transfer to the Molecular Imaging and Radionuclide Therapy all of the rights and interest in and the copyright of the work in its current form and in any form subsequently revised for publication and/or electronic dissemination.

This work is licensed under a Creative Commons Attribution-NonCommercial-NoDerivatives 4.0 International License.

Instructions for Authors

Instructions for authors are published in the journal and on the website <http://mirt.tsnmjournals.org>

Material Disclaimer

Scientific and legal responsibilities pertaining to the papers belong to the authors. Contents of the manuscripts and accuracy of references are also the author's responsibility. The Turkish Society of Nuclear Medicine, the Editor, the Editorial Board or the publisher do not accept any responsibility for opinions expressed in articles.

Financial expenses of the journal are covered by Turkish Society of Nuclear Medicine.

Correspondence Address

Editor in Chief Prof. Murat Fani Bozkurt, MD, FEBNM Hacettepe University, Medical School, Department of Nuclear Medicine, Ankara, Turkey

E-mail: fanibozkurt@gmail.com

Web page: <http://mirt.tsnmjournals.org/>

Publisher Corresponding Address

Galenos Yayınevi Tic. Ltd. Şti.

Address: Molla Gürani Mah. Kaçamak Sk. No: 21/1 34093 Fındıkzade, İstanbul, Turkey

Phone: +90 212 621 99 25

Fax: +90 212 621 99 27

E-mail: info@galenos.com.tr



INSTRUCTIONS TO AUTHORS

Molecular Imaging and Radionuclide Therapy (Mol Imaging Radionucl Ther, MIRT) publishes original research articles, short communications, invited reviews, editorials, case reports with a literature review on the topic, interesting images, consensus statements, guidelines, letters in the field of molecular imaging, multimodality imaging, nuclear medicine, radionuclide therapy, radiopharmacy, medical physics, dosimetry and radiobiology. MIRT is published by the Turkish Society of Nuclear Medicine three times a year (February, June, October).

Molecular Imaging and Radionuclide Therapy does not charge any article submission or processing fees.

GENERAL INFORMATION

MIRT commits to rigorous peer review, and stipulates freedom from commercial influence, and promotion of the highest ethical and scientific standards in published articles. Neither the Editor(s) nor the publisher guarantees, warrants or endorses any product or service advertised in this publication. All articles are subject to review by the editors and peer reviewers. If the article is accepted for publication, it may be subjected to editorial revisions to aid clarity and understanding without changing the data presented.

Manuscripts must be written in English and must meet the requirements of the journal. The journal is in compliance with the uniform requirements for manuscripts submitted to biomedical journals published by the International Committee of Medical Journal Editors (NEJM 1997; 336:309-315, updated 2016). Manuscripts that do not meet these requirements will be returned to the author for necessary revision before the review. Authors of manuscripts requiring modifications have a maximum of two months to resubmit the revised text. Manuscripts returned after this deadline will be treated as new submissions.

It is the authors' responsibility to prepare a manuscript that meets ethical criteria. The Journal adheres to the principles set forth in the Helsinki Declaration October 2013 (<https://www.wma.net/policies-post/wma-declaration-of-helsinki-ethical-principles-for-medical-research-involving-human-subjects/>) and holds that all reported research involving "Human beings" conducted in accordance with such principles.

Reports describing data obtained from research conducted in human participants must contain a statement in the MATERIALS AND METHODS section indicating approval by the ethical review board (including the approval number) and affirmation that INFORMED CONSENT was obtained from each participant.

All manuscripts reporting experiments using animals must include a statement in the MATERIALS AND METHODS section giving assurance that all animals have received humane care in compliance with the Guide for the Care and Use of Laboratory Animals (www.nap.edu) and indicating approval by the ethical review board.

If the study should have ethical approval, authors asked to provide ethical approval in order to proceed the review process. If they provide approval, review of the manuscript will continue.

In case report(s) and interesting image(s) a statement regarding the informed consent of the patients should be included in the manuscript and the identity of the patient(s) should be hidden.

Subjects must be identified only by number or letter, not by initials or names. Photographs of patients' faces should be included only if scientifically relevant. Authors must obtain written consent from the patient for use of such photographs. In cases of image media usage that potentially expose patients' identity requires

obtaining permission for publication from the patients or their parents/guardians. If the proposed publication concerns any commercial product, the author must include in the cover letter a statement indicating that the author(s) has (have) no financial or other interest with the product or explaining the nature of any relations (including consultancies) between the author(s) and editor the manufacturer or distributor of the product.

All submissions will be screened by Crossref Similarity Check powered by "iThenticate". Manuscripts with an overall similarity index of greater than 25%, or duplication rate at or higher than 5% with a single source will be returned back to authors.

MANUSCRIPT CATEGORIES

1. Original Articles
2. Short Communications are short descriptions of focused studies with important, but very straightforward results.
3. Reviews address important topics in the field. Authors considering the submission of uninvited reviews should contact the editor in advance to determine if the topic that they propose is of current potential interest to the Journal. Reviews will be considered for publication only if they are written by authors who have at least three published manuscripts in the international peer reviewed journals and these studies should be cited in the review. Otherwise only invited reviews will be considered for peer review from qualified experts in the area.
4. Editorials are usually written by invitation of the editor by the editors on current topics or by the reviewers involved in the evaluation of a submitted manuscript and published concurrently with that manuscript.
5. Case Report and Literature Reviews are descriptions of a case or small number of cases revealing a previously undocumented disease process, a unique unreported manifestation or treatment of a known disease process, unique unreported complications of treatment regimens or novel and important insights into a condition's pathogenesis, presentation, and/or management. The journal's policy is to accept case reports only if it is accompanied by a review of the literature on the related topic. They should include an adequate number of images and figures.
6. Interesting Image
One of the regular parts of Molecular Imaging and Radionuclide Therapy is a section devoted to interesting images. Interesting image(s) should describe case(s) which are unique and include interesting findings adding insights into the interpretation of patient images, a condition's pathogenesis, presentation, and/or management.
7. Consensus Statements or Guidelines may be submitted by professional societies. All such submissions will be subjected to peer review, must be modifiable in response to criticisms, and will be published only if they meet the Journal's usual editorial standards.
8. Letters to the Editor may be submitted in response to work that has been published in the Journal. Letters should be short commentaries related to specific points of agreement or disagreement with the published work.

Note on Prior Publication

Articles are accepted for publication on the condition that they are original, are not under consideration by another journal, or have not been previously published. Direct quotations, tables, or illustrations that have appeared in

INSTRUCTIONS TO AUTHORS

copyrighted material must be accompanied by written permission for their use from the copyright owner and authors. Materials previously published in whole or in part shall not be considered for publication. At the time of submission, authors must report that the manuscript has not been published elsewhere. Abstracts or posters displayed at scientific meetings need not be reported.

MANUSCRIPT SUBMISSION PROCEDURES

MIRT only accepts electronic manuscript submission at the web site <http://www.journalagent.com/mirt/>. After logging on to the website Click the 'online manuscript submission' icon. All corresponding authors should be provided with a password and a username after entering the information required. If you already have an account from a previous submission, enter your username and password to submit a new or revised manuscript. If you have forgotten your username and/or password, please send an e-mail to the editorial office for assistance. After logging on to the article submission system please read carefully the directions of the system to give all needed information and attach the manuscript, tables and figures and additional documents.

All Submissions Must Include:

1. Completed Copyright Assignment & Disclosure of Potential Conflict of Interest Form; This form should be downloaded from the website (provided in the author section), filled in thoroughly and uploaded to the website during the submission.
2. All manuscripts describing data obtained from research conducted in human participants must be accompanied with an approval document by the ethical review board.
3. All manuscripts reporting experiments using animals must include approval document by the animal ethical review board.
4. All submissions must include the authorship contribution form which is signed by all authors.

Authors must complete all online submission forms. If you are unable to successfully upload the files please contact the editorial office by e-mail.

MANUSCRIPT PREPARATION

General Format

The Journal requires that all submissions be submitted according to these guidelines:

- Text should be double spaced with 2.5 cm margins on both sides using 12-point type in Times Roman font.
- All tables and figures must be placed after the text and must be labeled.
- Each section (abstract, text, references, tables, figures) should start on a separate page.
- Manuscripts should be prepared as a word document (*.doc) or rich text format (*.rtf).
- Please make the tables using the table function in Word.
- Abbreviations should be defined in parenthesis where the word is first mentioned and used consistently thereafter.
- Results should be expressed in metric units. Statistical analysis should be done accurately and with precision. Please consult a statistician if necessary.
- Authors' names and institutions should not be included in the manuscript text and should be written only in the title page.

Title Page

The title page should be a separate form from the main text and should include the following:

- Full title (in English and in Turkish). Turkish title will be provided by the editorial office for the authors who are not Turkish speakers.
- Authors' names and institutions.
- Short title of not more than 40 characters for page headings.
- At least three and maximum eight keywords. (in English and in Turkish). Do not use abbreviations in the keywords. Turkish keywords will be provided by the editorial office for the authors who are not Turkish speakers. If you are not a native Turkish speaker, please reenter your English keywords to the area provided for the Turkish keywords. English keywords should be provided from <http://www.nlm.nih.gov/mesh> (Medical Subject Headings) while Turkish keywords should be provided from <http://www.bilimterimleri.com>.
- Word count (excluding abstract, figure legends and references).
- Corresponding author's e-mail and address, telephone and fax numbers.
- Name and address of person to whom reprint requests should be addressed.

Original Articles

Authors are required to state in their manuscripts that ethical approval from an appropriate committee and informed consents of the patients were obtained.

Original Articles should be submitted with a structured abstract of no more than 250 words. All information reported in the abstract must appear in the manuscript. The abstract should not include references. Please use complete sentences for all sections of the abstract. Structured abstract should include background, objective, methods, results and conclusions. Turkish abstract will be provided by the editorial office for the authors who are not Turkish speakers. If you are not a native Turkish speaker, please reenter your English abstract to the area provided for the Turkish abstract.

- Introduction
- Materials and Methods
- Results
- Discussion
- Study Limitations
- Conclusion

May be given for contributors who are not listed as authors, or for grant support of the research.

References should be cited in numerical order (in parentheses) in the text and listed in the same numerical order at the end of the manuscript on a separate page or pages. The author is responsible for the accuracy of references. Examples of the reference style are given below. Further examples will be found in the articles describing the Uniform Requirements for Manuscripts Submitted to Biomedical Journals (Ann Intern Med.1988; 208:258-265, Br Med J. 1988; 296:401-405). The titles of journals should be abbreviated according to the style used in the Index Medicus. Journal Articles and Abstracts: Surnames and initials of author's name, title of the article, journal name, date, volume number, and pages. All authors should be listed regardless of number. The citation of unpublished papers, observations or personal communications is not permitted. Citing an abstract is not recommended. Books: Surnames and initials of author's names, chapter title, editor's name, book title, edition, city, publisher, date and pages.

INSTRUCTIONS TO AUTHORS

Sample References

Journal Article: Sayit E, Söylev M, Çapa G, Durak I, Ada E, Yılmaz M. The role of technetium-99m-HMPAO-labeled WBC scintigraphy in the diagnosis of orbital cellulitis. *Ann Nucl Med* 2001;15:41-44.

Erselcan T, Hasbek Z, Tandogan I, Gumus C, Akkurt I. Modification of Diet in Renal Disease equation in the risk stratification of contrast induced acute kidney injury in hospital inpatients. *Nefrologia* 2009 doi: 10.3265/Nefrologia.2009.29.5.5449.en.full.

Article in a journal published ahead of print: Ludbrook J. Musculo-venous pumps in the human lower limb. *Am Heart J* 2009;00:1-6. (accessed 20 February 2009).

Lang TF, Duryea J. Peripheral Bone Mineral Assessment of the Axial Skeleton: Technical Aspects. In: Orwoll ES, Bliziotes M (eds). *Osteoporosis: Pathophysiology and Clinical Management*. New Jersey, Humana Press Inc, 2003;83-104.

Books: Greenspan A. *Orthopaedic Radiology a Practical Approach*. 3th ed. Philadelphia, Lippincott Williams Wilkins 2000, 295-330.

Website: Smith JR. 'Choosing Your Reference Style', *Online Referencing* 2(3), <http://orj.sagepub.com> (200, accessed October 2008).

- Tables

Tables must be constructed as simply as possible. Each table must have a concise heading and should be submitted on a separate page. Tables must not simply duplicate the text or figures. Number all tables in the order of their citation in the text. Include a title for each table (a brief phrase, preferably no longer than 10 to 15 words). Include all tables in a single file following the manuscript.

- Figure Legends

Figure legends should be submitted on a separate page and should be clear and informative.

- Figures

Number all figures (graphs, charts, photographs, and illustrations) in the order of their citation in the text. At submission, the following file formats are acceptable: AI, EMF, EPS, JPG, PDF, PPT, PSD, TIF. Figures may be embedded at the end of the manuscript text file or loaded as separate files for submission. All images MUST be at or above intended display size, with the following image resolutions: Line Art 800 dpi, Combination (Line Art + Halftone) 600 dpi, Halftone 300 dpi. Image files also must be cropped as close to the actual image as possible.

Short Communications:

Short communications should be submitted with a structured abstract of no more than 200 words. These manuscripts should be no longer than 2000 words, and include no more than two figures and tables and 20 references. Other rules which the authors are required to prepare and submit their manuscripts are the same as described above for the original articles.

Invited Review Articles:

- Title page (see above)

- Abstract: Maximum 250 words; without structural divisions; in English and in Turkish. Turkish abstract will be provided by the editorial office for the authors who are not Turkish speakers. If you are not a native Turkish speaker, please reenter your English abstract to the area provided for the Turkish abstract.

- Text

- Conclusion

- Acknowledgements (if any)

- References

Editorial:

- Title page (see above)

- Abstract: Maximum 250 words; without structural divisions; in English and in Turkish. Turkish abstract will be provided by the editorial office for the authors who are not Turkish speakers. If you are not a native Turkish speaker, please reenter your English abstract to the area provided for the Turkish abstract.

- Text

- References

Case Report and Literature Review

- Title page (see above)

- Abstract: Approximately 100-150 words; without structural divisions; in English and in Turkish. Turkish abstract will be provided by the editorial office for the authors who are not Turkish speakers. If you are not a native Turkish speaker, please re-enter your English abstract to the area provided for the Turkish abstract.

- Introduction

- Case report

- Literature Review and Discussion

- References

Interesting Image:

No manuscript text is required. Interesting Image submissions must include the following:

Title Page: (see Original article section)

Abstract: Approximately 100-150 words; without structural divisions; in English and in Turkish. Turkish abstract will be provided by the editorial office for the authors who are not Turkish speakers. If you are not a native Turkish speaker, please re-enter your English abstract to the area provided for the Turkish abstract. Image(s): The number of images is left to the discretion of the author. (See Original article section)

Figure Legend: Reference citations should appear in the legends, not in the abstract. Since there is no manuscript text, the legends for illustrations should be prepared in considerable detail but should be no more than 500 words total. The case should be presented and discussed in the Figure legend section.

References: Maximum eight references (see original article section).

Letters to the Editor:

- Title page (see above)

- Short comment to a published work, no longer than 500 words, no figures or tables.

- References no more than five.

Consensus Statements or Guidelines: These manuscripts should typically be no longer than 4000 words and include no more than six figures and tables and 120 references.

Proofs and Reprints

Proofs and a reprint orders are sent to the corresponding author. The author should designate by footnote on the title page of the manuscript the name and

INSTRUCTIONS TO AUTHORS

address of the person to whom reprint requests should be directed. The manuscript when published will become the property of the journal.

Archiving

The editorial office will retain all manuscripts and related documentation (correspondence, reviews, etc.) for 12 months following the date of publication or rejection.

Submission Preparation Checklist

As part of the submission process, authors are required to check off their submission's compliance with all of the following items, and submissions may be returned to authors that do not adhere to these guidelines.

1. The submission has not been previously published, nor is it before another journal for consideration (or an explanation has been provided in Comments to the Editor).
2. The submission file is in Microsoft Word, RTF, or WordPerfect document file format. The text is double-spaced; uses a 12-point font; employs italics, rather than underlining (except with URL addresses); and the location for all illustrations, figures, and tables should be marked within the text at the appropriate points.
3. Where available, URLs for the references will be provided.
4. All authors should be listed in the references, regardless of the number.
5. The text adheres to the stylistic and bibliographic requirements outlined in the Author Guidelines, which is found in About the Journal.
6. English keywords should be provided from [http://www.nlm.nih.gov/mesh\(Medical Subject Headings\)](http://www.nlm.nih.gov/mesh(Medical Subject Headings)), while Turkish keywords should be provided from <http://www.bilimterimleri.com>
7. The title page should be a separate document from the main text and should be uploaded separately.
8. The "Affirmation of Originality and Assignment of Copyright/The Disclosure Form for Potential Conflicts of Interest Form" and Authorship Contribution Form should be downloaded from the website, filled thoroughly and uploaded during the submission of the manuscript.

TO AUTHORS

Copyright Notice

The author(s) hereby affirms that the manuscript submitted is original, that all statement asserted as facts are based on author(s) careful investigation and research for accuracy, that the manuscript does not, in whole or part, infringe any copyright, that it has not been published in total or in part and is not being submitted or considered for publication in total or in part elsewhere. Completed

Copyright Assignment & Affirmation of Originality Form will be uploaded during submission. By signing this form;

1. Each author acknowledges that he/she participated in the work in a substantive way and is prepared to take public responsibility for the work.
2. Each author further affirms that he or she has read and understands the "Ethical Guidelines for Publication of Research".
3. The author(s), in consideration of the acceptance of the manuscript for publication, does hereby assign and transfer to the Molecular Imaging and Radionuclide Therapy all of the rights and interest in and the copyright of the work in its current form and in any form subsequently revised for publication and/or electronic dissemination.

Privacy Statement

The names and email addresses entered in this journal site will be used exclusively for the stated purposes of this journal and will not be made available for any other purpose or to any other party.

Peer Review Process

1. The manuscript is assigned to an editor, who reviews the manuscript and makes an initial decision based on manuscript quality and editorial priorities.
2. For those manuscripts sent for external peer review, the editor assigns at least two reviewers to the manuscript.
3. The reviewers review the manuscript.
4. The editor makes a final decision based on editorial priorities, manuscript quality, and reviewer recommendations.
5. The decision letter is sent to the author.

Contact Address

All correspondence should be directed to the Editorial Office:

Cinnah Caddesi Pilot Sokak No:10/12 06650 Çankaya / Ankara, Turkey

Phone: +90 312 441 00 45

Fax: +90 312 441 12 97

E-mail: info@tsnmjournals.org

CONTENTS

Original Articles

- 172** Contribution of Open Mouth Technique in ^{18}F -FDG PET/CT Imaging in Patients with Malignant Lip Neoplasm
Dudak Malign Neoplazmi Tanılı Hastaların ^{18}F -FDG PET/CT Görüntülemesinde Ağız Açık Pozisyonlamanın Katkısı
Gözde Mütevelizade, Ceren Sezgin, Yasemin Parlak, Gül Gümüşer, Elvan Sayit; Manisa, Turkey
- 179** The Effects of CoronaVac (Sinovac) and BNT162b2 (BioNTech/Pfizer) Vaccination on Oncologic ^{18}F -FDG PET/CT Studies
CoronaVac (Sinovac) ve BNT162b2 (BioNTech/Pfizer) Aşılmasının Onkolojik ^{18}F -FDG PET/CT Çalışmalarına Etkileri
Hüseyin Şan, Engin Alagöz; Ankara, Turkey
- 191** Comparison of Planar Imaging Using Dual-phase Tc-99m-sestamibi Scintigraphy and Single Photon Emission Computed Tomography/Computed Tomography in Hyperparathyroidism
Hiperparatiroidizmde Çift Fazlı Tc-99m-Sestamibi Planar Görüntüleme Sintigrafisi ve Tek Foton Emisyonlu Bilgisayarlı Tomografi/Bilgisayarlı Tomografi Karşılaştırılması
Halim Özçevik, Müge Öner Tamam, Mehmet Tarık Tatoğlu, Mehmet Mülazımoğlu; İstanbul, Turkey
- 200** Prognostic Significance of ^{18}F -FDG PET/CT Imaging in Survival Outcomes in Patients with Renal Cell Carcinoma
Renal Hücreli Karsinom Hastalarının Sağlık Sonuçlarında ^{18}F -FDG PET/CT Görüntülemenin Prognostik Önemi
Gamze Tatar, Cihan Gündoğan, Ömer Faruk Şahin, Esra Arslan, Nurhan Ergül, Tevfik Fikret Çermik; İstanbul, Diyarbakır, Turkey
- 207** The Role of ^{18}F -FLT PET/CT in Assessing Early Response to Transarterial Radioembolization and Chemoembolization in Patients with Primary and Metastatic Liver Tumors
Primer ve Metastatik Karaciğer Tümörlü Hastalarda Transarteriyel Radyoembolizasyon ve Kemoembolizasyona Erken Yanıtı Değerlendirmede ^{18}F -FLT PET/CT'nin Rolü
Demet Nak, Nuriye Özlem Küçük, Emre Can Çelebioğlu, Mehmet Sadık Bilgiç, Serhat Hayme, Kemal Metin Kır; Rize, Ankara, Erzincan, Turkey
- 216** Volumetric Evaluation of Staging ^{18}F -FDG PET/CT Images in Patients with Esophageal Cancer
Özofagus Kanserli Hastalarda Evreleme ^{18}F -FDG PET/CT Görüntülerinin Hacimsel Değerlendirilmesi
Nazlı Pınar Karahan Şen, Ayşegül Aksu, Gamze Çapa Kaya; İzmir, İstanbul, Turkey
- #### Interesting Images
- 223** Unexpected Metastatic Localizations of Prostate Cancer Determined by ^{68}Ga PSMA PET/CT: Series of Four Cases
 ^{68}Ga PSMA PET/CT'de Saptanan Prostat Kanserin Nadir Metastaz Lokalizasyonları: Dört Olgu
Gözde Mütevelizade, Ceren Sezgin, Gül Gümüşer, Elvan Sayit; Manisa, Turkey
- 227** Cerebellar Metastases from Prostate Cancer Detected by PET/CT with ^{18}F -Choline
 ^{18}F -Kolin PET/CT ile Saptanan Prostat Kanserin Serebellar Metastazları
Luca Filippi, Antonella Fontana, Francesco Guerrini, Angelo Pompucci, Oreste Bagni; Latina, Italy
- 231** COVID-19 Pneumonia was Incidentally Detected on ^{18}F -Fluorocholine PET/CT in a Work-up for Prostate Cancer
COVID-19 Pnömonisinin Prostat Kanseri Çalışmasında ^{18}F -Florokolin PET/CT'de Tesadüfen Tespit Edilmesi
Omar Ait Sahel, Yassir Benameur, Salah Oueriagli Nabih, Abderrahim Doudouh; Rabat, Morocco
- 234** Nasolacrimal Duct Obstruction on ^{131}I SPECT/CT: Atypical False-positive Paranasal Radioiodine Uptake as a Complication of Single-dose RAI Treatment
 ^{131}I SPECT/CT'de Nazolakrimal Kanal Tıkanıklığı: Tek-doza RAI Tedavisinin Bir Komplikasyonu Olarak Atipik Yanlış Pozitif Paranasal Radyoiodot Tutulumu
Nuh Filizoğlu, Kevser Öksüzöğlü, Salih Özgüven, Onur Buğdaycı, Tanju Yusuf Erdil; İstanbul, Turkey

CONTENTS

- 237** Isolated Scapular Lesion of Langerhans Cell Histiocytosis Detected by ^{18}F -FDG PET/CT
 ^{18}F -FDG PET/CT ile Saptanan Langerhans Hücreli Histiyoizozun İzole Skapula Lezyonu
Nuh Filizoğlu, Salih Özgüven, Hüseyin Kemal Türköz, Tunç Öneş, Halil Turgut Turoğlu, Tanju Yusuf Erdil; İstanbul, Turkey
- 239** ^{18}F -FDG PET/CT Showing Rare Mediastinal Growing Teratoma Syndrome Following Chemotherapy
Kemoterapi Sonrası Nadir Mediastinal Büyüyen Teratom Sendromu Gösteren ^{18}F -FDG PET/CT Uygulaması
Mihoko Sasahara, Takashi Abe, Yoichi Otomi, Yumi Abe, Hiroaki Toba, Takayoshi Shinya, Hideki Otsuka, Masafumi Harada; Tokushima, Nagoya, Japan
- 242** Neurolymphomatosis with Spinal Nerve Root Involvement Demonstrated on ^{18}F -FDG PET/CT
 ^{18}F -FDG PET/CT'de Spinal Sinir Kökü Tutulumu Olan Nörolenfomatosis
Ayça Arçay, Gonca Gül Bural, Utku Şenol; Antalya, Turkey
- 244** Mild ^{68}Ga PSMA-11 Uptake in Incidental Pituitary Adenoma
İnsidental Pitüiter Adenomda Hafif ^{68}Ga PSMA-11 Tutulumu
Ediz Beyhan, Özge Erol Fenercioğlu, Yeşim Karagöz, Nurhan Ergül, Tefvik Fikret Çermik; İstanbul, Turkey
- 246** A Case of Extracranial Metastasis of Glioblastoma Multiforme Seen on Bone Scintigraphy
Kemik Sintigrafisinde Görülen Glioblastoma Multiforme'dan Ekstrakraniyal Metastaz Olgusu
Hardik Veerwal, Anjali Meena, Vandana Dhingra; Rishikesh, India
- 250** Mass-like Appearance on ^{18}F -FDG PET/CT: Cascade Stomach
 ^{18}F -FDG PET/CT'de Kitlesel Görünüm: Kaskat Mide
Ayça Arçay, Funda Aydın, Mete Akın; Antalya, Turkey

Index

2022 Referee Index / 2022 Hakem Dizini

2022 Author Index / 2022 Yazar Dizini

2022 Subject Index / 2022 Konu Dizini



Contribution of Open Mouth Technique in ^{18}F -FDG PET/CT Imaging in Patients with Malignant Lip Neoplasm

Dudak Malign Neoplazmı Tanılı Hastaların ^{18}F -FDG PET/CT Görüntülemesinde Ağız Açık Pozisyonlamanın Katkısı

© Gözde Mütevelizade, © Ceren Sezgin, © Yasemin Parlak, © Gül Gümüşer, © Elvan Sayit

Manisa Celal Bayar University Faculty of Medicine, Department of Nuclear Medicine, Manisa, Turkey

Abstract

Objectives: ^{18}F -fluorodeoxyglucose (FDG) positron emission tomography/computed tomography (PET/CT) plays an important role in evaluating head and neck cancers. However, localization and size evaluation in this region can be rough due to the multitude of the anatomic structures and physiologic uptakes. The aim of this study was to evaluate malignant lip lesions with the contribution of open mouth (OM) imaging technique at PET/CT.

Methods: Fifty-six patients with malignant lip neoplasm underwent ^{18}F -FDG PET/CT imaging. Each patient was imaged twice as whole-body PET/CT with routine closed mouth (CM) position; and OM head and neck image, standardized with a special device. Lesion maximum standard uptake value (SUV_{max}), localization, size, and involvement of lymph nodes were evaluated.

Results: Lesion localization was correctly detected in 100% of the OM images. Lesion size in PET/CT was compared with clinical, radiological (magnetic resonance imaging and CT) and/or histopathological results and the size measurement was coherent at 47.1% and 95.6% for CM and OM images, respectively. It was observed that OM acquisition did not contribute additionally in detecting regional lymph node metastasis. Forty-one PET/CT scans with CT artifacts due to dental amalgams were evaluated and 46.3% dimensional and 53.7% localization errors were detected in the CM position. There was no statistically significant difference between OM and CM SUV_{max} ($p>0.05$).

Conclusion: We concluded that additional OM head and neck imaging is useful and necessary to accurately determine the localization and size of the tumor, thus enhancing the value of PET/CT in staging, treatment response assessment, and restaging of patients with malignant lip cancer with or without dental amalgam.

Keywords: Malignant lip neoplasm, open mouth technique, ^{18}F -FDG PET/CT

Öz

Amaç: Baş-boyun malignitelerinin değerlendirilmesinde ^{18}F -florodeoksiglukoz (FDG) pozitron emisyon tomografisi/bilgisayarlı tomografi (PET/CT) oldukça önemli bir yere sahiptir. Ancak bu bölgede yerleşimli anatomik yapıların çokluğu ve fizyolojik tutulum sıklığı nedeniyle lokalizasyon ve boyut değerlendirilmesinde güçlük yaşanabilmektedir. Bu çalışmada amaç, dudak malign neoplazmı evrelemesi amacıyla ^{18}F -FDG PET/CT çekilen hastalarda, ağız açık (AA) pozisyonlamanın primer tümörün lokalizasyon ve boyut değerlendirilmesine katkısını araştırmaktır.

Yöntem: Temmuz 2017-Ocak 2020 tarihleri arasında kliniğimizde dudak malign neoplazmı evrelemesi endikasyonu ile ^{18}F -FDG PET/CT çekilen 56 hasta çalışmaya dahil edilmiştir. Hastalara rutin uygulanan ağız kapalı (AK) pozisyonunda tüm vücut ^{18}F -FDG PET/CT görüntülemesi yapılmıştır. İlk görüntülemenin hemen ardından, özel aparat ile AA'lığı standardize edilerek AA pozisyonunda ek baş-boyun görüntüleri alınmıştır. Her iki görüntüde lezyon maksimum standartlaştırılmış alım değeri (SUV_{maks}), $\text{SUV}_{\text{ortalama}}$, lezyon boyutu, lezyon lokalizasyonu ve lenf nodu metastazı varlığı karşılaştırılmıştır.

Address for Correspondence: Gözde Mütevelizade MD, Manisa Celal Bayar University Faculty of Medicine, Department of Nuclear Medicine, Manisa, Turkey

Phone: +90 532 471 32 62 **E-mail:** gozdemutevelizadee@gmail.com ORCID ID: orcid.org/0000-0001-5986-8777

Received: 24.06.2022 **Accepted:** 08.07.2022

©Copyright 2022 by Turkish Society of Nuclear Medicine
Molecular Imaging and Radionuclide Therapy published by Galenos Yayınevi.

Bulgular: Lezyon lokalizasyonu AA görüntülerin tamamında doğru tespit edildi. Lezyon boyutu değerlendirilmesi açısından PET/BT görüntüleri, radyolojik, klinik ve histopatolojik veriler ile karşılaştırıldı; AK ve AA görüntülerde sırasıyla %47,1 ve %95,6 uyumlu olarak saptandı. AA görüntülemenin lenf nodu varlığını saptamada ek katkısı olmadığı izlendi. Kırk bir PET/BT görüntüsünde dental amalgamlara ait BT artefaktı mevcut olup, AK pozisyonda %46,3'ünde boyut ve %53,7'sinde lokalizasyon uyumsuz olarak saptandı. AA ve AK görüntülerde lezyon SUV_{maks}'ı açısından istatistiksel olarak anlamlı bir fark izlenmedi (p>0,05).

Sonuç: Dudak malign neoplazmi tanısı ile evreleme, yeniden evreleme ve tedaviye yanıt değerlendirme amacıyla çekilen ¹⁸F-FDG PET/BT görüntülerinde AA olarak yapılacak olan ek görüntülemenin, tümörün lokalizasyonunun ve boyutunun daha doğru belirlenmesinde faydalı ve gerekli olduğu sonucuna varılmıştır.

Anahtar kelimeler: Dudak malign neoplazmi, ağız açık pozisyonlama, ¹⁸F-FDG PET/BT

Introduction

Lip and oral cavity malignancies are the 16th most common neoplasms in the world, with nearly 355,000 new diagnoses and over 177,000 deaths in 2018 (1). Lip cancers are mostly seen in the 5th and 6th decades and are six times higher in males than in female patients. Lip cancers constitute 12% of head and neck cancers (HNC) and 25%-30% of oral cavity cancers. Lower lip cancer accounts for 88%-98% of lip cancers. The vast majority of lesions are located on the vermilion border of the lower lip. More than 95% are squamous cell carcinomas (SCC) and 70% are well differentiated. Basal cell carcinomas constitute 13% of upper lip cancers and less than 1% of lower lip cancers (2). Lip cancers are important diseases as they can affect patients' quality of life and cause cosmetic problems (3). Distant metastases due to lip carcinomas occur very rarely. Because it can be easily noticed by virtue of its localization, in 93% of patients, the tumor is at an early stage when diagnosed (4). Recurrence may develop in 15.1% of patients, and this is due to large size tumor and poor differentiation (5). The main risk factors associated with lip and oral cavity cancers are tobacco use, betel quid chewing, alcohol consumption, poor oral hygiene, low fruit and vegetable dietary habit, high exposure to ultraviolet light, radiotherapy, human papilloma virus infection and genetic factors (6,7). The major prognostic factor in lip carcinomas is the presence of cervical lymph node metastasis. The probability of cervical lymph node spread during diagnosis is between 2 and 16% in lower lip cancers (8). The gold standard treatment is neck dissection and resection of the primary tumor in the presence of lymph node metastasis (9). Accurate localization of a malignant neoplasm and early detection of cervical lymph node metastases play a critical roles in the management and survival of patients with this disease. Clinical examination and anatomical imaging with ultrasound (USG), computed tomography (CT) or magnetic resonance imaging (MRI) have proven to be of limited value for the correct staging of the cervical lymph nodes (10). The use of 2-deoxy-2-[¹⁸F] fluoro-D-glucose positron emission tomography/computed tomography

(¹⁸F-FDG PET/CT) is important in the initial assessment of early-stage and advanced-stage head and neck carcinomas. In the evaluation of primary lesions, nodal disease and distant metastases, sensitivity and specificity of ¹⁸F-FDG PET/CT were found to be superior to those of traditional imaging methods (11). Correct evaluation of the size and localization of the lesion is important in lip carcinomas because it affects treatment planning and follow-up parameters. Usually, clinical examination underestimates the actual thickness of the tumor and lymph node involvement (10). Studies have shown that ¹⁸F-FDG PET/CT has higher accuracy, sensitivity and positive predictive value than CT and MRI in determining the wideness and depth of the primary tumor (12). However, because of the closeness of anatomical structures of the head and neck region and increased physiologic uptake of ¹⁸F-FDG in this area, the spatial resolution of ¹⁸F-FDG PET/CT examination of the oral cavity and lip carcinoma may not be sufficient. ¹⁸F-FDG PET/CT shows high sensitivity but rather low specificity and weak spatial and anatomical resolution. Hence, it is often difficult to localize lip and oral cavity lesions with high accuracy. Therefore, some additional positional techniques may be useful for evaluating lip carcinomas.

We evaluated correct localization, wideness and depth of malignant lip neoplasms with the contribution of open mouth (OM) imaging technique at ¹⁸F-FDG PET/CT.

Materials and Methods

Fifty-six patients (17 women, 39 men; mean age 69±11.5 years) with histopathologically proven malignant lip neoplasm underwent ¹⁸F-FDG PET/CT (Philips, True Flight Select, USA) imaging in our clinic approximately 2017-2021 were included in the study. Manisa Celal Bayar University Faculty of Medicine Local Ethics Committee (decree number: 20.478.486/1069) approval was required and written informed consent was obtained from all patients. Patients fasted for at least 6 h and their blood glucose concentrations were measured to confirm the levels were below 200 mg/dL. Whole body images of the patients were taken after the 60 min resting phase following

intravenous injection of 370-555 MBq (10-15 mCi) ^{18}F -FDG. The patients spent the resting period without moving or speaking in a quiet room. Combined (fusion) whole body images of the patients in mouth close positions were acquired 60 min after intravenous injection of 5.2 MBq/kg ^{18}F -FDG. CT acquisition (16 slice; 120 kVp; 80 mA) was immediately followed by multibed PET acquisition (lutetium yttrium orthosilicate crystals; 3-dimensional 3D acquisition; 180 s per bed position; 5 bed positions). PET images were reconstructed using 3D ordered subsets expectation maximization as appropriate, in conjunction with the parameters described for the clinical protocol. Attenuation was corrected by the CT images obtained after ^{18}F -FDG injection. Intravenous contrast material was not used for the PET/CT scan. Immediately after, additional OM head and neck image acquired by a 50 mL syringe to standardize the position. A syringe was placed between the teeth to ensure correct and standardized immobilization (Figure 1). The acquisition was performed with quiet respiration for 5 min. All data were evaluated by two experienced nuclear



Figure 1. A 69 year old woman presented with lower lip squamous cell carcinoma. Additional open mouth head and neck image acquired by a 50 mL syringe placed between the teeth to ensure correct and standardized immobilization

medicine physicians blinded to each other, on a computer display in 3 orthogonal planes (i.e., axial, coronal, and sagittal). The observers did not have any information about the results of the conventional imaging modalities (USG, CT, MRI) and clinical examination findings. Closed mouth (CM) and OM scans were analyzed separately. Lip lesions were analyzed semiquantitatively according to maximum standard uptake value (SUV_{max}). The SUV_{max} was calculated automatically by software, as the ratio of the maximum tissue concentration of ^{18}F -FDG (kBq/mL) in the structure delineated by the region of interest to the activity injected per gram body weight of the patient (kBq/g). The PET/CT images suggested lymph node involvement in the case of any focal ^{18}F -FDG uptake greater than the background activity and correspond to nodular structures on CT. Lesion SUV_{max} , SUV_{mean} , lesion size, lesion localization and presence of lymph nodes were evaluated in OM and CM images. Findings were compared and correlated with radiological, histopathological and clinical findings.

Statistical Analysis

Data were recorded in the SPSS 21.0 data analysis program; lesion SUV_{max} , SUV_{mean} , lesion size, lesion localization and lymph node presence were compared between OM and CM images ($p < 0.05$ was considered as statistically significant).

Results

Lesion SUV_{max} , SUV_{mean} , lesion size and localization and presence of lymph nodes were evaluated both on OM and CM images. We calculated the lesion size by measuring the depth and wideness of the lesion. Since 10 patients had restaging and treatment response evaluation ^{18}F -FDG PET/CT, 68 images were included in the statistical evaluation. All the results were compared and correlated with radiological, histopathological and clinical findings. No statistical significant difference was detected between OM and CM SUV_{max} ($p > 0.05$) (Table 1). This revealed that openness or closure of the mouth did not affect SUV_{max} .

Distant metastasis was found in 13 of the 56 patients included in our study. There were 5 lung, 2 bones, 5 axillas and/or mediastinal lymph nodes and 1 lung and liver metastasis. There was no effect of mouth position on the detection of distant metastasis, as expected. Regional lymph node metastasis was not observed in 31 images (46%), whereas in 37 (54%) ^{18}F -FDG PET/CT images regional lymph node metastasis was detected. The presence of lymph nodes was correctly detected in all OM patients. While the presence of lymph nodes was correctly detected in 83.8% of CM patients, it was found to be inconsistent in 16.2%. It was observed that OM imaging

	n	Minimum	Maximum	Mean	Standard deviation	p
CM SUV _{max}	68	1.50	36.60	7.8618	7.59617	0.506
OM SUV _{max}	68	1.20	38.30	7.7632	8.13391	
CM SUV _{mean}	68	0.50	12.70	2.1015	1.95437	0.325
OM SUV _{mean}	68	0.40	22.40	1.9206	2.75180	
Valid n (listwise)	68	-	-	-	-	-

(p<0.05 was considered significant), CM: Closed mouth, OM: Open mouth, SUV_{max}: Maximum standard uptake value

		Frequency	Percent	Valid percent
CM lesion size	Incorrect	36	52.9	52.9
	Correct	32	47.1	47.1
	Total	68	100.0	100.0
OM lesion size	Incorrect	3	4.4	4.4
	Correct	65	95.6	95.6
	Total	68	100.0	100.0

CM: Closed mouth, OM: Open mouth

had no additional contribution in detecting lymph nodes. ¹⁸F-FDG PET/CT images were compared with the clinical, radiological (MRI and CT) and/or histopathological results in terms of lesion localization and dimension evaluation. Lesion size was correctly detected in 95.6% of OM images, but lesion size was correctly detected in only 47.1% of CM images (Table 2). OM positioning is much more correlated with the clinical findings on the basis of lesion size. While the lesion localization was detected correctly in all OM images, the localization assessment was incorrect in 57.4% of the CM images (Table 3). OM images are much more accurate in detecting both localization and the dimension of the lesions (Figure 2).

Forty-one PET/CT scans (60.3%) had CT artifacts due to dental amalgams. When these images are evaluated, 46.3% dimensional error is detected in the CM position, while this number decreases to 7.3% in the OM position. Similarly, 53.7% localization error was detected in the CM position in 41 images, but no error was determined in the localization evaluation in the OM position (Figure 3). Ten patients had more than one ¹⁸F-FDG PET/CT imaging. Two patients were imaged 3 times and 8 patients were imaged 2 times with PET/CT. One of these patients did not accept surgery, tumor growth was observed at follow-up and re-evaluated with PET/CT. The other 9 patients had various metastatic lesions and were treated with chemotherapy, radiotherapy, or chemoradiotherapy.

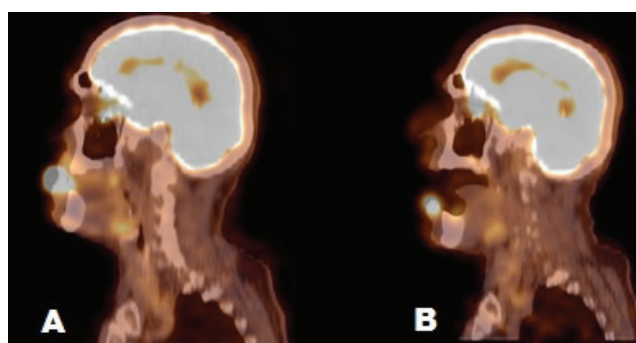


Figure 2. Closed (A) and open (B) mouth fused sagittal ¹⁸F-FDG PET/CT images of a 61 year old man with lower lip squamous cell carcinoma. Open mouth positioning helped to identify the lesion size and localization. SUV_{max}: Maximum standard uptake value, PET: Positron emission tomography, CT: Computed tomography, FDG: Fluorodeoxyglucose

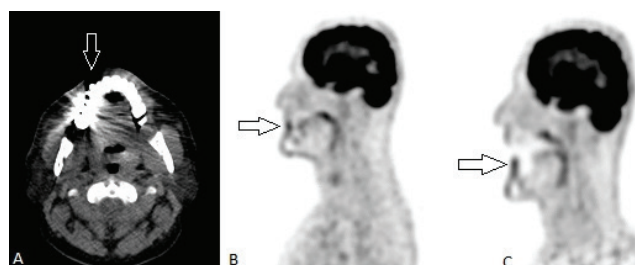


Figure 3. Sixty-four year old man presented with lip squamous cell carcinoma had dental amalgam artifact, which results in blind areas (arrow) at axial CT images (A). PET images were evaluated instead of CT and PET/CT due to amalgam artifact. Identification the localization of the very small lesion (arrow) in CM position is contradictory (B). The size and the localization of the lesion is unclear. It is easy to clearly identify the localization of the lesion (arrow) to the lower lip as his mouth is open at sagittal PET images (C). PET: Positron emission tomography, CT: Computed tomography, CM: Closed mouth

Discussion

Lip cancer is usually diagnosed earlier than other carcinomas of the oral cavity because it is easier to notice. The surgical treatment of lip cancer involves excision of the entire tumor while leaving an adequate margin of healthy tissue. The prognosis in patients diagnosed with lip carcinoma depends on the stage of the disease. The greater the

Table 3. Difference of closed mouth and open mouth imaging in terms of lesion localization assessment

		Frequency	Percent	Valid percent
CM lesion localization	Incorrect	39	57.4	57.4
	Correct	29	42.6	42.6
	Total	68	100.0	100.0
OM lesion localization	Correct	68	100.0	100.0
	Total	68	100.0	100.0

CM: Closed mouth, OM: Open mouth

thickness of the tumor, the higher the probability of lymph node metastasis (13). Therefore, it is critical to determine the size and thickness of the tumor correctly while staging (14). ^{18}F -FDG PET/CT plays an important role in evaluating HNC. However, localization and size evaluation of this region can be difficult due to the multiplicity of the anatomic structures and increased physiologic uptake of ^{18}F -FDG. PET/CT shows high sensitivity but rather low specificity and weak spatial and anatomic resolution. Therefore, it is often difficult to localize lip and oral cavity lesions with high accuracy. PET/CT plays an important role in the management of patients with HNC. The diagnostic success of PET/CT in different cancers compared to PET or CT alone is now an indisputable fact, and PET/CT has become the most important cancer imaging modality (15). Imaging methods in HNC make an important contribution to clinical examination. Various techniques and positioning methods have been studied to provide an optimal image of scanning methods in HNCs. OM imaging technique in oral cavity tumors was first described by Henrot et al. (16) in 2003. They indicated that OM technique allows a better visualization, especially in oral cavity lesions that cannot be localized because of CT artifacts due to dental amalgams. Henrot et al. (16) described dynamic maneuvers such as Puffed Cheek Technique, the modified Valsalva maneuver, phonation and The OM technique during the CT shoot. They have showed that the OM technique is especially effective in evaluating the CT images of patients with oral cavity and oropharynx tumors with dental amalgam, because of the attenuation created by the X-ray beam as it crosses dental amalgam (16). Kumar et al. (17) also evaluated the similar techniques (puffed-cheek, OM, modified valsalva maneuver, phonation) to better identify the lesions on PET/CT in HNC patients. They underlined that the OM technique is especially useful when a tumor of the oral cavity is not clearly visible because of dental amalgam artifact (17). Metal artifacts affect the image quality and give different results in OM and CM scans. Forty-one PET/CT scans (60.3%) had CT artifacts due to dental amalgams

in our study. In these patients, when comparing the OM and CM images, we observed that the OM scans are much more accurate in detecting both localization and the dimension of the primary lesions.

Pentenero et al. (12) evaluated the accuracy of PET/CT in oral SCC patients. They concluded that PET/CT scan showed good accuracy in determining tumor width and depth. They used the additional OM position, which revealed an increased space between the oral structures and provided a much clearer visualization (12).

Cistaro et al. (18) evaluated usefulness of the OM technique in patients with oral cavity carcinomas. They found that for anatomic localization and detection of tumor extent, OM images always resulted in better visualization than conventional CM images. They also found that in four patients, tumors were not detected using the CM technique but were correctly evaluated with the OM method because of better discrimination of the adjacent anatomical structures. They found no difference between the two techniques in terms of lymph node involvement, which was similarly concluded in our study. They included 34 patients with oral cavity tumors in their studies, and only one of them had lip cancer. Our study is the first and only to compare two techniques in patients with lip cancer homogeneously (18).

Lymph node involvement is the most important prognostic factor in patients with lip cancer, studies show that 5-year survival rates are reduced to approximately 50% in patients with nodal disease (19). Regional spread of lower lip carcinoma is unlikely, but death is mostly the result of uncontrolled disease in the neck. The role of elective neck dissection for treating lip cancer is controversial. Most surgeons do not recommend elective neck dissection for lower lip cancer. Onercl et al. (13) showed that tumor thickness correlated well with cervical lymph node metastasis in lower lip cancer. They showed that the risk of metastatic cervical lymph node increased if the primary lesion was above 5 mm (14). Supporting this data, in our study, all patients with cervical lymph node metastases had a tumor size above 5 mm. Regional lymph node metastasis was observed in 37 (54%) ^{18}F -FDG PET/CT images in our study and we found that OM imaging has no additional contribution to the detection of metastatic cervical lymph nodes.

When evaluating images of patients with HNC, optimal patient preparation technique can also help decrease unexpected ^{18}F -FDG uptake. To prevent non-pathologic increase orofarengal activity, patients are asked not to speak or chew during the waiting period and after ^{18}F -FDG injection. In our study, we informed all patients that

they should spend the waiting period under appropriate conditions. All patients were kept in the waiting room under optimized waiting conditions. Patients stayed in waiting rooms with a similar room temperature, and they were instructed not to use mobile phones, not to chew gum and not to talk.

Although lip cancer is usually an easily recognizable malignancy, some small and deeply located lesions may not be anatomically distinguishable. Especially in these patients, the location and extension of lesions are evaluated more easily from the OM positioning technique.

Since the primary treatment of lip cancer is surgery, it is critical to determine the extent of the lesion accurately (20,21). In our study, we observed that the OM images are very guidance for the surgeon who will perform the surgery in terms of determining the surgical margins. As seen in the results of our study, compared to conventional PET/CT imaging, OM PET/CT scanning improves the assessment of tumor localization and extent in the patients with carcinoma of the lip.

Study Limitations

Our study had several limitations: (1) The radiological images of the patients were in the form of MR or CT, and there was no single standard imaging method, (2) histopathological data were in the form of excision or wide resection, and there was no standard surgical procedure in this respect, (3) the number of patients was relatively small.

Conclusion

We conclude that additional OM head and neck imaging is useful and necessary for the accurate determination of the localization and size of the tumour, thus enhancing the value of PET/CT in staging, re-staging and response to the treatment of malignant lip neoplasms. We recommend routine OM positioning in patients with lip cancer to avoid additional X-ray exposure. Since it may be difficult to stand still with OM position during whole-body imaging, an additional OM head and neck scan is a good option for patients. We suggest that appropriate positioning techniques will also have beneficial results in other head and neck malignancies such as oral cavity, tongue, buccal mucosa, gingival mucosa, and oropharynx.

Ethics

Ethics Committee Approval: Manisa Celal Bayar University Faculty of Medicine Local Ethics Committee (decree number: 20.478.486/1069).

Informed Consent: Written informed consent was obtained from all patients.

Peer-review: Externally peer-reviewed.

Authorship Contributions

Surgical and Medical Practices: G.M., C.S., Concept: G.M., C.S., Y.P., G.G., E.S., Design: G.M., C.S., Y.P., G.G., E.S., Data Collection or Processing: G.M., C.S., Analysis or Interpretation: G.M., C.S., Y.P., Literature Search: G.M., G.G., E.S., Writing: G.M., G.G., E.S.

Conflict of Interest: No conflict of interest was declared by the authors.

Financial Disclosure: The authors declared that this study has received no financial support.

References

1. Bray F, Ferlay J, Soerjomataram I, Siegel RL, Torre LA, Jemal A. Global cancer statistics 2018: GLOBOCAN estimates of incidence and mortality worldwide for 36 cancers in 185 countries. *CA Cancer J Clin* 2018;68:394-424. Erratum in: *CA Cancer J Clin* 2020;70:313.
2. Jorgensen K, Elbrond O, Andersen AP. Carcinoma of the lip. A series of 869 cases. *Acta Radiol Ther Phys Biol* 1973;12:177-190.
3. Oskam IM, Verdonck-de Leeuw IM, Aaronson NK, Witte BI, de Bree R, Doornaert P, Langendijk JA, Leemans CR. Prospective evaluation of health-related quality of life in long-term oral and oropharyngeal cancer survivors and the perceived need for supportive care. *Oral Oncol* 2013;49:443-448.
4. de Visscher JG, Grond AJ, Botke G, van der Waal I. Results of radiotherapy for squamous cell carcinoma of the vermilion border of the lower lip. A retrospective analysis of 108 patients. *Radiother Oncol* 1996;39:9-14.
5. Zitsch RP, Park CW, Renner GJ, Rea JL. Outcome analysis for lip carcinoma. *Otolaryngol Head Neck Surg* 1995;113:589-596.
6. Petti S. Lifestyle risk factors for oral cancer. *Oral Oncol* 2009;45:340-350.
7. Tealab SH, Sedhom NFH, Hassouna A, Gouda I, Ismail H. Prevalence of human papilloma virus in oropharyngeal, tongue and lip squamous cell carcinoma: an experience from the Egyptian National Cancer Institute. *J Investig Med* 2019;67:1061-1066.
8. Genç O, Inançlı HM, Kürkçüoğlu SS, Tunçel U, Enöz M, Haksever M. Nüks alt dudak kanserlerine yaklaşım [Management of recurrent lower lip carcinomas]. *Kulak Burun Bogaz Ihtis Derg* 2010;20:237-242.
9. Olgun Y, Durmuşoğlu M, Doğan E, Erdağ TK, Sarıoğlu S, İköz AÖ. Role of elective neck dissection in early stage lip cancers. *Turk Arch Otorhinolaryngol* 2015;53:23-25.
10. Nahmias C, Carlson ER, Duncan LD, Blodgett TM, Kennedy J, Long MJ, Carr C, Hubner KF, Townsend DW. Positron emission tomography/computerized tomography (PET/CT) scanning for preoperative staging of patients with oral/head and neck cancer. *J Oral Maxillofac Surg* 2007;65:2524-2535.
11. Ha PK, Hdeib A, Goldenberg D, Jacene H, Patel P, Koch W, Califano J, Cummings CW, Flint PW, Wahl R, Tufano RP. The role of positron emission tomography and computed tomography fusion in the management of early-stage and advanced-stage primary head and neck squamous cell carcinoma. *Arch Otolaryngol Head Neck Surg* 2006;132:12-16.
12. Pentenero M, Cistaro A, Brusa M, Ferraris MM, Pezzuto C, Carnino R, Colombini E, Valentini MC, Giovannella L, Spriano G, Gandolfo S. Accuracy of 18F-FDG-PET/CT for staging of oral squamous cell carcinoma. *Head Neck* 2008;30:1488-1496.

13. Onerci M, Yilmaz T, Gedikoğlu G. Tumor thickness as a predictor of cervical lymph node metastasis in squamous cell carcinoma of the lower lip. *Otolaryngol Head Neck Surg* 2000;122:139-142.
14. Salgarelli AC, Sartorelli F, Cangiano A, Pagani R, Collini M. Surgical treatment of lip cancer: our experience with 106 cases. *J Oral Maxillofac Surg* 2009;67:840-845.
15. Czernin J, Allen-Auerbach M, Schelbert HR. Improvements in cancer staging with PET/CT: literature-based evidence as of September 2006. *J Nucl Med* 2007;48(Suppl 1):78S-88S.
16. Henrot P, Blum A, Toussaint B, Troufleau P, Stines J, Roland J. Dynamic maneuvers in local staging of head and neck malignancies with current imaging techniques: principles and clinical applications. *Radiographics* 2003;23:1201-1213.
17. Kumar R, Mukherjee A, Mittal BR. Special Techniques in PET/Computed Tomography Imaging for Evaluation of Head and Neck Cancer. *PET Clin* 2016;11:13-20. doi: 10.1016/j.cpet.2015.07.006.
18. Cistaro A, Palandri S, Balsamo V, Migliaretti G, Pentenero M, Testa C, Cusmà S, Ceraudo F, Gandolfo S, Ficola U. Assessment of a new 18F-FDG PET/CT protocol in the staging of oral cavity carcinomas. *J Nucl Med Technol* 2011;39:7-13.
19. Vartanian JG, Carvalho AL, de Araújo Filho MJ, Junior MH, Magrin J, Kowalski LP. Predictive factors and distribution of lymph node metastasis in lip cancer patients and their implications on the treatment of the neck. *Oral Oncol* 2004;40:223-227.
20. Lang K, Akbaba S, Held T, El Shafie R, Farnia B, Bougatf N, Bernhardt D, Freudlsperger C, Plinkert PK, Rieken S, Debus J, Adeberg S. Retrospective analysis of outcome and toxicity after postoperative radiotherapy in patients with squamous cell carcinoma of the lip. *Tumori* 2022;108:125-133.
21. Zhao R, Jia T, Qiao B, Liang J, Qu S, Zhu L, Feng H, Xing L, Ren Y, Wang F, Zhang H. Nomogram predicting long-term overall survival and cancer-specific survival of lip carcinoma patients based on the SEER database: a retrospective case-control study. *Medicine (Baltimore)* 2019;98:e16727.



The Effects of CoronaVac (Sinovac) and BNT162b2 (BioNTech/Pfizer) Vaccination on Oncologic ¹⁸F-FDG PET/CT Studies

CoronaVac (Sinovac) ve BNT162b2 (BioNTech/Pfizer) Aşılmasının Onkolojik ¹⁸F-FDG PET/CT Çalışmalarına Etkileri

✉ Hüseyin Şan¹, ✉ Engin Alagöz²

¹University of Health Sciences Turkey, Ankara City Hospital, Department of Nuclear Medicine, Ankara, Turkey

²University of Health Sciences Turkey, Gülhane Training and Research Hospital, Department of Nuclear Medicine, Ankara, Turkey

Abstract

Objectives: BioNTech (Pfizer) and CoronaVac (Sinovac) vaccines are two of the most administered coronavirus disease-2019 (COVID-19) vaccines worldwide. Vaccination against severe acute respiratory syndrome-coronavirus-2 has caused a diagnostic challenge in oncological ¹⁸F-fluorodeoxyglucose (FDG) positron emission tomography/computed tomography (PET/CT) studies. The aim of our study was to evaluate the ¹⁸F-FDG PET/CT findings of the two most commonly administered vaccines worldwide.

Methods: Patients over 18 years old who underwent ¹⁸F-FDG PET/CT for oncological purposes in our institution between January 13, 2021 and January 31, 2022, who received a single or second dose of the BioNTech or CoronaVac vaccines in the last two months, were included in the study. Descriptive analyses were presented as mean, standard deviation, frequency and ratio. Additionally, chi-square test was used to analyze categorical variables.

Results: Ipsilateral deltoid muscle hypermetabolism was observed in 6.9% (n=15) and 14.3% (n=22) patients who received CoronaVac and BioNTech vaccines, respectively. Ipsilateral axillary lymph node hypermetabolism was observed in 11% (n=24) and 41.6% (n=64) patients who received CoronaVac and BioNTech vaccines, respectively. Synchronous deltoid muscle and axillary lymph node hypermetabolism was observed in 4.14% (n=9) and 12.33% (n=19) patients who received CoronaVac and BioNTech vaccines, respectively. Significant differences were detected between CoronaVac and BioNTech vaccines in terms of ipsilateral deltoid muscle hypermetabolism, ipsilateral axillary lymph node hypermetabolism and synchronous deltoid muscle and axillary lymph node hypermetabolism (p<0.05).

Conclusion: COVID-19 vaccination may result in ipsilateral axillary lymph node hypermetabolism, ipsilateral deltoid muscle hypermetabolism, or synchronous deltoid muscle and axillary lymph node hypermetabolism with different frequencies depending on the type of vaccination. Although synchronous deltoid muscle and axillary lymph node hypermetabolism can reduce misinterpretation of ¹⁸F-FDG PET/CT, to avoid misinterpretation, it is important to question the vaccination history during ongoing COVID-19 vaccination process.

Keywords: ¹⁸F-FDG PET/CT, CoronaVac, BNT162b2, hypermetabolism, axillary lymph node

Öz

Amaç: BioNTech (Pfizer) ve CoronaVac (Sinovac) aşıları, dünya çapında en çok uygulanan koronavirüs hastalığı-2019 (COVID-19) aşılarından ikisi olmuştur. Şiddetli akut solunum yetmezliği sendromu-koronavirüs-2'ye karşı aşılama, onkolojik ¹⁸F-florodeoksiglukoz (FDG) pozitron emisyon tomografisi/bilgisayarlı tomografi (PET/CT) çalışmalarında tanınan zorluklara neden olmaktadır. Çalışmamızın amacı, dünya çapında en sık uygulanan iki aşının ¹⁸F-FDG PET/CT bulgularını değerlendirmektir.

Address for Correspondence: Hüseyin Şan MD, University of Health Sciences Turkey, Ankara City Hospital, Department of Nuclear Medicine, Ankara, Turkey

Phone: +90 312 552 60 00 **E-mail:** dr.huseyinsan@yahoo.com ORCID ID: orcid.org/0000-0002-2264-5446

Received: 05.06.2022 **Accepted:** 29.07.2022

©Copyright 2022 by Turkish Society of Nuclear Medicine
Molecular Imaging and Radionuclide Therapy published by Galenos Yayınevi.

Yöntem: 13 Ocak 2021 ile 31 Ocak 2022 tarihleri arasında kurumumuzda onkolojik amaçlı ¹⁸F-FDG PET/BT yapılan ve görüntüleme öncesi son iki ayda tek veya ikinci doz BioNTech veya CoronaVac aşısı yapılmış 18 yaş üstü hastalar çalışmaya dahil edildi. Tanımlayıcı analizler ortalama, standart sapma, frekans ve oran olarak sunuldu. Ayrıca kategorik değişkenlerin analizinde ki-kare testi kullanıldı.

Bulgular: CoronaVac ve BioNTech aşısı olan hastaların sırasıyla %6,9'unda (n=15) ve %14,3'ünde (n=22) ipsilateral deltoid kas hipermetabolizması gözlemlendi. CoronaVac ve BioNTech aşısı olan hastaların sırasıyla %11'inde (n=24) ve %41,6'sında (n=64) ipsilateral aksiller lenf nodu hipermetabolizması gözlemlendi. Senkron deltoid kas ve aksiller lenf nodu hipermetabolizması, CoronaVac ve BioNTech aşısı yapılan hastaların sırasıyla; %4,14'ünde (n=9) ve %12,33'ünde (n=19) gözlemlendi. CoronaVac ve BioNTech aşısı arasında ipsilateral deltoid kas hipermetabolizması, ipsilateral aksiller lenf nodu hipermetabolizması ve senkron deltoid kas ve aksiller lenf nodu hipermetabolizması açısından anlamlı fark saptandı (p<0,05).

Sonuç: COVID-19 aşısı, aşı tipine bağlı olarak farklı sıklıkta ipsilateral aksiller lenf nodu hipermetabolizması, ipsilateral deltoid kas hipermetabolizması veya senkron deltoid kas ve aksiller lenf nodu hipermetabolizması ile sonuçlanabilir. Senkron deltoid kas ve aksiller lenf nodu hipermetabolizması ¹⁸F-FDG PET/BT'nin yanlış yorumlanmasını azaltabilse de, yanlış yorumlamayı önlemek için devam eden COVID-19 aşılamada sürecinde aşı geçişini sorgulamak önemlidir.

Anahtar kelimeler: ¹⁸F-FDG PET/BT, CoronaVac, BNT162b2, hipermetabolizma, aksiller lenf nodu

Introduction

In late 2019, a new respiratory coronavirus disease-2019 (COVID-19) was detected in Wuhan, China's Hubei Province which was caused by a novel coronavirus named severe acute respiratory syndrome-coronavirus-2 (SARS-CoV-2) (1,2,3). A few months later, the World Health Organization (WHO) announced SARS-CoV-2 outbreak as a Public Health Emergency of International Concern on January 30, 2020 and subsequently reported COVID-19 as a pandemic on March 11, 2020 (1,3,4,5). With the aim of stopping the spread of the virus, many countries worldwide have reorganized the public order with strict restrictions that impact social life, businesses school, travel, economy and etc. (1,3).

To protect human health and reduce the unfavorable effects of COVID-19 on daily life, the development of vaccines and spread of vaccinations against SARS-CoV-2 has been accepted as the foremost prevention worldwide (6). As of January 12, 2022, WHO has evaluated that the AstraZeneca/Oxford, Johnson and Johnson, Moderna, BioNTech/Pfizer, Sinopharm, Sinovac, Covaxin, Covovax, Nuvaxovid vaccines against COVID-19 have met the necessary criteria for safety and efficacy (7). To date, BNT162b2 (BioNTech/Pfizer) and CoronaVac (Sinovac) have been the two of the most administered vaccines worldwide (8).

In a multicenter study by Dai et al. (9), it was revealed that cancer patients with COVID-19 have an almost threefold higher mortality ratio than COVID-19 patients without cancer. Prior vaccination of patients receiving cancer treatment, patients with advanced stage cancer and patients with hematologic malignancies and lung cancer have been recommended (10). Thus, vaccination prioritization of cancer and chronic diseases has been implemented in many countries.

Injection site pain and swelling, fatigue, headache, myalgia, chills, arthralgia, and lymphadenopathy are the adverse events after BNT162b2 and Coronavac vaccination (11,12). In addition to adverse events, vaccination against SARS-CoV-2 has caused a diagnostic challenge in oncologic ¹⁸F-fluorodeoxyglucose (FDG) positron emission tomography/computed tomography (PET/CT). Various studies have shown that ¹⁸F-FDG avid ipsilateral lymphadenopathy on ¹⁸F-FDG PET/CT was detected in approximately 50% and 10% of patients who received the BNT162b2 and CoronaVac vaccines, respectively (13,14). The aim of our study was to evaluate the ¹⁸F-FDG PET/CT findings of the two most commonly administered vaccines and possible factors affecting these findings as age, sex, systemic treatment, hematological malignancy, and days between vaccination and ¹⁸F-FDG PET/CT study. To the best of our knowledge, this study includes the largest number of participants comparing ¹⁸F-FDG PET/CT findings of both vaccines in the literature.

Materials and Methods

This retrospective study was conducted with the approval of the University of Health Sciences Turkey, Gulhane Scientific Research Ethics Committee of our institution (decision no: 2021/297). Patients over 18 years old who underwent ¹⁸F-FDG PET/CT for oncological purposes in our institution between January 13, 2021 and January 31, 2022 were reviewed. Patients who received a single or booster dose of the BNT162b2 or CoronaVac vaccines in the last two months before ¹⁸F-FDG PET/CT were included in the study. Patients who have not been vaccinated against COVID-19, patients who have been vaccinated after ¹⁸F-FDG PET/CT imaging, patients who have been vaccinated against other infections, ¹⁸F-FDG PET/CT imaging other than oncological purpose, patients who have missing data of vaccination and patient history, patients with known or congruent axillary

lymph node metastasis, patients who had undergone axillary lymph node dissection before and patients with more than two months between vaccination and ¹⁸F-FDG PET/CT imaging were excluded from the study (Figure 1).

CoronaVac vaccine contained SARS-CoV-2 antigen (600SU) and aluminum hydroxide (0.45 mg/mL) as an adjuvant (11). BNT162b2 vaccine contained 30 micrograms of tozinameran, a single-stranded, 5'-capped messenger RNA (mRNA) (12). The demographic data, medical diagnosis, and treatment history of patients, information about the date of vaccination, vaccination site and vaccine brand

were obtained from the patient anamnesis form filled before ¹⁸F-FDG PET/CT imaging.

A 64-slice CT-integrated PET scanner (Discovery 690-GE Healthcare, Milwaukee, Wisconsin, USA) was used for PET/CT imaging. After fasting for at least 6 h, patients with blood glucose levels below 150 mg/dL were intravenously injected with 3.7 MBq/kg (0.1 mCi/kg) ¹⁸F-FDG. Approximately one hour later, CT (120 kV, 10-90 mA) and PET (3 min per bed) images of the area from the vertex to mid-thigh were acquired. Sagittal, coronal, transverse sections and maximum intensity projection images were obtained by iterative reconstruction (12 subset and four iteration) and attenuation correction. The images were analyzed using Advantage Workstation 4.6 (GE Healthcare). All PET/CT images were analyzed by two nuclear medicine physicians with 6 and 13 years of ¹⁸F-FDG PET/CT experience. Considering previous studies, maximum standard uptake value (SUV_{max}) values were measured by placing a region of interest at the injection site and at the ipsilateral axillary lymph node with the highest ¹⁸F-FDG uptake and compared with the SUV_{max} values of the contralateral side. ¹⁸F-FDG uptake in the deltoid muscle and axillary lymph node was accepted as positive if the ipsilateral-to-contralateral SUV_{max} value ratio was at least 1.5 (13,15).

Statistical Analysis

Statistical analyzes were performed using version 26.0 SPSS (IBM Corp., Armonk, New York, USA) and Stata/MP 16 (Stata Corporation, College Station, Texas, USA) softwares. Descriptive analyzes were presented as mean, standard deviation (SD) and frequency. The Kolmogorov-Smirnov test was used to determine whether the obtained parameters confirmed a normal distribution. Chi-square test was used to analyze categorical variables. A tetrachoric correlation test was used to analyze the correlations between the binary variables. Student's t-test was used for comparing the normally distributed continuous variables. While investigating the associations between continuous, ordinal and dichotomous variables, the correlation coefficients (r) and their significance (p) were calculated using the Point Bi-serial and Pearson correlation tests.

Logistic regression models were fit with a binary dependent variable [ipsilateral deltoid muscle hypermetabolism (yes/no), ipsilateral axillary lymph node uptake (yes/no)] and with the following independent variables: Age, gender, systemic therapy (yes/no), hematologic malignancy (yes/no), vaccine brand, days after the single dose of vaccination, days after the booster dose of vaccination. The test of Hosmer and Lemeshow goodness of fit statistics were used to assess model fit. A 5% type-1 error level was used to infer statistical significance.

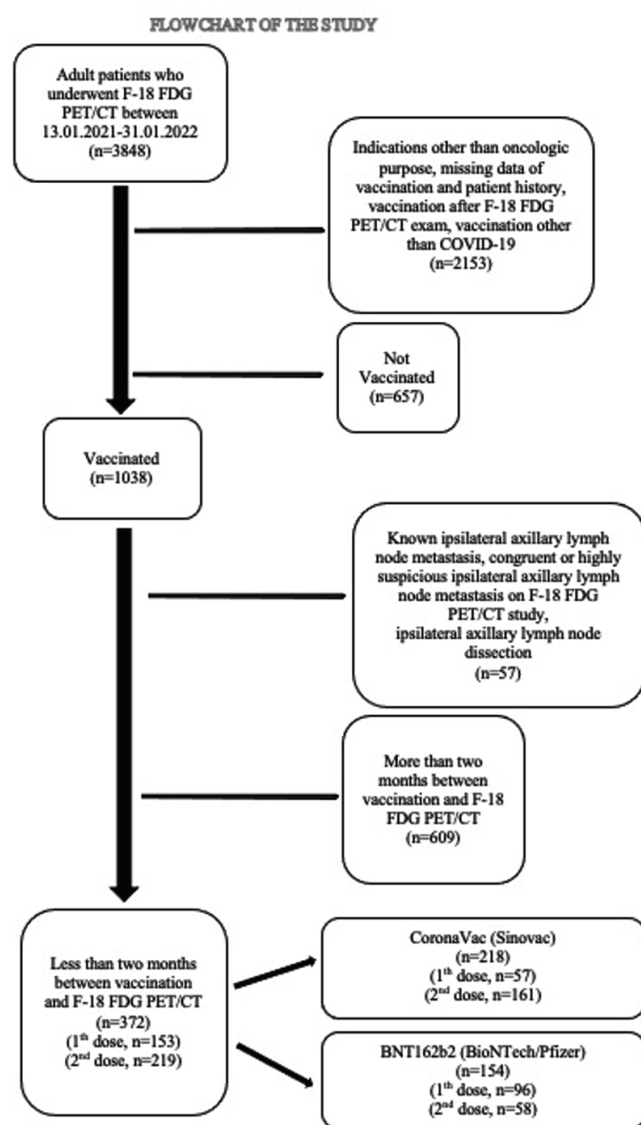


Figure 1. Flow chart of the study
FDG: Fluorodeoxyglucose, PET/CT: Positron emission tomography/computed tomography

Results

General Demographics

Of 372 adults analyzed in this study, 161 (43.27%) were female and 211 (56.72%) were male. Their mean age was 57.24 (SD: 12.73). The number of patients who received CoronaVac and BNT162b2 vaccines was 218 (58.60%) and 154 (41.39%), respectively. The number of patients who received the single dose and booster doses were 153 (41.12%) and 219 (58.87%), respectively. The number of patients who received the single dose and booster doses of CoronaVac vaccine was 57 (15.32%) and 161 (43.27%), respectively. The number of patients who received the single dose and booster doses of BNT162b2 vaccine was 96 (25.80%) and 58 (15.59%), respectively. Table 1 summarizes the demographic characteristics of the study population.

The distribution of the ¹⁸F-FDG PET/CT indications in numbers were; as head and neck cancer: 32 (8.6%), lung cancer: 84 (22.58%), breast cancer: 61 (16.39%), hematologic malignancy: 34 (9.13%), cutaneous cancer: 19 (5.1%), gynecologic cancer: 20 (5.37%), gastrointestinal cancer: 40 (10.75%), genitourinary cancer: 32 (8.6%), unknown primary: 27 (7.25%) and other tumors: 23 (6.18%).

The mean interval between the single dose of vaccination and ¹⁸F-FDG PET/CT imaging was 20.54 (SD: 13.89) (range, 1-59). The mean interval between the booster dose of vaccination and ¹⁸F-FDG PET/CT imaging was 31.12 (SD: 16.83) (range, 1-60).

In terms of positive ipsilateral axillary lymph node hypermetabolism, the median days after the single dose of CoronaVac and BNT162b2 vaccinations were 8 and 11, respectively. Additionally, in terms of positive ipsilateral axillary lymph node hypermetabolism, the median days after the booster dose of CoronaVac and BNT162b2 vaccination were 16 and 17, respectively.

The number of patients who received chemotherapy-chemoradiotherapy- surgery+chemotherapy, targeted therapy, radiotherapy, surgery and no treatment were 184 (49.46%), 49 (13.17%), 8 (2.1%) and 5 (1.3%) and 126 (33.87%) respectively. The number of patients who received systemic therapy (chemotherapy, chemoradiotherapy, surgery+chemotherapy and targeted therapy) was 233 (62.6%).

¹⁸F-FDG PET/CT study indications were diagnosis of malignancy and primary staging (n=79, 21.2%), assessment of treatment response (n=168, 45.2%) and restaging (n=125, 33.6%).

Vaccination caused ¹⁸F-FDG uptake in the ipsilateral deltoid muscle and axillary lymph nodes was detected in

9.9% (n=37) and 23.7% (n=88) of patients, respectively. Additionally, synchronous ipsilateral deltoid muscle and axillary lymph node hypermetabolism [Double sign ("DS")] (16) were detected in 28 patients (7.52%) (Figures 2, 3). Additionally, supraclavicular lymph node hypermetabolism was detected secondary to vaccination in 8 (2.15%) patients, 7 of whom (4.54%) were secondary to the BNT162b2 vaccine (Figure 4).

Ipsilateral Deltoid Muscle Hypermetabolism Based Analysis

Ipsilateral deltoid muscle hypermetabolism was detected in 6.9% (n=15) and 14.3% (n=22) patients who received CoronaVac and BNT162b2 vaccines, respectively. A significant difference was detected between CoronaVac and BNT162b2 vaccines in terms of ipsilateral deltoid muscle hypermetabolism (p<0.05). Ipsilateral deltoid muscle hypermetabolism was detected in 7.01% (n=4) and 9.37% (n=9) patients who received a single dose of CoronaVac and BNT162b2 vaccines, respectively. It was not detected any significant difference between only a single dose of CoronaVac and BNT162b2 vaccines in terms of ipsilateral deltoid muscle hypermetabolism (p>0.05). Ipsilateral deltoid muscle hypermetabolism was detected 6.83% (n=11) and 22.41% (n=13) patients who received booster doses of CoronaVac and BNT162b2 vaccines, respectively. A significant difference was detected between the booster doses of CoronaVac and BNT162b2 vaccines in terms of ipsilateral deltoid muscle hypermetabolism (p<0.05).

There was a significant correlation between BNT162b2 vaccination and ipsilateral deltoid muscle hypermetabolism (p<0.05, r_{tet} : 0.2562).

There was a significant association between ipsilateral deltoid muscle hypermetabolism and days passed after the booster dose of vaccination [Odds ratio (OR): 0.877; 95% confidence interval (CI), 0.829-0.928; p<0.05], days passed after the single dose of vaccination (OR, 0.748; 95% CI, 0.636-0.880; p<0.05) and age (OR, 0.965; 95% CI, 0.942-0.990; p<0.05).

Ipsilateral Axillary Lymph Node Hypermetabolism Based Analysis

Ipsilateral axillary lymph node hypermetabolism was detected in 11% (n=24) and 41.6% (n=64) patients who received CoronaVac and BNT162b2 vaccines, respectively. A significant difference was detected between CoronaVac and BNT162b2 vaccines in terms of ipsilateral axillary lymph node hypermetabolism (p<0.05). Ipsilateral axillary lymph node hypermetabolism was detected in 14.03% (n=8) and 41.66% (n=40) patients who received a single dose of CoronaVac and BNT162b2 vaccines, respectively.

Table 1. Demographic characteristics of study population			
Characteristics	Data (mean ±SD), n (%)	Characteristics	Data (mean ± SD), n (%)
Patient		¹⁸F-FDG uptake secondary to vaccination	
Age	57.24±12.73	All	
Female	161 (43.27%)	Deltoid muscle	37 (9.9%)
Male	211 (56.72%)	Axillary lymph node	88 (23.7%)
Vaccination		Double sign	28 (7.52%)
All		Single dose	
CoronaVac	218 (58.6%)	Deltoid muscle	13 (8.49%)
BNT162b2	154 (41.39%)	Axillary lymph node	48 (31.37%)
Single dose		Double sign	10 (6.53%)
All	153 (41.12%)	Booster dose	
CoronaVac	57 (15.32%)	Deltoid muscle	24 (10.95%)
BNT162b2	96 (25.80%)	Axillary lymph node	40 (18.26%)
Booster dose		Double sign	18 (8.21%)
All	219 (58.87%)	¹⁸F-FDG uptake secondary to CoronaVac	
CoronaVac	161 (43.27%)	All	
BNT162b2	58 (15.59%)	Axillary lymph node	24 (11%)
¹⁸F-FDG PET/CT		Double sign	9 (4.14%)
Tumour		Single dose	
Head and neck cancer	32 (8.6%)	Deltoid muscle	4 (7.01%)
Lung cancer	84 (22.58%)	Axillary lymph node	8 (14.03%)
Breast cancer	61 (16.39%)	Double sign	2 (3.5%)
Hematologic cancer	34 (9.13%)	Booster dose	
Cutaneous cancer	19 (5.1%)	Deltoid muscle	11 (6.83%)
Gynecologic cancer	20 (5.37%)	Axillary lymph node	16 (9.93%)
Gastrointestinal cancer	40 (10.75%)	Double sign	7 (4.34%)
Genitourinary cancer	32 (8.6%)	¹⁸F-FDG uptake secondary to BNT162b2	
Unknown primary	27 (7.25%)	All	
Other tumours	23 (6.18%)	Deltoid muscle	22 (14.3%)
Indication		Axillary lymph node	64 (41.6%)
Diagnosis of malignancy and primary staging	79 (21.2%)	Double sign	19 (12.33%)
Assessment of treatment response	168 (45.2%)	Single dose	
Restaging	125 (33.6%)	Deltoid muscle	9 (9.37%)
Treatment		Axillary lymph node	40 (41.66%)
Chemotherapy, chemoradiotherapy, chemotherapy+surgery	184 (49.46%)	Double sign	8 (8.33%)
Targeted therapy	49 (13.17%)	Booster dose	
Radiotherapy	8 (2.1%)	Deltoid muscle	13 (22.41%)
Surgery	5 (1.3%)	Axillary lymph node	24 (41.37%)
Without treatment	126 (33.87%)	Double sign	11 (18.96%)
Mean days between vaccination and ¹⁸F-FDG PET/CT			
Single	20.54±13.89		
Booster	31.12±16.83		

FDG: Fluorodeoxyglucose, PET/CT: Positron emission tomography/computed tomography, SD: Standard deviation

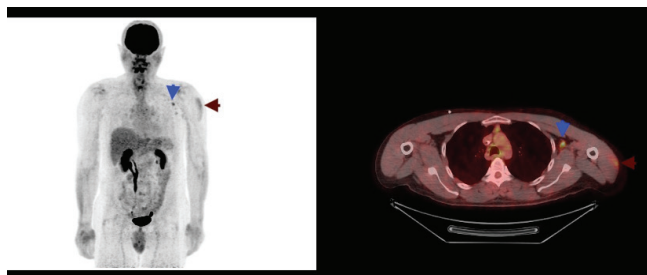


Figure 2. Maximum intensity projection and axial fusion image of ¹⁸F-FDG PET/CT. Synchronous hypermetabolism localised to the left deltoid muscle and left level 2 axillary lymph node secondary to BNT162b2 (BioNTech/Pfizer) vaccination (blue and claret arrows)
FDG: Fluorodeoxyglucose, PET/CT: Positron emission tomography/computed tomography

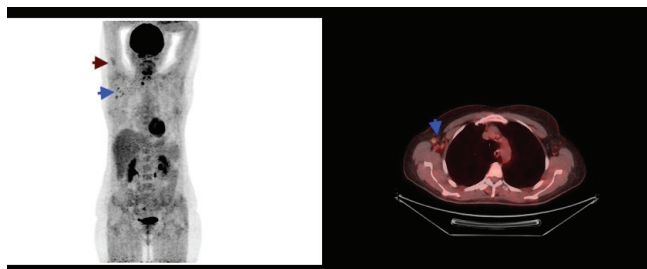


Figure 3. Maximum intensity projection and axial fusion image of ¹⁸F-FDG PET/CT. Synchronous hypermetabolism localised to the right deltoid muscle and right level 1 axillary lymph nodes secondary to BNT162b2 (BioNTech/Pfizer) vaccination (blue and claret arrows)
FDG: Fluorodeoxyglucose, PET/CT: Positron emission tomography/computed tomography

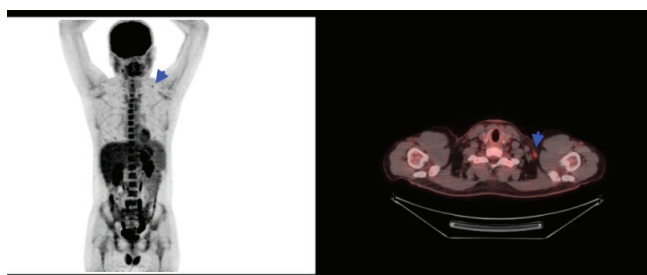


Figure 4. Maximum intensity projection and axial fusion image of ¹⁸F-FDG PET/CT. Left hypermetabolic supraclavicular lymph node secondary to BNT162b2 (BioNTech/Pfizer) vaccination (blue arrows)
FDG: Fluorodeoxyglucose, PET/CT: Positron emission tomography/computed tomography

A significant difference was detected between the single dose of CoronaVac and BNT162b2 vaccines in terms of ipsilateral axillary lymph node hypermetabolism ($p < 0.05$). Ipsilateral axillary lymph node hypermetabolism was detected in 9.93% ($n = 16$) and 41.37% ($n = 24$) patients who received booster doses of CoronaVac and BNT162b2 vaccines, respectively. A significant difference was

detected between the booster doses of CoronaVac and BNT162b2 vaccines in terms of ipsilateral axillary lymph node hypermetabolism ($p < 0.05$).

There was a significant correlation between BNT162b2 vaccination and ipsilateral axillary lymph node hypermetabolism ($p < 0.05$, r_{tet} : 0.5707).

There was a significant correlation between ipsilateral deltoid muscle hypermetabolism and ipsilateral axillary lymph node hypermetabolism ($p < 0.05$, r_{tet} : 0.7112).

There was a significant association between ipsilateral axillary lymph node hypermetabolism and days passed after the booster dose of vaccination (OR, 0.927; 95% CI, 0.898-0.958; $p < 0.05$), days passed after the single dose of vaccination (OR, 0.927; 95% CI, 0.893-0.962; $p < 0.05$) age (OR, 0.957; 95% CI, 0.936-0.976; $p < 0.05$) and booster dose (OR, 2.04; 95% CI, 1.261-3.319; $p < 0.05$).

“DS” Based Analysis

The percentage of “DS” in patients receiving CoronaVac and BNT162b2 vaccines were 4.14% ($n = 9$) and 12.33% ($n = 19$), respectively. A significant difference was detected between CoronaVac and BNT162b2 vaccines in terms of “DS” ($p < 0.05$). The percentage of “DS” in patients receiving the single dose of CoronaVac and BNT162b2 vaccines were 3.5% ($n = 2$) and 8.33% ($n = 8$), respectively. It was not detected any significant difference between the single dose of CoronaVac and BNT162b2 vaccines in terms of “DS” ($p > 0.05$). The percentage of “DS” in patients receiving booster doses of CoronaVac and BNT162b2 vaccines were 4.34% ($n = 7$) and 18.96% ($n = 11$), respectively. A significant difference was detected between the booster doses of CoronaVac and BNT162b2 vaccines in terms of “DS” ($p < 0.05$).

75.67% and 31.81% patients with ipsilateral deltoid muscle and axillary lymph node hypermetabolism had “DS”, respectively.

There was a significant correlation between BNT162b2 vaccination and “DS” ($p < 0.05$, r_{tet} : 0.3472).

There was a significant association between “DS” and days passed after the second dose of vaccination (OR, 0.878; 95% CI, 0.824-0.936; $p < 0.05$), days passed after the single dose of vaccination (OR, 0.768; 95% CI, 0.649-0.908; $p < 0.05$) and age (OR, 0.961; 95% CI, 0.934-0.988; $p < 0.05$).

Age, Gender, Therapy, Hematologic Malignancy Based Analysis

In terms of gender, it was not detected any significant difference between the positive and negative groups of ipsilateral deltoid muscle hypermetabolism, ipsilateral

axillary lymph node hypermetabolism and "DS" ($p>0.05$).

In terms of age, a significant difference was detected between the positive and negative groups of ipsilateral deltoid muscle hypermetabolism, ipsilateral axillary lymph node hypermetabolism and "DS" ($p<0.05$).

In terms of systemic therapy, it was not detected any significant difference between positive and negative groups of ipsilateral deltoid muscle hypermetabolism, ipsilateral axillary lymph node hypermetabolism and "DS" ($p>0.05$).

In terms of hematologic malignancy, it was not detected any significant difference between positive and negative groups of ipsilateral deltoid muscle hypermetabolism, ipsilateral axillary lymph node hypermetabolism and "DS" ($p>0.05$).

Time Based Analysis

In terms of days passed after the single and booster dose of vaccination, a significant difference was detected between positive and negative groups of ipsilateral deltoid muscle hypermetabolism, ipsilateral axillary lymph node hypermetabolism and "DS" ($p<0.05$).

In terms of days passed after the single dose of BNT162b2 vaccination, a significant difference was detected between positive and negative groups of ipsilateral deltoid muscle hypermetabolism, ipsilateral axillary lymph node hypermetabolism and "DS" ($p<0.05$). There was a significant and negative correlation between days passed after the single dose of BNT162b2 vaccination and ipsilateral deltoid muscle hypermetabolism ($p<0.05$, r_{pb} : -0.401), ipsilateral axillary lymph node hypermetabolism ($p<0.05$, r_{pb} : -0.539) and "DS" ($p<0.05$, r_{pb} : -0.371).

In terms of days passed after the booster dose of BNT162b2 vaccination, a significant difference was detected between positive and negative groups of ipsilateral deltoid muscle hypermetabolism, ipsilateral axillary lymph node hypermetabolism and "DS" ($p<0.05$). There was a significant and negative correlation between days passed after the booster dose of BNT162b2 vaccination and ipsilateral deltoid muscle hypermetabolism ($p<0.05$, r_{pb} : -0.651), ipsilateral axillary lymph node hypermetabolism ($p<0.05$, r_{pb} : -0.554) and "DS" ($p<0.05$, r_{pb} : -0.570).

In terms of days passed after the single and booster dose of CoronaVac vaccination, it was not detected any significant difference between positive and negative groups of ipsilateral deltoid muscle hypermetabolism, ipsilateral axillary lymph node hypermetabolism and "DS" ($p>0.05$).

In terms of single dose, ipsilateral axillary lymph node hypermetabolism was detected in 35.41%, 27.08%, 20.83%, 8.33%, 4.16%, 2.08%, and 2.08% patients at 1st-7th weeks after vaccination, respectively.

In terms of booster dose, ipsilateral axillary lymph node hypermetabolism was detected in 32.5%, 12.5%, 17.5%, 12.5%, 15%, 7.5%, and 2.5% of patients 1st-6th and 9th weeks after vaccination, respectively.

Discussion

Immunization against SARS-CoV-2 reduces the risk of life-threatening disease, therefore vaccination has been used as a necessary instrument against COVID-19 (4). Mass vaccination campaigns have been in progress worldwide by implementing additional booster dose. To date, BNT162b2 (BioNTech/Pfizer) and CoronaVac (Sinovac) vaccines have been the two of the most administered vaccines globally (8). BNT162b2 consist of "nucleoside-modified mRNA" encoding the "viral spike glycoprotein" of SARS-CoV-2 (12,17,18,19). CoronaVac is inactivated virus vaccine that contains inactivated SARS-CoV-2 as antigen (11). Although, BNT162b2 stimulates remarkably higher levels of SARS-CoV-2-specific binding and neutralizing antibody responses, CoronaVac elicits higher CD4+ and CD8+ T-cell responses than BNT162b2 (20). After vaccination, two main responses generated are the formation of cytotoxic T-lymphocytes in cellular response and formation of mature B-cells in the germinal center (GC) of the lymph node in humoral response (21,22). mRNA COVID-19 vaccines generate significant GC responses and the GC response substantially participates in the humoral response (22,23,24). In a study by Turner et al. (25), after examining the fine needle aspirates of draining axillary lymph nodes, it was detected that BNT162b2 vaccine stimulate GC B-cell responses eliciting the strong humoral immunity. In another study by Ellebedy et al. (24) similar results was founded that BNT162b2 vaccine has the capacity to elicit powerful GC reactions that are essential for durable humoral immunity.

The vulnerability of cancer patients to the influenza virus is a well-known and influenza infection increases the risk of death tenfold compared to patients without malignancy (4,26).

Based on this experience, the potential consequences of COVID-19 in cancer patients have been worrisome since the beginning of the pandemic. Patients with cancer have higher rates of severe disease and fatality after COVID-19 than the general population. In a recent meta-analysis (26 studies, 23,736 patients), Venkatesulu et al. (27) found nearly threefold higher odds of death in cancer patients affected by COVID-19 than in those without cancer (28). According to the Global Cancer Observatory Database, nearly 19.3 million new cancer cases have been declared in 2020 globally (29). Moreover, the incidence of cancer may increase, causing serious challenges for healthcare providers

in protecting cancer patients at risk of COVID-19 (4). Prior vaccination of patients receiving cancer treatment, patients with advanced stage cancer and patients with hematologic malignancies and lung cancer have been recommended (10). Therefore, considering the possible high risk of severe disease, cancer patients have been prioritized in vaccination campaigns in most countries (30,31).

In addition to adverse events, vaccination against SARS-CoV-2 has caused a diagnostic challenge in cancer patients. Solitary ¹⁸F-FDG avid axillary lymphadenopathy secondary to COVID-19 vaccination may challenge nuclear medicine physician and oncologist in patients diagnosed with lymphoma, breast cancer, malignant melanoma and other cutaneous malignancies (16). In the studies by Cohen et al. (32), Orevi et al. (16) and Eifer et al. (13) have shown that vaccination with BNT162b2 resulted in ¹⁸F-FDG-positive axillary (45.6%, 66%, and 45%, respectively) lymph nodes ipsilateral to the injection site, especially after the booster dose. In another study by Sahin (14), the ipsilateral hypermetabolic axillary lymph nodes were detected in 9.9% (18/182) patients vaccinated with CoronaVac and 37.5% (9/24) patients vaccinated with BNT162b2. In our study, findings followed previous studies as ipsilateral axillary lymph node hypermetabolism was detected in 11% and 41.6% of patients who received CoronaVac and BNT162b2 vaccines, respectively. It has been suggested that ¹⁸F-FDG avid lymph nodes are related to the activation of the immune response (13,16). Mok et al. (20) detected that BNT162b2 elicited significantly higher PRNT₅₀, PRNT₉₀, sVNT, spike receptor binding, spike N-terminal domain binding, spike S2 domain binding, spike FcR binding and antibody avidity levels than CoronaVac. The stronger humoral responses of BNT162b2 than the CoronaVac vaccine may explain the detection of ipsilateral hypermetabolic axillary lymph nodes in approximately 4 times more patients in favor of BNT162b2 vaccine in our study.

After the proximal arm injection, ¹⁸F-FDG uptake secondary to immune reaction is substantially limited to regionally draining axillary lymph nodes. Additionally, the subsequent draining to supraclavicular lymph nodes may also be uncommonly observed (16). In the studies by Orevi et al. (16) and Cohen et al. (32), ¹⁸F-FDG avid supraclavicular lymph nodes were detected in 5.7% and 7.9% of the BNT162b2 vaccination, respectively. In our study, supraclavicular lymph node hypermetabolism was detected secondary to vaccination in 8 (2.15%) patients, 7 of whom (4.54%) were secondary to BNT162b2 vaccine. In a study by Eifer et al. (13), it was detected a strong inverse association between hypermetabolic ipsilateral

lymph nodes secondary to BNT162b2 vaccination and patient age. In another study by Sahin (14), a statistically significant difference was detected between patients with and without hypermetabolic axillary lymph nodes in terms of age. In their study, Cohen et al. (32) stated that patients younger than 62 and 64 years of age show a higher incidence of vaccine-associated hypermetabolic lymphadenopathy (VAHL) after the single and booster dose of BNT162b2 vaccine, respectively. In our study, there was a significant and inverse association between age and ipsilateral axillary lymph node hypermetabolism. Brockman et al. (33) detected that responses to mRNA-based COVID-19 vaccination in older adults are quantitatively and functionally impaired. Additionally, age was found as the most crucial factor in the antibody response to COVID-19 mRNA vaccination (33). Impaired primary and secondary antibody responses to vaccination in the elderly are considered responsible for this situation (13,34).

Eifer et al. (13) detected that a strong inverse association between hypermetabolic ipsilateral lymph nodes secondary to BNT162b2 vaccination and immunosuppressive treatment and the presence of hematologic disease. In their study, Cohen et al. (32) stated that the detection of VAHL was not different in patients receiving chemotherapy, radiotherapy, biological treatment, or immunotherapy. In our study, it was not detected any significant association between ipsilateral axillary lymph node hypermetabolism and systemic treatment and presence of hematologic disease. Various chemotherapeutics and targeted therapies in the treatment plan, days passed after the last treatment, hematologic disease burden, bone-marrow reserves, and other differences in the study population may be responsible for the discordant results.

In a study by Orevi et al. (16), "DS" was detected in the 20% of the vaccinated patients. Additionally, it was determined that 95% of patients with ¹⁸F-FDG accumulation at the injection site had "DS" and both the specificity and positive predictive value of "DS" for vaccination-caused lymphadenopathy were 100%. Additionally, "DS" was considered a marker to prevent misinterpretation of ¹⁸F-FDG PET/CT studies and further unnecessary procedures (16). In our study 75.67% patients with ipsilateral deltoid muscle hypermetabolism had "DS" (higher for BNT162b2). Additionally, 31.81% patients with ipsilateral axillary lymph node hypermetabolism had "DS" (higher for CoronaVac). Although "DS" can reduce false positive results in cancer patients, in cases with only axillary lymph node hypermetabolism, vaccination history based follow-up and correlation with other imaging modalities would be useful to avoid misinterpretation.

In the study by Eifer et al. (13), the number of days from the last vaccine dose and the number of vaccine dose was significantly associated with increased odds of hypermetabolic lymph nodes. In our study, the number of days from the last vaccine dose was significantly associated with decreased odds of ipsilateral axillary lymph node hypermetabolism. Additionally, the number of vaccine doses was significantly associated with increased odds of ipsilateral axillary lymph node hypermetabolism. In a comparison of two studies, the direction of association between hypermetabolic axillary lymph node and the number of days from the last vaccine dose was incongruent. As the number of days after the last dose of vaccination increases, the detection of axillary lymph node hypermetabolism is expected to decrease. However, hypermetabolic axillary lymph nodes may not be detected if the interval is too short. In the study by Cohen et al. (32), the first five days after the first vaccine, the third week after the first vaccine and at least three weeks after the booster dose administration was defined as appropriate time window for ¹⁸F-FDG PET/CT imaging (the incidence of VAHL is lower).

In the study by Eifer et al. (13), no association was found between ipsilateral deltoid muscle hypermetabolism and patient age. The number of vaccine doses was associated with increased odds of ipsilateral deltoid muscle hypermetabolism. Additionally, the number of days from the last vaccination was associated with decreased odds of ipsilateral deltoid muscle hypermetabolism. In our study, the number of days from the last vaccine dose and age was associated with decreased odds of ipsilateral deltoid muscle hypermetabolism. Impaired inflammatory responses and wound healing in the elderly and resolution of inflammation with time after vaccination are considered responsible (35). Furthermore, in our study there was not any significant association between ipsilateral deltoid muscle hypermetabolism and the number of vaccine dose. Hypermetabolism at the injection site is induced by the traumatic and inflammatory effect of the injection (13,16). In contrast to the complicated immune response that causes axillary lymph node hypermetabolism, trauma and inflammation caused by hypermetabolism at the injection site may not depend on the number of vaccination.

In the study by Sahin (14), the rates of hypermetabolic axillary lymph node after 1st dose of CoronaVac and BNT162b2 vaccination were 9.6% and 35%, respectively. Additionally, the rates of hypermetabolic axillary lymph node after 2nd dose of CoronaVac and BNT162b2 vaccinations were 10.2% and 50%, respectively (14). In the study by Cohen et al. (32), VAHL secondary to BNT162b2 vaccination was detected in 36.4% of the patients after the first dose and

in 53.9% of patients after the booster dose. In our study, ipsilateral axillary lymph node hypermetabolism secondary to CoronaVac vaccination was detected in 14.03% (n=8) and 9.93% (n=16) patients after the single dose and booster dose, respectively. Additionally, ipsilateral axillary lymph node hypermetabolism secondary to BNT162b2 vaccination was detected in 41.66% (n=40) and 41.37% (n=24) patients after only a single and booster dose, respectively. It was determined that the results of our study were partially close to those of the aforementioned studies.

In the study by Sahin (14), the ipsilateral hypermetabolic axillary lymph nodes were detected in 9.9% patients vaccinated with CoronaVac and 37.5% (9/24) patients vaccinated with BNT162b2. However, the number of patients vaccinated with BNT162b2 was low (n=24) and statistical comparison could not be made between the two patient groups (14). In our study, ipsilateral axillary lymph node hypermetabolism was detected in 11% and 41.6% of patients who received CoronaVac and BNT162b2 vaccines, respectively. Additionally, a significant difference was detected between the CoronaVac and BNT162b2 vaccines with respect to ipsilateral axillary lymph node hypermetabolism. Furthermore, there was a significant correlation between BNT162b2 vaccination and ipsilateral axillary lymph node hypermetabolism. In their study, Mok et al. (20) found that 91.8% and 100% of the participants vaccinated with CoronaVac and BNT162b2, respectively, reached the 50% protection threshold 1 month after the second dose of vaccination. Further, 6 months after the second dose of vaccination, those ratios decreased to 16.3% and 79.6%, respectively. BNT162b2 was found to be more immunogenic and durable than the CoronaVac vaccine in terms of peak and waning antibody titers (20). In a study by Cohen et al. (22), correlation between VAHL secondary to BNT162b2 and humoral immunity in hematologic malignancy was researched. VAHL ratios were 10% in patients with negative serology, 31.3% in patients with low and 72.2% in patients with high anti-spike titers. Additionally, a positive statistically significant correlation was found between VAHL and serology ranks ($r_s=0.530$, $P_v < 0.001$) and it was suggested that the detection of VAHL indicates a higher likelihood of antibody production and an effective humoral response (22). We thought that the results of our study reflect the different immunogenic properties and effects of CoronaVac and BNT162b2 vaccines via ¹⁸F-FDG hypermetabolism. Although, BNT162b2 can cause a more hypermetabolic axillary lymph node than CoronaVac vaccine in parallel to its higher immunogenicity, to comment on serological antibody titer-related vaccine efficacy for COVID-19 infection is beyond the scope of the results of our study.

In a study by Eshet et al. (36), avid axillary lymphadenopathy was observed up to 7-10 weeks after the booster dose of BNT162b2 vaccination. In our study, ipsilateral axillary lymph node hypermetabolism was observed up to 7th and 9th week after the single and booster doses, respectively. Additionally, after the single and booster doses, ipsilateral axillary lymph node hypermetabolism was most frequently seen within the first month after vaccination and detected in 91.65% and 75% of patients, respectively. Further, after the single and booster dose, ipsilateral axillary lymph node hypermetabolism was most frequently seen within the first week after vaccination and detected in 35.41% and 32.5% of patients, respectively. Although postponing the ¹⁸F-FDG PET/CT study for a few weeks after COVID-19 vaccination reduces the possibility of ipsilateral hypermetabolic axillary lymph nodes, it cannot be completely prevented according to the results. Additionally, it should also be considered that long-term delay of ¹⁸F-FDG PET/CT study may adversely affect patient management.

Study Limitations

The main limitations of the study are the retrospective design, the inaccessibility to the vaccination records and patient histories of all patients who underwent ¹⁸F-FDG PET/CT. Axillary lymph nodes were not examined histopathologically due to invasive procedure. These studies were not repeated to follow-up the hypermetabolic axillary lymph nodes. Additionally, the association between vaccine-specific immune response and axillary lymph node hypermetabolism could not be investigated because to the lack of serological tests.

Conclusion

In our study population, ¹⁸F-FDG PET/CT detected ipsilateral axillary lymph node hypermetabolism in 11% and 41.6% of cancer patients receiving the inactivated SARS-CoV-2 vaccine and the novel mRNA-based COVID-19 vaccine, respectively. Although, the number of days after vaccination and age were negatively associated with ipsilateral axillary lymph node hypermetabolism, vaccination of booster dose was positively associated with ipsilateral axillary lymph node hypermetabolism. Additionally, BNT162b2 vaccination showed a positive relationship with ipsilateral axillary lymph node hypermetabolism. To avoid misinterpretation and unnecessary invasive procedures, it is necessary to enquire the COVID-19 vaccination history, particularly in young adults who received the booster dose of BNT162b2 vaccination recently. Although, misinterpretation of ¹⁸F-FDG PET/CT and further unnecessary invasive procedures could be reduced when "DS" was observed, in cases with only ipsilateral axillary lymph node hypermetabolism, vaccination

history based follow-up and correlation with other imaging modalities would be useful to avoid misinterpretation. In cancer patients who have tumors with a predilection for axillary lymph node involvement, it would be useful to perform vaccination in the contralateral arm, which is away from the tumoral nodal drainage zone. Ipsilateral axillary lymph node hypermetabolism was most frequently observed within the first month after vaccination. Postponing the ¹⁸F-FDG PET/CT study for a few weeks after COVID-19 vaccination reduces the possibility of ipsilateral hypermetabolic axillary lymph nodes. According to our results, the visualization of hypermetabolic axillary lymph nodes cannot be completely prevented as it can be seen up to 7th and 9th week after the single and booster dose. It should also be considered that long-term delays in ¹⁸F-FDG PET/CT study may adversely affect patient management. The results of our study reflect the different immunogenic properties and effects of CoronaVac and BNT162b2 vaccines via ¹⁸F-FDG hypermetabolism. BNT162b2 can cause more hypermetabolic axillary lymph nodes than CoronaVac vaccine in parallel to its higher immunogenicity. Prospective ¹⁸F-FDG PET/CT studies with specific serological antibody titers must evaluate the efficacy of vaccines against COVID-19 infection via ¹⁸F-FDG hypermetabolism.

Acknowledgments

We thank Nur Aydınbelge-Dizdar MD, Semra İnce MD, Kürşat Okuyucu MD, Aslı Ayan MD, Alev Noyaner Çınar MD, Alper Özgür Karaçalıoğlu MD, Bengül Günalp MD, Aylin Çomak MD for their contribution in routine ¹⁸F-FDG PET/CT reporting. In addition, we thank to Beyza Bedi MD and Serhan Mahmudov MD especially and nuclear medicine residency students for filling in the routine medical history forms.

Ethics

Ethics Committee Approval: This retrospective study was conducted with the approval of the University of Health Sciences Turkey, Gulhane Scientific Research Ethics Committee of our institution (decision no: 2021/297).

Informed Consent: Informed consent for using medical images was provided from the patients.

Peer-review: Internally peer-reviewed.

Authorship Contributions

Surgical and Medical Practices: H.Ş., E.A., Concept: H.Ş., E.A., Design: H.Ş., E.A., Data Collection or Processing: H.Ş., E.A., Analysis or Interpretation: H.Ş., E.A., Literature Search: H.Ş., E.A., Writing: H.Ş., E.A.

Conflict of Interest: No conflict of interest was declared by the authors.

Financial Disclosure: The authors declared that this study has received no financial support.

References

- Uddin M, Mustafa F, Rizvi TA, Loney T, Suwaidi HA, Al-Marzouqi AH, Eldin AK, Alsabeeha N, Adrian TE, Stefanini C, Nowotny N, Alsheikh-Ali A, Senok AC. SARS-CoV-2/COVID-19: viral genomics, epidemiology, vaccines, and therapeutic interventions. *Viruses* 2020;12:526.
- Ashour HM, Elkhatib WF, Rahman MM, Elshabrawy HA. Insights into the recent 2019 Novel Coronavirus (SARS-CoV-2) in light of past human coronavirus outbreaks. *Pathogens* 2020;9:186.
- World Health Organization, WHO. WHO Director-General's Opening Remarks at the Media Briefing on COVID-19—11 March 2020. Available from: <https://www.who.int/dg/speeches/detail/who-director-generals-opening-remarks-at-the-media-briefing-on-covid-19-11-march-2020> (accessed on 15.03.2022).
- Mandal A, Singh P, Samaddar A, Singh D, Verma M, Rakesh A, Ranjan R. Vaccination of cancer patients against COVID-19: towards the end of a dilemma. *Med Oncol* 2021;38:92.
- COVID-19 Public Health Emergency of International Concern (PHEIC) Global research and innovation forum. Available from: [https://www.who.int/publications/m/item/covid-19-public-health-emergency-of-international-concern-\(pheic\)-global-research-and-innovation-forum#:~:text=On%2030%20January%202020%20following,of%20International%20Concern%20\(PHEIC\)](https://www.who.int/publications/m/item/covid-19-public-health-emergency-of-international-concern-(pheic)-global-research-and-innovation-forum#:~:text=On%2030%20January%202020%20following,of%20International%20Concern%20(PHEIC)) (accessed on 15.03.2022).
- Klimek L, Agache I, Cooke E, Jutel M, Akdis CA, O'Hehir R. COVID-19 vaccines-The way forward. *Allergy* 2022;77:15-16.
- COVID-19 advice for the public: Getting vaccinated. Available from: <https://www.who.int/emergencies/diseases/novel-coronavirus-2019/covid-19-vaccines/advice> (accessed on 15.03.2022).
- Coronavirus Vaccine Tracker, By Carl Zimmer, Jonathan Corum, Sui-Lee Wee and Matthew Kristoffersen Updated March 11. Available from: <https://www.nytimes.com/interactive/2020/science/coronavirus-vaccine-tracker.html> (accessed on 15.03.2022).
- Dai M, Liu D, Liu M, Zhou F, Li G, Chen Z, Zhang Z, You H, Wu M, Zheng Q, Xiong Y, Xiong H, Wang C, Chen C, Xiong F, Zhang Y, Peng Y, Ge S, Zhen B, Yu T, Wang L, Wang H, Liu Y, Chen Y, Mei J, Gao X, Li Z, Gan L, He C, Li Z, Shi Y, Qi Y, Yang J, Tenen DG, Chai L, Mucci LA, Santillana M, Cai H. Patients with cancer appear more vulnerable to SARS-CoV-2: a multicenter study during the COVID-19 outbreak. *Cancer Discov* 2020;10:783-791.
- Ribas A, Sengupta R, Locke T, Zaidi SK, Campbell KM, Carethers JM, Jaffee EM, Wherry EJ, Soria JC, D'Souza G; AACR COVID-19 and Cancer Task Force. Priority COVID-19 vaccination for patients with cancer while vaccine supply is limited. *Cancer Discov* 2021;11:233-236.
- CoronaVac(Sinovac) package leaflet. Available from: https://www.covidvaccine.gov.hk/pdf/CoronaVac_ENG_PI_brief.pdf (accessed on 15.03.2022).
- Lamb YN. BNT162b2 mRNA COVID-19 vaccine: first approval. *Drugs* 2021;81:495-501.
- Eifer M, Tau N, Alhoubani Y, Kanana N, Domachevsky L, Shams J, Keret N, Gorfine M, Eshet Y. COVID-19 mRNA vaccination: age and immune status and its association with axillary lymph node PET/CT uptake. *J Nucl Med* 2022;63:134-139.
- Sahin O. Hypermetabolic axillary lymphadenopathy on FDG PET/CT Due to COVID-19 vaccination. *Selcuk Med J* 2021;37:269-275.
- Thomassen A, Lerberg Nielsen A, Gerke O, Johansen A, Petersen H. Duration of ¹⁸F-FDG avidity in lymph nodes after pandemic H1N1v and seasonal influenza vaccination. *Eur J Nucl Med Mol Imaging* 2011;38:894-898.
- Orevi M, Chicheportiche A, Ben Haim S. Lessons learned from post-COVID-19 vaccination PET/CT studies. *J Nucl Med* 2022;63:453-460.
- European Medicines Agency. Covid-19 mRNA vaccine (Comirnaty): EU summary of product characteristics. 2020. Available from: <https://www.ema.europa.eu/en/medicines/human/EPAR/comirnaty> (accessed 15.03.2022).
- European Medicines Agency. Comirnaty: CHMP public assessment report. 2020. Available from: <http://www.ema.europa.eu> (accessed 15.03.2022).
- Sahin U, Muik A, Vogler I, Derhovanessian E, Kranz LM, Vormehr M, Quandt J, Bidmon N, Ulges A, Baum A, Pascal K, Maurus D, Brachtendorf S, Lörks V, Sikorski J, Koch P, Hilker R, Becker D, Eller AK, Grütznert J, Tonigold M, Boesler C, Rosenbaum C, Heesen L, Kühnle MC, Poran A, Dong JZ, Luxemburger U, Kemmer-Brück A, Langer D, Bexon M, Bolte S, Palanche T, Schultz A, Baumann S, Mahiny AJ, Boros G, Reinholz J, Szabó GT, Karikó K, Shi PY, Fontes-Garfias C, Perez JL, Cutler M, Cooper D, Kyratsous CA, Dormitzer PR, Jansen KU, Türeci Ö. BNT162b2 induces SARS-CoV-2-neutralising antibodies and T cells in humans. doi: <https://doi.org/10.1101/2020.12.09.20245175>
- Mok CKP, Cohen CA, Cheng SMS, Chen C, Kwok KO, Yiu K, Chan TO, Bull M, Ling KC, Dai Z, Ng SS, Lui GC, Wu C, Amarasinghe GK, Leung DW, Wong SYS, Valkenburg SA, Peiris M, Hui DS. Comparison of the immunogenicity of BNT162b2 and CoronaVac COVID-19 vaccines in Hong Kong. *Respirology* 2022;27:301-310.
- Bettini E, Locci M. SARS-CoV-2 mRNA Vaccines: immunological mechanism and beyond. *Vaccines (Basel)* 2021;9:147.
- Cohen D, Hazut Krauthammer S, Cohen YC, Perry C, Avivi I, Herishanu Y, Even-Sapir E. Correlation between BNT162b2 mRNA Covid-19 vaccine-associated hypermetabolic lymphadenopathy and humoral immunity in patients with hematologic malignancy. *Eur J Nucl Med Mol Imaging* 2021;48:3540-3549.
- Lederer K, Castaño D, Gómez Atria D, Oguin TH, Wang S, Manzoni TB, Muramatsu H, Hogan MJ, Amanat F, Cherubin P, Lundgreen KA, Tam YK, Fan SHY, Eisenlohr LC, Maillard I, Weissman D, Bates P, Krammer F, Sempowski GD, Pardi N, Locci M. SARS-CoV-2 mRNA vaccines foster potent antigen-specific germinal center responses associated with neutralizing antibody generation. *Immunity* 2020;53:1281-1295.e5.
- Ellebedy A, Turner J, O'Halloran J, Kalaidina E, Kim W, Schmitz A, Lei T, Thapa M, Case J, Amanat F, Raouf A, Haile A, Klebert M, Suessen T, Middleton W, Krammer F, Teefey S, Diamond M, Presti R, Xie X, Shi PY. SARS-CoV-2 mRNA vaccines induce a robust germinal center reaction in humans. Available from: https://assets.researchsquare.com/files/rs-310773/v1_covered.pdf?c=1637595722
- Turner JS, O'Halloran JA, Kalaidina E, Kim W, Schmitz AJ, Zhou JQ, Lei T, Thapa M, Chen RE, Case JB, Amanat F, Raouf AM, Haile A, Xie X, Klebert MK, Suessen T, Middleton WD, Shi PY, Krammer F, Teefey SA, Diamond MS, Presti RM, Ellebedy AH. SARS-CoV-2 mRNA vaccines induce persistent human germinal center responses. *Nature* 2021;596:109-113.
- Bitterman R, Eliakim-Raz N, Vinograd I, Zalmanovici Trestioreanu A, Leibovici L, Paul M. Influenza vaccines in immunosuppressed adults with cancer. *Cochrane Database Syst Rev* 2018;2:CD008983.
- Venkatesulu B, Chandrasekar VT, Girdhar P, Advani P, Sharma A, Elumalai T, Hsieh CE, Elghazawy HI, Verma V, Krishnan S. A systematic review and meta-analysis of cancer patients affected by a novel coronavirus. *JNCI Cancer Spectr* 2021;5:pkaa102.
- Sengar M, Chinnaswamy G, Ranganathan P, Ashok A, Bhosale S, Biswas S, Chaturvedi P, Dhamne C, Divatia J, D'Sa K, Jain H, Laskar S, Moulik NR, Mummudi N, Nair S, Nayak L, Nayak P, Patkar S, Pawaskar P, Ramaswamy A, Shetty O, Singh A, Sridhar E, Thorat J, Badwe R, Pramesh CS; TMH COVID-19 action group. Outcomes of COVID-19 and risk factors in patients with cancer. *Nat Cancer* 2022;3:547-551.

29. GLOBOCAN 2020: New Global Cancer Data | UICC. Available from: <https://www.uicc.org/news/globocan-2020-new-global-cancer-data> (accessed 15.03.2022).
30. Giesen N, Sprute R, Rüttrich M, Khodamoradi Y, Mellinghoff SC, Beutel G, Lueck C, Koldehoff M, Hentrich M, Sandherr M, von Bergwelt-Baildon M, Wolf HH, Hirsch HH, Wörmann B, Cornely OA, Köhler P, Schalk E, von Lilienfeld-Toal M; COVID-19 guideline panel of the Infectious Diseases Working Party (AGIHO) of the German Society for Haematology and Medical Oncology (DGHO). 2021 update of the AGIHO guideline on evidence-based management of COVID-19 in patients with cancer regarding diagnostics, viral shedding, vaccination and therapy. *Eur J Cancer* 2021;147:154-160.
31. Fendler A, de Vries EGE, GeurtsvanKessel CH, Haanen JB, Wörmann B, Turajlic S, von Lilienfeld-Toal M. COVID-19 vaccines in patients with cancer: immunogenicity, efficacy and safety. *Nat Rev Clin Oncol* 2022;19:385-401.
32. Cohen D, Krauthammer SH, Wolf I, Even-Sapir E. Hypermetabolic lymphadenopathy following administration of BNT162b2 mRNA Covid-19 vaccine: incidence assessed by [¹⁸F]FDG PET-CT and relevance to study interpretation. *Eur J Nucl Med Mol Imaging* 2021;48:1854-1863.
33. Brockman MA, Mwimanzi F, Lapointe HR, Sang Y, Agafitei O, Cheung PK, Ennis S, Ng K, Basra S, Lim LY, Yaseen F, Young L, Umvilighozo G, Omondi FH, Kalikawe R, Burns L, Brumme CJ, Leung V, Montaner JSG, Holmes D, DeMarco ML, Simons J, Pantophlet R, Niikura M, Romney MG, Brumme ZL. Reduced magnitude and durability of humoral immune responses to COVID-19 mRNA vaccines among older adults. *J Infect Dis* 2022;225:1129-1140.
34. Castle SC. Clinical relevance of age-related immune dysfunction. *Clin Infect Dis* 2000;31:578-585.
35. Sgonc R, Gruber J. Age-related aspects of cutaneous wound healing: a mini-review. *Gerontology* 2013;59:159-164.
36. Eshet Y, Tau N, Alhoubani Y, Kanana N, Domachevsky L, Eifer M. Prevalence of increased FDG PET/CT axillary lymph node uptake beyond 6 weeks after mRNA COVID-19 vaccination. *Radiology* 2021;300:E345-E347.



Comparison of Planar Imaging Using Dual-phase Tc-99m-sestamibi Scintigraphy and Single Photon Emission Computed Tomography/Computed Tomography in Hyperparathyroidism

Hiperparatiroidizmde Çift Fazlı Tc-99m-sestamibi Planar Görüntüleme Sintigrafisi ve Tek Foton Emisyonlu Bilgisayarlı Tomografi/Bilgisayarlı Tomografi Karşılaştırılması

Halim Özçevik¹, Müge Öner Tamam², Mehmet Tarık Tatoğlu³, Mehmet Mülazımoğlu²

¹University of Health Sciences Turkey, Hamidiye Faculty of Medicine, Department of Nuclear Medicine, İstanbul, Turkey

²University of Health Sciences Turkey, Prof. Dr. Cemil Taşcıoğlu City Hospital, Clinic of Nuclear Medicine, İstanbul, Turkey

³Göztepe Prof. Dr. Süleyman Yalçın City Hospital, Clinic of Nuclear Medicine, İstanbul, Turkey

Abstract

Objectives: The aim of this study was to compare Technetium-99m (Tc-99m)-sestamibi dual-phase planar imaging method and delayed phase single photon emission computed tomography/computed tomography (SPECT/CT) imaging in patients with primary hyperparathyroidism and to evaluate the accuracy of scintigraphy with histopathological results.

Methods: Thirty-six patients with a prediagnosis of hyperparathyroidism, who had not been operated on the neck region before, and were not followed up for any other malignancy, and has confirmed histopathologic and biochemical diagnosis after parathyroidectomy, were retrospectively scanned and included in the study. The images of 36 patients who underwent dual-phase Tc-99m-sestamibi planar scintigraphy at the 20th and 120th minutes in the nuclear medicine clinic and delayed phase SPECT/CT imaging immediately after the 120th minute planar imaging were evaluated visually by two nuclear medicine specialists as positive or negative lesion. Dual-phase planar and SPECT/CT images were statistically compared in terms of sensitivity, specificity, positive predictive value, negative predictive value, and accuracy.

Results: Thirty-six patients with 41 lesions were evaluated. Comparing dual-phase planar imaging and delayed phase SPECT/CT revealed, sensitivity 84.21%-94.74%, specificity 66.67%-66.67%. Positive predictive value 96.97%-97.30%, negative predictive value 25%-50.0%, accuracy 82.93%-92.68% respectively. There was a statistically significant difference between planar imaging and SPECT/CT; SPECT/CT localized the lesion more accurately (p<0.05).

Conclusion: SPECT/CT is superior to planar imaging in determining the anatomical details and localization of the lesion, especially in determining the depth of the lesions in the neck and whether it is ectopic. In patients with hyperparathyroidism, SPECT/CT should be used routinely to detect parathyroid pathologies because it has a lower rate of error and higher accuracy rate.

Keywords: SPECT, SPECT/CT, hyperparathyroidism, parathyroid scintigraphy

Öz

Amaç: Bu çalışmanın amacı primer hiperparatiroidilli hastalarda Teknesyum-99m (Tc-99m)-sestamibi çift faz planar görüntüleme yöntemi ile geç faz tek foton emisyonlu bilgisayarlı tomografi/bilgisayarlı tomografi (SPECT/CT) görüntülemenin karşılaştırılması ve histopatolojik sonuçları ile sintigrafinin doğruluğunun değerlendirilmesidir.

Address for Correspondence: Asst. Prof. Halim Özçevik MD, University of Health Sciences Turkey, Hamidiye Faculty of Medicine, Department of Nuclear Medicine, İstanbul, Turkey

Phone: +90 212 638 30 00 **E-mail:** hozcevik@gmail.com ORCID ID: orcid.org/0000-0001-7201-9868

Received: 20.02.2022 **Accepted:** 26.06.2022

©Copyright 2022 by Turkish Society of Nuclear Medicine
Molecular Imaging and Radionuclide Therapy published by Galenos Yayınevi.

Yöntem: Hiperparatiroidi ön tanısı alan, daha önce boyun bölgesinden opere olmamış, 10 malignite nedeniyle takip edilmeyen, paratiroid cerrahisi uygulanarak patolojik incelemesi yapılan 36 olgu retrospektif taranarak çalışmaya dahil edildi. Nükleer tıp kliniğinde 20. ve 120. dakikada çift faz Tc-99m-sestamibi planar sintigrafisi ve 120. dakikadaki planar görüntülemenin hemen ardından geç faz SPECT/BT görüntülemesi yapılan 36 olgunun görüntüleri iki nükleer tıp uzmanı tarafından lezyon pozitif veya negatif şeklinde vizüel olarak değerlendirildi. Çift faz planar ve SPECT/BT görüntüleri duyarlılık, özgünlük, pozitif tahmin edici değer, negatif tahmin edici değer ve doğruluk açısından istatistiksel olarak karşılaştırıldı.

Bulgular: Otuz altı hastada cerrahi sonrası bulunan 41 lezyon değerlendirildiğinde çift faz planar görüntüleme ile geç faz SPECT/BT'nin karşılaştırılmasında sırayla duyarlılığı %84,21-%94,74, özgünlüğü %66,67-%66,67 Pozitif prediktif değeri %96,97-%97,30 negatif prediktif değeri %25-%50,0 doğruluk %82,93-20 %92,68 olarak bulunmuştur. Planar görüntüleme ile SPECT/BT arasında incelemede istatistiksel olarak anlamlı farklılık görülmektedir ($p<0,05$).

Sonuç: SPECT/BT, lezyonun anatomik detaylarını ve lokalizasyonunu belirlemede, özellikle lezyonun boyundaki derinliğini ve ektopik olup olmadığını belirlemede planar görüntülemeye üstündür. Hiperparatiroidizmlı hastalarda SPECT/BT'nin hata payı daha düşük, doğruluk oranı daha yüksek olduğundan paratiroid patolojilerini saptamak için rutin olarak kullanılmalıdır.

Anahtar kelimeler: SPECT, SPECT/BT, hiperparatiroidi, paratiroid sintigrafisi

Introduction

Primary hyperparathyroidism is the most common pathology of the parathyroid glands and is one of the most common endocrine disorders overall, usually resulting from solitary parathyroid adenoma, less frequently from multiple parathyroid gland disease, and rarely from parathyroid carcinoma (1). The diagnosis of primary hyperparathyroidism is diagnosed biochemically, and the only curative treatment is surgery (2).

Today, most patients do not have the classic symptoms or signs associated with primary hyperparathyroidism at the time of diagnosis and are diagnosed as asymptomatic or minimally symptomatic. With the introduction of routine serum calcium measurements, a significant increase in the incidence of primary hyperparathyroidism, which is mostly asymptomatic, has been observed. Parathyroid scintigraphy has proven to be a superior imaging modality for the preoperative localization of parathyroid adenomas (3,4). The main nuclear medicine method used in parathyroid imaging is dual-phase Technetium-99m-2-hexakis-methoxy-isobutyl-isonitrile (Tc-99m-sestamibi) imaging (5). Single photon emission computed tomography/computed tomography (SPECT/CT) is particularly useful for preoperative localization because it can evaluate the effectiveness of parathyroid adenoma localization in relation to adjacent anatomical structures and the depth in the neck or mediastinum.

The aim of this study was to compare Tc-99m-sestamibi dual-phase planar imaging method to delay SPECT/CT imaging in patients with primary hyperparathyroidism, to investigate whether it contributes in terms of accuracy, sensitivity, specificity, positive and negative predictive value (NPV), and to evaluate the accuracy of scintigraphy compared to histopathological results.

Materials and Methods

The images of 36 patients who applied to the Nuclear Medicine Clinic of Okmeydani Training and Research Hospital for dual-phase Tc-99m-sestamibi parathyroid scintigraphy due to primary hyperparathyroidism between March 2010 and March 2012 were evaluated retrospectively. Patients who were pre-diagnosed with hyperparathyroidism due to high parathyroid hormone (PTH) and calcium electrolyte levels in blood tests, and who underwent double-phase Tc-99m-sestamibi planar scintigraphy alongside delayed SPECT/CT examination in the Nuclear Medicine Clinic for localization, and who had a pathology report operated in the General Surgery Clinic of Okmeydani Training and Research Hospital were included in the study. Patients who had undergone previous neck surgery and were followed up for other malignancies, patients with secondary hyperparathyroidism due to chronic renal disease, patients who received parathyroidectomy more than 6 months after the scintigraphy, patients who had persistently rising intact PTH levels after surgery without compatible pathological findings of parathyroidectomy for hyperfunctioning parathyroid tissue, and patients with unavailable SPECT/CT data were excluded from the study.

Approximately 20 min after the intravenous injection of 20-25 mCi (740-925 MBq) Tc-99m-sestamibi, static images from the neck and mediastinum region, 2nd hour static images and 2nd hour SPECT/CT images were obtained in the anterior position of all patients.

Imaging Protocol

Imaging of all patients was performed using an Infinia Hawkeye 4 (General Electric Medical Systems, Milwaukee, WI) dual-headed SPECT/CT imaging system, which is a hybrid imaging technology. Planar images were recorded in a 128x128 matrix with a wide range of view, low-energy, high-resolution, parallel-hole collimator with a zoom value

of 2.5, peak energy level of 140 KeV and window spacing of 10%. With SPECT imaging, 60 images, each image for 30 seconds, was obtained at 360 degrees with a wide range of view, low energy, high resolution parallel hole collimator with peak energy level of 140 KeV, window interval of 10%, 128x128 matrix in 6 degree step and shoot mode. SPECT images were processed in Xeleris (General Electric Medical Systems, Milwaukee, WI) workstation.

After filtering with the Hann preconstruction filter, it was reconstructed with the 2-dimensional ordered-subset expectation maximization image refresh technique. Fusion images were obtained by combining SPECT images with computer attenuation correction and CT images. Areas with radiopharmaceutical involvement in SPECT/CT images on transverse, coronal, sagittal sections and 3D images were evaluated about whether they were synchronized and reported as negative or positive activity uptake.

Evaluation of Planar Imaging

Firstly, the homogeneity of the activity distribution in the early phase when the parathyroid and thyroid gland was observed together, and whether focal increased activity uptake compared to the thyroid tissue was investigated. Then, the early phase images were compared with the delayed phase images, and it was checked whether there was a persistent activity involvement that was not free from sestamibi activity. The results were recorded as negative or positive activity uptake and in terms of localization.

Evaluation of SPECT/CT Scintigraphy

Fusion images were obtained by combining SPECT images with attenuation correction by computer and CT images. Areas with radiopharmaceutical involvement in SPECT/CT images on transverse, coronal, sagittal sections and 3D images were evaluated about whether they were synchronized and reported as negative or positive activity uptake.

Evaluation of Images

Planar and SPECT/CT images were evaluated by two nuclear medicine specialists, unaware of each other. Nuclear medicine scintigraphic images of the patients were evaluated unaware of their clinical information, laboratory values and radiological imaging methods. The evaluations made by both experts were recorded as lesion positive and lesion negative. Localization of the lesions was recorded in a separate table. The images that were interpreted differently by the two experts were re-interpreted by the experts, and the positive or negative status of the lesion and the localization information were recorded.

Ethics Committee Approval

The study was approved by the Sisli Etfal Training and Research Hospital Clinical Research Ethics Committee (05/06/2012/89). All procedures performed in the studies involving human participants were in accordance with the ethical standards of the institutional research committee and with the 1964 Helsinki declaration and its later amendments or comparable ethical standards. All patients gave their informed consent before inclusion in the study.

Statistical Analysis

The NCSS (Number Cruncher Statistical System) 2007&PASS (Power Analysis and Sample Size) 2008 Statistical Software (Utah, USA) program was used for statistical analysis. While evaluating the study data, in addition to descriptive statistical methods (mean, standard deviation, frequency, rate), Mc-Nemar test and diagnostic screening tests (sensitivity, specificity, etc.) were used to compare the qualitative data of two separate tests. The Wilcoxon Signed Rank test was used to evaluate the difference between planar imaging and SPECT/CT imaging. Statistical significance was evaluated at the $p < 0.05$ level in all comparisons. Considering all healthy and diseased parathyroid glands, true positive (TP), true negative (TN), false positive (FP), and false negative (FN) variables were used. Sensitivity, specificity, positive predictive value (PPV), NPV, and accuracy were calculated.

Results

The patients were between the ages of 17-76. The mean age was 50.91 ± 13.39 years. Six (16.7%) of 36 patients were male and 30 (83.3%) were female.

Table 1 shows the "positive" and "negative" distributions of the lesions in pathology, planar imaging and SPECT/CT. Of the lesions, 92.7% were found to be positive on pathology, 80.5% on planar imaging, and 90.2% on SPECT/CT (Graph 1).

The comparison of pathology results and planar imaging results revealed that, pathology identified 92.7% of the

	Lesion	n	%
Pathology	Positive	38	92.7
	Negative	3	7.3
Planar imaging	Positive	33	80.5
	Negative	8	19.5
SPECT/CT	Positive	37	90.2
	Negative	4	9.8
SPECT/CT: Single photon emission computed tomography/computed tomography			

lesions, whereas the planar imaging method detected 80.5% of the lesions (Table 2). There was no significant difference between planar imaging and pathology results ($p>0.05$). Of 38 (92.7%) patients diagnosed with lesion by pathology, 32 (78%) were also diagnosed with a lesion on planar imaging. The sensitivity, specificity, PPV, NPV, and accuracy of planar imaging were 84.21%, 66.67%, 96.97%, 25%, and 82.93%, respectively.

When the distribution of the lesions in pathology and planar imaging evaluations were examined, two lesions detected in one patient were both lesion (+) in pathology, one of the two lesions was evaluated as lesions (+) and the other lesion (-) in planar imaging. Both lesions detected in one patient were lesion (+) in pathology, both were evaluated as the lesion (-) in planar imaging. Both lesions detected in the two patients were lesion (+) in pathology, both were evaluated as the lesion (-) in planar imaging. One of the two lesions detected in one patient was evaluated as lesions (+) in pathology and the other as lesions (-) in pathology, and both lesions were evaluated as lesions (-) by planar imaging. A lesion detected in one patient was evaluated as lesions (-) in both pathology and planar

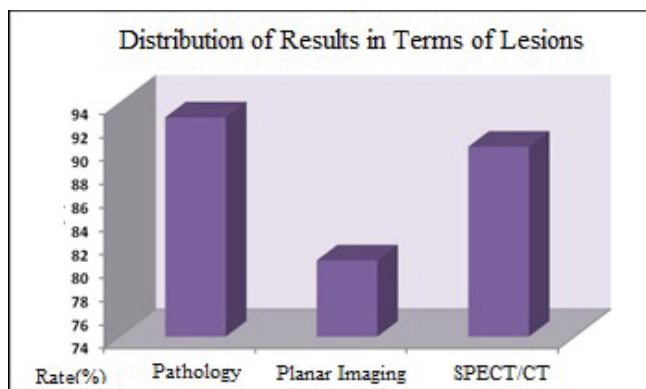
imaging. Two lesions detected in one patient were both evaluated as lesions (+) in pathology and planar imaging (Table 3) (Figures 1A, B, 2A, B).

The evaluation of the pathology results and SPECT/CT imaging results together revealed that lesions were detected in 92.7% of the patients with pathology, while lesions were detected in 90.2% of the patients with SPECT/CT (Table 4). The comparison of SPECT/CT results with the pathology results showed no significant difference between the two measurement methods ($p>0.05$). Lesions were positive in 36 (87.8%) patients in pathology and 38 (92.7%) of the patients in SPECT and were negative in the rest of the patients. The sensitivity, specificity, PPV, NPV, and accuracy of SPECT/CT was 94.74, 66.67, 97.30, 50.0, and 92.68%, respectively.

When planar imaging and SPECT/CT imaging were evaluated together on a lesion basis, 36 lesions were evaluated as TP in SPECT/CT imaging and 32 lesions in planar imaging. Four lesions were evaluated as FN only in planar imaging. Two lesions were evaluated as FN in planar imaging and SPECT/CT imaging. One lesion was evaluated as FP in planar imaging and SPECT/CT imaging. Two lesions were evaluated as TN in planar imaging and SPECT/CT imaging. SPECT/CT imaging detected four parathyroid lesions that could not be detected on planar imaging (Table 4).

There was a statistically significant difference in terms of the examination between planar imaging and SPECT/CT ($p<0.05$ Wilcoxon signed-rank test). SPECT/CT results were closer to the pathological results. The margin of error was found to be lower and the accuracy rate was higher.

When the patients were analyzed according to the surgical procedures performed, parathyroidectomy was performed together with thyroidectomy in 14 patients. In the other 22 patients, only the parathyroid gland underwent surgery.



Graph 1. Distribution of results in terms of lesions

		Pathology						p
		Lesion (+)		Lesion (-)		Total		
		n	%	n	%	n	%	
Planar imaging	Lesion (+)	32	78.0	1	2.4	33	80.5	0.125
	Lesion (-)	6	14.6	2	4.9	8	19.5	
	Total	38	92.7	3	7.3	41	100	
Sensitivity		84.21						
Specificity		66.67						
Positive predictive value		96.97						
Negative predictive value		25.00						
Accuracy		82.93						

Table 3. Distribution of planar imaging and SPECT/CT imaging results with surgical procedure and histopathology results

	Planar imaging	SPECT/CT imaging	Surgical procedure	Histopathology
1	LLQ+	LLQ+	Parathyroidectomy (L)	Parathyroid adenoma
2	LLQ+	LLQ+	Parathyroidectomy (L)	Parathyroid adenoma
3	LLQ+	LLQ+	Parathyroidectomy (L)	Parathyroid adenoma
4	RLQ+	RLQ (retrotracheal mediastinal area)	Thyroid lobectomy (R)+ parathyroidectomy (R)	Parathyroid hyperplasia +NG
5	LLQ+	LLQ (retrotracheal area)+	Parathyroidectomy (L)+ TT	Parathyroid adenoma +MNG
6	RLQ+	RLQ and LLQ+	Parathyroidectomy+ TT	Parathyroid adenoma (R) + Parathyroid hyperplasia (L)+ MTC
7	RQ+	RQ (posterior prevertebral area)	Parathyroidectomy (R)	Parathyroid adenoma
8	Negative	LLQ+	Parathyroidectomy	Parathyroid adenoma
9	LLQ+	LLQ+	Parathyroidectomy	Parathyroid adenoma
10	RLQ+	RLQ+	Parathyroidectomy+ TT	Parathyroid adenoma
11	RLQ+	RLQ+	Parathyroidectomy (R)+ TT	Parathyroid adenoma + MNG
12	LLQ+	LLQ+	Parathyroid mass excision	Parathyroid carcinoma
13	LUQ+	LUQ+	Parathyroidectomy (L)	Parathyroid adenoma
14	RUQ+	RUQ+	Thyroid lobectomy (R)+ parathyroidectomy (R)+	Parathyroid adenoma+ NG
15	LLQ+	LLQ+	Parathyroidectomy (L)	Parathyroid adenoma
16	Ectopic in midline mediastinum +	Ectopic in midline mediastinum (midclavicular area)+	Parathyroidectomy (mediastinum)	Parathyroid hyperplasia and thymus tissue
17	LLQ+	LLQ (paratracheal area)	Parathyroidectomy (L)	Parathyroid adenoma
18	RLQ+	RLQ+	Parathyroidectomy (R)+ TT	Parathyroid adenoma (R) + PTC (R+L)
19	Negative	Negative	Parathyroidectomy (L)	Parathyroid adenoma
20	Negative	LLQ and RLQ+	Parathyroidectomy (R+L)	Parathyroid hyperplasia (R+L)
21	LLQ+	LLQ+	Parathyroidectomy (L)	Parathyroid adenoma
22	RLQ+	RLQ+	Parathyroidectomy (R)	Parathyroid adenoma
23	LLQ+	LLQ+	Parathyroidectomy (L)	Parathyroid adenoma
24	Negative	Negative	Parathyroidectomy+ TT	Parathyroid hyperplasia + normal parathyroid tissue + MTC
25	LLQ+	LLQ+	Parathyroidectomy (L)	Parathyroid adenoma
26	Ectopic in midline mediastinum+	Ectopic in midline mediastinum (retrosternal area)+	Parathyroidectomy (mediastinum)	Parathyroid adenoma
27	RLQ+	RLQ (retrotracheal area)+	Thyroid lobectomy (R)+ parathyroidectomy	Parathyroid adenoma + NG
28	Ectopic in midline mediastinum+	Ectopic in midline mediastinum (retrosternal area)+	Parathyroidectomy (mediastinum)+ TT	Parathyroid adenoma+ PTC
29	LLQ+	LLQ (posterior paratracheal area)+	Parathyroidectomy (L)	Parathyroid adenoma
30	LLQ+	LLQ (posterior paratracheal area)+	Parathyroidectomy (L)+ TT	Parathyroid Adenoma+ PTC
31	Ectopic in midline mediastinum+	Ectopic in midline mediastinum (retrosternal area)+	Parathyroidectomy (mediastinum)	Parathyroid adenoma
32	LLQ and RUQ+	LLQ and RUQ+	Parathyroidectomy (R+L)+ TT	Parathyroid adenoma (L) + WDT-UMP (R)
33	Negative	Negative	Parathyroidectomy+ TT	Normal parathyroid tissue + MTC
34	LLQ+	LLQ+	Parathyroidectomy (L)	Parathyroid adenoma
35	LLQ+	LLQ+	Parathyroidectomy (L)	Parathyroid adenoma
36	LLQ and RLQ+	LLQ and RLQ+	Parathyroidectomy (R+L)+ TT	Parathyroid adenoma (R+L)+ MNG

SPECT/CT: Single photon emission computed tomography/computed tomography, RUQ: Right upper quadrant, RLQ: Right lower quadrant, LUQ: Left upper quadrant, LLQ: Left lower quadrant, +: Positive, TT: Total thyroidectomy, MTC: Medullary thyroid carcinoma, NG: Nodular goiter, PTC: Papillary thyroid carcinoma, WDT-UMP: Well differentiated thyroid tumor of uncertain malignant potential

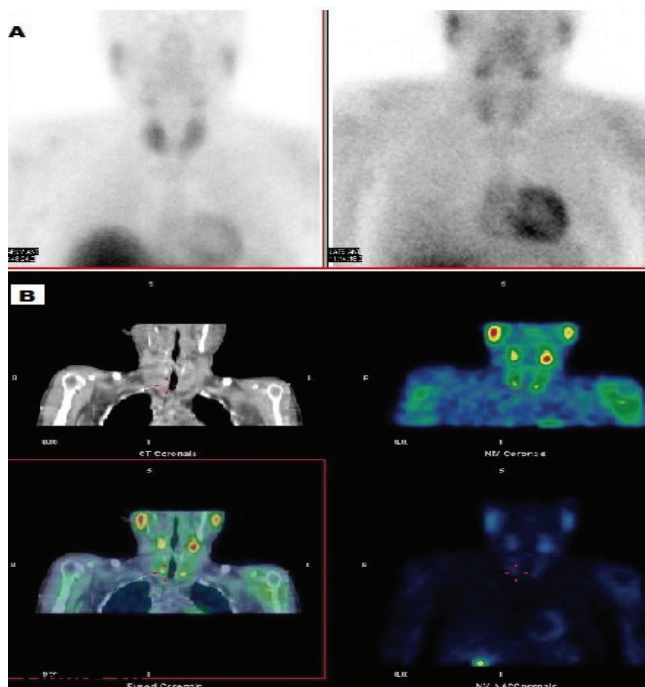


Figure 1. There was one lesion in the lower right pole in planar imaging (A), a lesion was also detected in the lower left pole in SPECT images, and the pathology report of both lesions was positive (B)
SPECT: Single photon emission computed tomography

Thyroid tumors were found in seven of 14 patients who underwent thyroid surgery, medullary carcinoma in three of them, papillary carcinoma in two, bilateral micropapillary carcinoma in one, and well-differentiated thyroid tumor in one with uncertain malignant potential. Benign thyroid pathologies were detected in the remaining seven patients. Out of 41 lesions detected in 36 patients, parathyroid hyperplasia was detected in six lesions (14.6%), parathyroid carcinoma in one lesion (2.43%), normal parathyroid tissue in two lesions (4.87%), parathyroid adenoma in 31 lesions (75.6%), and thyroid papillary carcinoma in one lesion (2.43%).

The lesion was mediastinal in four of eight patients with ectopic localized lesions, posterior to the trachea in three, and anterior to the vertebra in one patient. SPECT/CT provided information about ectopic locations, location, and neighborhood in each, and planar imaging provided information about ectopic location in four of these eight ectopic lesions but provided insufficient information about the location.

Of the three patients with double lesions, the lesion on the right was adenoma and the lesion on the left was hyperplasia in one patient, two lesions were hyperplasia in one patient, and two lesions were adenoma in another.

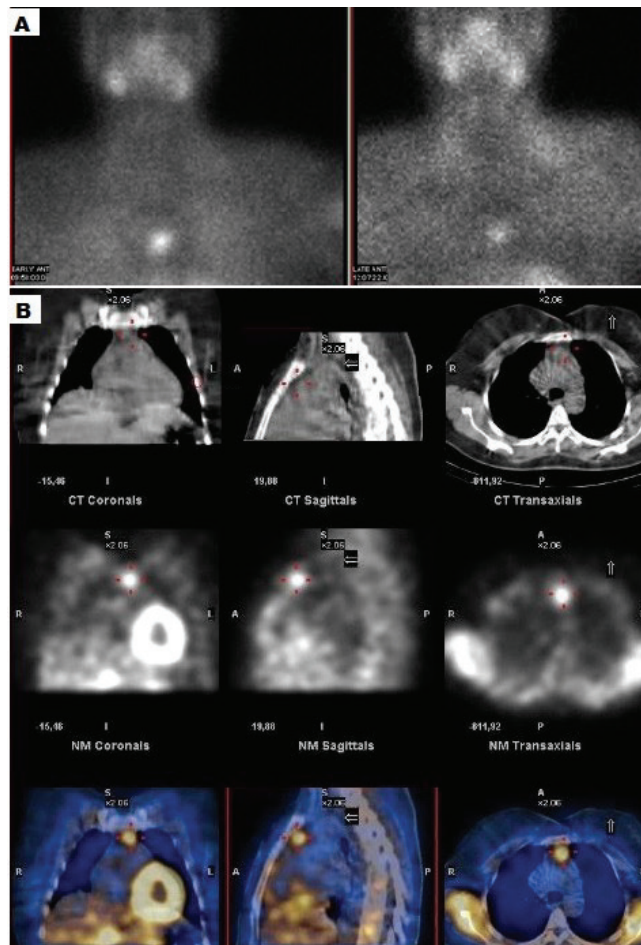


Figure 2. The lesion, which was detected intrathoracically in planar imaging (A), was localized in the anterior mediastinum in coronal, sagittal and axial SPECT/CT images (B)
SPECT/CT: Single photon emission computed tomography/computed tomography

		Pathology						p
		Lesion (+)		Lesion (-)		Total		
		n	%	n	%	n	%	
SPECT/CT	Lesion (+)	36	87.8	1	2.4	37	90.2	0.999
	Lesion (-)	2	4.9	2	4.9	4	9.8	
	Total	38	92.7	3	7.3	41	100	
Sensitivity		94.74						
Specificity		66.67						
Positive predictive value		97.30						
Negative predictive value		50.00						
Accuracy		92.68						
SPECT/CT: Single photon emission computed tomography/computed tomography								

Discussion

Pre-operative accurate localization has become extremely important in minimally invasive surgery in primary hyperparathyroidism. Preoperative imaging is important in distinguishing single-gland disease from multiglandular disease, in the differential diagnosis of co-existing thyroid pathology, and in defining ectopic parathyroid lesions (6).

Different scintigraphic methods and protocols have been defined for preoperative localization of hyperfunctioning parathyroid glands in studies conducted for many years. A wide variety of imaging protocols are available today. It explains the wide range of sensitivity reported in the literature, ranging from 70% to 95%, due to differences in protocols (7,8,9,10).

This study directly compared dual-phase Tc-99m-sestamibi planar imaging, which is frequently used in nuclear medicine clinics, and hybrid SPECT/CT imaging, one of the latest imaging methods, reporting statistical differences in terms of sensitivity, specificity, accuracy, PPV, and NPV.

Pre-operative accurate localization is required for successful minimally invasive parathyroid surgery. Because of embryological descent, the superior parathyroid glands tend to be located more posteriorly than the inferior parathyroid glands and are often located in the tracheoesophageal groove. In the ectopic infero-posterior location of superior parathyroids, surgery is often more complex because of its close relationship with the recurrent laryngeal nerve. Therefore, the use of SPECT/CT hybrid imaging in Tc-99m-sestamibi parathyroid scintigraphy is more useful in preoperative planning for minimally invasive surgery than planar and SPECT imaging. It is valuable in determining the surgical approach for the neck, particularly in ectopic glands and nodular thyroid diseases (9,10,11,12,13).

Among a wide variety of radiopharmaceutical and types of scintigraphic studies, SPECT improves the ability to detect lesions by providing superior contrast resolution compared with planar imaging. For parathyroid scintigraphy, many studies have reported that SPECT has 11-18% higher sensitivity than planar imaging (14,15,16).

SPECT is obtained in a single time interval, often early or delayed. Some studies in the literature have reported high sensitivity of 96% with an early SPECT (17,18). Civelek et al. (8) reported good sensitivity of 87% with delayed SPECT. Perez-Monte et al. (18), comparing delayed and early SPECT, found that early SPECT (91%) had higher sensitivity than delayed SPECT (74%), although no statistically significant difference was reported. Another study on early and delayed SPECT also showed that early SPECT tended to have higher sensitivity than delayed SPECT in parathyroid lesion localization; however, this trend did not reach a

statistically significant value, but dual-phase SPECT results were found to be statistically significantly superior to early or delayed single-phase SPECT results (13).

Hybrid SPECT/CT has the advantage of imaging in successive slices with the patient in the same position on the same imaging table. The hybrid system 2.5 mA low-resolution four-section CT scanner, which was used in this study, provided accurate anatomic localization with limited resolution in many patients. In the literature, some researchers have investigated the statistical contribution of SPECT/CT only to the diagnostic accuracy, and others have investigated the contribution of SPECT/CT to localization and surgery. The main purpose of our study was to investigate whether delayed-phase SPECT/CT contributed to the diagnostic accuracy of dual-phase planar imaging. In a study similar to this study, Huang et al. (19) performed dual-phase Tc-99m-sestamibi planar imaging at the 20th and 120th minutes and SPECT/CT imaging at the 90th minute in 27 patients. Compared with surgery results, they found 21 TP, four FP, four TN, and four FN results with planar imaging, and 22 TP, six FP, six TN, and three FN results with SPECT/CT. The sensitivity, specificity, and accuracy for SPECT/CT were 88%, 50%, and 75.7%, and 84%, and 50%, and 75.8% for planar imaging, respectively. It was found that the diagnostic accuracy of SPECT/CT did not differ statistically significantly from planar imaging (19). In our study, dual-phase Tc-99m-sestamibi planar imaging at the 20th and 120th minutes and SPECT/CT imaging at the 120th minute was performed in 36 patients. According to the surgical results of 41 lesions in 36 patients, 32 TP, one FP, two TN, and six FN results were found with planar imaging. With SPECT/CT, 36 TP, one FP, two TN, and two FN results were found. The sensitivity, specificity, and accuracy for SPECT/CT and planar imaging were 94.74%, 66.67%, and 92.68%, and 84.21%, 66.67%, and 82.93%, respectively. In our study, it was determined that the diagnostic accuracy of SPECT/CT was statistically significantly different from planar imaging ($p < 0.005$).

In a study by Lavelly et al. (13) in which 98 patients underwent early and delayed (dual-phase) imaging with planar, SPECT, and SPECT/CT, no significant difference was found between early SPECT/CT and dual-phase planar imaging in parathyroid lesion localization. However, dual-phase SPECT/CT was found to be statistically superior to single-phase SPECT/CT, dual-phase planar imaging, and dual-phase SPECT. The combination of early SPECT/CT with delayed SPECT or delayed planar imaging was also found to be statistically superior to dual-phase planar imaging or SPECT. In the study, the sensitivity values of dual-phase planar imaging and delayed-phase SPECT/CT imaging were 56.5% and 53.5%, specificity values were 98.7%

and 98.1%, PPVs were 79.0% and 75.8%, and NPVs were 96.4% and 96.2% (13). In our study, a lesion was evaluated as FP in both planar imaging and SPECT/CT imaging, resulting in decreased specificity. Additionally, the NPV was found to be low because the other intact parathyroid glands were not affected, and TN parathyroid glands could not be determined exactly because the intervention was made for pathological parathyroid glands during surgery.

In a meta-analysis in which 18 studies were evaluated, the sensitivity and PPV were 63% and 90% in planar scintigraphy, 66%, and 82% in SPECT, 84%, and 95% in SPECT/CT, respectively. SPECT/CT was found to be superior to the other two methods (20).

In the study by McCoy et al. (21), in which 1,388 patients were evaluated, 755 SPECT/CT and 633 SPECT examinations were compared. In 1,186 patients with solitary gland disease, SPECT/CT had higher sensitivity (96% vs. 91%), accuracy (83% vs. 77%), and PPV (90% vs. 85%) than SPECT. Although the rates of negative imaging in multigland disease were similar in both methods, the accuracy of SPECT/CT was found to be better than SPECT in predicting 202 patients with preoperative multigland disease (36% vs. 22%). Additionally, for multigland disease, the sensitivity (68% vs. 49%) and PPV (53% vs. 37%) of SPECT/CT were higher than in SPECT. They also stated that SPECT/CT provided a more reliable surgical guide in both single-gland and multi-gland disease (21).

A 48-patient study with hybrid SPECT/CT showed that the combination of dual-phase planar imaging and early SPECT with or without CT fusion confirmed 89% of the localization of parathyroid adenomas removed with surgery. The researchers concluded that the addition of CT fusion alone did not add value to SPECT. In another study of 36 patients, early SPECT/CT was performed only on patients whose planar imaging results were negative or diagnostically uncertain. It was shown that early SPECT/CT contributes to localization and surgical planning in 39% of patients (22).

Takami et al. (23) showed that localization of Tc-99m-sestamibi was impossible in delayed-phase images due to rapid excretion from parathyroid adenomas in 7% of patients with hyperparathyroidism in their study using Tc-99m-sestamibi dual-phase parathyroid scintigraphy. In another study, it was reported that Tc-99m-sestamibi caused false negativity in the delayed phase due to its early excretion from the parathyroid gland, particularly due to degeneration in hemorrhagic or large-hyperplastic parathyroid glands (24). Another factor thought to affect sestamibi uptake in parathyroid adenomas is the presence of P-glycoprotein or protein associated with multi-drug resistance in adenomas. There is insufficient sestamibi

uptake in adenomas with P-glycoprotein and this leads to FN results (25). In one patient in our study, a solitary parathyroid adenoma found in surgery could not be detected in either planar imaging or SPECT/CT imaging. This is a limitation of Tc-99m-sestamibi imaging methods with a single radionuclide.

MIBI uptake is related to cell function. Hence, some parathyroid lesions do not retain MIBI, whereas thyroid disease, lymphoma, lymph node diseases (lymph node metastatic disease, inflammation, and sarcoidosis) can lead to FP results. In our study, Thyroid tumors were found in seven of 14 patients who underwent thyroid surgery, medullary carcinoma in three of them, papillary carcinoma in two, bilateral micropapillary carcinoma in one, and well-differentiated thyroid tumor in one with uncertain malignant potential. Benign thyroid pathologies were detected in the remaining seven patients. SPECT/CT may decrease FP results attributable to thyroid nodules and FN results attributed to adenoma of a cystic nature or associated with concomitant thyroid nodules, which may go unidentified by scintigraphy (26). The failure of SPECT/CT to identify thyroid lesions may be associated with several factors, such as lesion size, resolution of the system, and amount of tracer uptake by thyroid tissue (27).

Study Limitations

Although SPECT/CT plays an important role in the diagnosis and location of parathyroid adenoma, evaluation together with ultrasonography would be more suitable for choosing an appropriate therapeutic regimen for identifying concomitant thyroid pathologies. Other limitations of our study were that: Our study was retrospective, USG findings were excluded from the study as they were evaluated by different physicians.

Conclusion

Hybrid SPECT/CT imaging is superior to planar imaging in terms of anatomic detail and localization of lesions, especially in determining the depth of lesions in the neck and in determining whether lesions are ectopic. Its margin of error is lower, and its sensitivity and accuracy are higher. Additionally, it increases PPV and NPV and the determination of the exact location of lesions in minimally invasive surgery. Therefore, it should be used routinely to detect parathyroid pathologies in patients with hyperparathyroidism.

Ethics

Ethics Committee Approval: The study was approved by the Sisli Etfal Training and Research Hospital Clinical Research Ethics Committee (05/06/2012/89).

Informed Consent: Retrospective study.

Peer-review: Externally peer-reviewed.

Authorship Contributions

Surgical and Medical Practices: H.Ö., M.Ö.T., M.M., Concept: H.Ö., M.Ö.T., M.M., Design: H.Ö., M.Ö.T., M.M., M.T.T., Data Collection or Processing: H.Ö., M.Ö.T., M.T.T., Analysis or Interpretation: H.Ö., M.Ö.T., M.T.T., Literature Search: H.Ö., M.Ö.T., M.T.T., Writing: H.Ö., M.Ö.T., M.M.

Conflict of Interest: No conflict of interest was declared by the authors.

Financial Disclosure: The authors declared that this study has received no financial support.

References

1. Heath H, Hodgson SF, Kennedy MA. Primary hyperparathyroidism. Incidence, morbidity, and potential economic impact in a community. *N Engl J Med* 1980;302:189-193.
2. Schell SR, Dudley NE. Clinical outcomes and fiscal consequences of bilateral neck exploration for primary idiopathic hyperparathyroidism without preoperative radionuclide imaging or minimally invasive techniques. *Surgery* 2003;133:32-39.
3. Ishibashi M, Nishida H, Hiromatsu Y, Kojima K, Tabuchi E, Hayabuchi N. Comparison of technetium-99m-MIBI, technetium-99m-tetrofosmin, ultrasound and MRI for localization of abnormal parathyroid glands. *J Nucl Med* 1998;39:320-324.
4. Anderson SR, Vaughn A, Karakla D, Wadsworth JT. Effectiveness of surgeon interpretation of technetium tc 99m sestamibi scans in localizing parathyroid adenomas. *Arch Otolaryngol Head Neck Surg* 2008;134:953-957.
5. Hindié E, Ugur O, Fuster D, O'Doherty M, Grassetto G, Ureña P, Kettle A, Gulec SA, Pons F, Rubello D; Parathyroid Task Group of the EANM. 2009 EANM parathyroid guidelines. *Eur J Nucl Med Mol Imaging* 2009;36:1201-1216.
6. Sharma J, Mazzaglia P, Milas M, Berber E, Schuster DM, Halkar R, Siperstein A, Weber CJ. Radionuclide imaging for hyperparathyroidism (HPT): which is the best technetium-99m sestamibi modality? *Surgery* 2006;140:856-863; discussion 863-865.
7. Geatti O, Shapiro B, Orsolon PG, Proto G, Guerra UP, Antonucci F, Gasparini D. Localization of parathyroid enlargement: experience with technetium-99m methoxyisobutylisonitrite and thallium-201 scintigraphy, ultrasonography and computed tomography. *Eur J Nucl Med* 1994;21:17-22.
8. Civelek AC, Ozalp E, Donovan P, Udelsman R. Prospective evaluation of delayed technetium-99m sestamibi SPECT scintigraphy for preoperative localization of primary hyperparathyroidism. *Surgery* 2002;131:149-157.
9. Cheng JL, Hsu CC, Wang PW, Sung KC, Chiu NT, Chiu LY, Huang YC. The feasibility of anterior 180° 99m Tc-sestamibi parathyroid SPECT/CT. *Ann Nucl Med* 2021;35:203-210.
10. Tawfik AI, Kamr WH, Mahmoud W, Abo Shady IA, Mohamed MH. Added value of ultrasonography and Tc-99m MIBI SPECT/CT combined protocol in preoperative evaluation of parathyroid adenoma. *Eur J Radiol Open* 2019;6:336-342. Erratum in: *Eur J Radiol Open* 2020;8:100308.
11. Wong KK, Fig LM, Gross MD, Dwamena BA. Parathyroid adenoma localization with 99mTc-sestamibi SPECT/CT: a meta-analysis. *Nucl Med Commun* 2015;36:363-375.
12. Assante R, Zampella E, Nicolai E, Acampa W, Vergara E, Nappi C, Gaudieri V, Fiumara G, Klain M, Petretta M, Cuocolo A. Incremental value of sestamibi SPECT/CT over dual-phase planar scintigraphy in patients with primary hyperparathyroidism and inconclusive ultrasound. *Front Med (Lausanne)* 2019;6:164.
13. Lavelly WC, Goetze S, Friedman KP, Leal JP, Zhang Z, Garret-Mayer E, Dackiw AP, Tufano RP, Zeiger MA, Ziessman HA. Comparison of SPECT/CT, SPECT, and planar imaging with single- and dual-phase (99m)Tc-sestamibi parathyroid scintigraphy. *J Nucl Med* 2007;48:1084-1089. Erratum in: *J Nucl Med* 2007;48:1430.
14. Moka D, Voth E, Dietlein M, Larena-Avellaneda A, Schicha H. Technetium 99m-MIBI-SPECT: a highly sensitive diagnostic tool for localization of parathyroid adenomas. *Surgery* 2000;128:29-35.
15. Lorberboym M, Minski I, Macadziob S, Nikolov G, Schachter P. Incremental diagnostic value of preoperative 99mTc-MIBI SPECT in patients with a parathyroid adenoma. *J Nucl Med* 2003;44:904-908.
16. Slater A, Gleeson FV. Increased sensitivity and confidence of SPECT over planar imaging in dual-phase sestamibi for parathyroid adenoma detection. *Clin Nucl Med* 2005;30:1-3.
17. Chen CC, Holder LE, Scovill WA, Tehan AM, Gann DS. Comparison of parathyroid imaging with technetium-99m-pertechnetate/sestamibi subtraction, double-phase technetium-99m-sestamibi and technetium-99m-sestamibi SPECT. *J Nucl Med* 1997;38:834-839.
18. Perez-Monte JE, Brown ML, Shah AN, Ranger NT, Watson CG, Carty SE, Clarke MR. Parathyroid adenomas: accurate detection and localization with Tc-99m sestamibi SPECT. *Radiology* 1996;201:85-91.
19. Huang J, Cheng M, Tzen K. The diagnostic effectiveness of 99mTc-sestamibi SPECT/CT in primary hyperparathyroidism. *Eur J Nucl Med Mol Imaging* 2012;39(Suppl 2):384-497. doi.org/10.1007/s00259-012-2224-7
20. Wei WJ, Shen CT, Song HJ, Qiu ZL, Luo QY. Comparison of SPET/CT, SPET and planar imaging using 99mTc-MIBI as independent techniques to support minimally invasive parathyroidectomy in primary hyperparathyroidism: a meta-analysis. *Hell J Nucl Med* 2015;18:127-135.
21. McCoy KL, Ghodadra AG, Hiremath TG, Albarano A, Joyce JM, Yip L, Carty SE, Muthukrishnan A. Sestamibi SPECT/CT versus SPECT only for preoperative localization in primary hyperparathyroidism: a single institution 8-year analysis. *Surgery* 2018;163:643-647.
22. Pata G, Casella C, Magri GC, Lucchini S, Panarotto MB, Crea N, Giubbini R, Salerni B. Financial and clinical implications of low-energy CT combined with 99m Technetium-sestamibi SPECT for primary hyperparathyroidism. *Ann Surg Oncol* 2011;18:2555-2563.
23. Takami H, Oshima M, Sugawara I, Satake S, Ikeda Y, Nakamura K, Kubo A. Pre-operative localization and tissue uptake study in parathyroid imaging with technetium-99m-sestamibi. *Aust N Z J Surg* 1999;69:629-631.
24. Chen EM, Mishkin FS. Parathyroid hyperplasia may be missed by double-phase Tc-99m sestamibi scintigraphy alone. *Clin Nucl Med* 1997;22:222-226.
25. Palestro CJ, Tomas MB, Tronco GG. Radionuclide imaging of the parathyroid glands. *Semin Nucl Med* 2005;35:266-276.
26. Shafiei B, Hoseinzadeh S, Fotouhi F, Malek H, Azizi F, Jahed A, Hadaegh F, Salehian M, Parsa H, Javadi H, Assadi M. Preoperative ^{99m}Tc-sestamibi scintigraphy in patients with primary hyperparathyroidism and concomitant nodular goiter: comparison of SPECT-CT, SPECT, and planar imaging. *Nucl Med Commun* 2012;33:1070-1076.
27. Guo R, Wang J, Zhang M, Zhang M, Meng H, Zhang Y, Li B. Value of 99mTc-MIBI SPECT/CT parathyroid imaging and ultrasonography for concomitant thyroid carcinoma. *Nucl Med Commun* 2017;38:676-682.



Prognostic Significance of ¹⁸F-FDG PET/CT Imaging in Survival Outcomes in Patients with Renal Cell Carcinoma

Renal Hücreli Karsinom Hastalarının Sağkalım Sonuçlarında ¹⁸F-FDG PET/BT Görüntülemenin Prognostik Önemi

✉ Gamze Tatar¹, ✉ Cihan Gündoğan², ✉ Ömer Faruk Şahin³, ✉ Esra Arslan³, ✉ Nurhan Ergül³, ✉ Tevfik Fikret Çermik³

¹University of Health Sciences Turkey, İstanbul Bağcılar Training and Research Hospital, Clinic of Nuclear Medicine, İstanbul, Turkey

²University of Health Sciences Turkey, Diyarbakır Gazi Yaşargil Training and Research Hospital, Clinic of Nuclear Medicine, Diyarbakır, Turkey

³University of Health Sciences Turkey, İstanbul Training and Research Hospital, Clinic of Nuclear Medicine, İstanbul, Turkey

Abstract

Objectives: Renal cell carcinoma (RCC) comprises 85%-90% of primary renal malignant tumors originating from the renal tubular epithelium and has different genetic characteristics. This study aimed to investigate the potential predictive role of ¹⁸F-fluorodeoxyglucose (FDG) positron emission tomography/computed tomography (PET/CT) and metabolic parameters in overall survival (OS) analysis in patients with RCC.

Methods: ¹⁸F-FDG PET/CT images of 100 patients performed for initial staging before surgical or oncological treatments were analyzed retrospectively. Maximum standard uptake value (SUV_{max}-T) of the primary tumor was calculated and its relationship to patient survival was analyzed. The median follow-up time was 5.61 years (0.01-8.7 years).

Results: SUV_{max}-T levels in the patients ranged from 2.1 to 48.9 (median 5.9, mean 9.0±7.9). SUV_{max}-T was significantly higher in RCC-related death more positive than in the negative cases (p<0.001). However, there was not any statistical significance for gender and pathological subtypes on the survival outcomes of patients (p=0.264 and p=0.784). The patients' 1-year, 3-year, and 5-year OS rates were 71%, 61%, and 57%, respectively. The highest action of SUV_{max}-T for estimating OS was a cut-off level of 5.4, which maintained sensitivity and specificity of 81% and 75%, respectively. However, cancer staging remained independent significance for OS (p<0.001).

Conclusion: SUV_{max} of primary tumor and cancer stage were demonstrated as significant prognostic factors for OS in patients with RCC. Evaluation of ¹⁸F-FDG accumulation with PET/CT may help plan treatment strategies and predict survival outcomes of these patients at diagnosis.

Keywords: Fluorine-18-fluorodeoxyglucose, positron emission tomography, prognosis, renal cell carcinoma, survival

Öz

Amaç: Renal hücreli karsinom (RHK), renal tübüler epitelden kaynaklanan primer renal malign tümörlerin %85-90'ını oluşturur ve farklı genetik özellikler içerir. Bu çalışmanın amacı RHK tanılı hastalarda genel sağkalım analizinde ¹⁸F-florodeoksiglukoz (FDG) pozitron emisyon tomografisi/bilgisayarlı tomografi (PET/BT) ve metabolik verilerin potansiyel öngörücü rolünü araştırmaktır.

Yöntem: Hastalar (n=100) geriye dönük olarak cerrahi veya onkolojik tedaviler uygulanmadan önce, evreleme ¹⁸F-FDG PET/BT görüntüleme ile incelendi. Primer tümörün maksimum standartlaştırılmış alım değeri (SUV_{maks}-T) hesaplandı ve hasta sağkalımı ile ilişkisi analiz edildi. Medyan takip süresi 5,61 yıl idi (0,01-8,7 yıl).

Bulgular: Tüm hastalarda SUV_{maks}-T ölçümleri 2,1 ile 48,9 arasında idi (medyan 5,9, ortalama 9,0±7,9). SUV_{maks}-T, RHK ile ilişkili eksitus pozitif olgularda negatif olgulardan anlamlı olarak daha yüksek idi (p<0,001), ancak hastaların sağkalım sonuçlarında cinsiyet ve patolojik alt tipler için

Address for Correspondence: Gamze Tatar MD, University of Health Sciences Turkey, İstanbul Bağcılar Training and Research Hospital, Clinic of Nuclear Medicine, İstanbul, Turkey

Phone: +90 536 452 11 71 **E-mail:** gamze_tatar@hotmail.com ORCID ID: orcid.org/0000-0002-4187-755X

Received: 16.05.2022 **Accepted:** 27.06.2022

©Copyright 2022 by Turkish Society of Nuclear Medicine
Molecular Imaging and Radionuclide Therapy published by Galenos Yayınevi.

istatistiksel bir anlamlılık yoktu ($p=0,264$ ve $p=0,784$). Tüm hastalar için 1-yıllık, 3-yıllık ve 5-yıllık genel sağkalım oranları sırasıyla %71, %61 ve %57 idi. Genel sağkalımı öngörmeye SUV_{max} -T'nin en yüksek performansı sırasıyla %81 ve %75 duyarlılık ve özgüllük sağlayan 5,4'lük bir cut-off seviyesi ile elde edildi. Öte yandan, kanser evrelemesi genel sağkalım için bağımsız bir öneme sahipti ($p<0,001$).

Sonuç: Primer tümör SUV_{max} ve kanser evresi, RHK'li hastalarda genel sağkalım için önemli prognostik faktörler olarak gösterildi. ^{18}F -FDG tutulumunun PET/BT ile değerlendirilmesi, tedavi stratejilerinin planlanmasına ve bu hastaların tanı anında sağkalım sonuçlarının tahmin edilmesine yardımcı olabilir.

Anahtar kelimeler: Flor-18-florodeksiglukoz, pozitron emisyon tomografisi, prognoz, renal hücreli karsinom, sağkalım

Introduction

Kidney cancers have histological subtypes with different characteristics, account for approximately 3% of adult cancers, and are in the third rank among urogenital cancers (1). Renal cell carcinoma (RCC) comprises 85%-90% of primary renal malignant tumors originating from the renal tubular epithelium and has different genetic characteristics (2). RCCs, highly angio-invasive tumors, tend to metastasize to the lungs, bones, liver, and brain by hematogenous and lymphatic spread. Survival in RCC is poor, especially in the clear cell subtype, which is prone to diagnosis at an advanced stage, and 20%-30% of patients are also in the metastatic stage during this period (3,4). Therefore, the management of these patients is very challenging. The 5-year survival rate is less than 20%, even if the metastatic tumor is removed, the survival is between 25 and 50% (5). However, the incidence of renal tumors, which are often incidentally diagnosed as smaller and low-grade tumors, is increasing because of the widespread use of non-invasive imaging tools. The histological subtype, grade, size, extracapsular spread, and lymphovascular invasion status can be considered among the main factors affecting the prognosis of renal tumors (6).

Positron emission tomography integrated with computed tomography (PET/CT) imaging has become a key modality for imaging patients with cancer and is frequently used in renal cancers, particularly to detect recurrence and evaluate treatment response. Cancer staging with ^{18}F -fluorodeoxyglucose (FDG) PET imaging is since malignant tumoral cells have higher glucose metabolism than normal cells (7). However, renal cancers are prone to exhibit low tracer uptake (8,9).

Whilst there is a wealth of literature addressing the use of ^{18}F -FDG PET/CT in renal tumors, the relationship between PET metabolic measurements obtained from the pre-treatment initial staging examination and patients' survival after long-term follow-up has not been well investigated. Therefore, we investigated the potential predictive role of ^{18}F -FDG PET/CT and metabolic data in the analysis of survival in patients with RCC.

Materials and Methods

Patients

A total of 100 patients [66 men and 34 women; mean age 58.1 ± 11.7 (range: 34-82 years)] with RCC were examined between August 2013 and March 2022 on ^{18}F -FDG PET/CT scans were retrospectively enrolled in the analyses at the initial staging before surgical or oncological treatments.

The University of Health Sciences Turkey, Istanbul Training and Research Hospital Clinical Research Ethics Committee approved the study protocol (number: 88, date: 02.03.2022) and the Declaration of Helsinki rules were followed to conduct this study.

^{18}F -FDG PET/CT Scan and Interpretation of Images

^{18}F -FDG doses according to patient weight (3.7 mBq/kg) were injected into the patients when their blood glucose values were <140 mg/dL. Initially, CT ($n=68$ with contrast-enhanced, $n=32$ without contrast-enhanced) data followed by PET scan were received 60 min after ^{18}F -FDG injection between the vertex-proximal thigh in an mCT 20 PET/CT scanner (Siemens Molecular Imaging, Hoffman Estates, IL) and all images were examined first visually and then semi-quantitatively. Regions with increased ^{18}F -FDG uptake than background and nearby structures in primary tumors, nodal and distant metastases were recorded. Maximum standardized uptake value (SUV_{max}) was measured automatically by drawing an elliptical volume of interest to include the pathological tumoral lesions in the three planes in ^{18}F -FDG PET/CT. The review process was carried out by combining the metabolic findings from the PET component with anatomical information obtained from the CT component. Initial staging images were evaluated to determine whether primary tumor SUV_{max} (SUV_{max} -T) predicted patient survival. According to the 8th edition of the American Joint Committee on Cancer 2018 tumor, node, and metastasis (TNM) staging system, the disease stage was determined, and the patients were followed up for at least 5 years or until death to evaluate their survival outcomes (10).

Statistical Analysis

Study data were evaluated by SPSS 25.0 software (IBM, Armonk, NY, USA) and $p<0.05$ was considered

statistically significant. Numbers and percentages were used to indicate the categorical data. Median and mean with standard deviation values were used to express the quantitative calculations. The relationship between survival and categorical variables was assessed by Pearson chi-squared. Time from PET/CT to death or final analysis of the study was calculated to determine overall survival (OS) and survival curves were performed and compared using the Kaplan-Meier method and Mantel-Cox Log-rank test. Receiver operating characteristic curve (ROC) analysis was used to express the cut-off values for OS. Univariate analyses of SUV_{max} on survival outcomes were measured using the Cox regression analysis. Independent variables related to OS were determined by significant factors by using multivariate logistic regression analysis. The data were expressed at a 95% confidence interval (CI).

Results

Overall, 65 patients had clear cell RCC, 21 had chromophobe RCC, nine had papillary RCC, and five had unclassified RCC. The clinicopathological TNM staging was stage 1 in 40 patients, stage 2 in 14 patients, stage 3 in 9 patients, and stage 4 in 37 patients. Distant metastases were visualized in 34 patients on ^{18}F -FDG PET/CT, and the lungs and bones were the most common sites of distant metastasis (Figure 1). Information on the characteristics of the patients is presented in Table 1. The median follow-up time was 5.61 years (range, 0.01-8.7 years; 0.78 years for deceased patients, 7.78 years for living patients). Fifty-two RCC-related deaths occurred; the remaining 48 patients were alive at the last check.

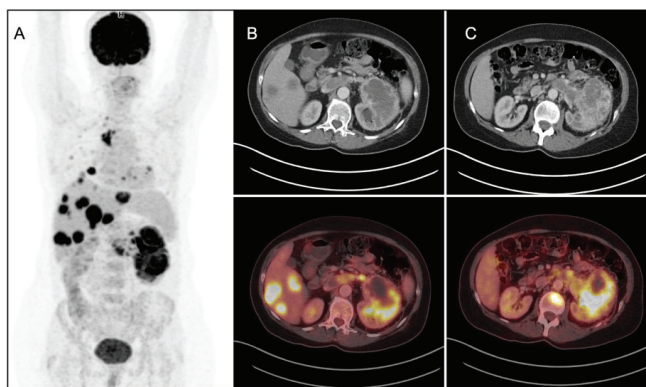


Figure 1. Maximal intensity projection (A), axial CT, and fusion PET/CT (B, C) images of a 57-year-old woman with clear cell RCC. The patient had T4 and stage 4 cancer with lung, liver, bone, and lymph node metastases. Primary tumor SUV_{max} was 25.1. She died 6 months after the initial evaluation ^{18}F -FDG PET/CT

PET/CT: Positron emission tomography/computed tomography, RCC: Renal cell carcinoma, SUV_{max} : Maximum standard uptake value, FDG: Fluorodeoxyglucose

SUV_{max} -T levels in the patients ranged from 2.1 to 48.9 (median 5.9, mean 9.0 ± 7.9). In our study, there were significant differences according to the PET metabolic parameters of the primary tumor. SUV_{max} -T was significantly higher in patients with distant metastases than in the negative ones ($p < 0.001$). Also, SUV_{max} -T was significantly higher in the RCC-related death group than in the other group ($p < 0.001$). There was statistical significance in OS between groups for tumor and cancer staging ($p < 0.001$). However, there was no statistical significance for gender and histological subtypes on patients' survival outcomes ($p = 0.264$ and $p = 0.784$) (Figure 2).

The time-dependent ROC curves were generated to analyze the efficacy of SUV_{max} -T to predict OS (Figure 3). High SUV_{max} -T was associated with a shorter OS and the highest SUV_{max} -T value to predict OS was a cut-off level of 5.4, which retained 81% and 75% sensitivity and specificity, respectively. Considering 1-year, 3-year, and 5-year survival, the best clinical performance of SUV_{max} -T was achieved at a cut-off level of 7.4, 5.5, and 5.5, which indicated the

Table 1. Characteristics of the patients

Variables	n
Age, median (range)	58 (34-82)
Sex	
Male	66
Female	34
Histopathological type	
Clear cell	65
Chromophobe	21
Papillary	9
Unclassified	5
Tumor stage	
T1	46
T2	22
T3	20
T4	12
TNM cancer staging	
I	40
II	14
III	9
IV	37
Nephrectomy	
Yes	66
No	34
RCC-related death	52
TNM: Tumor, node, and metastasis, RCC: Renal cell carcinoma	

highest sensitivity and specificity, respectively (Table 2). These results suggest that SUV_{max} -T is a reliable parameter for predicting OS. The patients' 1-year, 3-year, and 5-year OS rates were 71%, 61%, and 57%, respectively. Furthermore, OS rates were 52% vs. 48% in patients with $SUV_{max} \leq 5.4$ vs. >5.4 on ^{18}F -FDG PET/CT. Also, univariate Cox regression analysis identified the values of SUV_{max} -T as a significant prognostic marker for OS ($p < 0.001$, Odds ratio: 1.135, 95% CI: 1.098-1.173).

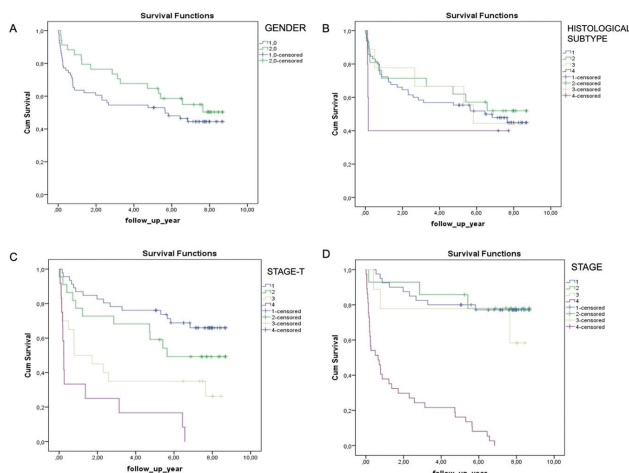


Figure 2. Kaplan-Meier curves of overall survival by patient's gender (A; blue: male, green: female), histological subtype (B), tumor staging (C), and cancer staging (D)

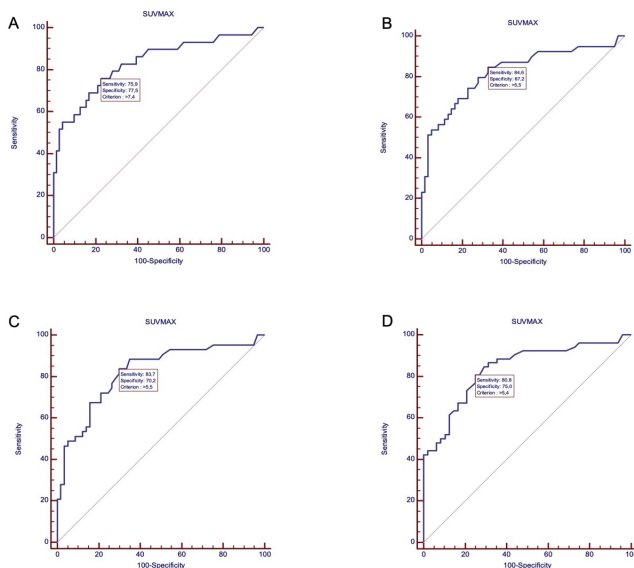


Figure 3. Receiver operating characteristic curve analysis of the patients comparing the prognostic accuracy for 1-year survival (A), 3-year survival (B), 5-year survival (C), and overall survival (D) and determining the cut-off values ($p < 0.0001$, each)

The effect of SUV_{max} on OS was compared with that of possible prognostic markers and the SUV_{max} levels exhibiting statistical significance in univariate analysis were included in the multivariate analysis. The findings of the multivariate analysis are indicated in Table 3. Analysis of SUV_{max} in association with patients' gender, histological tumor subtypes, and tumor staging at the initial pretreatment period revealed that SUV_{max} -T was a significant independent prognostic factor of OS in patients with RCC ($p < 0.001$). However, cancer staging remained independent significance for OS ($p < 0.001$). Regardless of the tumor stage and the histopathological subgroups, patients with a higher SUV_{max} had a shorter OS than patients with a lower SUV_{max} (Figure 4). In this study, the mean OS for 48 patients with $SUV_{max} \leq 5.4$ was 7.4 years (95% CI: 6.623-8.181), while in 52 patients with $SUV_{max} > 5.4$, the mean OS was 3.3 years (95% CI: 2.349-4.170). Differences in OS among these patients were statistically significant ($SUV_{max} \leq 5.4$ vs. > 5.4 , $p < 0.001$).

Discussion

Oncological PET/CT imaging has proven its importance in diagnosis, staging, evaluation of treatment response, and recurrence detection in most cancer types and is an indispensable modality in this field. Since RCC exhibits low glucose metabolism and tumoral ^{18}F -FDG uptake, PET/CT is more limitedly preferred as an imaging tool in the initial staging (11,12). However, several researchers have examined the efficacy of ^{18}F -FDG PET in determining the metabolic and molecular characterization of renal tumors (13,14). In a retrospective study investigating the impact of SUV_{max} levels on patient mortality in renal tumors, it was determined that patients with metastasis lived shorter, liver metastases showed shorter survival, and the lung metastases had higher SUV_{max} levels (15).

Diagnostic values of PET/CT at different SUV_{max} cut-off values in survival analysis are available for RCC in the literature (16,17). Komek et al. (18) investigated the relationship between the mortality results of 21 patients with RCC and showed that SUV_{max} values of ≥ 4.5 , obtained from pre-treatment ^{18}F -FDG PET/CT imaging, resulted in increased mortality. Furthermore, a cut-off value of 8.8 and SUV_{max} values higher than this have been reported as predictors of survival for advanced RCC (19). In this study, we evaluated the patient outcomes and mortality rates according to different SUV_{max} values, which refer to 1-year, 3-year, and 5-year results and we determined the patients' mortality rates as 29%, 39%, and 43%, respectively (Figure 5). Nakaigawa et al. (20) evaluated 101 patients with RCC during the pretreatment or follow-up period and classified study patients into three subgroups based on their highest

Table 2. Receiver operating characteristic analysis for the efficacy of SUV_{max} in predicting mortality relative to patient survival time

SUV_{max}	Cut-off level	Death	AUC	p value	Sensitivity (%)	Specificity (%)	95% CI
1-year survival	> 7.4	29	0.831	<0.0001	75.9	77.5	0.742-0.898
3-year survival	>5.5	39	0.821	<0.0001	84.6	67.2	0.732-0.891
5-year survival	>5.5	43	0.821	<0.0001	83.7	70.2	0.732-0.891
Overall survival	>5.4	52	0.837	<0.0001	80.8	75.0	0.750-0.903

SUV_{max} : Maximum standardized uptake value, AUC: Area under curve, CI: Confidence interval

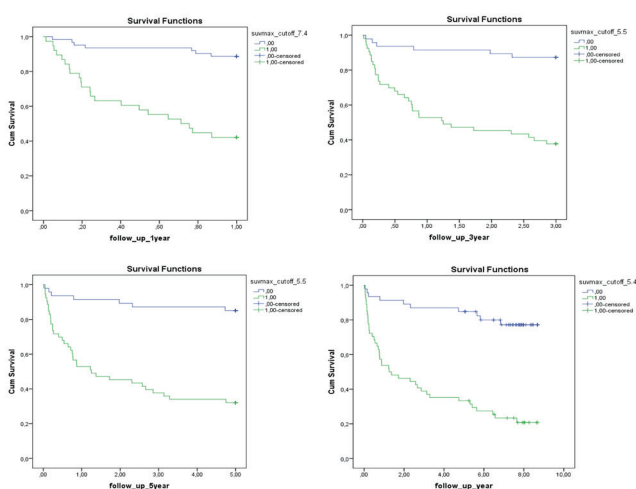


Figure 4. Kaplan-Meier survival graphs with log-rank (Mantel-Cox) present significant differences in survival outcomes of study patients classified by SUV_{max} values. $SUV_{max} > 7.5$ for 1-year survival (A), $SUV_{max} > 5.5$ for 3-year survival (B), $SUV_{max} > 5.5$ for 5-year survival (C), and $SUV_{max} > 5.4$ for overall survival (D) were associated with mortality and shorter OS ($p < 0.001$ for all)

SUV_{max} : Maximum standard uptake value, OS: Overall survival

SUV_{max} levels and reported significant differences in OS for RCC. Subjects were followed for a median of 18 months and the median OS of patients with $SUV_{max} < 7.0$, ≥ 7.0 , and < 12.0 , and ≥ 12.0 was found as 41.9, 20.6, and 4.2 months, respectively. In this study, the median follow-up time of our patients was 5.61 years, and we observed the mean OS as 7.4 and 3.3 years, respectively, for $SUV_{max} \leq 5.4$ vs. > 5.4 levels, with sensitivity and specificity results of 81% and 75%. Additionally, the SUV_{max} threshold of 7.4 was significant in distinguishing patient mortality and survival within 1 year after PET/CT evaluation (Figure 6).

The use of volumetric measures such as metabolic tumor volume (MTV) and total lesion glycolysis (TLG) provided a correlation with prognosis in published studies (21). Nakajima et al. (22) showed that MTV and TLG calculated from PET data are also important prognostic markers in the survival analysis of RCC patients. Further pre-treatment TLG was found to be an independent indicator of the prognosis of OS in another study (23). Besides PET measurements,

Table 3. Multivariate logistic regression analysis for patient survival outcomes

Variable	OR	95% CI	p value
SUV_{max}	1.076	1.036-1.118	<0.001
Age	1.028	0.997-1.060	0.081
Gender	0.660	0.358-1.218	0.184
T-stage	0.928	0.688-1.252	0.625
TNM stage	1.985	1.444-2.729	<0.001

SUV_{max} : Maximum standardized uptake value, OR: Odds ratio, CI: Confidence interval, TNM: Tumor, node, and metastasis

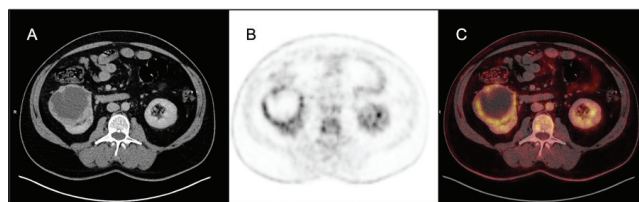


Figure 5. Axial CT (A), PET (B), and fusion PET/CT (C) images of a 54-year-old man patient with clear cell type RCC. The patient had stage 3 cancer with a T3 tumor on PET/CT performed at the initial staging. Primary tumor SUV_{max} was 6.5. He died of recurrent metastatic disease 2.7 years after initial evaluation ^{18}F -FDG PET/CT

PET/CT: Positron emission tomography/computed tomography, RCC: Renal cell carcinoma, SUV_{max} : Maximum standard uptake value, FDG: Fluorodeoxyglucose

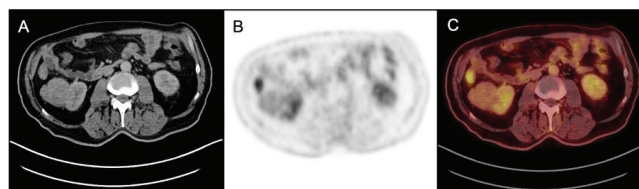


Figure 6. Axial CT (A), PET (B), and fusion PET/CT (C) images of a 67-year-old living patient with stage 1 cancer were received 7.4 years ago. He had chromophobe type RCC in the right kidney with a SUV_{max} value of 3.9

PET/CT: Positron emission tomography/computed tomography, RCC: Renal cell carcinoma, SUV_{max} : Maximum standard uptake value, FDG: Fluorodeoxyglucose

the prognostic value of pathological subtypes was investigated, and the clear cell variant was more prone to metastasis than the other two variants and exhibited a poor prognosis, but we did not observe any significant difference between the survival times of the histological

subgroups (24). Tumor size, grading system, various other markers, and different radiopharmaceuticals used in hybrid molecular imaging have been reported in several articles as potential predictors of the prognosis of patients with RCC (25,26,27).

Study Limitations

This study had some limitations. First, our retrospective study showed a heterogeneous distribution among pathological subgroups and tumor stages. Also, the differences in the patients' treatment protocols and follow-up strategies may have affected the survival analyses. Therefore, well-designed prospective studies are required to validate our findings.

Conclusion

Patients with high primary tumor SUV_{max} had increased mortality rates and shorter survival. SUV_{max} and the high-cancer stage were demonstrated as the significant prognostic predictors in patients with RCC. We think that SUV_{max} can act as a potential biomarker and reflect the disease prognosis. Evaluation of ^{18}F -FDG accumulation using PET/CT may help plan treatment strategies and predict survival outcomes of these patients at diagnosis.

Ethics

Ethics Committee Approval: The University of Health Sciences Turkey, Istanbul Training and Research Hospital Clinical Research Ethics Committee approved the study protocol (number: 88, date: 02.03.2022) and the Declaration of Helsinki rules were followed to conduct this study

Informed Consent: Externally peer-reviewed.

Peer-review: Externally peer-reviewed.

Authorship Contributions

Surgical and Medical Practices: G.T., C.G., Ö.F.Ş., E.A., N.E., T.F.Ç., Concept: G.T., C.G., Ö.F.Ş., E.A., N.E., T.F.Ç., Design: G.T., C.G., Ö.F.Ş., E.A., N.E., T.F.Ç., Data Collection or Processing: G.T., C.G., Ö.F.Ş., E.A., N.E., T.F.Ç., Analysis or Interpretation: G.T., C.G., Ö.F.Ş., E.A., N.E., T.F.Ç., Literature Search: G.T., C.G., Ö.F.Ş., E.A., Writing: G.T., T.F.Ç.

Conflict of Interest: No conflict of interest was declared by the authors.

Financial Disclosure: The authors declared that this study has received no financial support.

References

1. Siegel RL, Miller KD, Fuchs HE, Jemal A. Cancer statistics, 2021. *CA Cancer J Clin* 2021;71:7-33. Erratum in: *CA Cancer J Clin* 2021;71:359.
2. Ricketts CJ, De Cubas AA, Fan H, Smith CC, Lang M, Reznik E, Bowlby R, Gibb EA, Akbani R, Beroukhir R, Bottaro DP, Choueiri TK, Gibbs RA, Godwin AK, Haake S, Hakimi AA, Henske EP, Hsieh JJ, Ho TH, Kanchi RS, Krishnan B, Kwiatkowski DJ, Lui W, Merino MJ, Mills GB, Myers J, Nickerson ML, Reuter VE, Schmidt LS, Shelley CS, Shen H, Shuch B, Signoretti S, Srinivasan R, Tamboli P, Thomas G, Vincent BG, Vocke CD, Wheeler DA, Yang L, Kim WY, Robertson AG; Cancer Genome Atlas Research Network, Spellman PT, Rathmell WK, Linehan WM. The cancer genome atlas comprehensive molecular characterization of renal cell carcinoma. *Cell Rep* 2018;23:313-326.e5. Erratum in: *Cell Rep* 2018;23:3698.
3. Ferlay J, Soerjomataram I, Dikshit R, Eser S, Mathers C, Rebelo M, Parkin DM, Forman D, Bray F. Cancer incidence and mortality worldwide: sources, methods and major patterns in GLOBOCAN 2012. *Int J Cancer* 2015;136:E359-E386.
4. Zhang G, Wu Y, Zhang J, Fang Z, Liu Z, Xu Z, Fan Y. Nomograms for predicting long-term overall survival and disease-specific survival of patients with clear cell renal cell carcinoma. *Onco Targets Ther* 2018;11:5535-5544.
5. Klatte T, Rossi SH, Stewart GD. Prognostic factors and prognostic models for renal cell carcinoma: a literature review. *World J Urol* 2018;36:1943-1952.
6. Shao N, Wang HK, Zhu Y, Ye DW. Modification of American Joint Committee on cancer prognostic groups for renal cell carcinoma. *Cancer Med* 2018;7:5431-5438.
7. Gofrit ON, Orevi M. Diagnostic challenges of kidney cancer: a systematic review of the role of positron emission tomography-computerized tomography. *J Urol* 2016;196:648-657.
8. Alongi P, Picchio M, Zattoni F, Spallino M, Gianolli L, Saladini G, Evangelista L. Recurrent renal cell carcinoma: clinical and prognostic value of FDG PET/CT. *Eur J Nucl Med Mol Imaging* 2016;43:464-473.
9. Jena R, Narain TA, Singh UP, Srivastava A. Role of positron emission tomography/computed tomography in the evaluation of renal cell carcinoma. *Indian J Urol* 2021;37:125-132.
10. Amin MB, Greene FL, Edge SB, Compton CC, Gershenwald JE, Brookland RK, Meyer L, Gress DM, Byrd DR, Winchester DP. The Eighth Edition AJCC Cancer Staging Manual: continuing to build a bridge from a population-based to a more "personalized" approach to cancer staging. *CA Cancer J Clin* 2017;67:93-99.
11. Liu Y. The Place of FDG PET/CT in renal cell carcinoma: value and limitations. *Front Oncol* 2016;6:201.
12. Elahmadawy MA, Elazab MSS, Ahmed S, Salama M. Diagnostic value of F-18 FDG PET/CT for local and distant disease relapse surveillance in surgically treated RCC patients: Can it aid in establishing consensus follow up strategy? *Nucl Med Rev Cent East Eur* 2018;21:85-91.
13. Noda Y, Kanematsu M, Goshima S, Suzui N, Hirose Y, Matsunaga K, Nishibori H, Kondo H, Watanabe H, Kawada H, Kawai N, Tanahashi Y, Bae KT. 18-F fluorodeoxyglucose uptake in positron emission tomography as a pathological grade predictor for renal clear cell carcinomas. *Eur Radiol* 2015;25:3009-3016.
14. Takahashi M, Kume H, Koyama K, Nakagawa T, Fujimura T, Morikawa T, Fukayama M, Homma Y, Ohtomo K, Momose T. Preoperative evaluation of renal cell carcinoma by using 18F-FDG PET/CT. *Clin Nucl Med* 2015;40:936-940.
15. Komek H, Altindag S, Can C, Aguloglu N, Morcali H, Kepenek F, Karaoglan H. The effect on survival and mortality of the highest SUV_{max} value on metastatic foci in postoperative kidney tumors. *Niger J Clin Pract* 2018;21:163-169.
16. Toguchi M, Ishigami K, Goya M, Saito S, Murayama S, Nishie A. Efficacy of pre-operative 18F-FDG PET/CT in prognostic prediction in patients with renal cell carcinoma. *Cancer Diagn Progn* 2022;2:216-222.

17. Pankowska V, Malkowski B, Wedrowski M, Wedrowska E, Roszkowski K. FDG PET/CT as a survival prognostic factor in patients with advanced renal cell carcinoma. *Clin Exp Med* 2019;19:143-148.
18. Komek H, Altindag S, Can C, Aguloglu N, Morcali H, Tuzun A, Kavak S. The prognostic value of preoperative PET/CT evaluation of maximum standardized uptake value in renal cell carcinomas. *Ann Ital Chir* 2017;88:48-54.
19. Namura K, Minamimoto R, Yao M, Makiyama K, Murakami T, Sano F, Hayashi N, Tateishi U, Ishigaki H, Kishida T, Miura T, Kobayashi K, Noguchi S, Inoue T, Kubota Y, Nakaigawa N. Impact of maximum standardized uptake value (SUVmax) evaluated by 18-Fluoro-2-deoxy-D-glucose positron emission tomography/computed tomography (18F-FDG-PET/CT) on survival for patients with advanced renal cell carcinoma: a preliminary report. *BMC Cancer* 2010;10:667.
20. Nakaigawa N, Kondo K, Tateishi U, Minamimoto R, Kaneta T, Namura K, Ueno D, Kobayashi K, Kishida T, Ikeda I, Hasumi H, Makiyama K, Kubota Y, Inoue T, Yao M. FDG PET/CT as a prognostic biomarker in the era of molecular-targeting therapies: max SUVmax predicts survival of patients with advanced renal cell carcinoma. *BMC Cancer* 2016;16:67.
21. Kim D, Lee N, Lee SH, Kim HJ, Hong HS, Park JS, Cho NH, Choi YD, Ham WS, Lee SH, Han WK, Yun M. Metabolic tumour volume on 18F-FDG PET/CT predicts extended pathological T stages in patients with renal cell carcinoma at staging. *Sci Rep* 2021;11:23486.
22. Nakajima R, Matsuo Y, Kondo T, Abe K, Sakai S. Prognostic value of metabolic tumor volume and total lesion glycolysis on preoperative 18F-FDG PET/CT in patients with renal cell carcinoma. *Clin Nucl Med* 2017;42:e177-e182.
23. Farnebo J, Grybäck P, Harmenberg U, Laurell A, Wersäll P, Blomqvist LK, Ullén A, Sandström P. Volumetric FDG-PET predicts overall and progression-free survival after 14 days of targeted therapy in metastatic renal cell carcinoma. *BMC Cancer* 2014;14:408.
24. Leibovich BC, Lohse CM, Crispen PL, Boorjian SA, Thompson RH, Blute ML, Cheville JC. Histological subtype is an independent predictor of outcome for patients with renal cell carcinoma. *J Urol* 2010;183:1309-1315.
25. Mizuno T, Kamai T, Abe H, Sakamoto S, Kitajima K, Nishihara D, Yuki H, Kambara T, Betsunoh H, Yashi M, Fukabori Y, Kaji Y, Yoshida K. Clinically significant association between the maximum standardized uptake value on 18F-FDG PET and expression of phosphorylated Akt and S6 kinase for prediction of the biological characteristics of renal cell cancer. *BMC Cancer* 2015;15:1097.
26. Wang X, Li R, Chen R, Huang G, Zhou X, Liu J. Prognostic values of TIGAR expression and 18F-FDG PET/CT in clear cell renal cell carcinoma. *J Cancer* 2020;11:1-8.
27. Roussel E, Capitanio U, Kutikov A, Oosterwijk E, Pedrosa I, Rowe SP, Gorin MA. Novel imaging methods for renal mass characterization: a collaborative review. *Eur Urol* 2022;81:476-488.



The Role of ^{18}F -FLT PET/CT in Assessing Early Response to Transarterial Radioembolization and Chemoembolization in Patients with Primary and Metastatic Liver Tumors

Primer ve Metastatik Karaciğer Tümörlü Hastalarda Transarteriyel Radyoembolizasyon ve Kemoembolizasyona Erken Yanıtı Değerlendirmede ^{18}F -FLT PET/CT'nin Rolü

Demet Nak¹, Nuriye Özlem Küçük², Emre Can Çelebioğlu³, Mehmet Sadık Bilgiç³, Serhat Hayme⁴, Kemal Metin Kır²

¹Recep Tayyip Erdoğan Training and Research Hospital, Clinic of Nuclear Medicine, Rize, Turkey

²Ankara University Faculty of Medicine, Department of Nuclear Medicine, Ankara, Turkey

³Ankara University Faculty of Medicine, Department of Radiology, Ankara, Turkey

⁴Erzincan Binali Yıldırım University, Department of Biostatistics and Medical Informatics, Erzincan, Turkey

Abstract

Objectives: Metastases and primary malignancies are common in the liver. Local ablative applications such as transarterial chemoembolization (TACE), and transarterial radioembolization (TARE) provide minimally invasive and safe treatment in unresectable liver tumors. Early detection of response to treatment prevents unnecessary toxicity and cost in non-responder patients and provides an earlier use of other options that may be effective. This study aimed to identify the role of ^{18}F -fluorothymidine (FLT) positron emission tomography/computed tomography (PET/CT) in the assessment of early response to TACE and TARE treatments in patients with unresectable primary and metastatic liver tumors.

Methods: This single-center study included 63 patients who underwent ^{18}F -FLT PET/CT for response evaluation after TACE and TARE. After excluding 20 patients whose data were missing 43 TARE-receiving patients were analyzed. The compatibility of change in semi-quantitative values obtained from the ^{18}F -FLT PET/CT images with the treatment responses detected in ^{18}F -fluorodeoxyglucose PET/CT, CT, and MR images and survival was evaluated.

Results: There was no correlation between early metabolic, morphological response, and ^{18}F -FLT uptake pattern, and change in standardized uptake values (SUV) which were $\Delta\text{SUV}_{\text{max}}$, $\Delta\text{SUV}_{\text{mean}}$, $\Delta\text{SUV}_{\text{peak}}$, $\Delta\text{SUV}_{\text{mean}}$, $\Delta\text{SUV}_{\text{peak}}$ values. There was no significant correlation between ^{18}F -FLT uptake pattern, $\Delta\text{SUV}_{\text{max}}$, $\Delta\text{SUV}_{\text{mean}}$, $\Delta\text{SUV}_{\text{peak}}$, and overall survival, progression-free survival (PFS) for the target lobe PFS for the whole-body. The survival distributions for the patients with >30% change in $\Delta\text{SUV}_{\text{max}}$ and $\Delta\text{SUV}_{\text{peak}}$ values were statistically significantly longer than the patients with <30% change ($p<0.009$ and $p<0.024$, respectively).

Conclusion: There was significant longer PFS for target liver lobe in patients with more than 30% decrease in ^{18}F -FLT SUV_{max} and SUV_{peak} of the liver lesion in primary and metastatic unresectable liver tumors undergoing TARE.

Keywords: ^{18}F -FLT PET/CT, early response, primary, metastatic, chemoembolization, liver tumors, radioembolization, TACE, TARE

Öz

Amaç: Karaciğer hem metastazların hem de primer malignitelerin sık görüldüğü bir organdır. Transarteriyel kemoembolizasyon (TACE) ve transarteriyel radyoembolizasyon (TARE) gibi lokal ablatif uygulamalar, rezeke edilemeyen karaciğer tümörlerinde minimal invaziv ve güvenli tedavi sağlar. Tedaviye yanıtın erken tespiti, yanıt vermeyen hastalarda gereksiz toksisiteyi ve maliyeti önlerken etkili olabilecek diğer seçeneklerin

Address for Correspondence: Demet Nak MD, Recep Tayyip Erdoğan Training and Research Hospital, Clinic of Nuclear Medicine, Rize, Turkey

Phone: +90 464 213 0491-3618 **E-mail:** demet_nak@hotmail.com ORCID ID: orcid.org/0000-0002-9756-7788

Received: 09.12.2021 **Accepted:** 26.06.2022

©Copyright 2022 by Turkish Society of Nuclear Medicine
Molecular Imaging and Radionuclide Therapy published by Galenos Yayınevi.

daha erken kullanılmasını sağlar. Bu çalışmada, rezeke edilemeyen primer ve metastatik karaciğer tümürlü hastalarda TAKE ve TARE tedavilerine erken yanıtın değerlendirilmesinde ¹⁸F-FLT pozitron emisyon tomografisi/bilgisayarlı tomografinin (PET/BT) rolünün belirlenmesi amaçlanmıştır. **Yöntem:** Tek merkezli bu çalışmaya, TARE ve TAKE tedavileri öncesi ve sonrasında ¹⁸F-FLT PET/BT inceleme yapılarak yanıt değerlendirmesi yapılan 63 hasta dahil edilmiştir. Verileri eksik olan 20 hasta dışlanarak 43 TARE alan hasta analiz edilmiştir. ¹⁸F-FLT PET/BT görüntülerinden elde edilen semi-kantitatif değerlerdeki değişimin ¹⁸F-florodeoksiglukoz PET/BT, BT ve MR görüntülerinde saptanan tedavi yanıtları ile uyumluluğu ve sağkalımlarla ilişkisi araştırılmıştır.

Bulgular: Erken metabolik, morfolojik yanıt ile ¹⁸F-FLT tutulum paternindeki değişim, $\Delta\text{SUV}_{\text{maks}}$, $\Delta\text{SUV}_{\text{mean}}$, $\Delta\text{SUV}_{\text{peak}}$ olarak ifade edilen SUV değerlerindeki değişim arasında korelasyon saptanmamıştır. ¹⁸F-FLT tutulum paterninde değişim, $\Delta\text{SUV}_{\text{maks}}$, $\Delta\text{SUV}_{\text{mean}}$ ve $\Delta\text{SUV}_{\text{peak}}$ değerleri ile genel sağkalım, tüm vücut ve hedef lob için progresyonsuz sağkalım (PFS) arasında anlamlı ilişki gözlenmemiştir. $\Delta\text{SUV}_{\text{maks}}$ ve $\Delta\text{SUV}_{\text{peak}}$ değerlerinde >%30 değişiklik olan hastaların hedef lob için PFS'leri <%30 değişiklik olanlardan istatistiksel olarak anlamlı düzeyde uzun saptanmıştır (sırasıyla; $p<0,009$ ve $p<0,024$).

Sonuç: TARE uygulanan primer ve metastatik rezektabl olmayan karaciğer tümöründe karaciğer lezyonunun ¹⁸F-FLT SUV_{maks} ve SUV_{peak} 'inde >%30 azalma olan hastalarda hedef karaciğer lobu için daha uzun PFS saptanmıştır.

Anahtar kelimeler: ¹⁸F-FLT PET/BT, erken yanıt, primer, metastatik, kemoembolizasyon, karaciğer tümörleri, radyoembolizasyon, TAKE, TARE

Introduction

Both metastases and primary malignancies, such as hepatocellular carcinoma (HCC) and cholangiocellular cancer, are common in the liver. Metastases are the most common liver malignancy, and leading tumors metastasize to the liver are colorectal cancer, neuroendocrine tumors, other gastrointestinal cancers, and breast cancer. HCC is the sixth common cause of cancer and the third common cause of cancer-related deaths worldwide (1,2). Since the liver involvement is effective on survival, curative surgical applications are the first-line therapy, either with adjuvant chemotherapy or alone, providing the most significant survival advantage. However, surgery cannot be applied to most patients at diagnosis or tumor recurrence due to advanced-stage disease or inappropriate clinical status (1,3). Local ablative applications such as radiofrequency, microwave, and cryo-ablation, irreversible electroporation (IRE), endovascular transarterial chemoembolization (TACE), and transarterial radioembolization (TARE) provide minimally invasive and safe treatment (4,5,6,7,8). It has been reported that TARE and TACE provide long-term survival advantage and low toxicity, especially in patients with good performance and low tumor burden (5,7,8,9,10,11).

The prediction or early detection of response to therapy prevents unnecessary toxicity and cost that may be life-threatening in non-responder patients and provides an earlier use of other treatment options that may be effective. The morphological response evaluation with computed tomography (CT) and magnetic resonance (MR) requires a relatively long period and tumor shrinkage. Positron emission tomography (PET)/CT or PET/MR hybrid imaging, based on metabolic processes, provides earlier response assessment and concurrent anatomical information. ¹⁸F-fluorodeoxyglucose (FDG) is the most commonly used agent in PET imaging (12,13,14,15,16). However, since tumors with low-glucose metabolism and low cellularity,

small-sized and well-differentiated tumors show low ¹⁸F-FDG uptake, alternative agents such as thymidine analog 3'-deoxy-(F-18)-3'-fluorotimidin (¹⁸F-FLT), which reflects the proliferation of cells, ¹¹C-acetate, which reflects hypoxia, C11-choline or ¹⁸F-choline, which reflects aerobic metabolism (fatty acid synthesis) are being investigated (15,17,18,19,20,21,22,23).

¹⁸F-FLT, an analog of thymidine, is phosphorylated with thymidine kinase-1 (TK1) and is converted to ¹⁸F-FLT-monophosphate, which cannot penetrate DNA and is trapped in the cytosol. ¹⁸F-FLT is a TK1-specific substrate that increases in proliferating cells while not found in silent cells and correlates with a proliferation marker Ki-67 index (24,25). Imaging with ¹⁸F-FLT has advantages such as non-invasive quantitation of cell proliferation, three-dimensional tumor imaging, and evaluating the whole tumor proliferation heterogeneity in multiple tumor areas simultaneously. Studies show that tumor proliferation changes can be detected early with ¹⁸F-FLT PET/CT after radiotherapy (1,2,3). Knowing that TARE is an internal radiotherapy method, this study aimed to describe the role of ¹⁸F-FLT PET/CT in assessing the early response to TARE and TACE in patients with primary and metastatic liver tumors.

Materials and Methods

Ankara University Faculty of Medicine Human Research Ethics Committee Approval (i3-117-19) was obtained for this single-center study with prospective and retrospective components and was performed under the Helsinki Directive and Good Clinical Practices Guidelines. Informed consent was obtained from all volunteers included in the study.

Patients

The inclusion criteria of this study were TACE or TARE therapy for histologically/cytologically or radiologically diagnosed

primary (HCC, cholangiocellular carcinoma) or metastatic liver tumor; staged with CT/MR, ¹⁸F-FDG PET/CT, or PET/MR; Eastern Cooperative Oncology Group performance score ≤ 2 ; over 18 years of age; follow-up more than three months; available data. Patients with claustrophobia and pain that prevent imaging and patients who did not want to participate in the study were excluded. There was no intervention in the treatment selection or management of the patients. According to the standard evaluations, the relevant specialist (medical oncology, gastroenterology specialist, or general surgeon) chose the treatment.

¹⁸F-FLT and ¹⁸F-FDG PET/CT Imaging

The presence or history of systemic or local ablative therapy, chronic disease, etc., can affect the evaluation was questioned and noted. To reduce the total body radiation dose and increase the image quality, oral hydration and emptying of the bladder before imaging was provided. Approximately 60 min after the ¹⁸F-FDG and ¹⁸F-FLT were given intravenously, the whole-body PET/CT imaging was performed starting 60 min after injection. Following at least 6 hours of fasting, when blood glucose level was <150 mg/dL, ~ 4 -5 MBq/kg ¹⁸F-FDG was administered. Approximately 60 min after the administration of radiopharmaceutical, whole-body PET/CT images were obtained. FLT was synthesized in-house according to standard procedures (25). After administration of 3.4-9.3 mCi ¹⁸F-FLT intravenously, the whole-body PET/CT imaging was performed starting 60 min after injection (26,27,28,29,30). Following CT for attenuation correction, and anatomical correlation, whole-body PET images were obtained, in the supine position, from the vertex to the middle thigh, and 3 min per bed. PET/CT Discovery ST (GE Healthcare Waukesha, Wisconsin, USA) was used for PET/CT hybrid imaging. After assessing maximum intensity projection, cross-sectional and fusion images, areas with high, mixed (heterogeneous), equal and low uptake from adjacent liver parenchyma were noted. The same parameters and assessments were used for ¹⁸F-FDG and ¹⁸F-FLT imaging, which were performed twice, before the treatment as baseline and for response evaluation after therapy.

The target lesion was defined as sole or the largest lesion in the target lobe. Standardized uptake values (SUV): SUV_{max} , SUV_{mean} , SUV_{peak} were calculated automatically for hypermetabolic and heterogeneous (mixed) target lesions on a workstation by using PET software (GE Healthcare). A 2 cm region of interest was manually defined for isometabolic, and hypometabolic target lesions on the summed images by using the same software. Since the reference (non-tumoral) liver parenchymal SUV values of

the patients showed a significant difference both between the patients and the baseline and post-treatment images of the same patient, the target background ratio (TBR) of the target lesions were calculated by proportioning the SUV values of the target lesion to reference values and were evaluated separately. Reference SUV values were calculated by manually placing a 2 cm region of interest in the liver in a tumor-free area to measure background liver activity (26,28,29,30). Patients were divided into groups with and without the change of SUV values calculated from the difference between the target lesion's post-treatment and pre-treatment SUV values, which were calculated and referred to as delta (Δ) SUV values.

Statistical Analysis

The changes between baseline and post-treatment ¹⁸F-FLT PET/CT images were compared to the responses detected with ¹⁸F-FDG PET/CT and CT/MRI, evaluated according to the PERCIST and RECIST 1.1 criteria, respectively, and progression-free survival (PFS) and overall survival (OS). All statistical analyses were performed using IBM SPSS for Windows, version 25.0 (SPSS, Armonk, NY: IBM Corp.). Kolmogorov-Smirnov test was used to assess the assumption of normality. The continuous variables that did not have a normal distribution were expressed as medians (minimum-maximum). For non-normally-distributed continuous variables, differences between groups were tested using Mann-Whitney U test and Kruskal-Wallis test. Lastly, Pearson chi-square analysis and Fisher's Exact test determined associations between categorical variables, while Pearson and Spearman correlation analysis determined associations between continuous variables. The survival times of groups were obtained using Kaplan-Meier analysis and the difference in survival times between groups were compared with the Log Rank test. A two-sided p value <0.05 was considered as statistically significant.

Results

Patients

Sixty-three consecutive patients were included in the study between December 2018 and January 2020, who underwent pre- and post-treatment ¹⁸F-FLT PET/CT to evaluate their response to TARE and TACE treatments. Although all patients underwent baseline imaging, 4 of the TACE-receiving patients and 16 of the TARE-receiving patients could not undergo ¹⁸F-FLT PET/CT or other imaging for response evaluation either due to decreased performance status that hindered further procedure or death. Since the patients who received TACE did not

undergo PET/CT or CT/MRI to evaluate the response to treatment, and most of their data were missing TACE-receiving patients were excluded from the analysis. Forty-three TARE-receiving patients were analyzed to have a homogenous population and statistical analysis. Detailed patient characteristics are listed in Table 1.

¹⁸F-FLT, ¹⁸F-FDG PET/CT and CT/MRI

Other than one patient who did not undergo ¹⁸F-FDG PET/CT scanning for response evaluation because of the tumor’s ¹⁸F-FDG non-avidity at the baseline, all remaining patients underwent ¹⁸F-FLT PET/CT, ¹⁸F-FDG PET/CT, and CT/MR before and after TARE. The morphological response evaluation was performed with contrast-enhanced CT for 2 patients and with contrast-enhanced MR for 41 patients. Imaging characteristics of ¹⁸F-FLT PET/CT are given in Tables 2, 3; characteristics of ¹⁸F-FDG PET/CT and CT/MRI are given in Table 2. ¹⁸F-FLT PET/CT, ¹⁸F-FDG PET/CT, and contrast-enhanced liver MR of a patient with ¹⁸F-FDG non-avid, persistent ¹⁸F-FLT avid lesions and progressive disease are presented in Figure 1.

Correlation between the diagnosis, longest diameter of the target lesion, volume and percentage of tumors in the target lobe, age, the number of lesions in the target lobe, early metabolic, morphological response and ¹⁸F-FLT visual change, $\Delta\text{SUV}_{\text{max}}$, $\Delta\text{SUV}_{\text{mean}}$, $\Delta\text{SUV}_{\text{peak}}$, $\Delta\text{SUV}_{\text{max}}$ TBR, $\Delta\text{SUV}_{\text{mean}}$ TBR, and $\Delta\text{SUV}_{\text{peak}}$ TBR values were not significant. Calculated p values from statistical analyses are presented in Table 4.

Survival

During 18.4 months follow-up, 22 patients died. OS was median 7.0 (3.3-17.4) months, PFS was median 3.4 (1.3-17.4) months for the target lobe; and median 3.2 (1.3-17.4) months for whole-body. There was no significant correlation between ¹⁸F-FLT visual change, $\Delta\text{SUV}_{\text{max}}$, $\Delta\text{SUV}_{\text{mean}}$, $\Delta\text{SUV}_{\text{peak}}$, $\Delta\text{SUV}_{\text{max}}$ TBR, $\Delta\text{SUV}_{\text{mean}}$ TBR, and $\Delta\text{SUV}_{\text{peak}}$ TBR and OS, PFS for target lobes, and PFS for whole-body (Table 4). A log-rank test was run to determine whether there were differences in the target lobe’s PFS distribution for the $\Delta\text{SUV}_{\text{max}}$ and $\Delta\text{SUV}_{\text{peak}}$ groups when the cut-off >30% change was applied. The target lobe’s PFS for the patients with a >30% decrease in SUV_{max} was significantly longer than those without [350±57 days 95% confidence interval (CI) 238-463 vs. (130±21 days 95% CI 90-171 (χ^2 (1): 6.774) p=0.009]. The target lobe’s PFS for the patients with more than 30% change in SUV_{peak} was statistically significantly longer than the patients with <30% change [338±59 days 95% CI 222-453 vs. 1730±38 days 95% CI 98-247 (χ^2 (1): 5.095, p=0.024]. Estimated survival chance at 209th day was 0.549±0.129 for 17 patients with no change in SUV_{max} while the estimated survival chance at 92nd day was 0.500±0.098 in patients with more than 30%

Table 1. Patient characteristics

Characteristics	Median (minimum-maximum)	n=43	%
Gender			
Male	-	30	70
Female	-	13	30
Age	63 (38-79) years	-	-
Underlying liver disease			
Yes	-	15	35
No	-	28	65
Previous treatments			
Surgery	-	5	12
RFA	-	3	7
TACE	-	4	9
TARE	-	1	2
Chemotherapy alone	-	14	36
Chemotherapy + LRT	-	4	9
None	-	12	-
Microsphere			
Resine	0.65 (0.6-1.3) GBq	6	14
Glass	6.5 (3-18) GBq	37	86
Target lobe			
Right	-	34	79
Left	-	8	19
Transplanted liver	-	1	2
Primary tumor			
HCC	-	17	40
Klatskin	-	7	16
Colon	-	14	32.5
Gastric	-	2	4.6
Breast	-	2	4.6
Pancreas	-	1	2.3
Presence of primary tumor for liver metastasis			
Yes	-	3	16
No	-	16	37
Extrahepatic metastases			
Yes	-	20	47
No	-	23	54
The largest diameter of target lesion			
Pre-treatment	49.7 (8-190) mm	-	-
Post-treatment	60.3 (9-190) mm	-	-
Number of lesions on target lobe			
1	-	11	26

1-5	-	11	26
5-10	-	7	16
>10	-	14	32
Tumor volume percent on target lobe	14 (1-100) %	-	-
Event after TARE			
Alive-disease progression	-	13	30
Alive-partial response or stable disease	-	8	19
Died due to disease progression/other causes	-	14	32
Died due to liver failure	-	8	19
HCC: Hepatocellular carcinoma, LRT: Locoregional therapy, RFA: Radiofrequency ablation, TACE: Transarterial chemoembolization, TARE: Transarterial radioembolization			

decrease in SUV_{max} . Estimated survival proportion at 209th days were 0.514 ± 0.134 in 16 patients without change in SUV_{peak} value; while this proportion was 0.519 ± 0.096 at 90th day for the patients with more than 30% decrease in SUV_{peak} value (Figure 2, Table 4).

Discussion

This study assessed the role of PET/CT with ¹⁸F-FLT, a radiopharmaceutical reflecting cell proliferation, in response evaluation after TARE and found significant longer PFS for the target liver lobe in patients with more than 30% decrease in ¹⁸F-FLT SUV_{max} and SUV_{peak} of the target liver lesion. There was no significant relationship between SUV values and treatment response.

Although there are metabolic and morphological techniques used for assessing treatment response, there is no standard response evaluation and follow-up protocol for TARE. Response evaluation after TARE is performed at different times with PET/CT, CT, or MR depending on the center's practice. Since response assessment with CT and MRI takes a longer time and has their limitations, PET/CT and PET/MR, functional, molecular and anatomical imaging techniques, are used for early response evaluation with agents that reflect tumor-specific metabolism (13,14,15,16,18,21,22,23). ¹⁸F-FDG PET/CT is the most common metabolic imaging method due to increased glucose metabolism in many types of cancer. ¹⁸F-FDG PET/CT can be used to assess treatment response in poorly differentiated and high-grade tumors. However, since small and well-differentiated tumors (such as HCC, NET) show low or no ¹⁸F-FDG uptake due to low glucose metabolism and cellularity, imaging with new-tumor-specific agents is needed (13,16,21,22,23). PET/CT imaging with ¹⁸F-FLT, which reflects cell proliferation, is a non-invasive imaging

Table 2. ¹⁸F-FLT PET/CT, ¹⁸F-FDG PET/CT and CT/MRI characteristics

Characteristics	Median (minimum-maximum)	n=43	%
Time from pretreatment ¹⁸F-FLT PET/CT to TARE	8 (1-63) days	-	-
Administered activity for pretreatment ¹⁸F-FLT PET/CT	6.4 (4.6-10.4) mCi	-	-
Pretreatment ¹⁸F-FLT PET/CT	-	43	-
Hypermetabolic lesions	-	6	14
Mixed uptake pattern	-	5	12
Isometabolic	-	13	30
Hypometabolic	-	19	44
Time from TARE to post-treatment ¹⁸F-FLT PET/CT	48 (33-73) days	-	-
Administered activity for post-treatment ¹⁸F-FLT PET/CT	6.4 (3.4-9.3) mCi	-	-
Post-treatment ¹⁸F-FLT PET/CT	-	43	-
Hypermetabolic lesions	-	2	5
Mixed uptake pattern	-	2	5
Isometabolic	-	12	28
Hypometabolic	-	27	62
Visual change of target lesions on ¹⁸F-FLT PET/CT			
Yes	-	24	56
No	-	19	44
Persistent hypermetabolic	-	2	5
Hypermetabolic mixed uptake	-	1	2
Hypermetabolic isometabolic	-	1	2
Hypermetabolic hypometabolic	-	2	5
Persistent mixed uptake	-	1	2
Mixed uptake hypometabolic	-	4	10
Persistent isometabolic	-	12	28
Isometabolic hypometabolic	-	1	2
Persistent hypometabolic	-	19	44
Time from pretreatment ¹⁸F-FDG PET/CT to TARE	15 (1-64) days	43	-
Time from TARE to post-treatment ¹⁸F-FDG PET/CT	47 (34-72) days	42	-
Post-treatment ¹⁸F-FDG PET/CT response assessment on target lobe			
Complete response	-	5	12
Partial response	-	13	
Stable disease	-	14	
Progressive disease	-	10	
Time from pretreatment CT/MR to TARE	13 (1-79) days	43	
Time from TARE to post-treatment CT/MR	97 (46-171) days	43	
Post-treatment CT/MR response assessment on target lobe			
Complete response	-	2	4
Partial response	-	7	16
Stable disease	-	17	40
Progressive disease	-	17	40
CT: Computed tomography, FLT: Fluorothymidine, ¹⁸ F-FDG: ¹⁸ F-fluorodeoxyglucose, MRI: Magnetic resonance imaging, PET/CT: Positron emission tomography/computed tomography, TARE: Transarterial radioembolization			

Table 3. ¹⁸ F-FLT PET/CT values	
SUV value	Median (minimum-maximum)
Pre-treatment ¹⁸F-FLT PET/CT	
SUV _{max}	6.7 (2.7-22) g/mL
SUV _{mean}	4.4 (1.1-12.4) g/mL
SUV _{peak}	4.9 (1-18.2) g/mL
SUV _{max} TBR	0.9 (0.3-3.0)
SUV _{mean} TBR	0.8 (0.2-2.4)
SUV _{peak} TBR	0.9 (0.1-3.2)
Post-treatment ¹⁸F-FLT PET/CT	
SUV _{max}	5.9 (2.5-31.9) g/mL
SUV _{mean}	3.6 (0.9-14.9) g/mL
SUV _{peak}	4.9 (1-26.5) g/mL
SUV _{max} TBR	0.7 (0.3-3.8)
SUV _{mean} TBR	0.6 (0.1-3.3)
SUV _{peak} TBR	0.7 (0.1-4.1)
Difference between pre- and post-treatment ¹⁸F-FLT values	
ΔSUV _{max}	-2.0 (-9.3-25.2)
ΔSUV _{mean}	0.9 (-8.1-17.1)
ΔSUV _{peak}	-2.0 (-8.2 -21.2)
ΔSUV _{max} TBR	-1.0 (-1.3-0.8)
ΔSUV _{mean} TBR	0 (-1.5-0.9)
ΔSUV _{peak} TBR	0 (-1.4-1.0)
FLT: Fluorothymidine, SUV _{max} : Maximum standard uptake value, SUV _{mean} : Mean standard uptake value, SUV _{peak} : Peak standard uptake value, TBR: Tumor background rate, PET/CT: Positron emission tomography/computed tomography	

method and has been used for the response evaluation (24,25,26,27). In addition to complex and competing factors in the FLT uptake mechanism, there are notable differences between patient preparation, imaging time after injection, protocol, amount of injected activity, reconstruction method, analysis techniques, timing before and after treatment, patient numbers, and disease groups in studies with F-¹⁸FLT PET/CT (24,25,26,27,28,29,30,31,32). As far as it is known, this is the first study to investigate the role of ¹⁸F-FLT PET/CT in the early response evaluation after TARE. There are few studies investigating the role of FLT PET/CT in evaluating the liver-specific treatment response, considering high background liver uptake especially in HCC patients that hamper the detection of liver/lesions. Studies evaluated therapy of TACE-receiving HCC patients and systemic chemotherapy-receiving liver metastatic colorectal cancer patients (28,29,32).

Sharma et al. (32) investigated the role of ¹⁸F-FLT PET/CT in assessing treatment response to TACE in HCC patients. They used temporal-intensity voxel clustering [kinetic

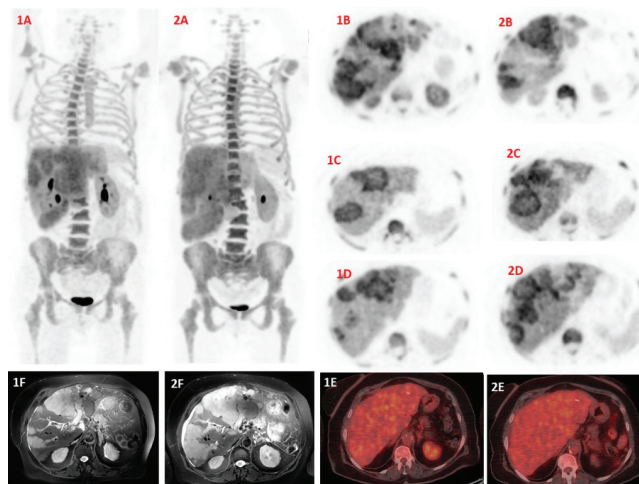


Figure 1. ¹⁸F-FLT PET MIP images before (1A) and after (2A) TARE therapy of a 70 years old female patient with HCC. Axial ¹⁸F-FLT PET images revealed hypermetabolic liver lesions (SUV_{max}: 16.1) before embolization (1B, 1C, 1D); post-therapy images revealed decreased activity on the left liver lobe, but most of the lesions were still hypermetabolic (SUV_{max}: 16.4) (2B, 2C, 2D). Pretreatment MR revealed multiple contrast-enhanced tumoral foci; after treatment, there were new lesions and progression on all lesions. T2-weighted MR shows multiple foci on both lobes before (1F) and after (2F) therapy. Tumoral foci were ¹⁸F-FDG non-avid (1E) and non-avidity did not change after TARE (2E)

FLT: Fluorothymidine, MIP: Maximum intensity projection, PET: Positron emission tomography, TARE: Transarterial radioembolization, SUV_{max}: Maximum standard uptake value, MR: Magnetic resonance

spatial filtering (KSF)] in lesion detection to overcome high background liver signal and thus ¹⁸F-FLT uptake but they could not achieve improvement in lesion detection by applying it. They reported 73% detection rate for pretreatment ¹⁸F-FLT PET, and 30% reduction in mean ¹⁸F-FLT PET uptake after TACE. In the current study, KSF could not be used due to unavailability, target lesion based detection rate for pretreatment ¹⁸F-FLT PET/CT was 53% (9/17) for HCC patients. In our study, although the change in ¹⁸F-FLT SUV_{max}, SUV_{mean} and SUV_{peak} values (Table 3) had no significant relationship with treatment response; patients with more than 30% decrease in ¹⁸F-FLT SUV_{max} and SUV_{peak} of the target lesion had significant longer PFS for target liver lobe after TARE.

Mogensen et al. (29) investigated the role of ¹⁸F-FLT PET/CT in patients with at least one measurable colorectal cancer liver metastasis and received first-line chemotherapy. They reported a reduction in ¹⁸F-FLT uptake in 85% patients, whereas there was no relationship between the early change in measured ¹⁸F-FLT SUV_{max} and RECIST 1.1 based response. In this study, similar to their study, there was no relationship between the change in SUV values (ΔSUV_{max}, ΔSUV_{mean} and ΔSUV_{peak}) and RECIST 1.1 and PERCIST-based responses. Contractor et al. (28) investigated the role of ¹⁸F-FLT PET/CT in evaluating the

Table 4. Statistical analysis of ¹⁸ F-FLT PET/CT values	
Parameter	p value
Visual change-early response	0.930 ^a
Visual change-anatomical response	0.710 ^a
¹⁸F-FLT SUV values-early response	
Δ SUV _{max}	0.290 ^a
Δ SUV _{mean}	0.100 ^b
Δ SUV _{peak}	0.430 ^a
Δ SUV _{max} TBR	0.600 ^a
Δ SUV _{mean} TBR	0.270 ^a
Δ SUV _{peak} TBR	0.280 ^a
¹⁸F-FLT SUV values-anatomical response	
Δ SUV _{max}	0.450 ^b
Δ SUV _{mean}	0.660 ^c
Δ SUV _{peak}	0.450 ^b
Δ SUV _{max} TBR	0.400 ^b
Δ SUV _{mean} TBR	0.400 ^b
Δ SUV _{peak} TBR	0.400 ^a
Overall survival-SUV values, visual change	
Δ SUV _{max}	0.630 ^c
Δ SUV _{mean}	0.160 ^c
Δ SUV _{peak}	0.870 ^c
Δ SUV _{max} TBR	0.210 ^c
Δ SUV _{mean} TBR	0.260 ^c
Δ SUV _{peak} TBR	0.590 ^c
Visual change	0.690 ^c
Progression free survival for target lobe	
Δ SUV _{max} [§]	0.009 ^c
Δ SUV _{mean} [§]	0.190 ^c
Δ SUV _{peak} [§]	0.024 ^c
^a Pearson chi-Square, ^b Fisher's Exact test, ^c Log Rank(Mantel-Cox), [§] if >30% percent change accepted as significant, FLT: Fluorothymidine, SUV _{max} : Maximum standard uptake value, SUV _{mean} : Mean standard uptake value, SUV _{peak} : Peak standard uptake value, TBR: Tumor background rate, PET/CT: Positron emission tomography/computed tomography	

treatment response of breast and colorectal cancer liver metastases. They reported that SUV_{ave} and SUV_{max} showed a significant decrease in responders two weeks after the first-line chemotherapy, and the change in FLT uptake can distinguish those who responded to the treatment from non-responders. In our study, ¹⁸F-FLT PET/CT was evaluated for the treatment response after TARE, an locoregional therapy (LRT), not a systemic treatment and there was no significant difference in the change in SUV_{max} , SUV_{mean} , and SUV_{peak} values among responder and non-responders.

The key point in the early evaluation of the treatment

response is to distinguish non-responder to discontinue unnecessary treatment, thus avoid toxicity and cost. It is critical to distinguish the resectable disease from those who require more aggressive treatment. Patients with shrinkage of tumors up to 30% are considered to have stable disease, according to RECIST 1.1, and are unresponsive to treatment (12,13,15,16). In this study, tumor sizes of patients with stable disease decreased, reflecting the beneficial effect of the treatment. However, since this decrease in size remained below the RECIST 1.1 response criteria, it was accepted as a stable disease and unresponsive to treatment. It should be recognized that patients with stable disease, especially with colon cancer, are accepted as responders and continue to receive systemic treatment in clinical practice (33). Generally, chemotherapy-refractory liver metastases are referred for LRTs such as TARE. Thus, even defined stable disease can provide longer survival and can be accepted as responsive. If patients with stable disease are accepted as responders to therapy, statistical analysis can be found significantly in long-term follow-up results. Because liver resection was not performed on any patient after radioembolization, except for the transplantation patient, post-treatment histopathological tumor changes, background of persistent ¹⁸F-FLT hypometabolism and correlation of histopathology with ¹⁸F-FLT values could not be evaluated.

It can be argued that the timing of the ¹⁸F-FLT was not right. But, TARE is an internal radiotherapy procedure, and response to radiotherapy is generally evaluated later than chemotherapy/selective systemic therapies (27,30). ¹⁸F-FDG PET/CT and ¹⁸F-FLT PET/CT imaging were done approximately ≥ 4 weeks after the procedure. Studies evaluating radiotherapy response revealed a significant relationship between ¹⁸F-FLT PET/CT and response or survival in patients with head-neck, esophageal, breast, lung, rectal, etc., cancer (30). This study distinguished real responders from non-responders who were grouped based on post-radiotherapy response assessment techniques ¹⁸F-FDG PET/CT and CT or MR. No correlation was found between the semi-quantitative values such as Δ SUV_{max}, Δ SUV_{mean}, Δ SUV_{peak}, SUV_{max} TBR, SUV_{mean} TBR, and SUV_{peak} TBR values calculated from ¹⁸F-FLT PET/CT images. There was a significant relationship with PFS for target liver lobe and >30% decrease in ¹⁸F-FLT SUV_{max} and SUV_{peak} of the target lesion.

Study Limitations

The most significant limitations of this study are the small sample size, consequent heterogeneous patient population, and the small number of patients who responded to the therapy. Therefore, in statistical analysis, results reaching

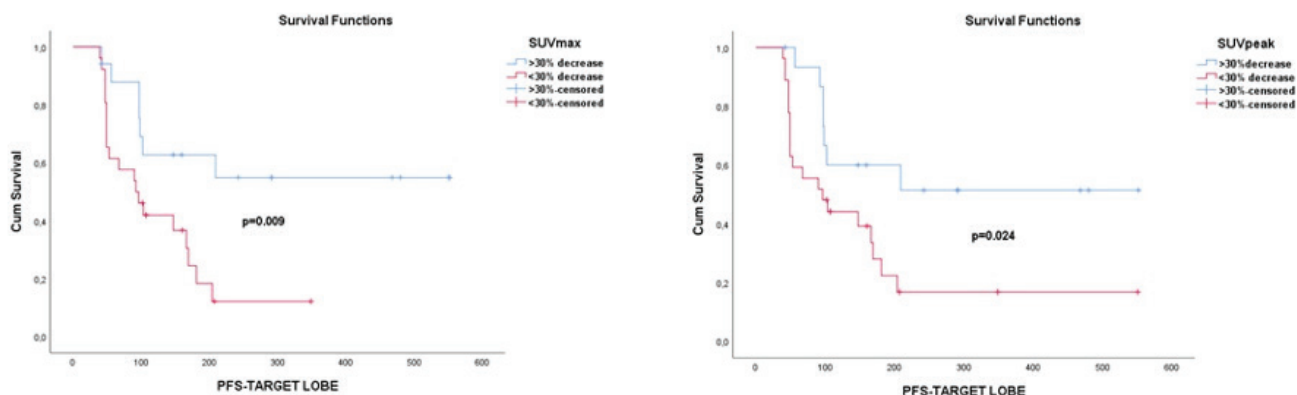


Figure 2. Kaplan-Meier method with log-rank test results revealing a significant difference in progression free survival distribution of target lobe for the patients with and without >30% change in SUV_{max} ($p=0.009$) and SUV_{peak} ($p=0.024$)
 SUV_{max} : Maximum standard uptake value, SUV_{peak} : Peak standard uptake value, PFS: Progression free survival

a significant degree could not be obtained for SUV parameters. TARE candidate patients have different clinical scenarios, such as highly variable liver lesion number and size, disease stage, history of single or multi-step systemic treatment, liver resection, transplant, and LRT's. Also, since there is a clear difference in disease etiologies, clinical and radiological status, it was not possible to standardize the patient group. Reproducible and re-applicable clinical data from a larger and standardized patient population are required to assess the role of ¹⁸F-FLT PET/CT in the evaluation of response to TARE treatment.

Conclusion

This study found significantly longer PFS for the target liver lobe in patients with more than 30% decrease in ¹⁸F-FLT SUV_{max} and SUV_{peak} of the liver lesion in patients with primary and metastatic unresectable liver tumors undergoing TARE. The changes in ¹⁸F-FLT PET/CT SUV_{max} , SUV_{mean} , SUV_{peak} , $SUV_{max\ TBR}$, $SUV_{mean\ TBR}$, and $SUV_{peak\ TBR}$ values had no significant relationship with response in ¹⁸F-FDG PET/CT or in contrast-enhanced CT/MR after TARE. ¹⁸F-FLT PET/CT can be used as an alternative/complementary imaging method to ¹⁸F-FDG PET/CT in the early evaluation of the treatment response in patients undergoing TARE for primary or secondary liver tumor.

Ethics

Ethics Committee Approval: Ankara University Faculty of Medicine Human Research Ethics Committee Approval (İ3-117-19).

Informed Consent: Informed consent was obtained from the volunteers included in the study.

Peer-review: Externally and internally peer-reviewed.

Authorship Contributions

Surgical and Medical Practices: M.S.B., E.C.Ç., D.N., Concept: D.N., N.Ö.K., M.S.B., E.C.Ç., Design: D.N., N.Ö.K., Data Collection or Processing: D.N., Analysis or Interpretation: S.H., D.N., Literature Search: D.N., N.Ö.K., Writing: D.N., N.Ö.K., K.M.K.

Conflict of Interest: No conflict of interest was declared by the authors.

Financial Disclosure: The authors declared that this study has received no financial support.

References

1. Bosch FX, Ribes J, Díaz M, Cléries R. Primary liver cancer: worldwide incidence and trends. *Gastroenterology* 2004;127(5 Suppl 1):S5-S16.
2. Sung H, Ferlay J, Siegel RL, Laversanne M, Soerjomataram I, Jemal A, Bray F. Global Cancer Statistics 2020: GLOBOCAN Estimates of Incidence and Mortality Worldwide for 36 Cancers in 185 Countries. *CA Cancer J Clin* 2021;71:209-249.
3. Yao FY, Bass NM, Nikolai B, Merriman R, Davern TJ, Kerlan R, Ascher NL, Roberts JP. A follow-up analysis of the pattern and predictors of dropout from the waiting list for liver transplantation in patients with hepatocellular carcinoma: implications for the current organ allocation policy. *Liver Transpl* 2003;9:684-692.
4. Harding JJ, Abou-Alfa GK. Treating advanced hepatocellular carcinoma: how to get out of first gear. *Cancer* 2014;120:3122-3130.
5. Memon K, Lewandowski RJ, Kulik L, Riaz A, Mulcahy MF, Salem R. Radioembolization for primary and metastatic liver cancer. *Semin Radiat Oncol* 2011;21:294-302.
6. Ryan MJ, Willatt J, Majdalany BS, Kielar AZ, Chong S, Ruma JA, Pandya A. Ablation techniques for primary and metastatic liver tumors. *World J Hepatol* 2016;8:191-199.
7. Viñal D, Minaya-Bravo A, Prieto I, Feliu J, Rodriguez-Salas N. Yttrium-90 transarterial radioembolization in patients with gastrointestinal malignancies. *Clin Transl Oncol* 2022;24:796-808.
8. Yu SCH, Hui JW, Li L, Cho CC, Hui EP, Chan SL, Yeo WM. Comparison of chemoembolization, radioembolization, and transarterial ethanol ablation for huge hepatocellular carcinoma (≥ 10 cm) in tumour

- response and long-term survival outcome. *Cardiovasc Intervent Radiol* 2022;45:172-181.
9. Kooby DA, Egnatashvili V, Srinivasan S, Chamsuddin A, Delman KA, Kauh J, Staley CA, Kim HS. Comparison of yttrium-90 radioembolization and transcatheter arterial chemoembolization for the treatment of unresectable hepatocellular carcinoma. *J Vasc Interv Radiol* 2010;21:224-230.
 10. Salem R, Gordon AC, Mouli S, Hickey R, Kallini J, Gabr A, Mulcahy MF, Baker T, Abecassis M, Miller FH, Yaghmai V, Sato K, Desai K, Thornburg B, Benson AB, Rademaker A, Ganger D, Kulik L, Lewandowski RJ. Y90 radioembolization significantly prolongs time to progression compared with chemoembolization in patients with hepatocellular carcinoma. *Gastroenterology* 2016;151:1155-1163.e2.
 11. Xing M, Kokabi N, Camacho JC, Kooby DA, El-Rayes BF, Kim HS. 90Y radioembolization versus chemoembolization in the treatment of hepatocellular carcinoma: an analysis of comparative effectiveness. *J Comp Eff Res* 2013;2:435-444.
 12. Duffaud F, Therasse P. New guidelines to evaluate the response to treatment in solid tumors. *Bull Cancer* 2000;87:881-886.
 13. Forner A, Ayuso C, Varela M, Rimola J, Hessheimer AJ, de Lope CR, Reig M, Bianchi L, Llovet JM, Bruix J. Evaluation of tumor response after locoregional therapies in hepatocellular carcinoma: are response evaluation criteria in solid tumors reliable? *Cancer* 2009;115:616-623.
 14. Miller FH, Kepcke AL, Reddy D, Huang J, Jin J, Mulcahy MF, Salem R. Response of liver metastases after treatment with yttrium-90 microspheres: role of size, necrosis, and PET. *AJR Am J Roentgenol* 2007;188:776-783.
 15. Singh P, Anil G. Yttrium-90 radioembolization of liver tumors: what do the images tell us? *Cancer Imaging* 2014;13:645-657.
 16. Wong CY, Salem R, Raman S, Gates VL, Dworkin HJ. Evaluating 90Y-glass microsphere treatment response of unresectable colorectal liver metastases by [18F]FDG PET: a comparison with CT or MRI. *Eur J Nucl Med Mol Imaging* 2002;29:815-820.
 17. Dubash SR, Idowu OA, Sharma R. The emerging role of positron emission tomography in hepatocellular carcinoma. *Hepat Oncol* 2015;2:191-200.
 18. Fortunati E, Argalia G, Zanoni L, Fanti S, Ambrosini V. New PET radiotracers for the imaging of neuroendocrine neoplasms. *Curr Treat Options Oncol* 2022;23:703-720.
 19. Ho CL, Chen S, Yeung DW, Cheng TK. Dual-tracer PET/CT imaging in evaluation of metastatic hepatocellular carcinoma. *J Nucl Med* 2007;48:902-909.
 20. Ho CL, Chen S, Cheung SK, Leung TWT. Significant Value of 11C-acetate and 18F-fluorodeoxyglucose PET/computed tomography on 90Y microsphere radioembolization for hepatocellular carcinoma. *PET Clin* 2019;14:459-467.
 21. Park JW, Kim JH, Kim SK, Kang KW, Park KW, Choi JI, Lee WJ, Kim CM, Nam BH. A prospective evaluation of 18F-FDG and 11C-acetate PET/CT for detection of primary and metastatic hepatocellular carcinoma. *J Nucl Med* 2008;49:1912-1921.
 22. Sacks A, Peller P, Surasi DS, Chatburn L, Mercier G, Subramaniam R. Value of PET/CT in the management of liver metastases, part 1. *AJR Am J Roentgenol* 2011;197:W256-259.
 23. Sacks A, Peller PJ, Surasi DS, Chatburn L, Mercier G, Subramaniam RM. Value of PET/CT in the management of primary hepatobiliary tumors, part 2. *AJR Am J Roentgenol* 2011;197:W260-265.
 24. Chalkidou A, Landau DB, Odell EW, Cornelius VR, O'Doherty MJ, Marsden PK. Correlation between Ki-67 immunohistochemistry and 18F-fluorothymidine uptake in patients with cancer: a systematic review and meta-analysis. *Eur J Cancer* 2012;48:3499-3513.
 25. Machulla HJ, Blocher A, Kuntzsch M, Piert M, Wei R, Grierson J. Simplified labeling approach for synthesizing 3'-Deoxy-3'-[18F]fluorothymidine ([18F]FLT). *J Radioanal Nucl Chem* 2000;243:843-846.
 26. Krohn KA, Mankoff DA, Eary JF. Imaging cellular proliferation as a measure of response to therapy. *J Clin Pharmacol* 2001;41:96S-103S.
 27. Peck M, Pollack HA, Friesen A, Muzi M, Shoner SC, Shankland EG, Fink JR, Armstrong JO, Link JM, Krohn KA. Applications of PET imaging with the proliferation marker [18F]-FLT. *Q J Nucl Med Mol Imaging* 2015;59:95-104.
 28. Contractor K, Challapalli A, Tomasi G, Rosso L, Wasan H, Stebbing J, Kenny L, Mangar S, Riddle P, Palmieri C, Al-Nahhas A, Sharma R, Turkheimer F, Coombes RC, Aboagye E. Imaging of cellular proliferation in liver metastasis by [18F]fluorothymidine positron emission tomography: effect of therapy. *Phys Med Biol* 2012;57:3419-3433.
 29. Mogensen MB, Loft A, Aznar M, Axelsen T, Vainer B, Osterlind K, Kjaer A. FLT-PET for early response evaluation of colorectal cancer patients with liver metastases: a prospective study. *EJNMMI Res* 2017;7:56.
 30. Sanghera B, Wong WL, Sonoda LI, Beynon G, Makris A, Woolf D, Ardeshta K. FLT PET-CT in evaluation of treatment response. *Indian J Nucl Med* 2014;29:65-73.
 31. Muzi M, Vesselle H, Grierson JR, Mankoff DA, Schmidt RA, Peterson L, Wells JM, Krohn KA. Kinetic analysis of 3'-deoxy-3'-fluorothymidine PET studies: validation studies in patients with lung cancer. *J Nucl Med* 2005;46:274-282.
 32. Sharma R, Inglese M, Dubash S, Lu H, Pinato DJ, Sanghera C, Patel N, Chung A, Tait PD, Mauri F, Crum WR, Barwick TD, Aboagye EO. Monitoring response to transarterial chemoembolization in hepatocellular carcinoma using 18F-fluorothymidine PET. *J Nucl Med* 2020;61:1743-1748.
 33. Chibaudel B, Maindrault-Goebel F, Lledo G, Mineur L, André T, Bennamoun M, Mabro M, Artru P, Carola E, Flesch M, Dupuis O, Colin P, Larsen AK, Afchain P, Tournigand C, Louvet C, de Gramont A. Can chemotherapy be discontinued in unresectable metastatic colorectal cancer? The GERCOR OPTIMO2 Study. *J Clin Oncol* 2009;27:5727-5733.



Volumetric Evaluation of Staging ¹⁸F-FDG PET/CT Images in Patients with Esophageal Cancer

Özofagus Kanseri Hastalarda Evreleme ¹⁸F-FDG PET/CT Görüntülerinin Hacimsel Değerlendirilmesi

✉ Nazlı Pınar Karahan Şen¹, ✉ Ayşegül Aksu², ✉ Gamze Çapa Kaya¹

¹Dokuz Eylül University Faculty of Medicine, Department of Nuclear Medicine, İzmir, Turkey

²University of Health and Sciences Turkey, Başakşehir Çam and Sakura City Hospital, Clinic of Nuclear Medicine, İstanbul, Turkey

Abstract

Objectives: The aim of this study was to evaluate the metastatic potential of primary tumor and survival in esophageal cancer (EC) patients by using metabolic tumor volume (MTV) and total lesion glycolysis (TLG) from the staging ¹⁸F-fluorodeoxyglucose (FDG) positron emission tomography/computed tomography (PET/CT) images. Another aim is to determine a tumor volume-based cut-off value to predict long-term survival.

Methods: Medical records of EC patients were retrospectively evaluated. Sixty-two patients with staging ¹⁸F-FDG PET/CT and at least five years of follow-up were included in the study. The region of interest to the primary tumor and all metastatic sites was created and MTV and TLG values of the primary tumor (MTVp, TLGp) and total tumor volume (MTVt and TLGt) values were obtained. The relationship between the obtained MTV and TLG values and short-time (one-year) and long time (five-year) survival was investigated.

Results: Significant factors on survival were determined as lymph node or distant metastasis (p=0.024, 0.008, respectively) at the staging PET/CT. A significant relationship between volumetric parameters of the primary tumor and total tumor burden (MTVp, TLGp, MTVwb and TLGwb) between survivors and non-survivors for one-year and five-year was detected. In receiver operating characteristics analysis, the most significant volumetric parameter was MTVwb, with area under curve 0.771 in estimated five-year survival. The best cut-off value was detected as 36.1 mL with 78% sensitivity and 75% specificity for MTVwb in determining long-term survivors.

Conclusion: Tumor burden in ¹⁸F-FDG PET/CT images at the time of staging of patients with EC will contribute to the prediction of long-term survivors.

Keywords: ¹⁸F-FDG PET/CT, metabolic tumor volume, esophageal cancer

Öz

Amaç: Bu çalışmanın amacı evreleme ¹⁸F-florodeoksiglukoz (FDG) pozitron emisyon tomografisi/bilgisayarlı tomografi (PET/CT) görüntülerinden metabolik tümör hacmi (MTV) ve toplam lezyon glikolizini (TLG) kullanarak özofagus kanseri (ÖK) hastalarında primer tümörün metastatik potansiyelini ve sağkalımı değerlendirmektir. Diğer bir amaç, uzun süreli sağkalımı tahmin etmek için tümör hacmine dayalı bir eşik değeri belirlemektir.

Yöntem: ÖK tanılı hastaların tıbbi kayıtları geriye dönük olarak değerlendirildi. Evreleme anında ¹⁸F-FDG PET/CT yapılan ve en az beş yıllık takip süresi olan 62 hasta çalışmaya dahil edildi. Primer tümörün ve tüm metastatik bölgelerin ilgi alanı oluşturuldu ve primer tümörün MTV ve TLG değerleri (MTVp, TLGp) ve toplam tümör hacmi (MTVt ve TLGt) değerleri elde edildi. Elde edilen MTV ve TLG değerleri ile kısa süreli (bir yıllık) ve uzun süreli (beş yıllık) sağkalım arasındaki ilişki araştırıldı.

Address for Correspondence: Nazlı Pınar Karahan Şen MD, Dokuz Eylül University Faculty of Medicine, Department of Nuclear Medicine, İzmir, Turkey

Phone: +90 232 412 42 90 **E-mail:** drpinarkarahan@hotmail.com ORCID ID: orcid.org/0000-0002-1562-9085

Received: 03.11.2021 **Accepted:** 20.02.2022

©Copyright 2022 by Turkish Society of Nuclear Medicine
Molecular Imaging and Radionuclide Therapy published by Galenos Yayınevi.

Bulgular: Sağkalım üzerinde önemli faktörler evreleme PET/BT'de lenf nodu veya uzak metastaz bulunması (sırasıyla; $p=0,024$, $0,008$) olarak belirlendi. Primer tümörün volumetrik parametreleri ile toplam tümör yükü (MTVp, TLGp, MTVwb ve TLGwb) arasında, bir yıl ve beş yılda sağ kalanlar ve ölenler arasında anlamlı bir ilişki tespit edildi. Alıcı işlem karakteristikleri analizinde, beş yıllık sağkalımı tahmin etmede en önemli hacimsel parametre eğrinin altındaki alan $0,771$ ile MTVwb idi. Uzun süreli sağ kalanların belirlenmesinde MTVwb için en iyi kesim değeri %78 duyarlılık ve %75 özgüllük ile $36,1$ mL olarak tespit edildi.

Sonuç: ÖK'li hastaların evreleme anındaki ^{18}F -FDG PET/BT görüntülerindeki tümör yükü, uzun dönemde sağ kalanların tahminine katkıda bulunacaktır.

Anahtar kelimeler: ^{18}F -FDG PET/BT, metabolik tümör hacmi, özofagus kanseri

Introduction

Esophageal cancer (EC) ranks seventh cause in terms of incidence and the sixth most common cause of mortality across the world (1). Five-year survival rate is 19.9% (2). In distant metastatic (DM) disease, worse prognosis and lower five-year survival rates are declared (5.2%) (2).

^{18}F -fluorodeoxyglucose (FDG) positron emission tomography/computed tomography (PET/CT) is a standard diagnostic workup in EC. PET/CT provides essential information about the distribution of the lesions, size, and presence of metastases at the time of staging. As a quantitative parameter standard uptake value (SUV) provides information about the intensity of the uptake in the lesion and most commonly maximum standard uptake value (SUV_{max}) is used to determine the tumor metabolic activity (3). However, SUV do not represent the whole tumor (4). Metabolic tumor volume (MTV) and tumor lesion glycolysis (TLG) are the parameters that are increasingly being studied to define the combined volumetric and metabolic characteristics of the tumors (5,6).

This study evaluates the relationship between the volumetric characteristics of the primary tumor obtained from the staging ^{18}F -FDG PET/CT images and the metastatic potential of the primary tumor at the time of diagnosis in EC patients. Another aim is, use volumetric parameters, to determine a volume-based cut-off value to predict long-term survival in EC patients.

Materials and Methods

Patients' medical records, who had undergone ^{18}F -FDG PET/CT at the time of initial staging with EC, between January 2008 and September 2019 at our department, were retrospectively analyzed. Patients whose follow-up was insufficient (less than five-years) were excluded. In total, 62 patients were included in this study. This study was approved by the Local Ethical Committee at Dokuz Eylül University Institution (decision no: 2019/23-09, date: 16.09.2019).

^{18}F -FDG PET/CT

Patients with appropriate patient preparation (fasting for at least 4 h and adequate blood glucose levels) were enrolled in PET/CT. Approximately 1 h after the average injection of 4.1 MBq/kg ^{18}F -FDG all scan was performed using a Philips Gemini TOF PET/CT (Eindhoven, Netherlands). The emission scans were 10-12 beds per patient and for 1.5 minutes/bed position and the transmission scans were obtained from low-dose CT with 50 mAs and 120 kVp, 5 mm re-structured section thickness.

Determination of Region of Interest (ROI)

Conventional and volumetric data of the primary tumor and all metastatic sites were obtained by drawing the ROI of the primary tumors from PET/CT images via LIFEX software (<http://www.lifexsoft.org>) by a nuclear medicine physician (12 years of experience) (7,8). To prevent manual error, the area of interest was drawn in the tumor area with a minimum SUV of 2 and above (Figure 1). SUV (maximum and mean), MTV and TLG of the primary tumor (MTVp, TLGp) and total tumor volume in the whole body (MTVwb and TLGwb) values were obtained.

Statistical Analysis

Statistical Package for the Social Sciences software version 22.0 for Windows was used for statistical analysis. A statistically significant difference between the obtained SUV, MTV and TLG values and short-time (one-year), long time (five-year) survival; lymph node (LN) and DM in subgroups according to the localization and histopathology were investigated. Non-parametric tests (The Mann-Whitney U test and Kruskal-Wallis test) were used because of the heterogeneity of our data. A p value of <0.05 was set as significant. The receiver operating characteristics (ROC) analysis was performed for significant parameters ($p<0.05$) to determine a cut-off value to predict long and short-time survival. Median overall survival (OS) and cumulative survival were calculated using Kaplan-Meier analysis.

Patient Group and Treatment Procedure

Thirty-one patients were administered neoadjuvant chemotherapy (NCRT) but only 13 of them had surgery

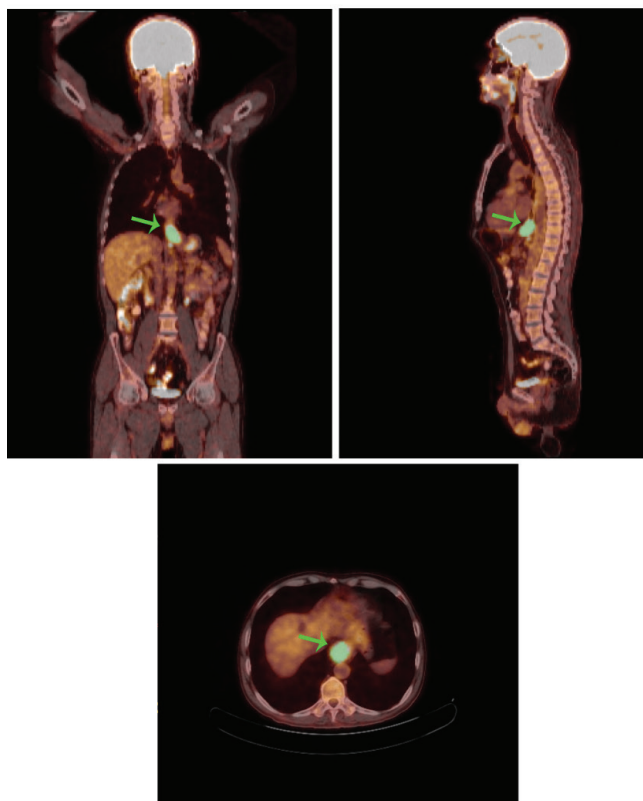


Figure 1. Arrows depicts an example of region of interest in a patient after NCRT. One patient underwent surgery after only neoadjuvant chemotherapy. Four patients underwent surgery as first-line treatment. Thirteen patients with no chance of surgery or local treatment were administered only chemotherapy. After diagnosis, twelve patients had no chance to start a treatment procedure. One patient with only local disease had no chance to administer chemotherapy, only radiotherapy applied, resulted with progression.

Results

Seventeen (27.4%) of 62 patients had DM and 42 (67.7%) had local lymph node metastasis (LNM). Twenty patients (32.3%) had only a local tumor with no metastasis (NM) (no LNM or DM). Twenty-five patients (40.3%) had primary tumor and local only lymph node metastasis (OLNM), and seventeen patients (27.4%) had both local LN and DM (lung, bone, liver or distant lymph node). Fifty patients (80.6%) had squamous cell cancer (SCC) and 12 patients (19.4%) had adeno cancer (AC). Primary tumors were located in the upper, middle and lower esophagus, in 10 (16.1%), 26 (41.9%), and 26 (41.9%) patients, respectively (Table 1).

LNM was detected in 62% of the SCC and 91.7% of the AC groups, and DM rates were 24% and 41.7%, respectively.

	Total (all patients)
Patient number	62 (100%)
Mean age	60±12 (26-85)
AC	12 (19.4%)
SCC	50 (80.69%)
Upper	10 (16.1%)
Middle	26 (41.9%)
Lower	26 (41.9%)
1-year survivors	30 (48.4%)
1-year non-survivors	32 (51.6%)
5-year survivors	12 (19.4%)
5-year non-survivors	50 (80.6%)
Female	22 (35.5%)
Male	40 (64.5%)
NM	20 (32.3%)
LNM	42 (67.7%)
OLNM	25 (40.3%)
DM	17 (27.4%)

AC: Adeno cancer, SCC: Squamous cell cancer, NM: No metastasis, LNM: Lymph node metastasis positive, OLNM: Only lymph node metastasis, DM: Distant metastasis

According to metastasis rates, no significant difference was detected between pathological subgroups ($p>0.05$). It was observed that primary tumor volumetric parameters (MTVp, TLGp, SUV_{max} and SUV_{mean}) were not significant indicators in predicting LN or DM at the time of staging.

Median OS was detected 13.3 ± 2.0 months [95% confidence interval (CI): 9.35-17.26]. Median OS for NM, OLNM and DM was detected 20.9 ± 16.4 months, 12.6 ± 2.2 and 8.3 ± 3.2 , respectively ($p=0.004$) (Figure 2). LNM and DM at the staging PET/CT were detected as significant factors ($p=0.024$, 0.008 , respectively) on OS in the Kaplan-Meier analysis. However, location of the tumor, gender, or histopathological subtype were not significant factors ($p>0.05$). One-year and five-year cumulative OS were determined as $56.5\pm 0.63\%$ and $19.4\pm 0.50\%$, respectively.

When evaluated according to histopathological subtypes, MTVp, TLGp, and SUV_{max} and SUV_{mean} of the primary tumor had no significant difference between SCC and AC patients ($p>0.05$). Similarly, MTVp, TLGp, and SUV_{max} and SUV_{mean} of the primary tumor were not related to the tumor's localization ($p>0.05$). According to the localization of the primary tumor, a significant difference was detected between SCCs and AC ($p<0.005$). SCCs were detected mainly located in the middle esophagus, unlike AC located mainly in the lower esophagus.

A significant relationship between volumetric parameters of the primary tumor and total tumor burden (MTVp, TLGp, MTVwb and TLGwb) between survivors and non-survivors for one-year and five-year was detected. In ROC analysis, the most significant volumetric parameter was MTVwb, with area under curve (AUC) 0.771 in estimated five-year survival. The results are given in Table 2. According to the

Youden index, the best cut-off value was detected as 36.1 mL with 78% sensitivity and 75% specificity for MTVwb in determining long-term survivors (Figure 3). When patients were divided into groups according to the cut-off value as low (<36.1 mL) and high (≥36.1 mL) MTVwb, Kaplan-Meier analysis demonstrated high and low MTVwb as a significant factor on OS (p<0.001). In the low MTVwb and high MTVwb groups, OS was detected as 10.1±1.94 and 35.9±19.34 months, respectively (Figure 4).

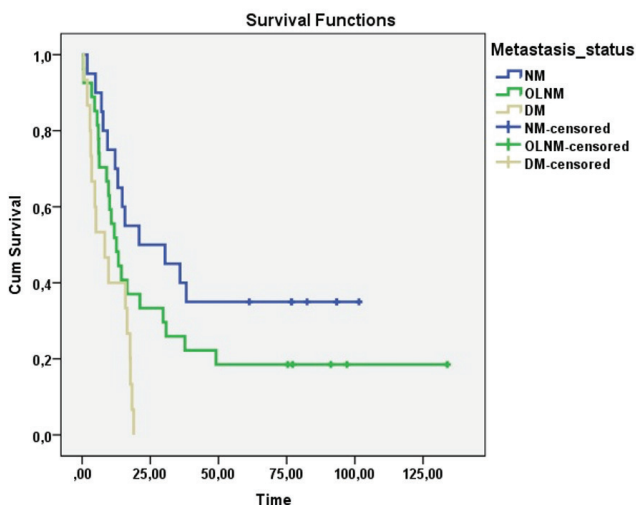


Figure 2. Kaplan-Meier curves demonstrate 5-year survival in patient groups according to metastasis (no metastasis, only lymph node metastasis, and distant metastasis)

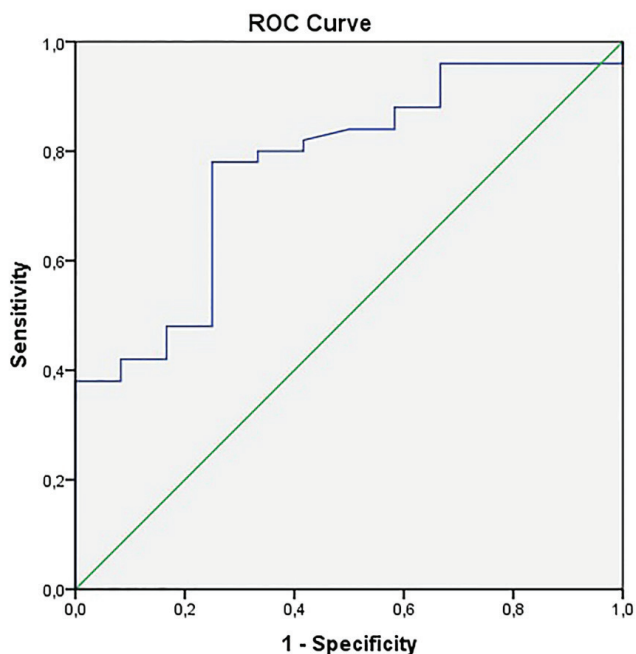


Figure 3. Receiver operating characteristics curve of MTVwb for 5-year survival is given in the figure
MTVwb: Metabolic tumor volume of whole body

Discussion

In this study, we investigated the metastatic potential of the primary tumor at the time of diagnosis and the role of metabolic parameters (MTV and TLG) in OS for both the primary tumor and metastasis obtained from ¹⁸F-FDG PET/CT images. We determined a cut-off value for tumor volume to predict long-time survivors. Among the volumetric parameters, MTVwb, which depicts whole-body tumor volume (tumor burden) in a patient, was determined to be the most significant parameter in detecting five-year survival in patients with EC.

An endpoint of our study was whether the primary tumor’s metabolic features obtained from staging PET/CT was associated with LN or DM. Studies investigate the relation between the metabolic parameters in EC patients and LN or DM or response to treatment. A study, which investigated LNM status at baseline PET/CT, determined in multivariate analysis that MTV of primary tumor with 40% threshold method [Odds ratio (OR): 1.127, p=0.04] and SUR_{max} (maximum tumor-to-blood SUV ratio) (OR:

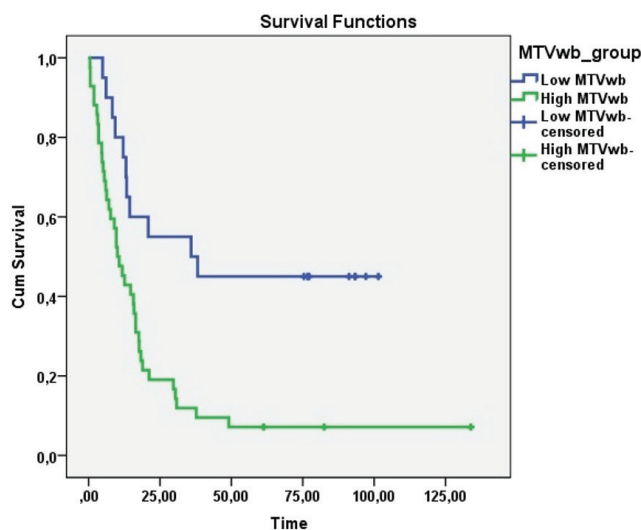


Figure 4. Kaplan-Meier curves demonstrate 5-year survival in patient groups according to low (<36.1 mL) and high (≥36.1 mL) MTVwb groups
MTVwb: Metabolic tumor volume of whole body

Table 2. Receiver operating characteristics analysis results of survival

	1-year survival			5-year survival		
	p value	AUC	(95% CI)	p value	AUC	(95% CI)
MTVp	0.048	0.646	(0.508-0.785)	0.041	0.691	(0.525-0.857)
TLGp	0.053	0.643	(0.505-0.782)	0.089	0.659	(0.500-0.819)
MTVwb	0.012	0.686	(0.553-0.820)	0.004	0.771	(0.631-0.911)
TLGwb	0.009	0.694	(0.562-0.826)	0.011	0.739	(0.597-0.882)

AUC: Area under curve, CI: Confidence interval, MTVp: Metabolic tumor volume of primary tumor, TLGp: Total lesion glycolysis of primary tumor, MTVwb: Metabolic tumor volume of whole body, TLGwb: Total lesion glycolysis of whole body

1.446, $p=0.004$) were independent predictors of LNM, with sensitivity and specificity were 51.2%, 83.7% vs. 53.7%, 79.1% respectively. In the detection of occult LNM, only MTV was detected significantly ($p=0.024$) (9). However, our study revealed that primary tumor metabolic parameters (MTVp, TLGp, SUV_{max} and SUV_{mean}) were not significant indicators in predicting LN or DM at the time of staging. Also, the discrimination of histopathological subtypes of EC is impossible with current imaging modalities. One study suggested that SUV_{max} was not related to histopathological subtypes of EC but, MTV values of AC patients were significantly higher than those of SCC patients (10). However, there are also studies, which could not determine histopathological subtypes with SUV_{max} or MTV (11). Similarly, in our study, primary tumor's volumetric parameters have no significant difference in discriminating histopathological subtypes or localization of the primary tumor ($p>0.05$). Two main histological subtypes, SCC and AC, account for 95% of all EC cases (12). SCC is the most commonly seen subtype and mainly located in the mid to upper part of the esophagus (13). However, AC is mainly located in the distal esophagus. In accordance with literature, according to the localization of primary tumors, a significant difference was detected between the two histopathological subtypes ($p=0.005$) in our study.

Comparison of primary tumor MTV and TLG calculated from initial PET/CT images in patients with EC and treatment response, OS and progression-free survival have been investigated in various studies (14,15,16,17,18,19). A study reported that MTV and TLG of the primary tumor were associated with survival after surgery ($p\leq 0.05$) (16). Another study, which included 151 EC patients, while MTV of the primary tumor was detected as an independent prognostic factor on OS ($p=0.021$), the SUV_{max} of the primary tumor was not significant (17). Similarly, in our study, among the metabolic features of the primary tumor (SUV_{max} , SUV_{mean} , MTVp and TLGp) only MTVp was significantly related to one-year and five-year OS ($p=0.048$, 0.041, respectively).

There are studies have investigated the role of whole-body TLG and MTV on survival in EC patients. Kitajima et al. (20) stated that MTVwb and TLGwb are predictors of OS in univariate analysis ($p<0.0001$), but multivariate analysis pointed to a reduction rate of TLG [Hazard ratios (HR): 2.21, 95% CI, 1.04-4.68; $p=0.040$] as an independent predictor of OS. In a study in which pretreatment whole-body TLG, MTV and SUV_{max} were investigated in patients with EC, while SUV_{max} was not significant, whole-body TLG and MTV were determined as independent predictors of OS, local control, and progression-free survival. HR of TLG and MTV for OS were determined as HR: 2.15 and HR: 2.36, respectively (21). Similarly, our results demonstrate that MTVwb and TLGwb are significant predictors of OS. Apart from our study, Takahashi et al. (21) studied in a limited group and included in their study only patients with stage 2 and 3 thoracic esophageal SCC patients and created the groups for low and high MTV and TLG based on median values (15.57 mL for MTV and 103.68 for TLG). Additionally, in their study, they underline that whole-body TLG has a higher HR than MTV. However, our results determined MTVwb has a higher predictive value than TLGwb. In another study, the five-year survival rate was detected as 49.8%, and MTVp, TLGp and TLGwb were associated with OS. The only significant parameter was TLGwb in multivariate analysis. However, that study included only stage 1-3 SCC EC patients and did not calculate MTVwb values (22). Similar to our results, Zhang et al. (11) reported in their study, in which 36 patients evaluated for short (less than one-year) and long (higher than one-year) survival, higher MTV values were related to short OS in EC. In our study, LNM and DM at the staging PET/CT were detected as significant factors ($p=0.024$, 0.008, respectively) on OS in EC patients. Additionally, metastasis groups (NM, OLN and DM) were significant factors in long-term survival ($p=0.004$). However, the determined MTVwb cut-off value was demonstrated as the most significant factor on OS ($p<0.001$).

Study Limitations

Limited sample size, heterogeneity in the number of patients in the pathological subgroups and the retrospective design of the study are the main limitations.

Our patient group is a heterogeneous group consisting of patients with a diagnosis of EC who underwent PET/CT at the time of staging, but in clinically different stages, with different treatment and management processes. In the treatment management, patients with EC are primarily evaluated in terms of operability, and even in locally advanced stages, the lesion size is reduced with neoadjuvant treatment methods. The surgery option is considered first because surgery is accepted as the most effective treatment strategy (23). In metastatic patients, chemotherapy regimens are the first choice. However, some patients may die before starting or completing treatment regimens, with complications such as bleeding due to the disease, fistula, aspiration, decreased oral intake due to mass effect, while still at the time of staging. Although heterogeneity may seem like a disadvantage in our study group, in general practice, we already encounter a heterogeneous patient group.

In our data, in predicting long-term survivors, AUC was calculated 0.771 for MTVwb. This value is acceptable for determine a cut-off value. The ROC curve is a plot of sensitivity versus 1-specificity at all possible cut-off values. Different cut-off values could be calculated from ROC plot. However, we determined our best cut-off value as 36.1 mL using Youden index. In it is also possible to determine different cut-off values for different patient groups. Including only local/or only metastatic patients could give different cut-off values. Heterogeneity of our data could be seen as an advantage in this regard. Conducting similar studies in different clinics will be beneficial for consolidating the results of our study.

Conclusion

This study suggests that, in addition to the role of metabolic volume of the primary tumor in initial ^{18}F -FDG PET/CT, tumor burden (MTVwb) in ^{18}F -FDG PET/CT images at the time of staging of patients with EC will contribute to the prediction of the long-term survivors. Patients with MTVwb <36.1 mL at the staging ^{18}F -FDG PET/CT could demonstrate better OS results and this value could predict long-term survivors.

Ethics

Ethics Committee Approval: This study was approved by the Local Ethical Committee at Dokuz Eylul University Institution (decision no: 2019/23-09, date: 16.09.2019).

Informed Consent: Retrospective cross sectional study.

Peer-review: Externally peer-reviewed.

Authorship Contributions

Surgical and Medical Practices: N.P.K.Ş., A.A., G.Ç.K., Concept: N.P.K.Ş., G.Ç.K., Design: N.P.K.Ş., G.Ç.K., Data Collection or Processing: N.P.K.Ş., Analysis or Interpretation: N.P.K.Ş., A.A., Literature Search: N.P.K.Ş., Writing: N.P.K.Ş.

Conflict of Interest: No conflict of interest was declared by the authors.

Financial Disclosure: The authors declared that this study has received no financial support.

References

1. Sung H, Ferlay J, Siegel RL, Laversanne M, Soerjomataram I, Jemal A, Bray F. Global Cancer Statistics 2020: GLOBOCAN estimates of incidence and mortality worldwide for 36 cancers in 185 countries. *CA Cancer J Clin* 2021;71:209-249.
2. Howlader N, Noone AM, Krapcho M, Miller D, Brest A, Yu M, Ruhl J, Tatalovich Z, Mariotto A, Lewis DR, Chen HS, Feuer EJ, Cronin KA (eds). SEER Cancer Statistics Review, 1975-2018, National Cancer Institute. Bethesda. Available from: https://seer.cancer.gov/csr/1975_2018/ based on November 2020 SEER data submission, posted to the SEER web site, April 2021.
3. Makino T, Yamasaki M, Tanaka K, Tatsumi M, Takiguchi S, Hatazawa J, Mori M, Doki Y. Importance of positron emission tomography for assessing the response of primary and metastatic lesions to induction treatments in T4 esophageal cancer. *Surgery* 2017;162:836-845.
4. Meacham CE, Morrison SJ. Tumour heterogeneity and cancer cell plasticity. *Nature* 2013;501:328-337.
5. Hanamoto A, Tatsumi M, Takenaka Y, Hamasaki T, Yasui T, Nakahara S, Yamamoto Y, Seo Y, Isohashi F, Ogawa K, Hatazawa J, Inohara H. Volumetric PET/CT parameters predict local response of head and neck squamous cell carcinoma to chemoradiotherapy. *Cancer Med* 2014;3:1368-1376.
6. Hofheinz F, Li Y, Steffen IG, Lin Q, Lili C, Hua W, van den Hoff J, Zschaek S. Confirmation of the prognostic value of pretherapeutic tumor SUR and MTV in patients with esophageal squamous cell carcinoma. *Eur J Nucl Med Mol Imaging* 2019;46:1485-1494.
7. Wheeler JM, Warren BF, Mortensen NJ, Ekanyaka N, Kulacoglu H, Jones AC, George BD, Kettlewell MG. Quantification of histologic regression of rectal cancer after irradiation: a proposal for a modified staging system. *Dis Colon Rectum* 2002;45:1051-1056.
8. Nioche C, Orlhac F, Boughdad S, Reuzé S, Goya-Outi J, Robert C, Pellet-Barakat C, Soussan M, Frouin F, Buvat I. LIFEX: A freeware for radiomic feature calculation in multimodality imaging to accelerate advances in the characterization of tumor heterogeneity. *Cancer Res* 2018;78:4786-4789.
9. Xu M, Wang L, Ouyang M, Lin J, Wang L, Zheng X, Miao S, Tang K. Prediction of lymph node metastasis by PET/CT metabolic parameters in patients with esophageal squamous cell carcinoma. *Nucl Med Commun* 2019;40:933-939.
10. Korkmaz U, Hacıoğlu MB, Kostek O, Sut N, Kodaz H, Erdoğan B, Ustun F, Saynak M, Tastekin E, Cicin I, Durmus-Altun G. The relationship between FDG PET/CT-defined metabolic parameters and the histopathological subtype of oesophageal carcinomas. *Pol J Radiol* 2020;85:e254-e260.
11. Zhang YH, Herlin G, Rouvelas I, Nilsson M, Lundell L, Brismar TB. Texture analysis of computed tomography data using morphologic and

- metabolic delineation of esophageal cancer-relation to tumor type and neoadjuvant therapy response. *Dis Esophagus* 2019;32:doy096.
12. Thrumurthy SG, Chaudry MA, Thrumurthy SSD, Mughal M. Oesophageal cancer: risks, prevention, and diagnosis. *BMJ* 2019;366:l4373. Erratum in: *BMJ* 2019;366:l5391.
 13. Martin-Richard M, Díaz Beveridge R, Arrazubi V, Alsina M, Galan Guzmán M, Custodio AB, Gómez C, Muñoz FL, Pazo R, Rivera F. SEOM Clinical Guideline for the diagnosis and treatment of esophageal cancer (2016). *Clin Transl Oncol* 2016;18:1179-1186.
 14. I H, Kim K, Kim SJ, Kim IJ, Pak K, Kim H. Prognostic value of metabolic volume measured by F-18 FDG PET-CT in patients with esophageal cancer. *Thorac Cancer* 2012;3:255-261.
 15. Martínez A, Infante JR, Quirós J, Rayo JI, Serrano J, Moreno M, Jiménez P, Cobo A, Baena A. Baseline 18F-FDG PET/CT quantitative parameters as prognostic factors in esophageal squamous cell cancer. *Rev Esp Med Nucl Imagen Mol (Engl Ed)* 2021:S2253-654X(21)00107-4.
 16. Tustumi F, Duarte PS, Albenda DG, Takeda FR, Sallum RAA, Junior UR, Buchpiguel CA, Ceconello I. Prognostic value of 18F-fluorodeoxyglucose PET/computed tomography metabolic parameters measured in the primary tumor and suspicious lymph nodes before neoadjuvant therapy in patients with esophageal carcinoma. *Nucl Med Commun* 2021;42:437-443.
 17. Hyun SH, Choi JY, Shim YM, Kim K, Lee SJ, Cho YS, Lee JY, Lee KH, Kim BT. Prognostic value of metabolic tumor volume measured by 18F-fluorodeoxyglucose positron emission tomography in patients with esophageal carcinoma. *Ann Surg Oncol* 2010;17:115-122.
 18. Jayachandran P, Pai RK, Quon A, Graves E, Krakow TE, La T, Loo BW Jr, Koong AC, Chang DT. Postchemoradiotherapy positron emission tomography predicts pathologic response and survival in patients with esophageal cancer. *Int J Radiat Oncol Biol Phys* 2012;84:471-477.
 19. Domachevsky L, Kashtan H, Brenner B, Nidam M, Morgenstern S, Kundel Y, Groshar D, Bernstine H. Baseline 18F-FDG PET/CT as predictor of the pathological response to neoadjuvant therapy in esophageal cancer: a retrospective study. *Medicine (Baltimore)* 2018;97:e13412.
 20. Kitajima K, Kaida H, Nakatani K, Ishibashi M, Morita T, Nakajo M, Tamaki Y, Minamimoto R. Assessment of tumor response to definitive chemoradiotherapy and prognosis prediction in patients with esophageal cancer judged by PET response criteria in solid tumors: multicenter study in Japan. *Nucl Med Commun* 2020;41:443-451.
 21. Takahashi N, Umezawa R, Takanami K, Yamamoto T, Ishikawa Y, Kozumi M, Takeda K, Kadoya N, Jingu K. Whole-body total lesion glycolysis is an independent predictor in patients with esophageal cancer treated with definitive chemoradiotherapy. *Radiother Oncol* 2018;129:161-165.
 22. Park SY, Lee SJ, Yoon JK. The prognostic value of total lesion glycolysis via 18F-fluorodeoxyglucose PET-CT in surgically treated esophageal squamous cell carcinoma. *Ann Nucl Med* 2016;30:81-88.
 23. Harada K, Rogers JE, Iwatsuki M, Yamashita K, Baba H, Ajani JA. Recent advances in treating oesophageal cancer. *F1000Res* 2020;9:F1000 Faculty Rev-1189.



Unexpected Metastatic Localizations of Prostate Cancer Determined by ⁶⁸Ga PSMA PET/CT: Series of Four Cases

⁶⁸Ga PSMA PET/BT'de Saptanan Prostat Kanserinin Nadir Metastaz Lokalizasyonları: Dört Olgu

© Gözde Mütevelizade, © Ceren Sezgin, © Gül Gümüşer, © Elvan Sayit

Manisa Celal Bayar University Faculty of Medicine, Department of Nuclear Medicine, Manisa, Turkey

Abstract

Prostate-specific membrane antigen (PSMA) is a transmembrane protein with overexpression in most prostate cancer cells. Gallium-68-⁶⁸Ga PSMA positron emission tomography/computed tomography (PET/CT) imaging is a game-changer in the management of prostate cancer. ⁶⁸Ga PSMA PET/CT scan is advanced and a promising radioligand has high sensitivity in determining lesions of prostate cancer with a high tumor to background ratio. The most common areas of metastasis are the bone and pelvic lymph nodes. The prognosis of prostate cancer is mainly determined by the status of metastases. The presence and the localization of metastases affects treatment planning. In our cases, we presented some examples of uncommon sites of metastases such as the brain, adrenal glands, penis and orbit. Improvements in imaging techniques, such as ⁶⁸Ga PSMA PET/CT have led to the possibility to make more determination of rare metastase sites in prostate cancer patients.

Keywords: Prostate cancer, unexpected, metastases, ⁶⁸Ga PSMA PET/CT

Öz

Prostat-spesifik membran antijen (PSMA) çoğu prostat kanseri hücresinde bulunan bir transmembran proteinidir. PSMA son yıllarda prostat kanserinin görüntüleme ve tedavisinde hedef molekül olarak ilgi çekmektedir. Galyum-68-⁶⁸Ga PSMA pozitron emisyon tomografi/bilgisayarlı tomografi (PET/BT) günümüzde prostat kanseri görüntülemesinde sıklıkla kullanılmaktadır. Prostat kanserinin en sık metastaz lokalizasyonları iskelet sistemi ve pelvik lenf nodlarıdır. Prognoz ve tedavi yönetimi metastaz varlığına ve lokalizasyonuna bağlı değişmektedir. Yayınımızda beyin, adrenal bez, penis ve orbita gibi prostat kanserine ait nadir metastaz lokalizasyonlarından örnek olgular göstermeyi amaçladık. Görüntüleme tekniklerinde ve moleküler ajanlarda gelişmeler devam ettikçe, beklenmedik metastatik lokalizasyonların saptanmasının giderek artacağını düşünmekteyiz.

Anahtar kelimeler: Prostat kanseri, nadir, metastaz, ⁶⁸Ga PSMA PET/BT

Address for Correspondence: Gözde Mütevelizade MD, Manisa Celal Bayar University Faculty of Medicine, Department of Nuclear Medicine, Manisa, Turkey
Phone: +90 532 471 32 62 **E-mail:** gozdemutevelizadee@gmail.com ORCID ID: orcid.org/0000-0001-5986-8777

Received: 02.04.2021 **Accepted:** 16.06.2021

©Copyright 2022 by Turkish Society of Nuclear Medicine
Molecular Imaging and Radionuclide Therapy published by Galenos Yayınevi.

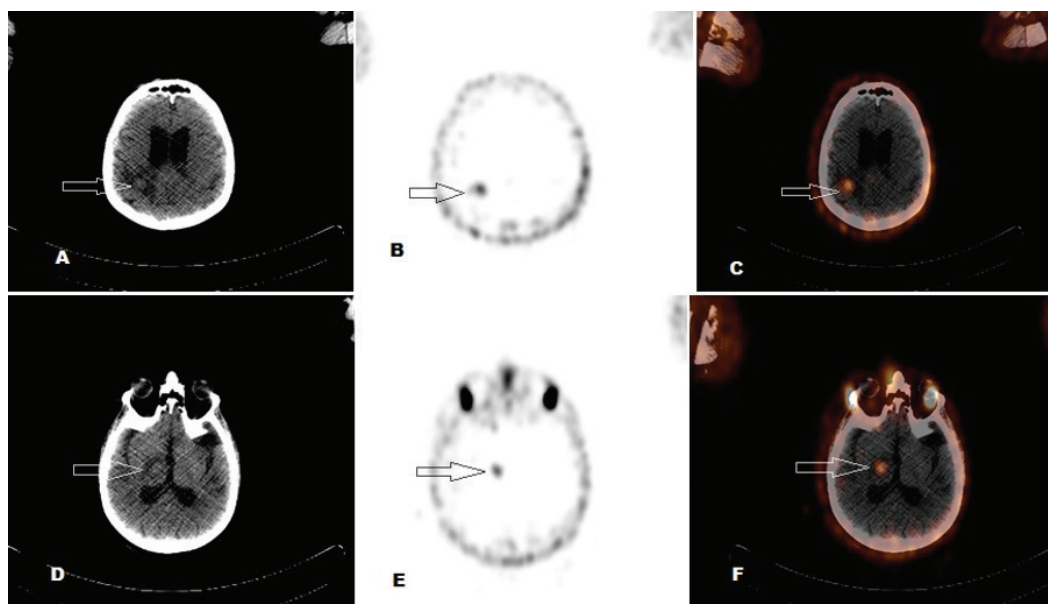


Figure 1. In prostate cancer, correct evaluation of extraprostatic spread is of great importance for estimated prognosis and in treatment planning. The most common areas of metastasis are pelvic lymph nodes and bone (1). Hatzoglou et al. (2) identified the incidence of brain metastasis from prostate carcinoma as 0.16%. They also stated that non-adenocarcinoma pathology are more likely to develop brain metastasis (2). Gallium-68- ^{68}Ga prostate-specific membrane antigen (PSMA) positron emission tomography/computed tomography (PET/CT) (Philips, True Flight Select, USA) scan was performed on a 62-year-old patient with prostate adenocarcinoma (Gleason's score 4+3, PSA 12.2 ng/mL). ^{68}Ga PSMA avid lesions in the right parietal (A, B, C) and thalamic (D, E, F) regions with perilesional edema were detected [maximum standardized uptake value (SUV_{max}): 1.3-2.6] (arrow). Magnetic resonance imaging (MRI) was performed for further evaluation. MRI report was consistent with our findings, demonstrating a 2 cm diameter mass in the right frontal lobe-precentral gyrus localization with peripheral diffusion restriction and a similar lesion in the right thalamus with a diameter of 1.3 cm. Radiotherapy was planned for cranial metastases.

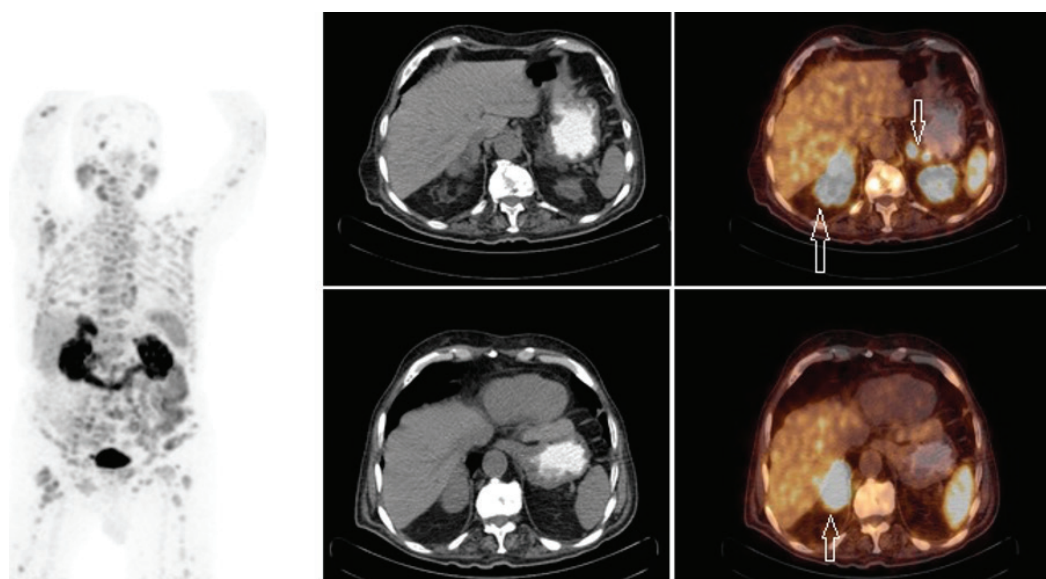


Figure 2. Metastases are the most common malignant lesions of adrenal gland. Adrenal metastasis can originate mostly from the lung (39%) and breast (35%) cancers (3). Even if the frequency of adrenal metastases was shown as 13% in an autopsy series, there are few publications in the literature with adrenal metastases of prostate cancer (4). ^{68}Ga PSMA PET/CT was performed in an 83-year-old patient who had prostate adenocarcinoma (Gleason's score of 4+5, PSA 809 ng/mL). Invasive prostate lesions to seminal vesicles, bilateral adrenal masses with the largest diameter of 61x33 mm (SUV_{max} : 26.2) (arrow), abdominopelvic lymph nodes, and widespread sclerotic skeletal metastases with intense PSMA expression were detected. Androgen deprivation therapy and chemotherapy were started and he has been for follow-up.

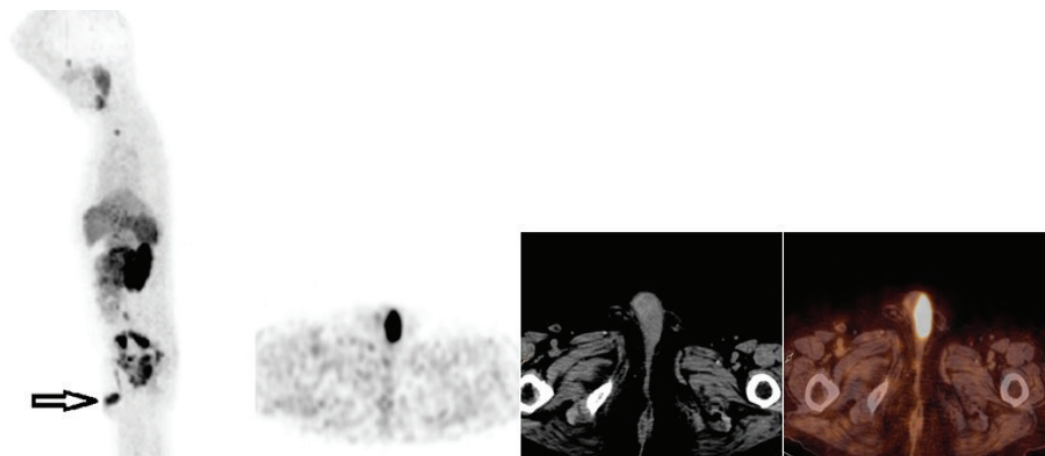


Figure 3. Secondary malignancy of the penis is a rare condition despite its rich vascularization. Tatkovic et al. (5) observed the incidence of penile metastasis of prostate cancer was 0.1% at 4860 ^{68}Ga PSMA PET/CT examinations. Seventy two year-old patient with prostate adenocarcinoma (Gleason's score of 4+5) had significant PSA progression (22.6 ng/mL and 47.9 ng/mL, respectively) despite eight cycles of chemotherapy and enzalutamide treatment. ^{68}Ga PSMA PET/CT revealed a large prostate mass with rectal and vesical invasion, PSMA avid inferior cervical, abdominal, and pelvic lymph nodes. Additionally, there was an intense ^{68}Ga PSMA expression noted in the penile shaft with a diameter of approximately 40x20 mm (SUV_{max} : 14.9) (arrow). Colour-coded duplex ultrasonography was used to evaluate the penile metastasis, radiotherapy was started for pencil metastasis and Lutetium-177 (^{177}Lu) PSMA was planned.

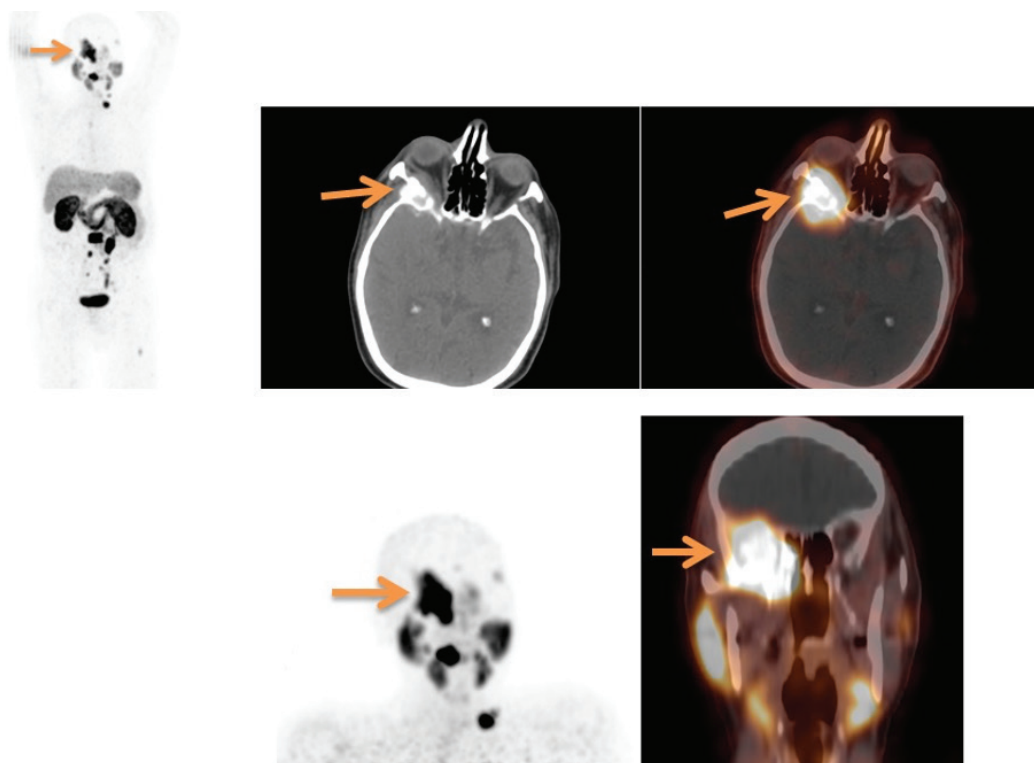


Figure 4. More than 90% of distant metastases in prostate cancer patients are found in the bones. The axial skeleton is the most commonly affected (1). Although the osseous metastases are common in prostate cancer, orbital metastases are very rare. Adenocarcinoma of the prostate is implicated in 3.6% to 4% of all orbital metastases (6). Cranial and orbital MRI was performed on 84-year-old patient with castrate-resistant prostate cancer (PSA 17 ng/mL) who developed diplopia and proptosis in the right eye. ^{68}Ga PSMA PET/CT was performed upon seeing a periorbital mass in the MRI. Pathological PSMA involvement (SUV_{max} : 19.4) was observed in the lesion, approximately 3.5x2.5 cm in size, located in the sphenoid bone in the right and invading the temporal lobe, maxillary sinus and orbit (arrow). ^{68}Ga PSMA PET/CT also demonstrated multiple cervical, abdominal and pelvic nodal involvement and sclerotic skeletal metastases. 7400 MBq ^{177}Lu PSMA radionuclide therapy was administered to the patient. He did not have any side effects during treatment or in the following weeks. The patient died from posttraumatic intracranial bleeding during follow-up.

Ethics

Informed Consent: Written informed consent was obtained from the patients who participated in this study.

Peer-review: Externally and internally peer-reviewed.

Authorship Contributions

Surgical and Medical Practices: G.M., C.S., Concept: G.M., E.S., Design: G.M., G.G., Data Collection or Processing: G.M., C.S., Analysis or Interpretation: G.M., G.G., Literature Search: G.M., E.S., Writing: G.M.

Conflict of Interest: No conflict of interest was declared by the authors.

Financial Disclosure: The authors declared that this study received no financial support.

References

1. Morigi JJ, Stricker PD, van Leeuwen PJ, Tang R, Ho B, Nguyen Q, Hruby G, Fogarty G, Jagavkar R, Kneebone A, Hickey A, Fanti S, Tarlinton L, Emmett L. Prospective comparison of 18F-fluoromethylcholine versus 68Ga-PSMA PET/CT in prostate cancer patients who have rising PSA after curative treatment and are being considered for targeted therapy. *J Nucl Med* 2015;56:1185-1190.
2. Hatzoglou V, Patel GV, Morris MJ, Curtis K, Zhang Z, Shi W, Huse J, Rosenblum M, Holodny AI, Young RJ. Brain metastases from prostate cancer: an 11-year analysis in the MRI era with emphasis on imaging characteristics, incidence, and prognosis. *J Neuroimaging* 2014;24:161-166.
3. Dhamija E, Panda A, Das CJ, Gupta AK. Adrenal imaging (part 2): medullary and secondary adrenal lesions. *Indian J Endocrinol Metab* 2015;19:16-24.
4. Bubendorf L, Schöpfer A, Wagner U, Sauter G, Moch H, Willi N, Gasser TC, Mihatsch MJ. Metastatic patterns of prostate cancer: an autopsy study of 1,589 patients. *Hum Pathol* 2000;31:578-583.
5. Tatkovic A, McBean R, Schoeman J, Wong D. Prostate penile metastasis: incidence and imaging pattern on 68Ga-PSMA PET/CT. *J Med Imaging Radiat Oncol* 2020;64:499-504.
6. Saadi A, Kerkeni W, Bouzouita A, Ayed H, Gaja A, Cherif M, Slama RB, Mnif N, Derouiche A, Chebil M. Bilateral orbital metastasis of prostatic adenocarcinoma. *Urology* 2016;94:e3-4.



Cerebellar Metastases from Prostate Cancer Detected by PET/CT with ¹⁸F-Choline

¹⁸F-Kolin PET/BT ile Saptanan Prostat Kanserinin Serebellar Metastazları

Luca Filippi¹, Antonella Fontana², Francesco Guerrini³, Angelo Pompucci³, Oreste Bagni¹

¹Santa Maria Goretti Hospital, Nuclear Medicine Unit, Latina, Italy

²Santa Maria Goretti Hospital, Radiotherapy Unit, Latina, Italy

³Santa Maria Goretti Hospital, Neurosurgery Unit, Latina, Italy

Abstract

A 76-year-old male, previously submitted enucleation renal-cell carcinoma (pT1) and prostatectomy for prostate cancer (Gleason score 3+5, pT3b pN0 pMx), was submitted to positron emission/computed tomography (PET/CT) with ¹⁸F-choline for restaging due to raised levels of prostate-specific antigen. PET/CT scan showed increased tracer incorporation corresponding to bone metastases in the left ischio-pubic ramus, also revealing 2 areas of increased tracer uptake in the cerebellum, subsequently confirmed by brain magnetic resonance imaging. The patient was urgently submitted to neurosurgery. Post-operative histology was positive for brain metastases from prostate cancer.

Keywords: Prostate neoplasm, positron emission tomography, molecular imaging, neurosurgery, personalized medicine

Öz

Daha önce renal hücreli karsinoma (pT1) için enükleasyon ve prostat kanseri nedeniyle prostatektomi (Gleason skoru 3+5, pT3b pN0 pMx) uygulanan 76 yaşındaki bir erkek hasta, prostat spesifik antijen seviyelerinin yükselmesi nedeniyle yeniden evreleme için ¹⁸F-kolin kullanılarak yapılan pozitron emisyon tomografisi/bilgisayarlı tomografiye (PET/BT) gönderildi. PET/BT taraması, sol ischio-pubik ramustaki kemik metastazlarına karşılık gelen radyofarmasötik tutulumunda artış gösterdi. Ayrıca beyincikte 2 alanda radyofarmasötik tutulumunda artış görüldü ve sonrasında uygulanan beyin manyetik rezonans görüntüleme ile doğrulandı. Hasta acilen beyin cerrahisine sevk edildi. Ameliyat sonrası histoloji, prostat kanserinden beyin metastazi için pozitif.

Anahtar kelimeler: Prostat neoplazmı, pozitron emisyon tomografisi, moleküler görüntüleme, beyin cerrahisi, kişiselleştirilmiş tıp

Address for Correspondence: Luca Filippi MD, Santa Maria Goretti Hospital, Nuclear Medicine Unit, Latina, Italy

Phone: +393921247921 **E-mail:** l.filippi@ausl.latina.it ORCID ID: orcid.org/0000-0003-4423-5496

Received: 16.04.2021 **Accepted:** 29.06.2021

©Copyright 2022 by Turkish Society of Nuclear Medicine
Molecular Imaging and Radionuclide Therapy published by Galenos Yayınevi.

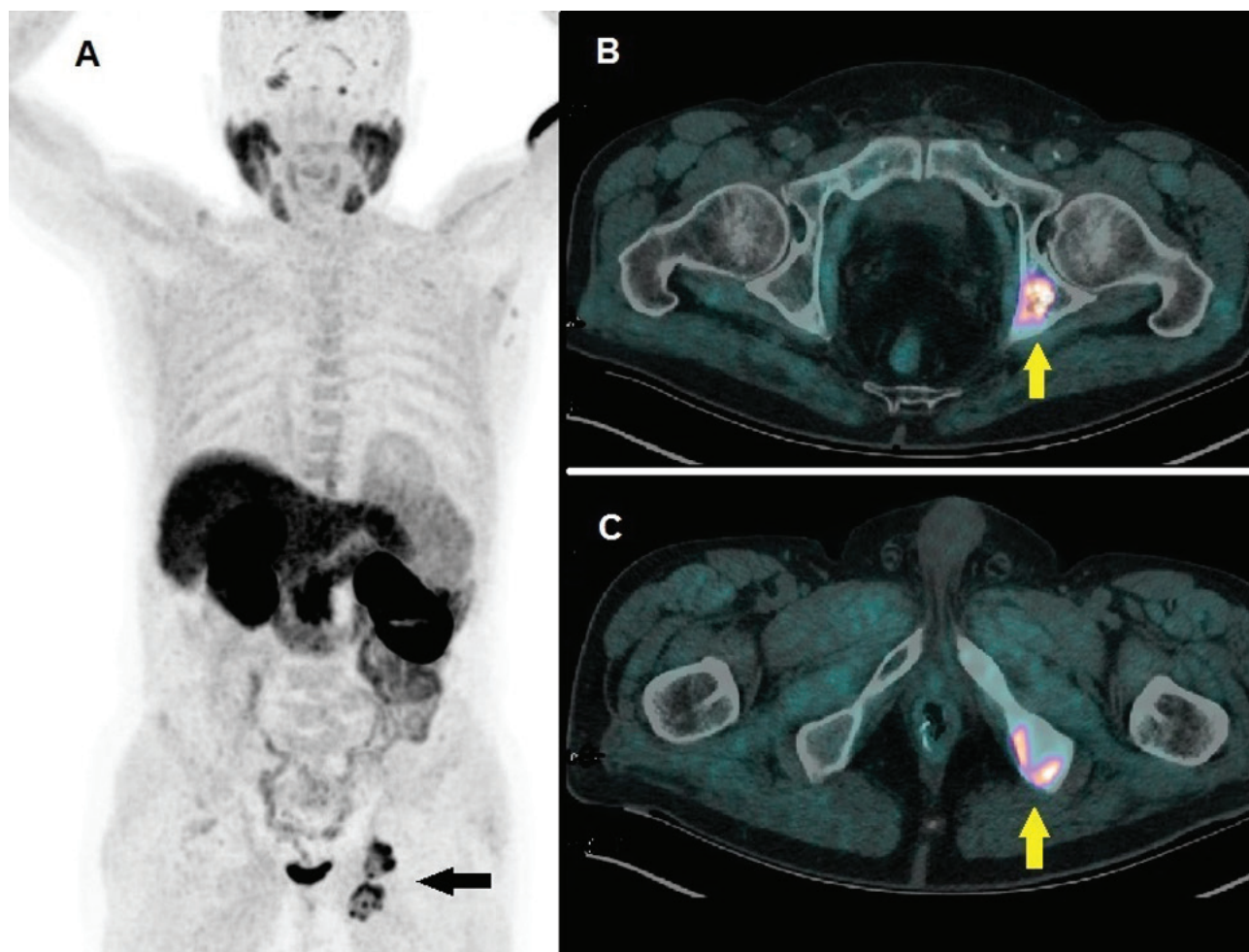


Figure 1. In 2003, a 76-year-old male patient was contextually submitted for prostatectomy due to prostate cancer (PCa) (pT3b pN0 pMx) and enucleation of a tumor mass in the right kidney resulted in renal cell-carcinoma (pT1m). He received adjuvant radiotherapy and was then monitored for the following years by clinical and laboratory examination. In 2018, due to raising values prostate-specific antigen (PSA) level, he was submitted to positron emission tomography/computed tomography (PET/CT) with ^{18}F -choline that was positive for bone metastases. He underwent radiotherapy on the skeletal lesions and started androgen deprivation therapy with complete PSA response. After 12 years, a further progressive increase in PSA level up to a value of 4.8 ng/mL was registered. Therefore, the patient underwent a further PET/CT with ^{18}F -choline for restaging. Maximum intensity projection demonstrated highly intense tracer incorporation in the bones of the left pelvis (A, black arrow). Fused corresponding axial PET/CT images showed ^{18}F -choline in the para-acetabular region of the left ischium [B, yellow arrow; standardized uptake value (SUV_{max}): 18.8] and in the ipsilateral ischio-pubic ramus (C, yellow arrow, SUV_{max} : 11.8).

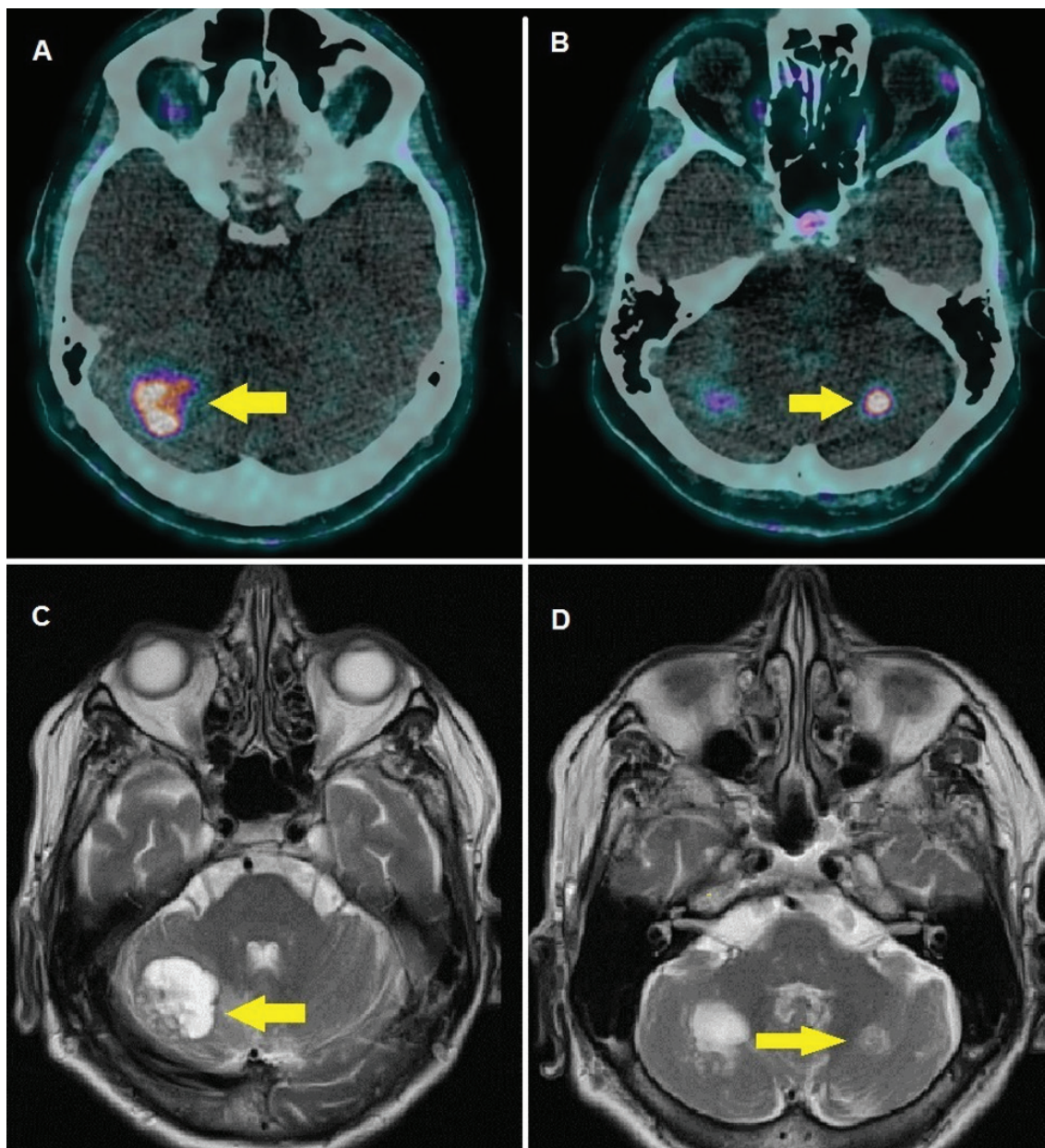


Figure 2. PET/CT images of the cranial region demonstrate 2 unexpected areas of increased tracer uptake in the right (A, yellow arrow; $\text{SUV}_{\text{max}}: 7.7$) and left (B, yellow arrow; $\text{SUV}_{\text{max}}: 8.9$) posterior fossa, highly suspected for cerebellar metastases. The patient underwent brain magnetic resonance imaging, whose T2-weighted sequences showed hyperintense lesions in the right cerebellar hemisphere (C, yellow arrow) and in the contralateral one (D, yellow arrow), with maximum transverse diameters of 32 mm and 13 mm, respectively. The subject was promptly submitted to neurosurgery of the largest lesion in the right cerebellar hemisphere. Definitive histology showed a glandular pattern of PSA-positive cells, compatible with PCa brain metastasis. The patient is in good clinical condition, actually undergoing gamma knife on the lesion in the left cerebellar hemisphere. Brain metastases from PCa cancer are rarely reported (1). In a published retrospective study including a large cohort of 2,194 subjects affected by PCa, only 1 case having brain metastases was identified (2). PET/CT with ^{18}F -choline is routinely used for the imaging of PCa recurrence and monitoring the response to treatment, but it has also been successfully applied for detecting brain tumors (3,4). Gizewska et al. (5) reported the case of a patient, affected by metastatic castration-resistant prostate cancer treated with docetaxel, diagnosed with brain metastases through ^{18}F -choline PET/CT, although a histological confirmation was not obtained. It must be highlighted that, in contrast with the case described in the aforementioned paper, our patient was chemotherapy-naïve and completely asymptomatic for both bone pain and neurological signs. Furthermore, aside PCa, our patient had undergone surgery for renal-cell carcinoma, thus neurosurgery and subsequent histology was crucial to achieve an unambiguous diagnosis. Our report highlights that when reading PET/CT scans with ^{18}F -choline, particular attention should be paid to brain evaluation, for the early detection of eventual primitive or secondary lesions.

Ethics

Informed Consent: Each patient must sign a written consent authorizing the use of anonymous data for research purpose before performing PET/CT scan.

Peer-review: Externally peer-reviewed.

Authorship Contributions

Surgical and Medical Practices: L.P., A.F., F.G., A.P., O.B., Concept: L.P., A.F., F.G., A.P., O.B., Design: L.P., A.F., F.G., A.P., O.B., Data Collection or Processing: L.P., A.F., F.G., A.P., O.B., Analysis or Interpretation: L.P., A.F., F.G., A.P., O.B., Literature Search: L.P., A.F., F.G., A.P., O.B., Writing: L.P., A.F., F.G., A.P., O.B.

Conflict of Interest: No conflict of interest was declared by the authors.

Financial Disclosure: The authors declared that this study received no financial support.

References

1. Estebanez J, Teyrouz A, Gutierrez MA, Linazasoro I, Bellosso J, Cano C, Peralta JM, Sanz JP. Natural history of prostate cancer. *Arch Esp Urol* 2014;67:383-387.
2. Macedo J, Carneiro E, Ferreira D, Verdelho A, Afonso LP, Maurício J, Silva SM, Arantes M. Neuroimaging analysis of rare brain metastases from prostate cancer: PS171. *Porto Biomed J* 2017;2:220.
3. Filippi L, Basile P, Schillaci O, Bagni O. The Relationship between total lesion activity on ¹⁸F choline positron emission tomography-computed tomography and clinical outcome in patients with castration-resistant prostate cancer bone metastases treated with ²²³Radium. *Cancer Biother Radiopharm* 2020;35:398-403.
4. Treglia G, Muoio B, Trevisi G, Mattoli MV, Albano D, Bertagna F, Giovanella L. Diagnostic performance and prognostic value of PET/CT with different tracers for brain tumors: a systematic review of published meta-analyses. *Int J Mol Sci* 2019;20:4669.
5. Gizewska A, Witkowska-Patena E, Stembrowicz-Nowakowska Z, Buraczewska A, Dziuk M. Brain metastases in patient with prostate cancer found in ¹⁸F-choline PET/CT. *Nucl Med Rev Cent East Eur* 2015;18:39-41.



COVID-19 Pneumonia was Incidentally Detected on ^{18}F -Fluorocholine PET/CT in a Work-up for Prostate Cancer

COVID-19 Pnömonisinin Prostat Kanseri Çalışmasında ^{18}F -Florokolin PET/BT'de Tesadüfen Tespit Edilmesi

© Omar Ait Sahel, © Yassir Benameur, © Salah Oueriagli Nabih, © Abderrahim Doudouh

Mohammed V University of Rabat, Mohammed V Military Teaching Hospital, Departments of Nuclear Medicine, Rabat, Morocco

Abstract

This is a presentation of the case of a patient who underwent ^{18}F -fluorocholine positron emission/computed tomography to stage a prostate cancer with incidentally found bilateral pneumonia. A high prevalence of incidental pneumonia is very probable under the current circumstance of coronavirus disease-2019 (COVID-19) pandemic, and oncological patients are at increased risk of COVID-19 with poorer outcome. The lung inflammatory burden in the case of COVID-19 infection can be demonstrated by ^{18}F -fluorocholine.

Keywords: COVID-19, pneumonia, prostate cancer, ^{18}F -fluorocholine, PET/CT

Öz

Bu çalışmada, prostat kanseri evrelemesi için ^{18}F -florokolin pozitron emisyon tomografisi/bilgisayarlı tomografi çekilen ve tesadüfen bilateral pnömoni tespit edilen bir hasta sunulmaktadır. Koronavirüs hastalığı-2019 (COVID-19) pandemisinin mevcut koşullarında yüksek insidental pnömoni prevalansı çok olasıdır ve onkolojik hastalar daha kötü sonuçlarla birlikte COVID-19 açısından yüksek risk altındadır. COVID-19 enfeksiyonu durumunda akciğer enflamatuvar yükü, ^{18}F -florokolin ile gösterilebilir.

Anahtar kelimeler: COVID-19, pnömoni, prostat kanseri, ^{18}F -florokolin, PET/BT

Address for Correspondence: Omar Ait Sahel PhD, Mohammed V University of Rabat, Mohammed V Military Teaching Hospital, Departments of Nuclear Medicine, Rabat, Morocco

Phone: +90 212 662 84 17 84 **E-mail:** omaraitsahel85@gmail.com ORCID ID: orcid.org/0000-0002-5294-9731

Received: 11.06.2021 **Accepted:** 06.07.2021

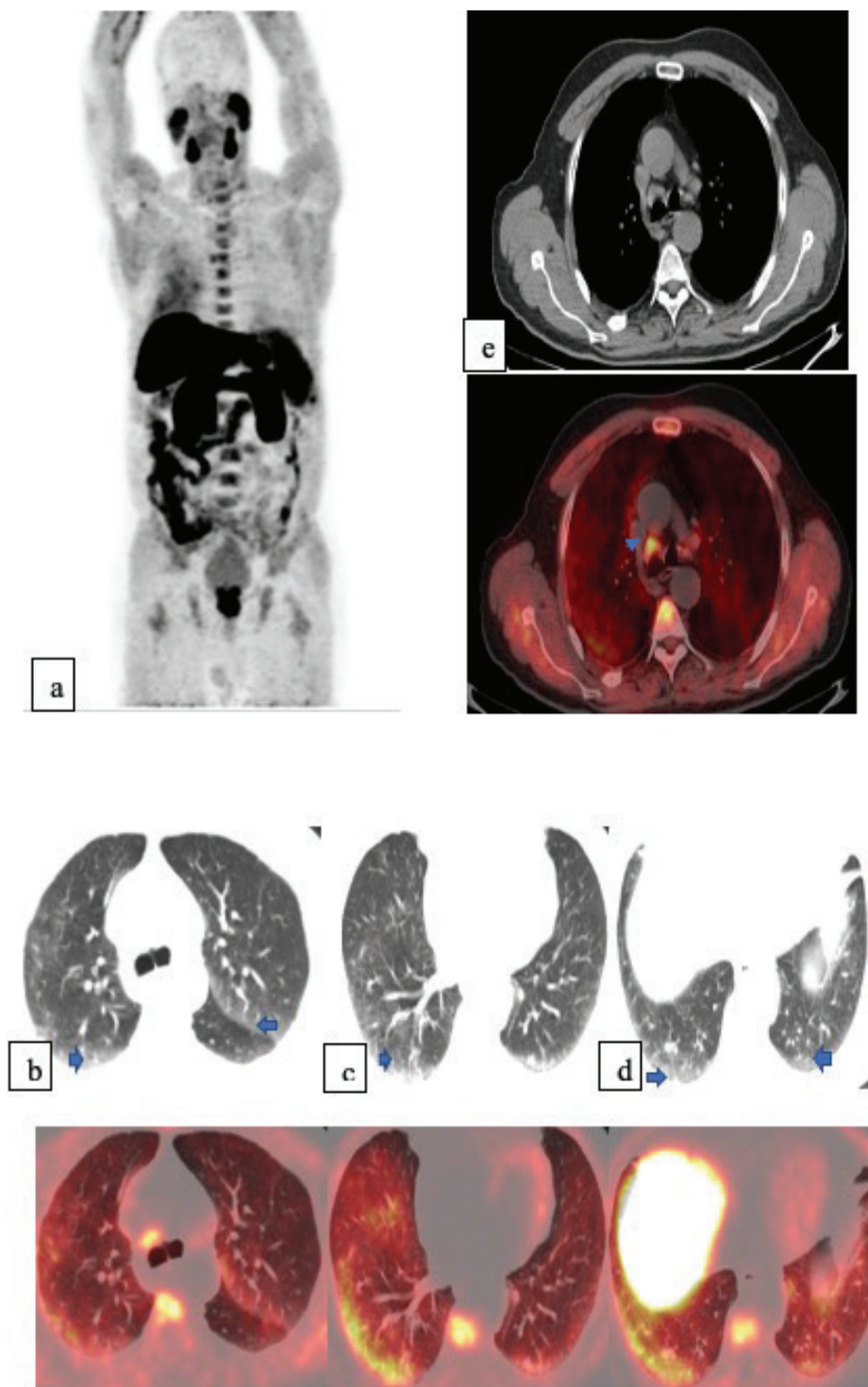


Figure 1. A recent diagnosis of a prostate adenocarcinoma has been made out in a 75-year-old man with a Gleason score of 7 (4+3) and a prostate-specific antigen value of 25 ng/mL. We performed a positron emission tomography/computed tomography (PET/CT) scan with ¹⁸F-choline to stage the disease. Immediately after intravenous injection of tracer (255 MBq), we acquired dynamic images of the pelvis. Sixty min after the injection, we performed a whole-body scan from the head to mid-thighs. Maximum intensity projection showed mild uptake in the right lung, with intense and diffuse uptake of the prostate gland with a standardized uptake value (SUV_{max}) of 13.2 (a). Moderate tracer uptake was shown in the subpleural region of both right and left lungs with SUV_{max}: 5.0 and SUV_{max}:

2.7 respectively. The extent of pneumonia was greater in the right lung, which corresponds to CT findings of ground glass opacities and a reticular pattern, particularly in the posterior segments (b, c, d) (arrows). We also detected a focal uptake of the tracer in the right hilar (SUV_{max} : 3.2), and right paratracheal lymph node with SUV_{max} : 4.5 (e) due to infection (arrowhead).

The general practitioner was warned to manage the patient and undergo a pharyngeal swab to test for severe acute respiratory syndrome-coronavirus-2 infection. Real-time polymerase chain reaction (RT-PCR), to detect viral nucleotides on pharyngeal swab, was positive for COVID-19. Hydroxychloroquine and azithromycin were administered to treat the patient, who did not need for hospitalization.

Patients with cancer and cardiovascular disease face with increased risk and worse clinical outcomes of COVID-19 infections (1). Nucleic acid testing (RT-PCR) is the standard test for the diagnosing of COVID-19 infection, but with a high false negative rate. The chest CT findings demonstrated high sensitivity for diagnosis and monitoring of COVID-19. Although many reports highlight the usefulness of PET/CT with ¹⁸F-fluorodeoxyglucose in the early detection of asymptomatic patients with COVID-19 (2,3), very few reports demonstrate incidental detection of COVID-19 infection in ¹⁸F-fluorocholine PET/CT examination in patients with malignancy (4,5). The lung inflammatory burden in a COVID-19 infection can be demonstrated by ¹⁸F-fluorocholine. An upregulation of choline kinase in the activated macrophages may explain the accumulation of ¹⁸F-fluorocholine in the inflammatory tissue (6,7).

Ethics

Informed Consent: Written informed consent of the patient was obtained.

Peer-review: Externally peer-reviewed.

Authorship Contributions

Surgical and Medical Practices: O.A.S., A.D., Concept: O.A.S., A.D., Design: O.A.S., A.D., Data Collection or Processing: O.A.S., Y.B., Analysis or Interpretation: O.A.S., Y.B., S.O.N., Literature Search: O.A.S., S.O.N., Writing: O.A.S.

Conflict of Interest: No conflict of interest was declared by the authors.

Financial Disclosure: The authors declared that this study received no financial support.

References

- Dai M, Liu D, Liu M, Zhou F, Li G, Chen Z, Zhang Z, You H, Wu M, Zheng Q, Xiong Y, Xiong H, Wang C, Chen C, Xiong F, Zhang Y, Peng Y, Ge S, Zhen B, Yu T, Wang L, Wang H, Liu Y, Chen Y, Mei J, Gao X, Li Z, Gan L, He C, Li Z, Shi Y, Qi Y, Yang J, Tenen DG, Chai L, Mucci LA, Santillana M, Cai H. Patients with cancer appear more vulnerable to SARS-CoV-2: a multicenter study during the COVID-19 outbreak. *Cancer Discov* 2020;10:783-791.
- Scarlattei M, Baldari G, Silva M, Bola S, Sammartano A, Migliari S, Graziani T, Cidda C, Sverzellati N, Ruffini L. Unknown SARS-CoV-2 pneumonia detected by PET/CT in patients with cancer. *Tumori Journal* 2020;106:325-332.
- Minamimoto R, Hotta M, Ishikane M, Inagaki T. FDG-PET/CT images of COVID-19: a comprehensive review. *Glob Health Med* 2020;2:221-226.
- Olivari L, Riccardi N, Rodari P, Angheben A, Artioli P, Salgarello M. COVID-19 pneumonia: increased choline uptake with ¹⁸F-choline PET/CT. *Eur J Nucl Med Mol Imaging* 2020;47:2476-2477.
- García Vicente AM, Soriano Castrejón Á. Incidental COVID-19 pneumonia on ¹⁸F-fluorocholine PET/CT. *Clin Nucl Med* 2020;45:e376-e377.
- Savelli G, Bonacina M, Rizzo A, Zaniboni A. Activated macrophages are the main inflammatory cell in COVID-19 interstitial pneumonia infiltrates. Is it possible to show their metabolic activity and thus the grade of inflammatory burden with ¹⁸F-fluorocholine PET/CT? *Med Hypotheses* 2020;144:109885.
- Wyss MT, Weber B, Honer M, Späth N, Ametamey SM, Westera G, Bode B, Kaim AH, Buck A. ¹⁸F-choline in experimental soft tissue infection assessed with autoradiography and high-resolution PET. *Eur J Nucl Med Mol Imaging* 2004;31:312-316.



Nasolacrimal Duct Obstruction on ¹³¹I SPECT/CT: Atypical False-positive Paranasal Radioiodine Uptake as a Complication of Single-dose RAI Treatment

¹³¹I SPECT/BT'de Nazolakrimal Kanal Tıkanıklığı: Tek-doz RAI Tedavisinin Bir Komplikasyonu Olarak Atipik Yanlış Pozitif Paranasal Radyoiodin Tutulumu

✉ Nuh Filizoğlu¹, ✉ Kevser Öksüzoğlu¹, ✉ Salih Özgüven¹, ✉ Onur Buğdaycı², ✉ Tanju Yusuf Erdil¹

¹Marmara University, Pendik Training and Research Hospital, Clinic of Nuclear Medicine, İstanbul, Turkey

²Marmara University, Pendik Training and Research Hospital, Clinic of Radiology, İstanbul, Turkey

Abstract

Nasolacrimal duct obstruction (NLDO) is a rare complication after radioiodine therapy and may cause false positive ¹³¹I uptake at the point of obstruction in ¹³¹I whole body scan. Here, we report a 59-year-old female patient with papillary thyroid cancer treated with total thyroidectomy followed by ¹³¹I therapy. ¹³¹I whole body scan revealed focal uptake in the head. Single photon emission computed tomography/computed tomography (CT) showed focal uptake at the right proximal nasolacrimal duct. The ophthalmologic examination and the diagnostic maxillofacial CT confirmed the diagnosis of NLDO.

Keywords: ¹³¹I, radioiodine therapy, nasolacrimal duct obstruction, thyroid cancer

Öz

Nazolakrimal kanal tıkanıklığı (NLKT), radyoiodin tedavisi sonrası nadir görülen bir komplikasyondur ve ¹³¹I tüm vücut tarama sintigrafisinde tıkanma noktasında yanlış pozitif ¹³¹I tutulumuna neden olabilir. Burada, 59 yaşında papiller tiroid kanserli, total tiroidektomi ve ardından ¹³¹I tedavisi uygulanan bir kadın hasta sunuldu. ¹³¹I tüm vücut tarama sintigrafisinde kafada odaksal bir ¹³¹I tutulumu izlendi. Tek foton emisyon tomografisi/bilgisayarlı tomografi (BT) sağ nazolakrimal kanal proksimal kesiminde fokal ¹³¹I tutulumu gösterdi. Oftalmolojik muayene ve tanısal maksillofasial BT, NLKT tanısını doğruladı.

Anahtar kelimeler: ¹³¹I, radyoiodin tedavi, nazolakrimal kanal tıkanıklığı, tiroid kanseri

Address for Correspondence: Nuh Filizoğlu MD, Marmara University, Pendik Training and Research Hospital, Clinic of Nuclear Medicine, İstanbul, Turkey

Phone: + 90 216 396 86 48 **E-mail:** nuhfilizoglu@gmail.com ORCID ID: orcid.org/0000-0002-9139-9752

Received: 10.03.2021 **Accepted:** 08.07.2021

©Copyright 2022 by Turkish Society of Nuclear Medicine
Molecular Imaging and Radionuclide Therapy published by Galenos Yayınevi.

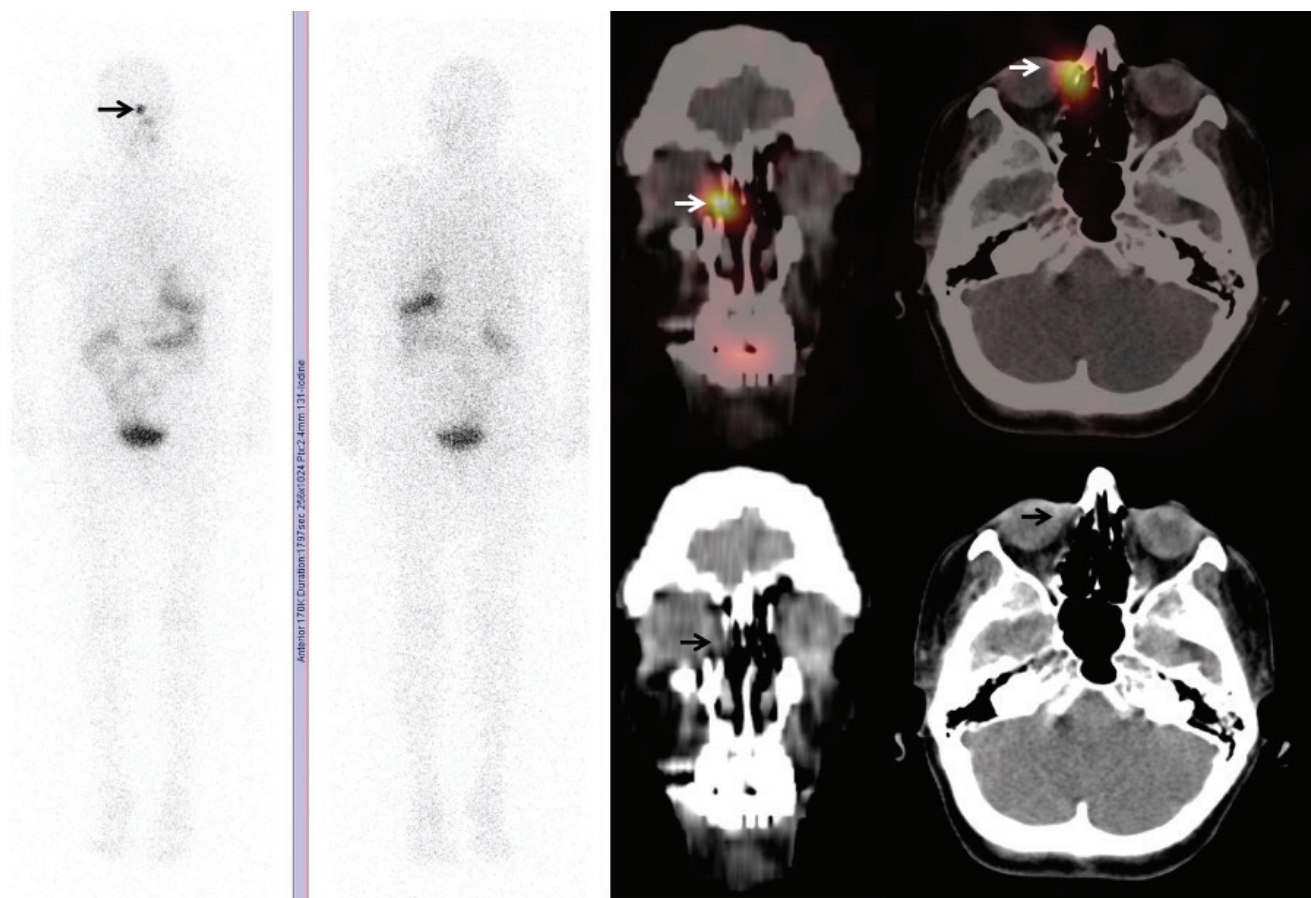


Figure 1. ^{131}I whole body scan was performed on a 59-year-old female patient with papillary thyroid cancer (T3N1bM0), who was treated 5 years ago with total thyroidectomy followed by a single dose 150 mCi ^{131}I therapy. A planar ^{131}I whole body scan with single photon emission computed tomography/computed tomography (SPECT/CT) and spot neck pinhole images were obtained at the 48th hour after 5 mCi ^{131}I oral administration. At the time of imaging, stimulated thyroid-stimulating hormone level was 280 IU/mL, thyroglobulin (Tg) level was 0.20 ng/mL and anti-Tg antibody level was <0.9 IU/mL. The patient had no symptoms at the time of imaging. Planar ^{131}I whole body scan showed no significant radioactivity uptake that may be compatible with residual thyroid tissue or recurrent thyroid cancer, on the other hand a suspicious focus of intense increased uptake was noted at the right paranasal region, which mimics a metastatic lesion (arrow in planar images). SPECT/CT images revealed 7x4 mm sized soft tissue density lesion-demonstrating ^{131}I uptake, in the right infraorbital region next to the lateral wall of ethmoid sinus (arrows in fused SPECT/CT images) suggesting nasolacrimal duct obstruction (NLDO). Subsequently, an ophthalmologic examination and a diagnostic maxillofacial CT were performed to confirm the diagnosis. ^{131}I has been used for many years as a valuable treatment in thyroid diseases such as hyperthyroidism and differentiated thyroid carcinomas (1,2,3). NLDO is an uncommon complication of ^{131}I therapy, especially rarely occurs after a single dose of radioiodine treatment. Morgenstern et al. (4) reported that the cells of the lacrimal drainage system have the same Na/I symporters expressed by the cells of the thyroid gland and eventually the accumulation of ^{131}I in these cells results in radiation induced damage. Fibrosis and obstruction of lacrimal drainage system will cause ^{131}I uptake at the point of obstruction in whole body ^{131}I scan and that may be misinterpreted as a metastasis (5,6). SPECT/CT can be useful to discriminate these false positive findings of planar ^{131}I whole-body imaging, as in this study (7). Beside that early identification of these lesions may hasten the subsequent appropriate treatment of the patients and improve quality of life (8).

Ethics

Informed Consent: Informed consent form was obtained.

Peer-review: Externally peer-reviewed.

Authorship Contributions

Surgical and Medical Practices: N.F., K.Ö., S.Ö., O.B., T.Y.E.,
Concept: N.F., T.Y.E., Design: N.F., T.Y.E., Data Collection or
Processing: N.F., K.Ö., Analysis or Interpretation: N.F., T.Y.E.,
Literature Search: N.F., T.Y.E., Writing: N.F., S.Ö.

Conflict of Interest: No conflict of interest was declared
by the authors.

Financial Disclosure: The authors declared that this study
received no financial support.

References

1. Ali MJ. Iodine-131 Therapy and nasolacrimal duct obstructions: what we know and what we need to know. *Ophthalmic Plast Reconstr Surg* 2016;32:243-248.
2. Burns JA, Morgenstern KE, Cahill KV, Foster JA, Jhiang SM, Kloos RT. Nasolacrimal obstruction secondary to I(131) therapy. *Ophthalmic Plast Reconstr Surg* 2004;20:126-129.
3. Fard-Esfahani A, Mirshekarpour H, Fallahi B, Eftekhari M, Saghari M, Beiki D, Ansari-Gilani K, Takavar A. The effect of high-dose radioiodine treatment on lacrimal gland function in patients with differentiated thyroid carcinoma. *Clin Nucl Med* 2007;32:696-699.
4. Morgenstern KE, Vadysirisack DD, Zhang Z, Cahill KV, Foster JA, Burns JA, Kloos RT, Jhiang SM. Expression of sodium iodide symporter in the lacrimal drainage system: implication for the mechanism underlying nasolacrimal duct obstruction in I(131)-treated patients. *Ophthalmic Plast Reconstr Surg* 2005;21:337-344.
5. Yuoness S, Rachinsky I, Driedger AA, Belhocine TZ. Differentiated thyroid cancer with epiphora: detection of nasolacrimal duct obstruction on I-131 SPECT/CT. *Clin Nucl Med* 2011;36:1149-1152.
6. Fard-Esfahani A, Farzanefer S, Fallahi B, Beiki D, Saghari M, Emami-Ardekani A, Majdi M, Eftekhari M. Nasolacrimal duct obstruction as a complication of iodine-131 therapy in patients with thyroid cancer. *Nucl Med Commun* 2012;33:1077-1080.
7. Brockmann H, Wilhelm K, Joe A, Palmedo H, Biersack HJ. Nasolacrimal drainage obstruction after radioiodine therapy: case report and a review of the literature. *Clin Nucl Med* 2005;30:543-545.
8. Ali MJ, Vyakaranam AR, Rao JE, Prasad G, Reddy PV. Iodine-131 therapy and lacrimal drainage system toxicity: nasal localization studies using whole body nuclear scintigraphy and SPECT-CT. *Ophthalmic Plast Reconstr Surg* 2017;33:13-16.



Isolated Scapular Lesion of Langerhans Cell Histiocytosis Detected by ¹⁸F-FDG PET/CT

¹⁸F-FDG PET/BT ile Saptanan Langerhans Hücreli Histiyoitozun İzole Skapula Lezyonu

• Nuh Filizoğlu¹, • Salih Özgüven¹, • Hüseyin Kemal Türköz², • Tunç Öneş¹, • Halil Turgut Turoğlu¹, • Tanju Yusuf Erdil¹

¹Marmara University, Pendik Training and Research Hospital, Clinic of Nuclear Medicine, İstanbul, Turkey

²Marmara University, Pendik Training and Research Hospital, Clinic of Pathology, İstanbul, Turkey

Abstract

Langerhans cell histiocytosis (LCH) is a rare disease that occurs mainly in pediatric patients and most adult LCH is considered a part of multisystem or multifocal disease. Only 7.3% of cases present as unifocal bone lesion. Herein, we present a case of an isolated scapular lesion of LCH in a 48-year-old man.

Keywords: Langerhans cell histiocytosis, ¹⁸F-FDG PET/CT, bone

Öz

Langerhans hücreli histiyoitoz (LHH), çoğunlukla pediatrik hastalarda ortaya çıkar ve yetişkin LHH genellikle multisistem veya multifokal hastalığın bir parçası olarak görülen nadir bir hastalıktır. Olguların sadece %7,3'ü tek odaklı kemik lezyonu olarak karşımıza çıkmaktadır.

Anahtar kelimeler: Langerhans hücreli histiyoitoz, ¹⁸F-FDG PET/BT, kemik

Address for Correspondence: Nuh Filizoğlu MD, Marmara University, Pendik Training and Research Hospital, Clinic of Nuclear Medicine, İstanbul, Turkey

Phone: + 90 216 396 86 48 **E-mail:** nuhfilizoglu@gmail.com ORCID ID: orcid.org/0000-0002-9139-9752

Received: 12.03.2021 **Accepted:** 22.07.2021

©Copyright 2022 by Turkish Society of Nuclear Medicine
Molecular Imaging and Radionuclide Therapy published by Galenos Yayınevi.

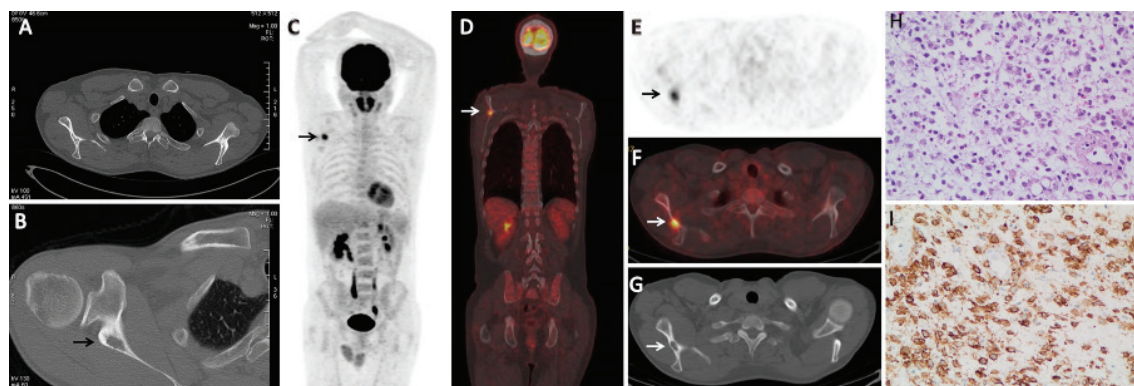


Figure 1. A 48-year-old man who was diagnosed with ankylosing spondylitis was admitted to a hospital for right shoulder pain. Computed tomography (CT) showed no lesions, which may cause the pain at shoulder area (A, transaxial CT image). Six months after his first CT, another CT was performed due to progression of his pain and revealed a lytic lesion in the right scapula (arrow in B, transaxial CT image). He was suspected to have scapular metastases or primary bone malignancies and was referred to ^{18}F -fluorodeoxyglucose (FDG) positron emission tomography (PET)/CT for further investigation. ^{18}F -FDG PET/CT showed 20x8 mm sized intense hypermetabolic [maximum standardized uptake value (SUV_{max}): 9.7] lytic lesion in the right scapula (arrows in C, coronal PET image; D, coronal fused PET/CT image; E, transaxial PET image; F, transaxial fused PET/CT image; G, transaxial CT image) and physiologic ^{18}F -FDG distribution on the rest of the body. Next a bone biopsy was performed. Histopathologic examination revealed neoplastic cells with vesicular nuclei, small nucleoli and nuclear grooves that were admixed with inflammatory cells including plasmacytes and eosinophils (H). Immunohistochemical examination of the tumor cells showed S100, tangerine and CD1a positivity (I). These findings were consistent with diagnosis of langerhans cell histiocytosis (LCH). LCH is a rare disease characterized by abnormal clonal proliferation and accumulation of pathological LC. Clinical presentation of LCH varies from isolated benign localization to multisystemic aggressive lesions (1). Although any organ can be affected, the most common site of involvement in LCH is skeletal. The accumulation of osteoclast-like multinucleated giant cells causes necrosis of the bone and consequently lead to formation of osteolytic lesions. The most common sites of involvement are the skull (27%) and involvement of other bones, such as the femur, humerus, spine, ribs and mandible, has also been reported. Isolated bony lesions of LCH are associated with a good prognosis and the lesion spontaneously regresses regardless of the type of treatment (2,3,4,5). Therefore, the most important aspect for treating LCH is categorizing the case correctly. ^{18}F -FDG PET/CT is superior at detecting new disease sites, recurrence, evaluating response to therapy, and distinguishing the metabolically active disease from inactive diseases to conventional imaging modalities (6). The utility of ^{18}F -FDG PET/CT for screening and follow-up in patients with LCH has been well established in the literature (7,8,9). LCH exhibits a relatively high SUV on ^{18}F -FDG PET/CT. Although the presence of scapular lesion as a part of the disseminated disease has been reported by prior publications, a case of LCH involving only the scapula has not been reported previously.

Ethics

Informed Consent: Obtained all appropriate patient consent forms.

Peer-review: Externally peer-reviewed.

Authorship Contributions

Surgical and Medical Practices: N.F., S.Ö., H.K.T., T.Ö., H.T.T., T.Y.E., Concept: N.F., S.Ö., Design: N.F., T.Y.E., Data Collection or Processing: N.F., S.Ö., Analysis or Interpretation: N.F., T.Y.E., Literature Search: N.F., S.Ö., Writing: N.F., S.Ö.

Conflict of Interest: No conflict of interest was declared by the authors.

Financial Disclosure: The authors declared that this study received no financial support.

References

1. Monsereenusorn C, Rodriguez-Galindo C. Clinical characteristics and treatment of langerhans cell histiocytosis. *Hematol Oncol Clin North Am* 2015;29:853-873.
2. Agarwal KK, Seth R, Behra A, Jana M, Kumar R. ^{18}F -fluorodeoxyglucose PET/CT in Langerhans cell histiocytosis: spectrum of manifestations. *Jpn J Radiol* 2016;34:267-276.
3. Albano D, Bosio G, Giubbini R, Bertagna F. Role of ^{18}F -FDG PET/CT in patients affected by Langerhans cell histiocytosis. *Jpn J Radiol* 2017;35:574-583.
4. Chen L, Chen Z, Wang Y. Langerhans cell histiocytosis at L5 vertebra treated with en bloc vertebral resection: a case report. *World J Surg Oncol* 2018;16:96.
5. Sasaki H, Nagano S, Shimada H, Nakamura S, Setoguchi T, Komiya S. Clinical course of the bony lesion of single-system single-site Langerhans cell histiocytosis - is appropriate follow-up sufficient treatment? *J Orthop Sci* 2018;23:168-173.
6. Ferrell J, Sharp S, Kumar A, Jordan M, Picarsic J, Nelson A. Discrepancies between F-18-FDG PET/CT findings and conventional imaging in Langerhans cell histiocytosis. *Pediatr Blood Cancer* 2021;68:e28891.
7. Nguyen BD, Roarke MC, Chivers SF. Multifocal Langerhans cell histiocytosis with infiltrative pelvic lesions: PET/CT imaging. *Clin Nucl Med* 2010;35:824-826.
8. Obert J, Vercellino L, Van Der Gucht A, de Margerie-Mellon C, Bugnet E, Chevret S, Lorillon G, Tazi A. ^{18}F -fluorodeoxyglucose positron emission tomography-computed tomography in the management of adult multisystem Langerhans cell histiocytosis. *Eur J Nucl Med Mol Imaging* 2017;44:598-610.
9. Lee HJ, Ahn BC, Lee SW, Lee J. The usefulness of F-18 fluorodeoxyglucose positron emission tomography/computed tomography in patients with Langerhans cell histiocytosis. *Ann Nucl Med* 2012;26:730-737.



¹⁸F-FDG PET/CT Showing Rare Mediastinal Growing Teratoma Syndrome Following Chemotherapy

Kemoterapi Sonrası Nadir Mediastinal Büyüyen Teratom Sendromu Gösteren ¹⁸F-FDG PET/BT Uygulaması

✉ Mihoko Sasahara¹, ✉ Takashi Abe², ✉ Yoichi Otomi¹, ✉ Yumi Abe², ✉ Hiroaki Toba³, ✉ Takayoshi Shinya¹, ✉ Hideki Otsuka¹, ✉ Masafumi Harada¹

¹Tokushima University, Department of Radiology, Tokushima, Japan

²Nagoya University Hospital, Department of Radiology, Nagoya, Japan

³Tokushima University, Department of Thoracic and Endocrine Surgery and Oncology, Tokushima, Japan

Abstract

Growing teratoma syndrome (GTS) is a condition in which poorly differentiated cells in a mixed-germ cell tumor (GCT) regress after chemotherapy, and the number of well-differentiated components increases. A 60-year-old man had an 8.0 cm mediastinal tumor with strong ¹⁸F-fluorodeoxyglucose (FDG) uptake [maximum standardized uptake value (SUV_{max}): 9.2], which was diagnosed as a GCT. After chemotherapy, serum alpha fetoprotein, beta-human chorionic gonadotropin, and tumor ¹⁸F-FDG uptake decreased (SUV_{max}: 3.9), but the tumor volume increased. The tumor was completely resected, and pathology confirmed the diagnosis of GTS. ¹⁸F-FDG positron emission tomography after chemotherapy reflects the proliferation of highly differentiated tumor components with poor ¹⁸F-FDG uptake.

Keywords: Growing teratoma syndrome, ¹⁸F-FDG PET, mediastinum, germ cell tumor

Öz

Büyüyen teratom sendromu (GTS), mikst germ hücreli tümörde (GCT) kötü diferansiye hücrelerin kemoterapiden sonra gerilediği ve iyi diferansiye komponentlerin sayısının arttığı bir durumdur. Altmış yaşındaki bir erkek hastada, yüksek ¹⁸F-florodeoksiglukoz (FDG) tutulumu [maksimum standartlaştırılmış tutulum değeri (SUV_{maks}): 9,2] olan 8,0 cm'lik ve GCT tanısı konulan bir mediastinal tümör vardı. Kemoterapiden sonra serum alfa fetoprotein, beta-insan koryonik gonadotropin ve tümör ¹⁸F-FDG tutulumu azaldı (SUV_{maks}: 3,9), ancak tümör hacmi arttı. Tümör tamamen rezeke edildi ve patoloji sonucu GTS tanısını doğruladı. Kemoterapi sonrası uygulanan ¹⁸F-FDG pozitron emisyon tomografisi, zayıf ¹⁸F-FDG tutulumu ile oldukça diferansiye tümör komponentlerinin proliferasyonunu yansıtır.

Anahtar kelimeler: Büyüyen teratom sendromu, ¹⁸F-FDG PET, mediasten, germ hücreli tümör

Address for Correspondence: Mihoko Sasahara MD, Tokushima University, Department of Radiology, Tokushima, Japan

Phone: +81-88-633-7173 **E-mail:** k.mihoko.928@gmail.com ORCID ID: orcid.org/0000-0001-6855-7030

Received: 27.05.2021 **Accepted:** 05.09.2021

©Copyright 2022 by Turkish Society of Nuclear Medicine
Molecular Imaging and Radionuclide Therapy published by Galenos Yayınevi.

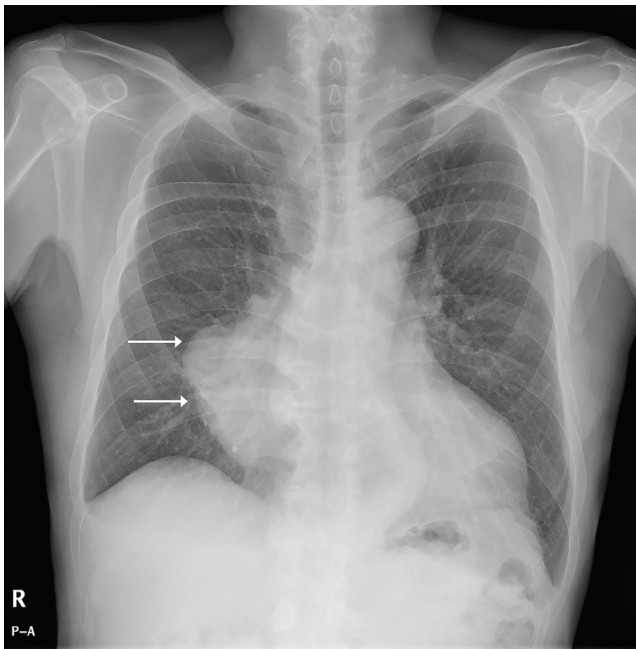


Figure 1. Chest X-ray image of an asymptomatic 60-year-old male during a routine medical check-up. A large mass was found in the right mediastinum (arrows).

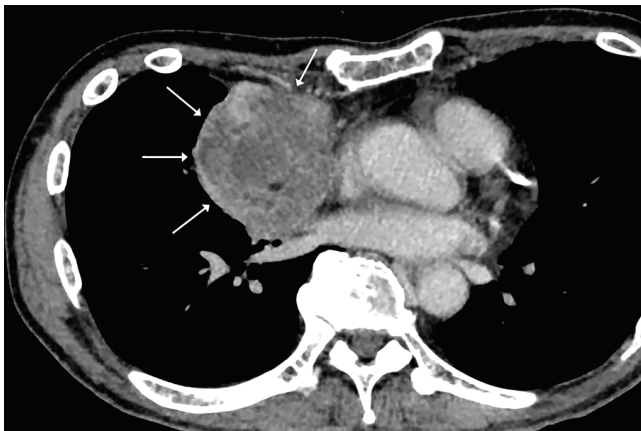


Figure 2. Contrast-enhanced computed tomography (CT) showed a mass, 8.0 cm in diameter, in the right anterior mediastinum (arrows).

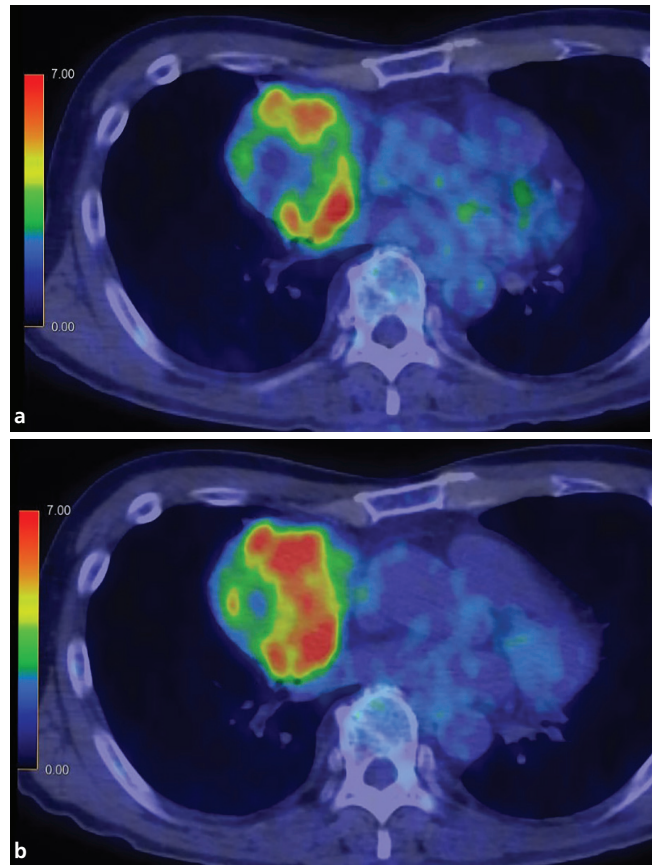


Figure 3. ^{18}F -fluorodeoxyglucose (FDG) positron emission tomography (PET)/CT fusion images at initial diagnosis. In the solid part of the tumor, the uptake of ^{18}F -FDG was strong with a maximum standardized uptake value (SUV_{max}): 9.2 in the early phase (a: 1 h after ^{18}F -FDG injection) and 10.4 in the delayed phase (b: 2 h after ^{18}F -FDG injection). Both serum alpha fetoprotein (971 ng/mL) and beta-human chorionic gonadotropin (3.8 mIU/mL) levels were increased. Percutaneous needle biopsy showed undifferentiated tumor cells, which were considered to be part of a non-seminomatous germ cell tumor (GCT).

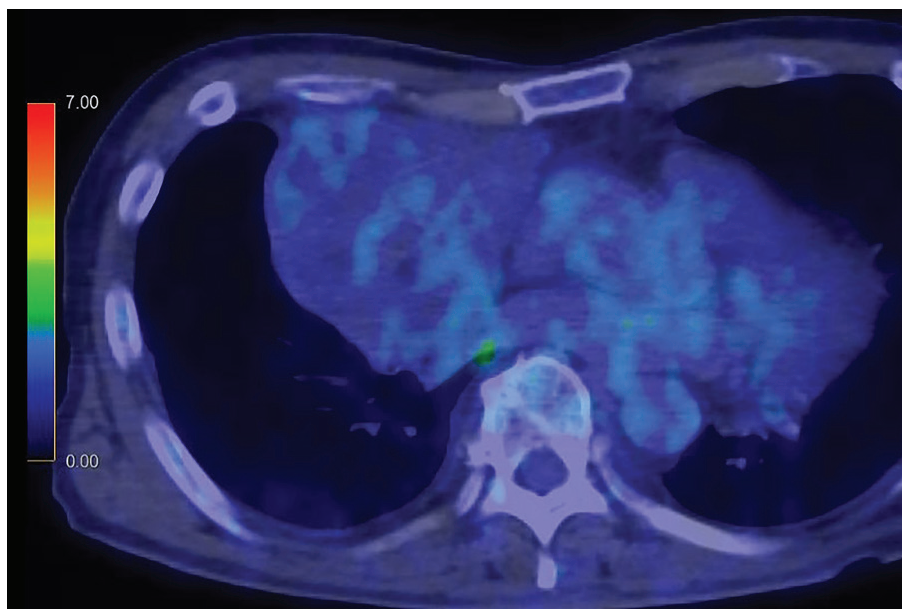


Figure 4. ^{18}F -FDG PET/CT fusion image after chemotherapy. After two courses of chemotherapy with bleomycin, etoposide, and cisplatin, the tumor size increased. Meanwhile, tumor marker levels decreased (alpha fetoprotein 230 ng/mL, beta-human chorionic gonadotropin 2.7 mIU/mL), and ^{18}F -FDG uptake decreased to a SUV_{max} of 3.9. The tumor was completely resected and histologically diagnosed as mature teratomas (MT) with growing teratoma syndrome (GTS). GCTs of the mediastinum occur mostly during the third to fourth decade of life (1). Chemotherapy is generally effective for GCTs, but the tumor may become unresponsive to treatment, which is a sign of poor prognosis. However, chemotherapy may reduce the malignant component of the tumor, resulting in an increased benign component. This phenomenon, called GTS, is defined as an increase in tumor size in a patient with a GCT, either during or after chemotherapy, while the initial tumor markers are normal and histology shows only MT (2,3). The treatment for GTS is the complete removal of the mass (4). To the best of our knowledge, this is the first report showing a decrease in ^{18}F -FDG uptake of mediastinal GTS after chemotherapy. In past reports of GTS, ^{18}F -FDG SUV_{max} was 4.9 in mediastinal tumors and 4.0, 4.1 and 8.1 in ovarian tumors (5,6). Hariprasad et al. (7) reported one patient with GTS in an ovary that showed positive ^{18}F -FDG uptake. The mature components of the teratoma in the specimen that they resected were brain, thyroid, hair follicle, cartilage, and adipose tissue. They suspected that the brain tissue components had a high rate of glucose metabolism that might be the main reason for ^{18}F -FDG uptake. Our case also included brain tissue, but the proportion was not high; so it is possible that the post-chemotherapeutic tumor uptake was not particularly high. It is not easy to diagnose GTS in such cases with strong ^{18}F -FDG uptake; however, the diagnosis of GTS can be made more reliably when the ^{18}F -FDG uptake decreases after treatment, as in our case, even if conventional imaging techniques, such as CT and magnetic resonance imaging, show tumor growth.

Ethics

Informed Consent: Written informed consent of the patient was obtained.

Peer-review: Externally peer-reviewed.

Authorship Contributions

Surgical and Medical Practices: Y.O., Y.A., H.T., T.S., H.O., Concept: T.A., T.S., Design: M.S., T.A., Data Collection or Processing: M.S., Y.O., M.H., Analysis or Interpretation: M.S., M.H., Literature Search: M.S., T.A., Writing: M.S., T.A., Y.O.

Conflict of Interest: No conflict of interest is declared by the authors.

Financial Disclosure: The authors declare that this study received no financial support.

References

1. Dulmet EM, Macchiarini P, Suc B, Verley JM. Germ cell tumors of the mediastinum. A 30-year experience. *Cancer* 1993;72:1894-1901.
2. Logothetis CJ, Samuels ML, Trindade A, Johnson DE. The growing teratoma syndrome. *Cancer* 1982;50:1629-1635.
3. DiSaia PJ, Saltz A, Kagan AR, Morrow CP. Chemotherapeutic retroconversion of immature teratoma of the ovary. *Obstet Gynecol* 1977;49:346-350.
4. Saso S, Galazis N, Iacovou C, Kappatou K, Tzafetas M, Jones B, Yazbek J, Lathouras K, Anderson J, Jiao LR, Smith RJ. Managing growing teratoma syndrome: new insights and clinical applications. *Future Sci OA* 2019;5:FSO419.
5. Omachi N, Kawaguchi T, Shimizu S, Okuma T, Kitaichi M, Atagi S, Yoon HE, Matsumura A. Life-threatening and rapidly growing teratoma in the anterior mediastinum. *Intern Med* 2015;54:2487-2489.
6. Kikawa S, Todo Y, Minobe S, Yamashiro K, Kato H, Sakuragi N. Growing teratoma syndrome of the ovary: a case report with FDG-PET findings. *J Obstet Gynaecol Res* 2011;37:926-932.
7. Hariprasad R, Kumar L, Janga D, Kumar S, Vijayaraghavan M. Growing teratoma syndrome of ovary. *Int J Clin Oncol* 2008;13:83-87.



Neurolymphomatosis with Spinal Nerve Root Involvement Demonstrated on ¹⁸F-FDG PET/CT

¹⁸F-FDG PET/CT'de Spinal Sinir Kökü Tutulumu Olan Nörolenfomatozis

✉ Ayça Arçay¹, ✉ Gonca Gül Bural¹, ✉ Utku Şenol²

¹Akdeniz University Faculty of Medicine, Department of Nuclear Medicine, Antalya, Turkey

²Akdeniz University Faculty of Medicine, Department of Radiology, Antalya, Turkey

Abstract

A 56 years old woman with a diagnosis of diffuse large B-cell lymphoma had dyspnea, weakness in the left upper extremity and vocal cord paralysis after chemotherapy. She underwent cervical, thoracic and lumbosacral magnetic resonance imaging (MRI) however findings on MRI could not entirely explain the symptoms of the patient. Therefore, the patient underwent ¹⁸F-fluorodeoxyglucose (FDG) positron emission tomography/computed tomography and the scan revealed focal symmetrical ¹⁸F-FDG uptake on the cervical, thoracic and lumbar spinal nerve roots. Considering the symptoms of the patient and cerebrospinal fluid cytology findings, hypermetabolic spinal nerve roots were interpreted as lymphoma involvement.

Keywords: Neurolymphomatosis, ¹⁸F-FDG PET/CT, MRI, lymphoma, spinal nerve root

Öz

Diffüz büyük B-hücreli lenfoma tanılı 56 yaşındaki kadın hastada kemoterapi sonrası dispne, sol üst ekstremitede güçsüzlük ve vokal kord paralizisi izlendi. Hastaya servikal, torakal ve lumbosakral manyetik rezonans görüntüleme (MRG) yapıldı ancak MRG bulguları hastanın semptomlarını tam olarak açıklayamadı. Bu nedenle hastaya ¹⁸F-florodeoksiglukoz (FDG) pozitron emisyon tomografisi/bilgisayarlı tomografi yapıldı ve taramada servikal, torakal, lumbal spinal sinir köklerinde fokal simetrik ¹⁸F-FDG tutulumu izlendi. Hastanın semptomları ve beyin omurilik sıvısı sitolojik bulguları dikkate alındığında, hipermetabolik spinal sinir kökleri lenfoma tutulumu olarak yorumlandı.

Anahtar kelimeler: Nörolenfomatozis, ¹⁸F-FDG PET/CT, MRG, lenfoma, spinal sinir kökü

Address for Correspondence: Prof. Gonca Gül Bural MD, Akdeniz University Faculty of Medicine, Department of Nuclear Medicine, Antalya, Turkey

Phone: +90 533 058 98 46 **E-mail:** buralgonca@gmail.com ORCID ID: orcid.org/0000-0002-6608-6770

Received: 22.08.2021 **Accepted:** 26.09.2021

©Copyright 2022 by Turkish Society of Nuclear Medicine
Molecular Imaging and Radionuclide Therapy published by Galenos Yayınevi.

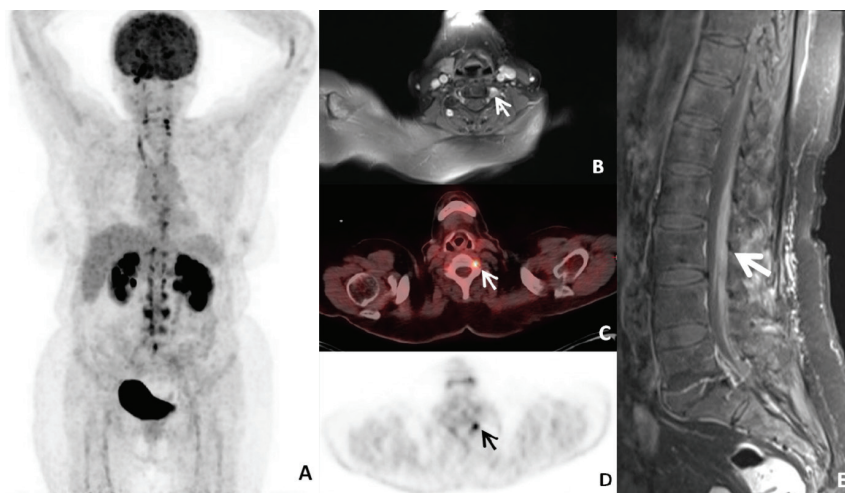


Figure 1. A 56 years old woman diagnosed with diagnosis diffuse large B-cell lymphoma had dyspnea, weakness in the left upper extremity and vocal cord paralysis beginning one month after 4 cycles of chemotherapy. She underwent cervical, thoracic and lumbosacral magnetic resonance imaging (MRI) revealing diffuse thickening and contrast enhancement on cauda equina and filum terminale (E, T1 weighted fat sat postcontrast sagittal image, arrow), also asymmetric contrast enhancement on cervical 5-6 left spinal nerve root (B, T1 weighted fat sat postcontrast axial image, arrow) suspicious for lymphoma involvement, however these findings could not entirely explain the symptoms of the patient. Four days after MRI, the patient underwent ¹⁸F-fluorodeoxyglucose (FDG) positron emission tomography/computed tomography (PET/CT) for treatment response evaluation and the scan revealed focal symmetrical ¹⁸F-FDG uptake on the cervical (C, axial fused PET/CT; D, axial PET with maximum standardized uptake value: 8.95, arrows), thoracic and lumbal spinal nerve roots (A, MIP yerrine maximum intensity projection). Cerebrospinal fluid (CSF) cytology examination was done two days after PET/CT and it was reported as consistent with lymphoma involvement. Considering the symptoms of the patient and CSF cytology findings, hypermetabolic spinal nerve roots were interpreted as lymphoma involvement.

Neurolymphomatosis (NL) is a rare entity defined as the infiltration of the nervous system by lymphoma. NL can lead to the development of symptoms of neuropathy, including pain, hypoesthesia, paresthesia and palsy. NL is most frequently associated with B-cell non-Hodgkin's lymphoma (NHL), though there are reported cases of non-B-cell NHL (1,2). Generally, NL present after several courses of treatment, it is uncommonly a primary presentation of lymphoma (1,2). Diagnosing NL is challenging due to the variable symptoms and the large number of differential diagnosis. Nerve biopsy result is the gold standard, however it is invasive with the risk of permanent nerve damage and blind biopsies have high false-negative rates. Therefore, imaging can play an important role in diagnosis, can also guide nerve biopsies and help avoid unnecessary biopsies. NL is increasingly being recognized with the increasing use of MRI and ¹⁸F-FDG PET/CT in the evaluation of peripheral nervous system disorders (3). NL on ¹⁸F-FDG PET/CT can be seen as the involvement of cranial nerves (1,4,5,6,7), peripheral nerves (1,3,6,7,8), neural plexuses (1,3,5,6) or -as in this case- spinal nerve roots (1,3,5,6,7). We should be familiar with the appearance patterns of NL on ¹⁸F-FDG PET/CT and consider this entity while evaluating the lymphoma patients with neurological symptoms.

Ethics

Informed Consent: Consent form was filled out by the patient.

Peer-review: Externally peer-reviewed.

Authorship Contributions

Surgical and Medical Practices: A.A., G.G.B., U.Ş., Concept: A.A., G.G.B., Design: A.A., G.G.B., Data Collection or Processing: A.A., G.G.B., U.Ş., Analysis or Interpretation: A.A., G.G.B., U.Ş., Literature Search: A.A., Writing: A.A.

Conflict of Interest: No conflict of interest was declared by the authors.

Financial Disclosure: The authors declared that this study received no financial support.

References

1. Salm LP, Van der Hiel B, Stokkel MP Increasing importance of ¹⁸F-FDG PET in the diagnosis of neurolymphomatosis. *Nucl Med Commun* 2012;33:907-916.
2. Baehring JM, Batchelor TT. Diagnosis and management of neurolymphomatosis. *Cancer J* 2012;18:463-468.
3. Shree R, Goyal MK, Modi M, Gaspar BL, Radotra BD, Ahuja CK, Mittal BR, Prakash G. The diagnostic dilemma of neurolymphomatosis. *J Clin Neurol* 2016;12:274-281.
4. Tsang HH, Lee EY, Anthony MP, Khong PL. ¹⁸F-FDG PET/CT diagnosis of vagus nerve neurolymphomatosis. *Clin Nucl Med* 2012;37:897-898.
5. Davidson T, Kedmi M, Avigdor A, Komisar O, Chikman B, Lidar M, Goshen E, Tzila Zwas S, Ben-Haim S. FDG PET-CT evaluation in neurolymphomatosis: imaging characteristics and clinical outcomes. *Leuk Lymphoma* 2018;59:348-356.
6. Strobel K, Fischer K, Hany TF, Poryazova R, Jung HH. Sciatic nerve neurolymphomatosis - extent and therapy response assessment with PET/CT. *Clin Nucl Med* 2007;32:646-648.
7. Singh SS, Mittal BR, Kumar R, Singh H, Balaini N, Goyal M. Primary central nervous system lymphoma with diffuse neurolymphomatosis involving multiple cranial and spinal nerve roots. *Clin Nucl Med* 2020;45:e285-e287.
8. Byun JM, Kim KH, Kim M, Kim TM, Jeon YK, Park JH, Paik JH, Lee JM, Lee HY, Lee JS, Heo DS, Lee JO. Diagnosis of secondary peripheral neurolymphomatosis: a multi-center experience. *Leuk Lymphoma* 2017;58:2624-2632.



Mild ^{68}Ga PSMA-11 Uptake in Incidental Pituitary Adenoma

İnsidental Pitüiter Adenomda Hafif ^{68}Ga PSMA-11 Tutulumu

Ediz Beyhan¹, Özge Erol Fenercioğlu¹, Yeşim Karagöz², Nurhan Ergül¹, Tevfik Fikret Çermik¹

¹University of Health Sciences Turkey, İstanbul Training and Research Hospital, Clinic of Nuclear Medicine, İstanbul, Turkey

²University of Health Sciences Turkey, İstanbul Training and Research Hospital, Clinic of Radiology, İstanbul, Turkey

Abstract

A 76-year-old man with metastatic prostate cancer was referred to ^{68}Ga prostate-specific membrane antigen (PSMA) positron emission tomography/computed tomography (PET/CT) for restaging. A consecutive ^{18}F -fluorodeoxyglucose (FDG) PET/CT was performed due to the history of lung cancer in the left lung treated with stereotactic radiotherapy. Intense ^{18}F -FDG uptake was detected in the pituitary gland despite the mild uptake of ^{68}Ga PSMA. Contrast-enhanced magnetic resonance imaging confirmed pituitary adenoma.

Keywords: ^{68}Ga PSMA PET/CT, pituitary adenoma, ^{18}F -FDG PET/CT

Öz

Metastatik prostat kanseri tanılı 76 yaşında erkek hasta yeniden evreleme amacıyla ^{68}Ga prostat-spesifik membran antijen (PSMA) pozitron emisyon tomografi/bilgisayarlı tomografi (PET/BT) görüntüleme için yönlendirildi. Akciğer kanseri öyküsü olan ve sol akciğere stereotaktik radyoterapi uygulanan hastaya ayrıca ^{18}F -fluorodeoxyglucose (FDG) PET/BT görüntüleme de yapıldı. Hipofiz glandında yoğun ^{18}F -FDG tutulumu saptanırken, ^{68}Ga PSMA görüntülemesinde hafif tutulum saptandı. Kontrastlı manyetik rezonans görüntüleme ile pitüiter adenom tanısını doğrulandı.

Anahtar kelimeler: ^{68}Ga PSMA PET/BT, pitüiter adenom, ^{18}F -FDG PET/BT

Address for Correspondence: Ediz Beyhan MD, University of Health Sciences Turkey, İstanbul Training and Research Hospital, Clinic of Nuclear Medicine, İstanbul, Turkey

Phone: +90 535 713 24 98 **E-mail:** edizbeyhan@gmail.com ORCID ID: orcid.org/0000-0001-6833-4830

Received: 10.07.2021 **Accepted:** 10.10.2021

©Copyright 2022 by Turkish Society of Nuclear Medicine
Molecular Imaging and Radionuclide Therapy published by Galenos Yayınevi.

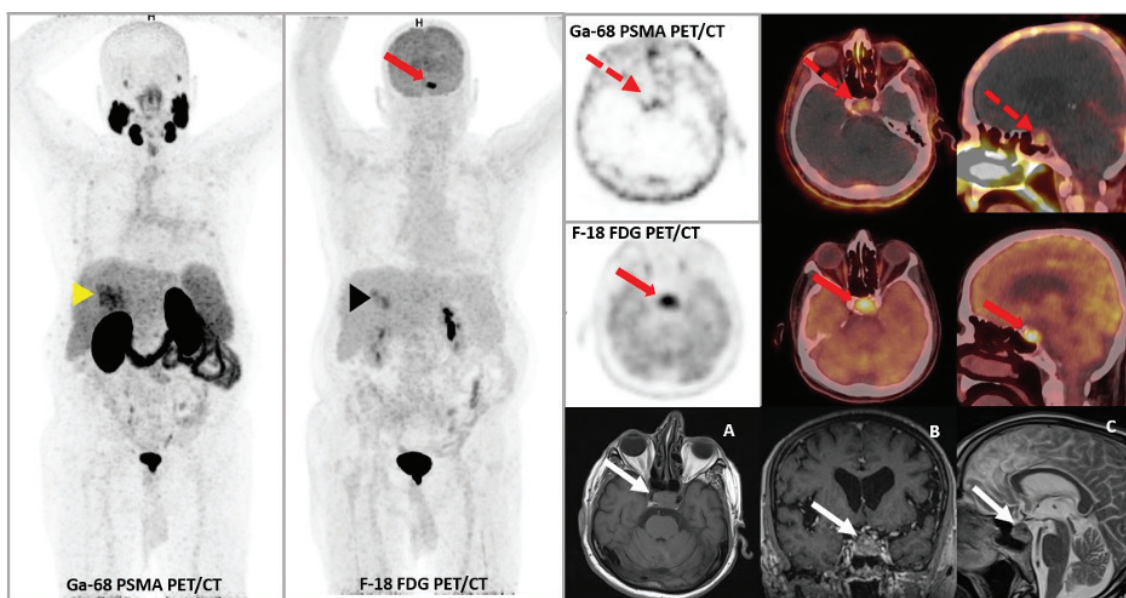


Figure 1. A 76-year-old man underwent radical prostatectomy for prostate adenocarcinoma 4 years ago. The patient received chemoradiotherapy due to castration resistance and was referred to ⁶⁸Ga prostate-specific membrane antigen (PSMA) positron emission tomography/computed tomography (PET/CT) for restaging. He also had a history of lung cancer and stereotactic radiotherapy to a lesion in left lung. A consecutive ¹⁸F-fluorodeoxyglucose (FDG) PET/CT was performed for evaluation of lung cancer remission. Metastatic lesions in liver are seen in both PET/CT images (maximum intensity projection images, arrowheads). Intense ¹⁸F-FDG uptake was observed in pituitary gland in axial and sagittal slices of ¹⁸F-FDG PET/CT [maximum standardized uptake value (SUV_{max}): 13.94] (red arrows). Axial and sagittal PET and fusion images showed mild ⁶⁸Ga PSMA uptake (SUV_{max}: 1.88) in the pituitary gland (dashed arrows). Magnetic resonance imaging (MRI) examination of pituitary gland-verified macroadenoma filling and expanding the sella in T1 weighted sequences axial slice (A), contrast-enhanced coronal slice (B), and T2 weighted sequences sagittal slice (C). Pituitary adenomas are detected incidentally in oncological ¹⁸F-FDG PET/CT and the incidence was found as 0.073% in a multi-center study (1,2). The SUV_{max} value was determined as 4.1 in another study conducted with ¹⁸F-FDG PET/CT to discriminate physiological and pathological involvement (3). Pituitary lesions can be detected with high accuracy in contrast-enhanced MRI (4). PSMA PET/CT plays a significant role in diagnosis and treatment response assessment in prostate cancer patients (5). Various benign lesions with PSMA uptake have been reported (6,7,8). We showed the mild uptake on ⁶⁸Ga PSMA PET/CT in a pituitary adenoma for the first time to our knowledge.

Ethics

Informed Consent: Obtained from the patient.

Peer-review: Externally peer-reviewed.

Authorship Contributions

Concept: T.F.Ç., N.E., Design: T.F.Ç., N.E., Data Collection or Processing: Y.K., Ö.E.F., E.B., Analysis or Interpretation: T.F.Ç., N.E., Literature Search: E.B., T.F.Ç., N.E., Writing: E.B., Y.K., Ö.E.F., T.F.Ç., N.E.

Conflict of Interest: No conflict of interest was declared by the authors.

Financial Disclosure: The authors declared that this study received no financial support.

References

- Jeong SY, Lee SW, Lee HJ, Kang S, Seo JH, Chun KA, Cho IH, Won KS, Zeon SK, Ahn BC, Lee J. Incidental pituitary uptake on whole-body ¹⁸F-FDG PET/CT: a multicentre study. *Eur J Nucl Med Mol Imaging* 2010;37:2334-2343.
- Maffei P, Marzola MC, Musto A, Dassie F, Grassetto G, De Carlo E, Rampin L, Chondrogianis S, Massaro A, Pelizzo MR, Rubello D. A very

rare case of nonfunctioning pituitary adenoma incidentally disclosed at ¹⁸F-FDG PET/CT. *Clin Nucl Med* 2012;37:e100-e101.

- Hyun SH, Choi JY, Lee KH, Choe YS, Kim BT. Incidental focal ¹⁸F-FDG uptake in the pituitary gland: clinical significance and differential diagnostic criteria. *J Nucl Med* 2011;52:547-550.
- Bashari WA, Senanayake R, Fernández-Pombo A, Gillett D, Koulouri O, Powlson AS, Matys T, Scoffings D, Cheow H, Mendichovszky I, Gurnell M. Modern imaging of pituitary adenomas. *Best Pract Res Clin Endocrinol Metab* 2019;33:101278.
- Sheikhabahei S, Afshar-Oromieh A, Eiber M, Solnes LB, Javadi MS, Ross AE, Pienta KJ, Allaf ME, Haberkorn U, Pomper MG, Gorin MA, Rowe SP. Pearls and pitfalls in clinical interpretation of prostate-specific membrane antigen (PSMA)-targeted PET imaging. *Eur J Nucl Med Mol Imaging* 2017;44:2117-2136.
- Bilgin R, Ergül N, Çermik TF. Incidental meningioma mimicking metastasis of prostate adenocarcinoma in ⁶⁸Ga-labeled PSMA ligand PET/CT. *Clin Nucl Med* 2016;41:956-958.
- Strele-Trieb P, Dunzinger A, Sonnberger M, Wolfsgruber J, Pichler R. Uptake of ⁶⁸Ga-prostate-specific membrane antigen PET in adrenal gland: a potential pitfall. *Clin Nucl Med* 2018;43:50-51.
- Pfob CH, Karimov I, Jesinghaus M, Novotny A, Weber WA, Eiber M, Feuercker B. Pitfalls in ⁶⁸Ga-PSMA-PET/CT: incidental finding of parathyroid adenoma. *Eur J Nucl Med Mol Imaging* 2019;46:1041.



A Case of Extracranial Metastasis of Glioblastoma Multiforme Seen on Bone Scintigraphy

Kemik Sintigrafisinde Görülen Glioblastoma Multiforme'dan Ekstrakraniyal Metastaz Olgusu

Hardik Veerwal, Anjali Meena, Vandana Dhingra

All India Institute of Medical Sciences, Department of Nuclear Medicine, Rishikesh, India

Abstract

Glioblastoma multiforme (GBM) is the most common primary malignant tumor of the central nervous system in adults. It is known for its devastating intracranial progress thus attributing to its very short survival. Here, we report a case of 37-year-old female with GBM post surgery, chemotherapy and radiotherapy who presented with pain in right hip region. She was referred to our department for evaluation of skeletal metastasis. Tc-99m methylene diphosphonate bone scan revealed an expansile lesion involving the right iliac blade along with extensive lytic bony lesions throughout the axial skeleton.

Keywords: Glioblastoma multiforme, bone scan, metastasis, Tc-99m MDP, extraosseous

Öz

Glioblastoma multiforme (GBM), erişkinlerde merkezi sinir sisteminin en sık görülen primer malign tümörüdür. Yıkıcı intrakraniyal gelişimi ve bu nedenle çok kısa bir hayatta kalma oranı ile bilinir. Bu çalışmada sağ kalça bölgesinde ağrı şikayeti ile başvuran, ameliyat, kemoterapi ve radyoterapi uygulanan 37 yaşındaki bir kadın GBM hastası sunuldu. İskelet metastazının değerlendirilmesi için bölümümüze sevk edildi. Tc-99m metilen difosfonat kemik taraması, aksiyel iskelet boyunca geniş litik kemik lezyonları ile birlikte sağ iliak kemiği kapsayan ekspansil bir lezyon ortaya çıkardı.

Anahtar kelimeler: Glioblastoma multiforme, kemik taraması, metastaz, Tc-99m MDP, ekstraosseöz

Address for Correspondence: Assoc. Prof. Vandana Dhingra MD, All India Institute of Medical Sciences, Department of Nuclear Medicine, Rishikesh, India

Phone: +918433295564 **E-mail:** modisbanu@yahoo.com ORCID ID: orcid.org/0000-0002-3006-8597

Received: 13.09.2021 **Accepted:** 24.10.2021

©Copyright 2022 by Turkish Society of Nuclear Medicine
Molecular Imaging and Radionuclide Therapy published by Galenos Yayınevi.

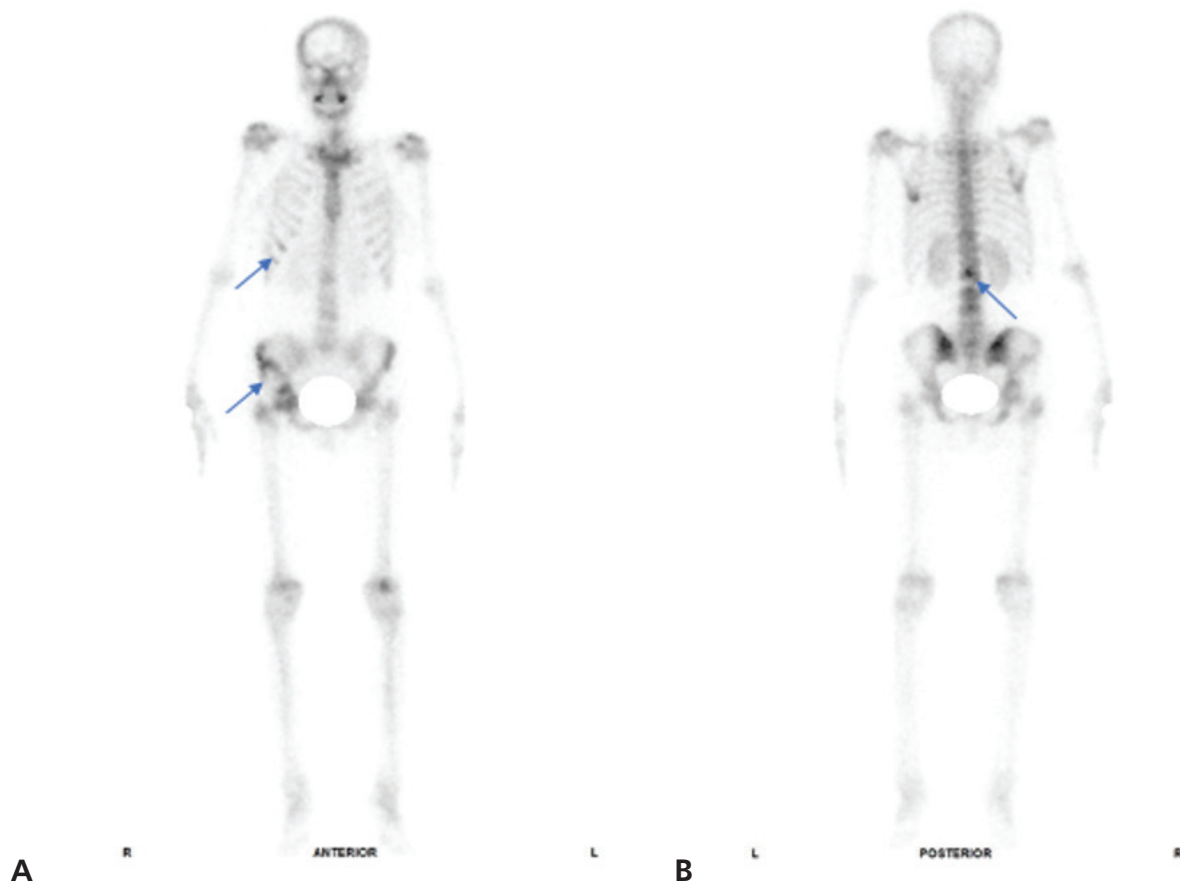


Figure 1. A 37-year-old female, known case of glioblastoma multiforme (GBM) status post-surgery followed by adjuvant chemotherapy and radiotherapy presented to our hospital OPD with recent onset pain in the right hip region 1 year post surgery. Initial workup with contrast-enhanced magnetic resonance imaging brain revealed no residual or recurrent disease at the primary tumour site. Patient was referred to the nuclear medicine department for whole body skeletal screening. Tc-99m methylene diphosphonate (MDP) whole body bone scan in anterior and posterior views (A and B) revealed heterogeneous increased tracer uptake involving right iliac blade, right 7th rib and L2 lumbar vertebra.

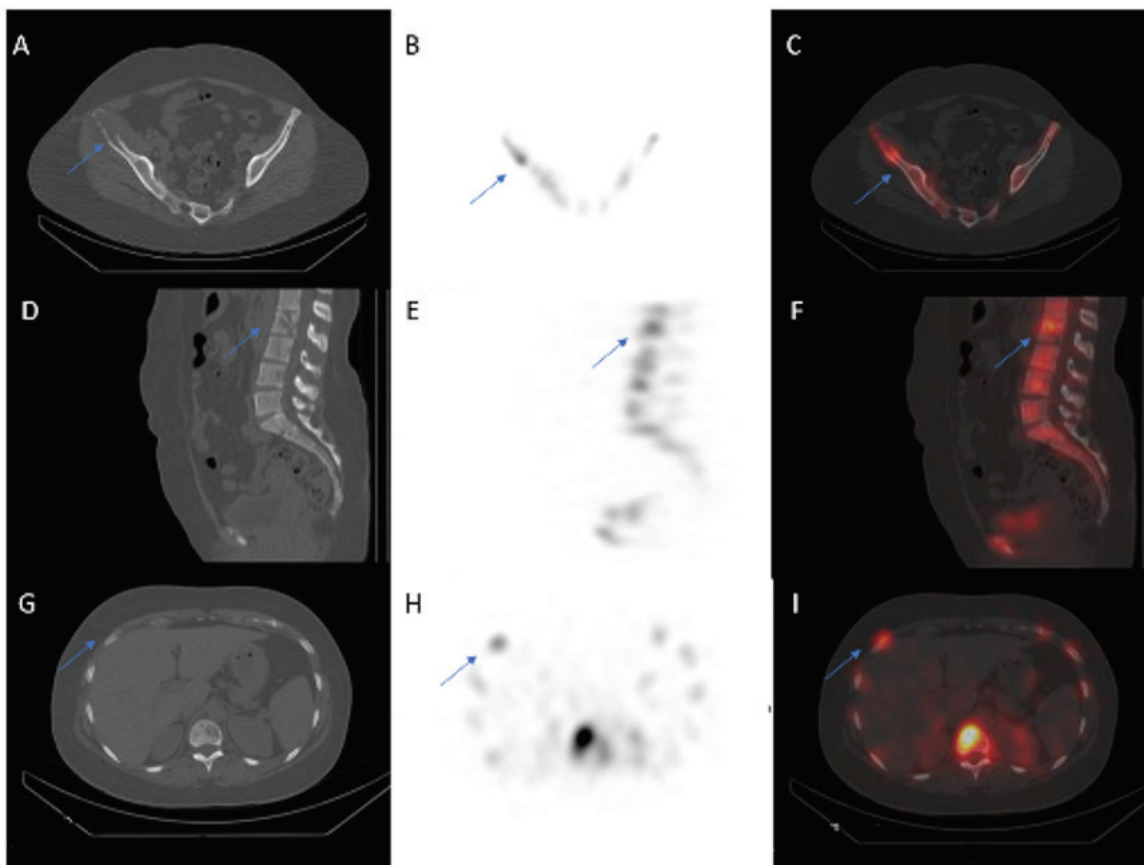


Figure 2. Thorax and pelvis with lumbar region single photon emission computed tomography/computed tomography (SPECT/CT) was performed. The transaxial and sagittal CT, SPECT, fused SPECT/CT images of the lumbar region showed a lytic expansile lesion measuring 5x5 cm seen in the right iliac blade with soft tissue component (A, B, C). The lesion was infiltrating into the surrounding muscular structure. Multiple, well-defined lytic lesions involving left clavicle, left 7th rib, bilateral scapulae, bilateral pelvic bone, bilateral proximal femur, and multiple cervical, thoracic, lumbosacral, vertebrae were also seen on the CT images (D, E, F). A biopsy of the right iliac lesion was performed, which was suggestive of metastasis from GBM. GBM has an extracranial metastasis rate of 0.4-0.5% (1). Only limited cases have reported till now of extracranial metastasis of GBM (2,3,4,5,6,7,8). Radiotherapy has been suggested as one of the causes for the extracranial involvement of GBM caused by metaplasia of tumor cells and barrier breach (9). Disruption of dura due to surgery and certain chemotherapeutic agents has also been postulated as a causative factor for extracranial spreads of GBM (10,11). This case presented with multiple extracranial metastases 1 year post-surgery, and chemoradiotherapy. Extracranial metastasis, although being rare, should be considered a possibility in post-surgery, chemotherapy, and radiotherapy patients. Further research is required to determine whether ancillary therapy can have positive causation with extracranial metastasis and the role Tc-99m MDP bone scan plays in the evaluation of GBM patients.

Ethics

Informed Consent: Patient consent was obtained.

Peer-review: Externally peer-reviewed.

Authorship Contributions

Concept: H.V., V.D., Design: H.V., V.D., Data Collection or Processing: H.V., A.M., V.D., Analysis or Interpretation: H.V., A.M., V.D., Literature Search: H.V., A.M., V.D., Writing: H.V., A.M., V.D.

Conflict of Interest: No conflict of interest was declared by the authors.

Financial Disclosure: The authors declare that this study has received no financial support.

References

1. Simonetti G, Silvani A, Fariselli L, Hottinger AF, Pesce GA, Prada F, Gaviani P. Extra central nervous system metastases from glioblastoma: a new possible trigger event? *Neurol Sci* 2017;38:1873-1875.
2. Seo YJ, Cho WH, Kang DW, Cha SH. Extraneural metastasis of glioblastoma multiforme presenting as an unusual neck mass. *J Korean Neurosurg Soc* 2012;51:147-150.
3. Ricard JA, Cramer SW, Charles R, Tommee CG, Le A, Bell WR, Chen CC, Flanagan E. Infratentorial glioblastoma metastasis to bone. *World Neurosurg* 2019;131:90-94.

4. Rossi J, Giaccherini L, Cavallieri F, Napoli M, Moratti C, Froio E, Serra S, Fraternali A, Ghadirpour R, Cozzi S, Ciammella P, Iaccarino C, Pascarella R, Valzania F, Pisanello A. Extracranial metastases in secondary glioblastoma multiforme: a case report. *BMC Neurol* 2020;20:382.
5. Sibanda Z, Farahani N, Ogbonnaya E, Albanese E. Glioblastoma multiforme: a rare case of spinal drop metastasis. *World Neurosurg* 2020;144:24-27.
6. Undabeitia J, Castle M, Arrazola M, Pendleton C, Ruiz I, Úrculo E. Multiple extraneural metastasis of glioblastoma multiforme. *An Sist Sanit Navar* 2015;38:157-161.
7. Shastin D, Mathew RK, Ismail A, Towns G. Cervical spinal glioblastoma multiforme in the elderly. *BMJ Case Rep* 2017;2017:bcr2016217742.
8. Forsyth TM, Bi WL, Abedalthagafi M, Dunn IF, Chiocca EA. Extracranial growth of glioblastoma multiforme. *J Clin Neurosci* 2015;22:1521-1523.
9. Rosen J, Blau T, Grau SJ, Barbe MT, Fink GR, Galldiks N. Extracranial metastases of a cerebral glioblastoma: a case report and review of the literature. *Case Rep Oncol* 2018;11:591-600.
10. Pietschmann S, von Bueren AO, Kerber MJ, Baumert BG, Kortmann RD, Müller K. An individual patient data meta-analysis on characteristics, treatments and outcomes of glioblastoma/ gliosarcoma patients with metastases outside of the central nervous system. *PLoS One* 2015;10:e0121592.
11. Beauchesne P. Extra-neural metastases of malignant gliomas: myth or reality? *Cancers (Basel)* 2011;3:461-477.



Mass-like Appearance on ¹⁸F-FDG PET/CT: Cascade Stomach

¹⁸F-FDG PET/BT'de Kitlesel Görünüm: Kaskat Mide

✉ Ayça Arçay¹, ✉ Funda Aydın¹, ✉ Mete Akın²

¹Akdeniz University Hospital, Department of Nuclear Medicine, Antalya, Turkey

²Akdeniz University Hospital, Department of Internal Medicine, Division of Gastroenterology, Antalya, Turkey

Abstract

A 56-year-old female patient who had involuntary weight loss underwent ¹⁸F-fluorodeoxyglucose positron emission tomography/computed tomography (PET/CT) for detection of malignancy. The scan revealed non-metabolic soft tissue density in the posterior wall of the stomach requiring endoscopy. Endoscopic examination was performed 9 days after PET/CT and cascade stomach was detected. Cascade stomach is a rare entity that can be diagnosed by radiographic barium evaluations and endoscopy, the appearance on CT is largely incidental and CT has rarely been relied on for the diagnosis. We present this incidental case of cascade stomach on PET/CT to be familiar with the appearance.

Keywords: Cascade stomach, ¹⁸F-FDG PET/CT, CT

Öz

İstemsiz kilo kaybı şikayeti olan 56 yaşında kadın hastaya malignite araştırılması için ¹⁸F-florodeoksiglukoz pozitron emisyon tomografisi/bilgisayarlı tomografi (PET/BT) yapıldı. Görüntülerde mide posterior duvarda endoskopi gerektiren metabolik aktivitesi olmayan yumuşak doku dansitesi izlendi. PET/BT görüntülemeye 9 gün sonra yapılan endoskopik incelemede kaskat mide tespit edildi. Kaskat mide, baryum grafi ve endoskopi ile tanı konabilen nadir bir antitedir, BT'de görünümü büyük oranda insidentaldir ve çok nadiren tanıda BT kullanılır. PET/BT'de insidental izlenen bu kaskat mide olgusunu görünümüne aşina olmak için sunuyoruz.

Anahtar kelimeler: Kaskat mide, ¹⁸F-FDG PET/BT, BT

Address for Correspondence: Prof. Funda Aydın MD, Akdeniz University Hospital, Department of Nuclear Medicine, Antalya, Turkey

Phone: +90 242 249 60 00 **E-mail:** afunda@akdeniz.edu.tr ORCID ID: orcid.org/0000-0001-7110-549X

Received: 08.10.2021 **Accepted:** 01.01.2022

©Copyright 2022 by Turkish Society of Nuclear Medicine
Molecular Imaging and Radionuclide Therapy published by Galenos Yayınevi.

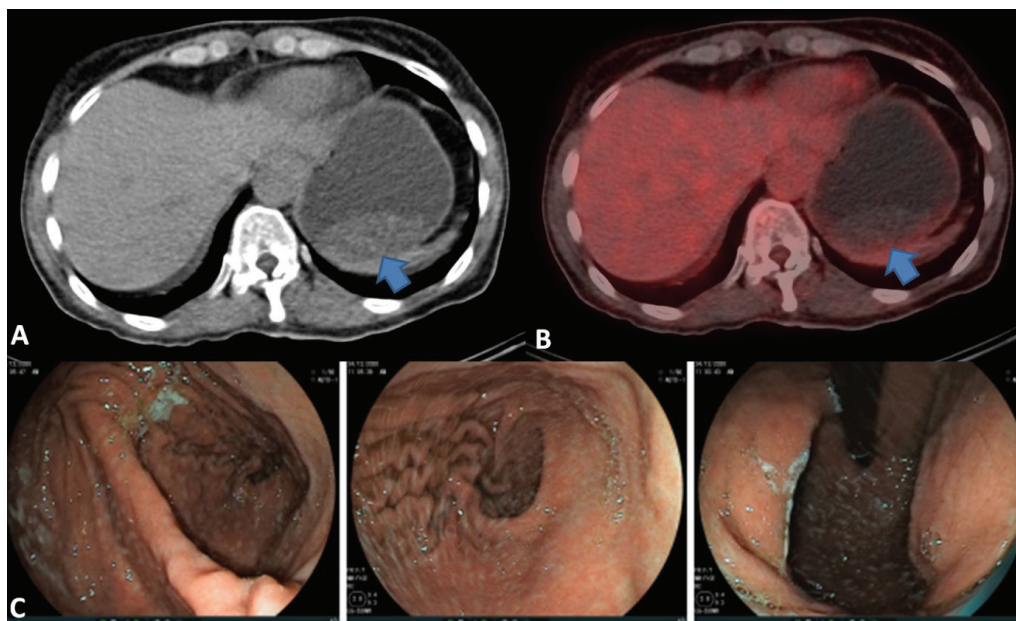


Figure 1. We present the case of a 56-year-old female patient who had more than 20% body weight loss involuntarily in the last 6 months. ¹⁸F-fluorodeoxyglucose (FDG) positron emission tomography/computed tomography (PET/CT) was performed for investigation of malignancy. The scan demonstrated a non-metabolic well-demarcated mass-like soft tissue appearance in the posterior wall of the stomach extending into the lumen (A, axial CT; B axial fused PET/CT, arrows). Because of the involuntary weight loss and the appearance on PET/CT, the patient underwent endoscopy 9 days after the scan. The endoscopic examination revealed no mass formation, however, a cascade stomach was observed (C). Cascade stomach (“cup-and-spill” stomach) is a deformity of the stomach in which the fundus is folded over corpus in a dorsal direction and its actual incidence is not known (1,2,3). Various causes of cascade stomach, including congenital, functional, and organic disorders, have been described in the literature (2,4,5). A cascade stomach is a rare cause of upper gastrointestinal symptoms and is often difficult to diagnose (6). Mostly barium studies and endoscopic examination have been relied on for the diagnosis (7,8). CT appearance of the cascade stomach is not well known, therefore we present this case of an incidental finding. This mass-like well-demarcated non-metabolic soft tissue appearance on PET/CT may be attributed to bezoar or non-¹⁸F-FDG-avid tumoral lesions. However, it should be kept in mind that structural abnormalities and deformities of the stomach, as in this case, cascade stomach can also appear similarly. We emphasize the significance of endoscopic guidance for differential diagnosis in such cases.

Ethics

Informed Consent: Written informed consent was obtained from the patient.

Peer-review: Externally peer-reviewed.

Authorship Contributions

Surgical and Medical Practices: A.A., F.A., M.A., Concept: A.A., F.A., Design: A.A., Data Collection or Processing: A.A., F.A., M.A., Analysis or Interpretation: A.A., Literature Search: A.A., Writing: A.A.

Conflict of Interest: No conflict of interest was declared by the authors.

Financial Disclosure: The authors declared that this study received no financial support.

References

- Gulsen MT, Koruk I, Dogan M, Beyazit Y. Diagnostic accuracy of cascade stomach by upper gastrointestinal endoscopy in patients with obscure symptoms: a multi-center prospective trial. *Clin Res Hepatol Gastroenterol* 2011;35:489-493.
- Schouten R, Freijzer PL, Greve JW. Laparoscopic sleeve resection of a recurrent gastric cascade: a case report. *J Laparoendosc Adv Surg Tech A* 2007;17:307-310.
- Spriggs EA, Marxer OA. Kinking, rotation, and twisting of the stomach, with special reference to cascade stomach and chronic gastric volvulus. *Br Med J* 1954;2:325-330.
- Sirakov V, Stefanov R, Shipkov C. The most common cause of cascade stomach. *Folia Med (Plovdiv)* 1994;36:37-39.
- Battisti G, Natali G, Manno A, Stio F, Palazzini G, Granai AV, Scaldaferrì T, Porcelli C, Gabatel R, Messinetti S. “Cascade stomach”: laparoscopic treatment. *Endoscopy* 1998;30:S92-S93.
- Kusano M, Hosaka H, Moki H, Shimoyama Y, Kawamura O, Kuribayashi S, Mori M, Akuzawa M. Cascade stomach is associated with upper gastrointestinal symptoms: a population-based study. *Neurogastroenterol Motil* 2012;24:451-455, e214.
- Keller RJ, Khilnani MT, Wolf BS. Cascade stomach. Roentgen appearance and significance. *Am J Roentgenol Radium Ther Nud Med* 1975;123:746-754.
- Kusano M, Hosaka H, Yasuoka H, Kawamura O, Kawada A, Kuribayashi S, Shimoyama Y, Mizuide M, Tomizawa T, Ishihara S, Sagawa T, Akiyama J, Sato K, Kakizaki S, Moki F. New endoscopic classification of cascade stomach, a risk factor for reflux esophagitis. *J Gastroenterol* 2017;52:211-217.

2022 Referee Index - 2022 Hakem Dizini

A. Cahid Civelek
Ahmet Tutuř
Ali Sarıkaya
Ayře Mavi
Ayřegöl Akgün
Bedri Seven
Berna Okudan Tekin
Bilge Volkan Salancı
Bircan Sönmez
Bölent Turgut
Cengiz Tařçı
Corinna Altini
Dragana Sobic Saranovic
Elgin Özkan
Emre Demirci
Emre Entok

Esra Arslan
Fatma Suna Kıraç
Feyza řen
Fikriye Gül Gümüşer
Funda Üstün
Gamze Çapa Kaya
Gonca G. Bural
Gözde Dağlıöz Görür
Hakan Demir
Hülya Yalçın
Irena Dimitrova Kostadinova
İlknur Ak Sivrikoz
Mahmut Yüksel
Majid Assadi
Maria Lyra Georgosopoulou
Mehmet Reyhan

Meliha Korkmaz
Meryem Kaya
Mine Araz
Mustafa Demir
Mustafa Yıldız
Nedim Cüneyt Murat Gülaldi
Nilüfer Yıldırım
Nosheen Fatimn
Rabia Lebriz Uslu Beřli
Sevin Cořar Ayaz
Seyhan Karaçavuş
Suna Erdoğan
Tarık řengöz
Tunç Öneř
Yakup Yüreklı
Zekiye Hasbek

2022 Author Index - 2022 Yazar Dizini

Aamna Hassan.....	66	Esra Arslan.....	72, 75, 200
Abderrahim Doudouh.....	231	Evangelos Ntais.....	63
Ahmet Emre Eşkazan.....	57	Ezgi Başak Erdoğan.....	23
Ahmet Eren Şen.....	151	Filiz Özülker.....	96
Ahmet Volkan Sünter.....	75	Francesco Guerrini.....	227
Alain Seret.....	7	Francisco Manuel Cañete Sánchez.....	145
Ali İbrahim Hatemi.....	57	François-Xavier Hanin.....	7
Ali Kibar.....	57	Funda Aydın.....	250
Alper Özgür Karaçalıoğlu.....	89	Gamze Çapa Kaya.....	216
Andreas Fotopoulos.....	63	Gamze Tatar.....	123, 200
Angelo Pompucci.....	227	Göksel Alçın.....	72
Anjali Meena.....	246	Göksel Alçın.....	123
Antonella Fontana.....	227	Gonca Gül Bural.....	242
Antonio Cabrera Villegas.....	145	Gözde Mütevelizade.....	172,223
Aris Bechlioulis.....	63	Gül Gümüşer.....	172, 223
Atilla Halil Elhan.....	114	Gülçin Yeğen.....	72
Ayça Arçay.....	242, 250	Gülen Hatemi.....	57
Ayça Kırmızı.....	49	Halil Kömek.....	104
Ayşegül Aksu.....	16, 216	Halil Turgut Turoğlu.....	69, 237
Batuhan Bakırarar.....	49	Halim Özçevik.....	191
Bernard Willemart.....	7	Hardik Veerwal.....	246
Berrin İmge Ergüder.....	114	Hasan Öner.....	33
Buğra Kaya.....	151, 163	Hideki Otsuka.....	169, 239
Burak İnce.....	57	Hiroaki Inoue.....	169
Büşra Aydur Püren.....	82	Hiroaki Toba.....	239
Ceren Sezgin.....	172, 223	Hüseyin Kemal Türköz.....	237
Chrissa Sioka.....	63	Hüseyin Ozan Tekin.....	82
Christos Katsouras.....	63	Hüseyin Şan.....	42, 89, 179
Cihan Gündoğan.....	200	Hwan Lee.....	1
Çağlagül Erol.....	151	Imran Khalid Niazi.....	66
Çağlar Uyulan.....	82	Isabelle Mathieu.....	7
Çiğdem Soydal.....	49, 114	İbrahim Ethem Geçim.....	114
Demet Nak.....	207	Jeremie Tordo.....	166
Didem Can Trabulus.....	75	Kemal Metin Kır.....	207
Ediz Beyhan.....	157, 160, 244	Kerim Sönmezöğlü.....	57, 154
Eleni Kapsalı.....	63	Kevser Öksüzöğlü.....	234
Elgin Özkan.....	49, 114	Leonardo Gabriel Romero Robles.....	145
Elvan Sayit.....	172, 223	Levent Kabasakal.....	139
Emre Can Çelebioğlu.....	207	Luca Filippi.....	227
Emre Demirci.....	139	María Mangas Losada.....	145
Engin Alagöz.....	89, 179	Masafumi Harada.....	169, 239

2022 Author Index - 2022 Yazar Dizini

Matthieu Dietz.....	166	Özgül Ekmekçioğlu.....	154
Maythinee Chantadisai.....	130	Özlem Özkul.....	123
Mehmet Aydın.....	23	Özlem Şahin.....	151
Mehmet Mülazimoğlu.....	191	Pinar Gündüz.....	49
Mehmet Reyhan.....	60	Pinar Pelin Özcan.....	60
Mehmet Sadık Bilgiç.....	207	Puy Garrastachu.....	145
Mehmet Tarık Tatoğlu.....	191	Rabia Lebriz Uslu Beşli.....	57
Meltem Ocak.....	139	Rabiye Uslu Erdemir.....	82
Meryem İlkay Eren Karanis.....	33	Rafael Ramírez Lasanta.....	145
Mete Akın.....	250	Rahime Şahin.....	157, 160
Michel Destine.....	7	Reyhane Ahmadi.....	142
Mihoko Sasahara.....	239	Roberto Delgado Bolton.....	145
Mine Araz.....	49, 114	Sadık Bilgiç.....	114
Mohsen Qutbi.....	142	Sadife Rüya Erinç.....	16
Muhammet Sait Sağer.....	57	Saho Irahara.....	169
Murat Akyol.....	104	Salah Oueriagli Nabih.....	231
Mustafa Durmaz.....	114	Salih Özgüven.....	69, 234, 237
Mustafa Erol.....	33	Sana Munir Gill.....	66
Mustafa Özdeş Emer.....	89	Sasitorn Sirisalipoch.....	130
Mustafa Taşar.....	89	Selçuk Ergen.....	139
Müge Öner Tamam.....	16, 191	Selim Bakan.....	154
Nalan Alan Selçuk.....	139	Selin Kesim.....	69
Namra Asghar.....	66	Semra İnce.....	89
Nazım Coşkun.....	33	Semra Özdemir.....	82
Nazlı Pinar Karahan Şen.....	216	Serhat Hayme.....	207
Necdet Poyraz.....	163	Serpil Dizbay Sak.....	49
Nedim Tokgözoğlu.....	16	Sertaç Asa.....	57
Nesrin Aslan.....	148	Seval Erhamamcı.....	148
Nilay Ermantaş.....	72	Sıddıka Fındık.....	163
Nuh Filizoğlu.....	234, 237	Sinan Demircioğlu.....	163
Nuran Katgı.....	104	Sira Vachatimanont.....	130
Nurhan Ergül.....	157, 160, 200, 244	Sotirios Giannopoulos.....	63
Nuri Arslan.....	89	Şeyma Babaoğlu.....	163
Nuriye Özlem Küçük.....	114, 207	Taha Cumhan Şavlı.....	75
Nurşin Agüloğlu.....	104	Takashi Abe.....	239
Omar Ait Sahel.....	231	Takayoshi Shinya.....	169, 239
Onur Buğdaycı.....	234	Tamer Aksoy.....	72, 75
Oreste Bagni.....	227	Tamer Özülker.....	96
Ömer Faruk Şahin.....	200	Tanju Yusuf Erdil.....	69, 234, 237
Özge Erol Fenercioğlu.....	157, 160, 244	Tevfik Fikret Çermik.....	72, 75, 157, 160, 200, 244
Özge Vural Topuz.....	16	Tunç Öneş.....	69, 237

2022 Author Index - 2022 Yazar Dizini

Türkay Toklu	139	Yasemin Özlük	72
Türker Tekin Ergüzel.....	82	Yasemin Parlak.....	172
Uğur Bozlar	89	Yassir Benameur	231
Umm e Kalsoom Awan	66	Yavuz Sami Salihoğlu	82
Usman Ahmad.....	66	Yoichi Otomi.....	169, 239
Utku Şenol.....	242	Yumi Abe.....	239
Vandana Dhingra	246	Yeşim Karagöz	244
Vehbi Erçolak	60	Zehra Pınar Koç	60
Xavier Louis Boulevard Chollet.....	145	Zeynep Aydın	151
Yasemin Gökden.....	96		

“Picture-in-Picture” artifact/“Resim-İçinde-Resim” artefaktı.....	142	Coronary stenosis/Koroner stenoz	89
¹³¹ I/ ¹³¹ I	234	CoronaVac/CoronaVac.....	179
¹⁸ F-FDG PET/ ¹⁸ F-FDG PET	239	COVID-19/COVID-19	169, 231
¹⁸ F-FDG PET/CT/ ¹⁸ F-FDG PET/BT	16, 66, 104, 157, 166, 169, 172, 179, 216, 237, 242, 244, 250	CT/BT	250
¹⁸ F-FDG-PET/ ¹⁸ F-FDG-PET.....	160	Deconvolution/Dekonvolüsyon.....	7
¹⁸ F-FDG/ ¹⁸ F-FDG	57, 72, 148	Denoising/Gürültü giderme.....	7
¹⁸ F-FLT PET/CT/ ¹⁸ F-FLT PET/BT.....	207	Diagnostic performance/Tanısıl performans	130
¹⁸ F-fluorocholine/ ¹⁸ F-florokolin.....	231	Diffuse large B-cell lymphoma/Diffüz büyük B-hücreli lenfoma	148
¹⁸ F-fluorodeoxyglucose (¹⁸ F-FDG)/ ¹⁸ F-florodeoksiglukoz (¹⁸ F-FDG).....	23	Diffuse large B-cell non-Hodgkin lymphoma/Diffüz büyük B hücreli non-Hodgkin lenfoma	72
¹⁸ F-fluorodeoxyglucose/ ¹⁸ F-florodeoksiglukoz	123	Dosimetry/Dozimetri.....	1
²²⁵ Ac targeted alpha therapy/ ²²⁵ Ac hedeflendirilmiş alfa tedavisi	139	Early response/Erken yanıt	207
⁶⁸ Ga PSMA PET/CT/ ⁶⁸ Ga PSMA PET/BT	223, 244	Echocardiography/Ekokardiyografi	63
⁶⁸ Ga/ ⁶⁸ Ga.....	60	EGFR/EGFR	104
Accuracy/Doğruluk	130	Endometrial cancer/Endometriyum kanseri	16
Acrometastasis/Akrometastaz	160	Enoxaparin/Enoksaparin.....	157
Acute myeloid leukemia/Akut miyeloid lösemi	63	Esophageal cancer/Özofagus kanseri	216
Acute myeloid leukemia/Akut miyeloid lösemi	57	Extranodal-multiorgan involvement/Ekstranodal- multiorgan tutulumu	72
Alpha particle/Alfa parçacığı.....	1	Extraosseous/Ekstraosseöz.....	246
Angiography/Anjiyografi	63	Fluorine-18-fluorodeoxyglucose/Flor-18-florodeoksiglukoz... ..	200
Attenuation correction/Atenüasyon düzeltmesi.....	130	Fluorodeoxyglucose/Florodeoksiglukoz	33, 49
Axillary lymph node/Aksiller lenf nodu.....	179	Gastrointestinal Behcet’s disease/Gastrointestinal Behçet hastalığı.....	57
Behcet syndrome/Behçet sendromu.....	57	Gastrointestinal tract/Gastrointestinal sistem	96
Beta particle/Beta parçacığı	1	Germ cell tumor/Germ hücreli tümör.....	239
BNT162b2/BNT162b2	179	Giant cell tumor of tendon sheath/Tendon kılıfının dev hücreli tümörü	145
Bone/Kemik.....	237	Glioblastoma multiforme/Glioblastoma multiforme	246
Bone metastasis/Kemik metastazı.....	160	Granuloma/Granülom.....	157
Bone scan/Kemik taraması.....	166, 246	Growing teratoma syndrome/Büyüyen teratom sendromu	239
Bone scintigraphy/Kemik sintigrafisi	151	Heterotopic ossification/Heterotopik ossifikasyon	166
Breast cancer/Meme kanseri.....	23, 49, 123	Hormone receptor/Hormon reseptörü	49
Breast/Meme.....	163	Hypermetabolism/Hipermetabolizma	179
Cardiac hybrid imaging/Kardiyak hibrid görüntüleme	89	Hyperparathyroidism/Hiperparatiroidi	191
Cascade stomach/Kaskat mide	250	Incidental ¹⁸ F-FDG uptake/İnsidental ¹⁸ F-FDG tutulumu....	96
Caudal regression syndrome/Kaudal regresyon sendromu....	69	Incidentally detected lesions/İnsidental olarak saptanan lezyonlar	96
Chemoembolization/Kemoembolizasyon	207	Integrin alpha-3/İntegrin alfa-3.....	75
Colon/Kolon	96	Integrin beta-1/İntegrin beta-1	75
Colorectal cancer/Kolorektal kanser.....	114	Internet/İnternet	42
Coronary artery disease/Koroner arter hastalığı	63, 130		
Coronary CT angiography/Koroner BT anjiyografi	89		

2022 Subject Index / 2022 Konu Dizini

Langerhans cell histiocytosis/Langerhans hücreli histiyositoz.....	237	Papillary thyroid cancer/Papiller tiroid kanseri.....	75
Legendre polynomials/Legendre polinomları.....	7	Parathyroid scintigraphy/Paratiroid sintigrafisi.....	191
Liver metastasis/Karaciğer metastazi.....	114	Peptide receptor radionuclide therapy/Peptid reseptör radyonüklid tedavisi.....	139
Liver tumors/Karaciğer tümörleri.....	207	Personalized medicine/Kişiselleştirilmiş tıp.....	227
Lu-177/Lu-177.....	60	PET scan/PET tarama.....	57
Lung adenocarcinoma/Akciğer adenokarsinomu.....	33	PET/CT/PET/BT.....	49, 82, 72, 148, 154, 160, 163, 231
Lung cancer/Akciğer kanseri.....	104	Pituitary adenoma/Pitüiter adenom.....	244
Lung carcinoma/Akciğer kanseri.....	160	Plasmacytoma/Plazmositom.....	163
Lymphoma/Lenfoma.....	242	Pneumonia/Pnömoni.....	231
Machine learning/Makine öğrenmesi.....	82	Positron emission tomography/computed tomography (PET/CT)/Pozitron emisyon tomografisi/bilgisayarlı tomografi (PET/BT).....	23
MAG3/MAG3.....	7	Positron emission tomography/Pozitron emisyon tomografisi.....	123, 200, 227
Magnetic resonance imaging/Manyetik rezonans görüntüleme.....	145	Post-therapeutic ¹³¹ I survey/Tedavi sonrası ¹³¹ I tarama....	142
Malignant lip neoplasm/Dudak malign neoplazmı.....	172	Primary cardiac tumor/Primer kardiyak tümörler.....	148
Mammography/Mamografi.....	163	Primary/Primer.....	207
MDP/MDP.....	151	Prognosis/Prognoz.....	33, 200
Mediastinum/Mediasten.....	239	Progression-free survival/Progresyonsuz sağkalım.....	104
Mesenteric panniculitis/Mezenterik pannikülit.....	154	Prone position/Pron pozisyonu.....	23
Metabolic tumor volume/Metabolik tümör hacmi.....	216	Prostate cancer/Prostat kanseri.....	1, 223, 231
Metastases/Metastaz.....	223	Prostate cancer/Prostat karsinomu.....	60
Metastasis/Metastaz.....	246	Prostate neoplasm/Prostat neoplazmı.....	227
Metastatic/Metastatik.....	207	Prostate-specific membrane antigen/Prostata özgü membran antijeni.....	1
Molecular imaging/Moleküler görüntüleme.....	227	PSMA/PSMA.....	60
Monosomy 7/Monozomi 7.....	57	Pulmonary alveolar microlithiasis/Pulmoner alveolar mikrolitiazis.....	151
Moore-Penrose/Moore-Penrose.....	7	Radiation-induced osteosarcoma/Radyasyona bağlı osteosarkom.....	66
MRI/MRG.....	57, 242	Radioactive iodine/Radyoaktif iyot.....	42
Myelodysplastic syndromes/Myelodisplastik sendrom...	57	Radioembolization/Radyoembolizasyon.....	207
Myocardial ischemia/Miyokardiyal iskemi.....	63	Radioiodine therapy/Radyoiyot tedavisi.....	234
Myocardial perfusion imaging/Miyokardiyal perfüzyon görüntüleme.....	63, 130	Radiomic/Radyomik.....	82
Myocardial perfusion scintigraphy/Miyokard perfüzyon sintigrafisi.....	89	Radiomics/Radyomiks.....	33
Nasolacrimal duct obstruction/Nazolakrimal kanal tıkanıklığı.....	234	Radionuclide therapy/Radyonüklid tedavi.....	1
Neoadjuvant chemotherapy/Neoadjuvan kemoterapi....	123	Renal cell carcinoma/Renal hücreli karsinom.....	200
Neuroendocrine tumors/Nöroendokrin tümörler.....	139	Renal transit time/Renal geçiş süresi.....	7
Neurolymphomatosis/Nörolenfomatozis.....	242	Sacral agenesis/Sakral agenezi.....	69
Neurosurgery/Beyin cerrahisi.....	227	Scintigraphy/Sintigrafisi.....	145
Open mouth technique/Ağız açık pozisyonlama.....	172		
Ovary carcinoma/Over kanseri.....	154		
Overall survival/Genel sağkalım.....	104		

Serum angiogenic factors/Serum anjiyojenik faktörler	114	Tc-99m MDP/Tc-99m MDP.....	246
Single photon emission computed tomography/Tek foton emisyonlu bilgisayarlı tomografi	130	Textural analysis/Doku analizi	33
Solitary plasmacytoma/Soliter plazmasitoma	66	Thyroid cancer/Tiroid kanseri	75, 234
Solitary pulmonary nodule/Soliter pulmoner nodül	82	Thyroid neoplasms/Tiroid neoplazmaları	145
SPECT/CT/SPECT/BT	69, 191	Transarterial radioembolization/Transarteriyel radyoembolizasyon	114
SPECT/SPECT	191	Treatment/Tedavi	42
Spinal nerve root/Spinal sinir kökü	242	Ultrasonography/Ultrasonografi	163
Survival/Sağkalım.....	200	Unexpected/Nadir	223
SUV _{max} /SUV _{maks}	16	Vaccination/Aşı.....	169
TACE/TAKE	207	VACTERL association/VACTERL asosiyasyonu	69
TARE/TARE.....	207	Video/Video	42
Tc-99m DMSA renal scintigraphy/Tc-99m DMSA böbrek sintigrafisi	69	Volumetric parameters/Volumetrik parametreler.....	16
		Whole-body scanning/Tüm vücut taraması	142